4,7-Diarylbenzo[*c*][1,2,5]thiadiazoles as Fluorophores and Visible Light Organophotocatalysts

Electronic Supplementary Information

Dominic Taylor,[a] Thomas Malcomson,[b] Adilet Zhakeyev,[c] Shengxian Cheng,[d] Georgina M. Rosair,[a] Jose Marques-Hueso,[c] Zhengtao Xu,[e] Martin J. Paterson,[a] Scott. J. Dalgarno,[a,*] and Filipe Vilela[a,*]

[a]*Institute of Chemical Sciences, School of Engineering and Physical Science, Heriot-Watt University, Riccarton, Edinburgh, EH14 4AS, UK.*

[b]*Department of Chemistry, Lancaster University, Lancaster, LA1 4YB, UK.*

[c]*Institute of Sensors, Signals and Systems, School of Engineering and Physical Science, Heriot-Watt University, Riccarton, Edinburgh, EH14 4AS, UK.*

[d]*Department of Chemistry, City University of Hong Kong, 83 Tat Chee Avenue, Kowloon, Hong Kong.*

[e]*Institute of Materials Research and Engineering (IMRE), Agency of Science, Technology and Research (A*STAR), 2 Fusionopolis Way, Innovis, Singapore 138634.*

E-mail: f.vilela@hw.ac.uk, s.j.dalgarno@hw.ac.uk

Table of Contents

1.	**General Details**		**3**
	1.1	General Experimental Details	3
	1.2	Structures of Fluorophores/Photocatalysts and Abbreviations Used	5
2.	**Synthetic Details**		**6**
	2.1	Synthesis of Starting Materials	6
	2.2	Synthesis of Photocatalysts	7
3.	**Single Crystal X-ray Structures**		**20**
4.	**Photophysical Properties of the Photocatalysts**		**35**
	4.1	UV-Vis Absorption and Emission Spectra	35
	4.2	Molar Attenuation Coefficient Measurements	51

4.3 Summary of Photophysical Results 52
4.4 Photobleaching Studies 53
5. Computational Studies 54
5.1 General Information 54
5.2 Theoretical Absorption and Emission Spectra 55
5.3 Summary of Results 68
5.4 Excited State Orbitals 69
5.5 Theoretical Analysis of Selenophene and Tellurophene Analogues of **Th-BTZ** 83
5.6 Energy Barriers to Bond Rotation of Selected Photocatalysts 86
5.7 Geometry Comparison Table 89
6. Cyclic Voltammetry Studies **90**
6.2 Cyclic Voltammograms 90
6.3 Summary of Results 103
7. Decarboxylative C-H Functionalisation of Heteroarenes 104
7.1 Procedures for Batch Photocatalysis 104
7.2 Optimisation of Reaction Conditions 106
7.3 Reaction Scope 107
7.4 Photocatalysis in Flow 111
8. Characterisation of Photocatalysts **113**
9. Characterisation of Photocatalytic Reaction Products **164**
10 References **174**

1. General Details

1.1 General Experimental Details

All commercially available compounds were used as received and purchased from Sigma-Aldrich, Fluorochem, Apollo Scientific or Fischer Scientific. Where stated, reactions were carried out under an atmosphere of oxygen free nitrogen purchased from BOC using oven dried glassware. Column chromatography was performed using Silicagel 60 Å 40 – 63 microns from Fluorochem. Thin layer chromatography was run using Silica gel 60 F254 TLC plates and the spots were visualised using UV illumination.

NMR spectra of synthetic products were recorded using a Bruker AVIII 300 MHz spectrometer using the residual solvent peak as an internal reference unless stated otherwise. For selected compounds exhibiting low solubility, ^{13}C NMR spectra were recorded using a Bruker AVIIIHD 400 MHz spectrometer, with the D_1 relaxation delay increased from 2 to 20 s and a total of 2048 scans recorded. Quantitative NMR spectra of photoredox catalytic experiments were also carried out using the Bruker AVIII 300 MHz spectrometer using $CDCl_3$ as the solvent.

All IR spectra were recorded on solid powder/crystals using a Nicolet™ iS™ 5 FTIR spectrometer.

UV-Vis absorption spectra for the synthesised photocatalysts were obtained using a Perkin-Elmer Lambda 35 spectrometer in chloroform solution in quartz cuvettes with a path length of 1 cm. Emission spectra in the visible region were recorded using a Perkin Elmer LS 55 fluorescence spectrometer in chloroform solution using quartz cuvettes with a path length of 1 cm. The excitation wavelength used was the wavelength of maximum absorption for each individual photocatalyst. For comparison between different spectra, each set of data was normalised to the maximum absorbance observed in the region of 350 – 800 nm.

The PLQYs were measured following the conventions and considerations from Jones *et al.*[1] A FLS920 spectrofluorometer (Edinburgh Instruments Ltd) equipped with an extended red-sensitive photon multiplier detector (Hamamatsu, R2658P) and an integrating sphere with a 102 mm inner diameter (Yobin Yvon) were used for all PLQY measurements. For the excitation, a 450 W Xenon lamp (Edinburgh Instruments Ltd, Xe2) was employed. The samples consisted of 2 mL diluted dyes in chloroform, typically at 20 μM. The sample was contained in a square quartz cuvette with 10 mm light path and placed in the centre of the integrating sphere. The reference sample, or blank, was pure chloroform. The excitation wavelengths were set to the peak absorption of each sample with a bandwidth set to 5 nm. The excitation and emission regions were typically measured with a 0.25 nm step size. The associated measurement error was 3%.

Single crystal x-ray structures were collected using a Bruker D8 venture using either a Cu-K_α (λ = 1.5418 Å) or a Mo-K_α (0.7107 Å) IμS 3.0 microfocus source, using the APEX3 program suite, with the crystal kept at 100.0 K during data collection. The structures were solved using Olex2, using the SHELXT structure solution program using Intrinsic Phasing and refined with the SHELXL refinement package using Least Squares minimisation.[2–4]

ESI-MS spectra of the synthesised photocatalysts were measured using time-of-flight mass spectrometry using a Waters Acquity UPLC-Xevo G2 QTof with the electrospray ionisation source in positive mode. Samples were prepared by dissolving 1 mg of sample in 4 mL of acetonitrile.

Cyclic voltammetry measurements were performed using an IviumStat potentiostat using a glassy carbon working electrode, a platinum wire counter electrode and a standard calomel reference electrode. The solutions were degassed with nitrogen prior to measurements and carried out under a protective layer of nitrogen. All measurements were carried out using dry dichloromethane as the solvent and 0.25 M tetra(*n*-butylammonium) hexafluorophosphate dissolved in dry DCM as the electrolyte.

Irradiation during batch photochemical experiments was achieved using in-house constructed light source. An array of four 3 W 420 nm LED modules purchased from Future Eden were mounted onto an aluminium heat sink using thermal glue for attachment.

For photocatalytic reactions performed under flow conditions, an easy-Photochem E-Series flow machine was utilised. The reaction mixture was flowed through a coiled section of transparent fluorinated ethylene propylene tubing (total volume 5 mL), that was irradiated using the same violet LED source as described above. Separate to this, the Vapourtec UV-150 photochemical reactor equipped with a blue LED module (410 – 420 nm, 60 W) was also tested using the same 5 mL coiled tubing.

1.2 Structures of Fluorophores/Photocatalysts and Abbreviations Used

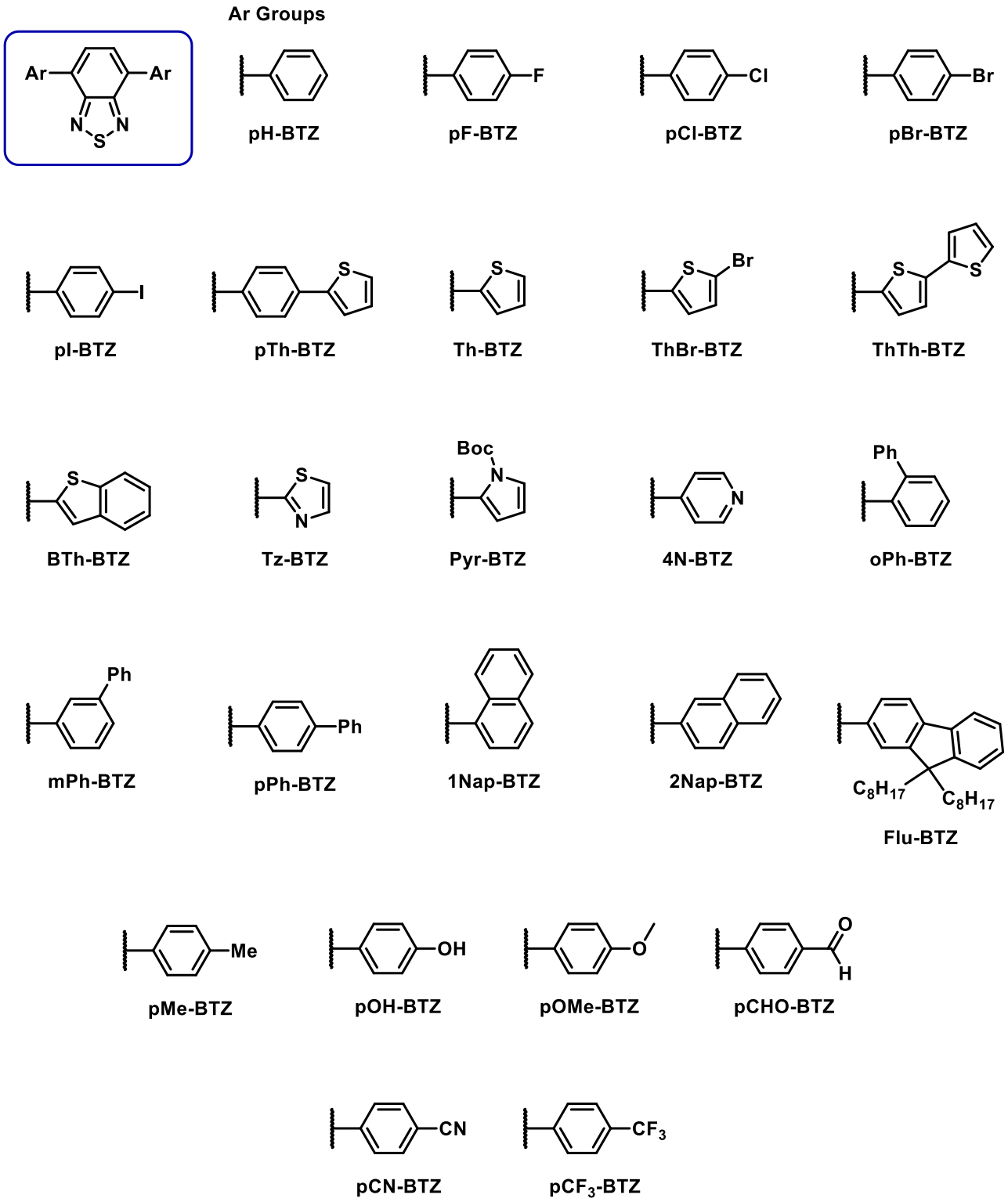

Figure S1 Structure of **BTZ** photocatalysts and their abbreviations used in this study.

2. Synthetic Details

2.1 Synthesis of Starting Materials

Tetrakis(triphenylphosphine) palladium (0)[5]

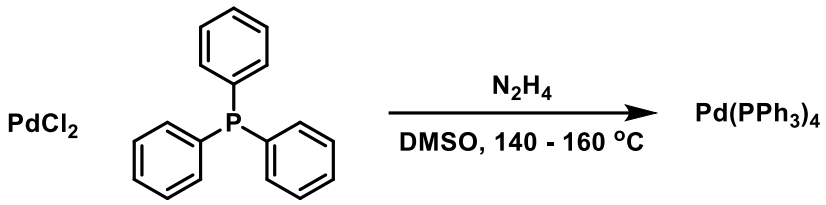

A dry 250 mL 2-neck flask was charged with triphenylphosphine (2.63 g, 10 mmol) and palladium (II) chloride (351 mg, 2 mmol) then evacuated and back-filled with nitrogen three times. The flask was then charged with anhydrous DMSO (25 mL) and rapidly evacuated and backfilled with nitrogen three times. The mixture was then heated to 140 – 160 °C under nitrogen until an orange solution formed, then stirring continued for 15 minutes. Hydrazine hydrate (50 – 60%, 0.6 mL) was added then the mixture was removed from the heat and stirring stopped. The mixture was then allowed to cool to room temperature and left to sit for approximately 1 hour. During this time, yellow crystals formed that were then filtered through a sintered glass adaptor under nitrogen. The crystals were then washed with dry methanol (5 x 15 mL) and dry diethyl ether (5 x 10 mL) then allowed to dry under nitrogen and vacuum. The crystals were then transferred to a dry round bottom flask, sealed with a septum then evacuated and backfilled with nitrogen five times. The final mass of dried crystals was 2.057 g (89%).

4,7-Dibromobenzo[*c*][1,2,5]thiadiazole (Br_2BTZ)

For the synthesis of 4,7-dibromobenzo[*c*][1,2,5]thiadiazole, two different literature procedures were utilised.[6,7]

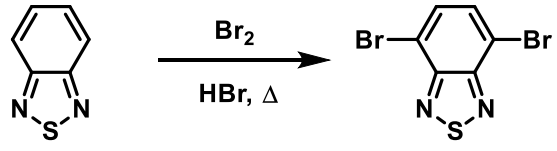

Procedure 1: A 2-neck round bottom flask was charged with benzo[*c*][1,2,5]thiadiazole (12.0 g, 88.1 mmol) and hydrobromic acid (47%, 30 mL) added. The mixture was heated to reflux and bromine (13.54 mL, 264.3 mmol) added slowly over 20 minutes then the refluxed for 2.5 hours. The mixture was cooled to room temperature and the residue washed with deionised water to yield a yellow powder. Recrystallisation from hot

chloroform yielded light yellow needles (22.055 g, 86%). **^{1}H NMR** ($CDCl_3$, 300 MHz, 25.0 °C) δ_H 7.73 (s, 2 *H*).

Procedure 2:

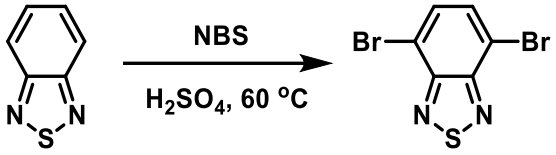

Benzo[*c*][1,2,5]thiadiazole (2.5 g, 18.4 mmol) and *N*-bromosuccinimide (NBS) (6.877 g, 38.64 mmol) were dissolved in concentrated sulfuric acid (25 mL) and the mixture heated to 60 °C for 4 hours. Following this, the reaction was allowed to cool to room temperature and then poured onto an ice-water mixture. The precipitate that formed was then filtered and washed with copious amounts of water. The final product was dried under vacuum to give an off-white powder (4.524 g, 85%). Characterisation as above.

2.2 Synthesis of Photocatalysts

General Procedure A for Synthesis of Photocatalysts *via* Suzuki-Miyaura Cross Coupling

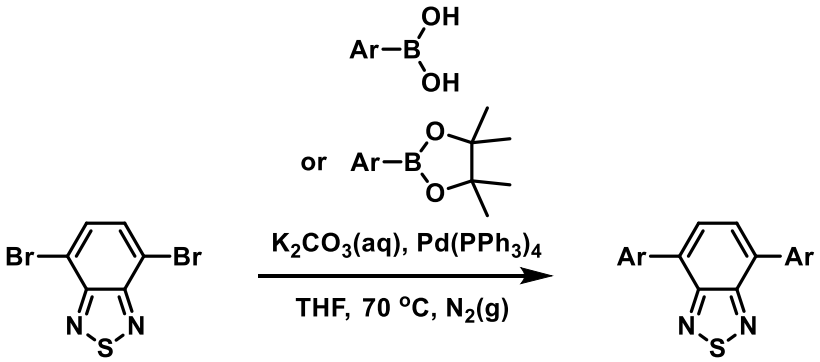

A dry 2-neck flask was charged with 4,7-dibromobenzo[*c*][1,2,5]thiadiazole (1.0 equivalent), the appropriate aryl boronic acid or boronic acid pinacol ester (2.5 equivalents), potassium carbonate (2.0 equivalents) and $Pd(PPh_3)_4$ (5 mol%). The flask was connected to a Schlenk line then evacuated and backfilled with nitrogen three times. Degassed THF (40 mL) and degassed deionised water (5 mL) were added and the reaction heated to 70 °C for 16 h. Following this time, the mixture was allowed to cool to room temperature, poured onto deionised water and extracted with DCM (3 x 25 mL). The combined organic phases were washed with deionised water (50 mL), dried over $MgSO_4$ and the solvent removed under reduced pressure. Purification of the crude product was achieved either by recrystallisation, washing with hot solvent or column chromatography.

General Procedure B for Synthesis of Photocatalysts *via* Suzuki-Miyaura Cross Coupling

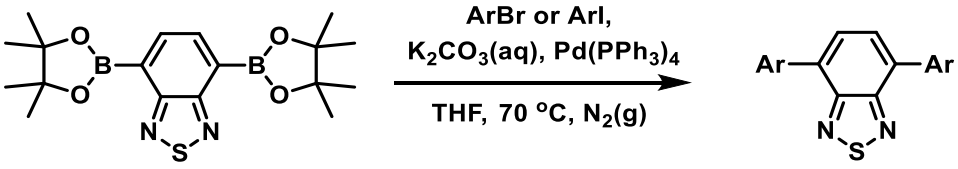

A dry 2-neck flask was charged with 4,7-bis(4,4,5,5-tetramethyl-1,3,2-dioxaborolan-2-yl)benzo[*c*][1,2,5]thiadiazole (1.0 equivalents), the appropriate aryl bromide or iodide (2.5 equivalents), potassium carbonate (2.0 equivalents) and $Pd(PPh_3)_4$ (5 mol%). The flask was connected to a Schlenk line then evacuated and backfilled with nitrogen three times. Degassed THF (40 mL) and degassed deionised water (5 mL) were added and the reaction heated to 70 °C for 16 h. Following this time, the mixture was allowed to cool to room temperature, poured onto deionised water and extracted with DCM (3 x 25 mL). The combined organic phases were washed with deionised water (50 mL), dried over $MgSO_4$ and the solvent removed under reduced pressure. Purification of the crude product was achieved either by recrystallisation or washing with hot solvent.

4,7-Diphenylbenzo[*c*][1,2,5]thiadiazole (pH-BTZ)

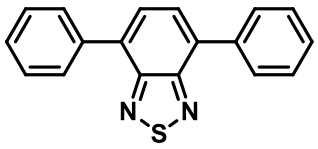

$C_{18}H_{12}N_2S$
288.37 g mol^{-1}

General procedure A for Suzuki-Miyaura coupling using benzene boronic acid (305 mg, 2.5 mmol), 4,7-dibromobenzo[*c*][1,2,5]thiadiazole (294 mg, 1.0 mmol), potassium carbonate (276 mg, 2.0 mmol) and $Pd(PPh_3)_4$ (58 mg, 0.05 mmol). Crude product was recrystallised from methylated spirits to give yellow needles (173 mg, 60%). **^{1}H NMR** ($CDCl_3$, 300 MHz, 25.0 °C) δ_H 7.97 (m, 4 *H*), 7.80 (s, 2 *H*), 7.59 (m, 4 *H*), 7.47 (m, 2 *H*). **^{13}C NMR** ($CDCl_3$, 75.5 MHz, 25.0 °C) δ_C 154.1 (C), 137.5 (C), 133.4 (C), 129.3 (CH), 128.7 (CH), 128.4 (CH), 128.2 (CH). **UV-Vis** ($CHCl_3$) λ_{max} (nm) 380. **IR** $\bar{\nu}$ (cm^{-1}) 3027 (w, C-H str.). **HRMS** (ES+, MeCN) m/z = 289.0800 $[M+H]^+$, calc. 289.0799.

4,7-Bis(4-fluorophenyl)benzo[*c*][1,2,5]thiadiazole (pF-BTZ)

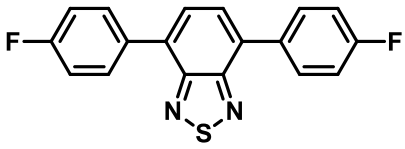

$C_{18}H_{10}F_2N_2S$
324.35 g mol^{-1}

General procedure A for Suzuki-Miyaura coupling using 4-fluorophenylboronic acid (0.33 mL, 350 mg, 2.5 mmol), 4,7-dibromobenzo[*c*][1,2,5]thiadiazole (294 mg, 1.0 mmol), potassium carbonate (276 mg, 2.0 mmol) and $Pd(PPh_3)_4$ (58 mg, 0.05 mmol). Crude product was recrystallised from methylated spirits to yield yellow-green crystals (152 mg, 47%). **^{1}H NMR** ($CDCl_3$, 300 MHz,

25.0 °C) δ_H 7.96 (m, 4 *H*), 7.75 (s, 2 *H*), 7.25 (m, 4 *H*). **^{13}C NMR** ($CDCl_3$, 75.5 MHz, 25.0 °C) δ_C 133.3 (C), 132.4 (C), 131.0 (CH), 130.9 (CH), 127.9 (CH), 115.8 (CH), 155.5 (CH). **^{19}F NMR** ($CDCl_3$, 282.4 MHz, 25.0 °C) δ_F -133.3 (m, 2 *F*). **UV-Vis** ($CHCl_3$) λ_{max} (nm) 381. **IR** $\bar{\nu}$ (cm^{-1}) 3070 (w, C-H str.). **HRMS** (ES+, MeCN) m/z = 325.0612 $[M+H]^+$, calc. 325.0611.

4,7-Bis(4-chlorophenyl)benzo[*c*][1,2,5]thiadiazole (pCl-BTZ)

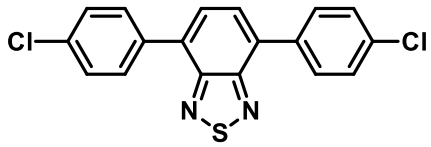

$C_{18}H_{10}Cl_2N_2S$
357.25 g mol^{-1}

General procedure A for Suzuki-Miyaura coupling using 4-chlorophenylboronic acid (391 mg, 2.5 mmol), 4,7-dibromobenzo[*c*][1,2,5]thiadiazole (294 mg, 1.0 mmol), potassium carbonate (276 mg, 2.0 mmol) and $Pd(PPh_3)_4$ (58 mg, 0.05 mmol). Crude product was recrystallised from hot methylated spirits to yield yellow-green crystals (225 mg, 63%). **^{1}H NMR** ($CDCl_3$, 300 MHz, 25.0 °C) δ_H 7.92 (m, 2 *H*), 7.74 (s, 2 *H*), 7.53 (m, 2 *H*). **^{13}C NMR** ($CDCl_3$, 75.5 MHz, 25.0 °C) δ_C 153.9 (C), 135.6 (C), 134.6 (C), 132.4 (C), 130.5 (CH), 128.9 (CH), 128.0 (CH). **UV-Vis** ($CHCl_3$) λ_{max} (nm) 383. **IR** $\bar{\nu}$ (cm^{-1}) 3037 (w, C-H str.). **HRMS** (ES+, MeCN) m/z = 357.0022 $[M+H]^+$, calc. 357.0020.

4,7-Bis(4-bromophenyl)benzo[*c*][1,2,5]thiadiazole (pBr-BTZ)

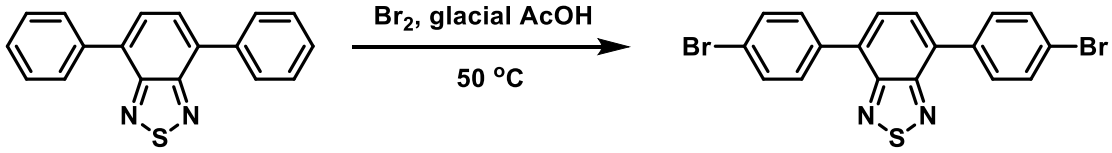

$C_{18}H_{10}Br_2N_2S$
446.16 g mol^{-1}

A 2-neck round bottom flask was charged with 4,7-diphenylbenzo[*c*][1,2,5]thiadiazole (721 mg, 2.5 mmol) then glacial acetic acid (20 mL) added. Bromine (1 mL) was added and the reaction mixture heated to 50 °C for 16 hours. Following this time, the mixture was allowed to cool to room temperature then filtered under gravity. The solid was then washed thoroughly with deionised water and air dried. The crude product was then recrystallised twice from hot toluene to yield yellow-green crystals (520 mg, 47%). **^{1}H NMR** ($CDCl_3$, 300 MHz, 25.0 °C) δ_H 7.86 (m, 4 *H*), 7.77 (s, 2 *H*), 7.68 (m, 4 *H*). **UV-Vis** ($CHCl_3$) λ_{max} (nm) 381. **IR** $\bar{\nu}$ (cm^{-1}) 3046 (w, C-H str.). **HRMS** (ES+, MeCN) m/z = 444.9007 $[M+H]^+$, calc. 444.9010. Due to the low solubility of 4,7-bis(4-bromophenyl)benzo[*c*][1,2,5]thiadiazole, a ^{13}C NMR of sufficient quality could not be obtained.

4,7-Bis(4-iodophenyl)benzo[*c*][1,2,5]thiadiazole (pI-BTZ)

pI-BTZ was synthesised by first coupling **Br_2BTZ** with (4-(trimethylsilyl)phenyl)boronic acid then carrying out an *ipso*-iodination using iodine monochloride.[8]

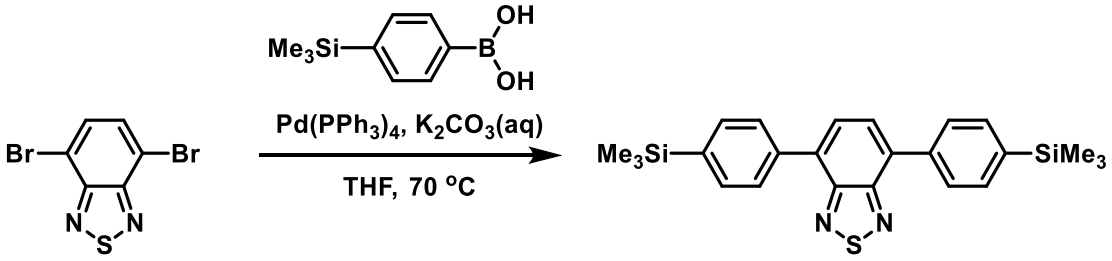

Step 1

General procedure A for Suzuki-Miyaura coupling using (4-(trimethylsilyl)phenyl)boronic acid (485 mg, 2.5 mmol), 4,7-dibromobenzo[*c*][1,2,5]thiadiazole (294 mg, 1.0 mmol), potassium carbonate (276 mg, 2.0 mmol) and $Pd(PPh_3)_4$ (58 mg, 0.05 mmol). Crude product was recrystallised from hot methylated spirits to yield green crystals (151 mg, 35%). **^{1}H NMR** ($CDCl_3$, 300 MHz, 25.0 °C) δ_H 7.94 (m, 4 *H*), 7.79 (s, 2 *H*), 7.71 (m, 4 *H*), 0.33 (s, 18 *H*). **^{13}C NMR** ($CDCl_3$, 75.5 MHz, 25.0 °C) δ_C 155.2 (C), 141.9 (C), 138.9 (C), 134.8 (CH), 134.6 (C), 129.6 (CH), 129.2 (C), 0.0 (CH_3). **UV-Vis** ($CHCl_3$) λ_{max} (nm) 385.

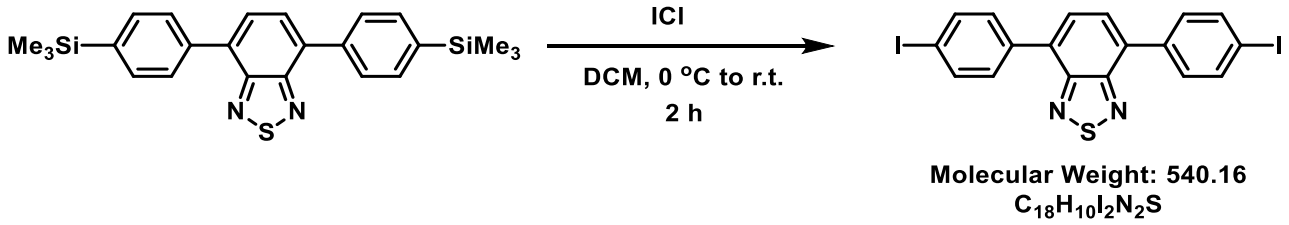

Step 2

4,7-Bis(4-(trimethylsilyl)phenyl)benzo[*c*][1,2,5]thiadiazole (108 mg, 0.25 mmol) was dissolved in DCM (5 mL) and cooled using an ice-water bath. Iodine monochloride (0.1 mL) was added then the mixture stirred with cooling for 10 minutes then slowly warmed to room temperature and further stirred for 2 hours. The reaction mixture was then poured onto a saturated sodium thiosulfate solution (40 mL), extracted with DCM (3 x 40 mL) then washed with water (30 mL). The crude reaction mixture was filtered through a layer of silica then the solvent removed under reduced pressure and the residue washed with hot methylated spirits to give a yellow powder (69 mg, 51%). **^{1}H NMR** ($CDCl_3$, 300 MHz, 25.0

°C) δ_H 7.88 (m, 4 *H*), 7.77 (s, 2 *H*), 7.71 (m, 4 *H*). **UV-Vis** ($CHCl_3$) λ_{max} (nm) 384. **IR** $\bar{\nu}$ (cm^{-1}) 3038 (w, C-H str.). **HRMS** (ES+, MeCN) m/z = 540.8744 $[M+H]^+$, calc. 540.8732. Due to the low solubility of 4,7-bis(4-iodophenyl)benzo[*c*][1,2,5]thiadiazole, a ^{13}C NMR of sufficient quality could not be obtained.

4,7-Bis(4-(thiophen-2-yl)phenyl)benzo[*c*][1,2,5]thiadiazole (pTh-BTZ)

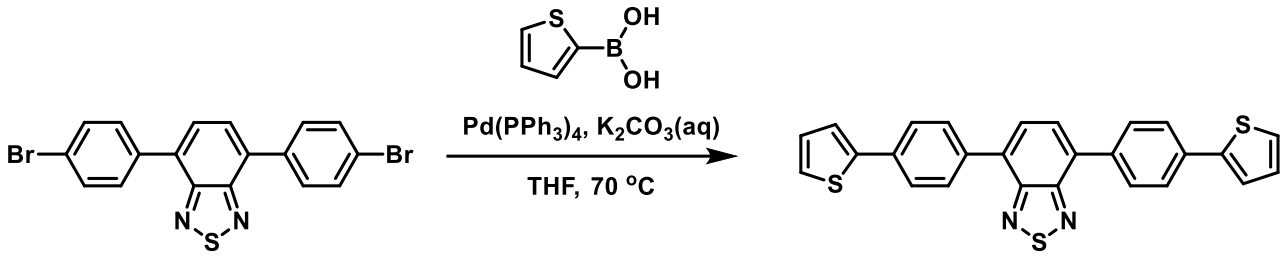

$C_{26}H_{16}N_2S_3$
452.61 g mol^{-1}

A dry 2-neck flask was charged with 4,7-bis(4-bromophenyl)benzo[*c*][1,2,5]thiadiazole (223 mg, 0.5 mmol), thiophen-2-yl boronic acid (160 mg, 1.25 mmol), potassium carbonate (138 mg, 1.0 mmol) and $Pd(PPh_3)_4$ (29 mg, 0.025 mmol). The flask was connected to a Schlenk line then evacuated and back-filled with nitrogen three times. Degassed THF (40 mL) and degassed deionised water (5 mL) were added and the reaction heated to 70 °C for overnight. Following this time, the mixture was allowed to cool to room temperature, poured onto deionised water and extracted with DCM (3 x 25 mL). The combined organic phases were washed with deionised water (50 mL), dried over $MgSO_4$ and the solvent removed under reduced pressure. The crude product was then washed with hot methylated spirits to give a yellow-brown powder (115 mg, 51%). **^{1}H NMR** ($CDCl_3$, 300 MHz, 25.0 °C) δ_H 8.03 (m, 4 *H*), 7.84 (s, 2 *H*), 7.81 (m, 4 *H*), 7.42 (dd, J = 3.6, 1.1 Hz, 2 *H*), 7.34 (dd, J = 5.1, 1.1 Hz, 2 *H*), 7.13 (dd, J = 5.1, 3.6 Hz, 2 *H*). **^{13}C NMR** ($CDCl_3$, 75.5 MHz, 25.0 °C) δ_C 154.1 (C), 144.0 (C), 136.4 (C), 134.5 (C), 132.8 (C), 129.7 (CH), 128.2 (CH), 127.9 (CH), 126.2 (CH), 125.2 (CH), 123.5 (CH). **UV-Vis** ($CHCl_3$) λ_{max} (nm) 409. **IR** $\bar{\nu}$ (cm^{-1}) 3038 (w, C-H str.). **HRMS** (ES+, MeCN) m/z = 453.0548 $[M+H]^+$, calc. 453.0554.

4,7-Di(thiophen-2-yl)benzo[*c*][1,2,5]thiadiazole (Th-BTZ)

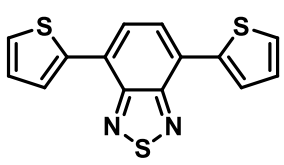

$C_{14}H_8N_2S_3$
300.41 g mol^{-1}

General procedure A for Suzuki-Miyaura coupling using 2-thiophene boronic acid pinacol ester (525 mg, 2.5 mmol), 4,7-dibromobenzo[*c*][1,2,5]thiadiazole (294 mg, 1.0 mmol), potassium carbonate (276 mg, 2.0 mmol) and $Pd(PPh_3)_4$ (58 mg, 0.05 mmol). Crude product was recrystallised from hot methylated spirits to give

red needles (200 mg, 67%). **^{1}H NMR** ($CDCl_3$, 300 MHz, 25.0 °C) δ_H 8.13 (dd, J = 3.7, 1.1 Hz, 2 *H*), 7.89 (s, 2 *H*), 7.45 (dd, J = 5.1, 1.1 Hz, 2 *H*), 7.22 (dd, J = 5.1 Hz, 3.7 Hz, 2 *H*). **^{13}C NMR** ($CDCl_3$, 75.5 MHz, 25.0 °C) δ_C 152.7 (C), 139.4 (C), 128.0 (CH), 127.5 (CH), 126.8 (CH), 126.1 (C), 125.8 (CH). **UV-Vis** ($CHCl_3$) λ_{max} (nm) 446. **IR** $\bar{\nu}$ (cm^{-1}) 2990 (w, C-H str.). **HRMS** (ES+, MeCN) m/z = 300.9922 $[M+H]^+$, calc. 300.9928.

4,7-Bis(5-bromothiophen-2-yl)benzo[*c*][1,2,5]thiadiazole (ThBr-BTZ)[9]

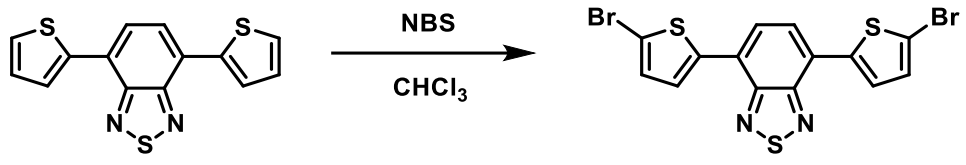

$C_{14}H_6Br_2N_2S_3$
458.20 g mol^{-1}

4,7-Di(thiophen-2-yl)benzo[*c*][1,2,5]thiadiazole (300 mg, 1 mmol) and NBS (534 mg, 3 mmol) were dissolved in $CHCl_3$ (15 mL) and stirred in the dark at room temperature for 3 days. Following this time, the precipitate that formed was filtered off and then washed with deionised water. Drying under vacuum yielded a dark red powder (403 mg, 88%). **^{1}H NMR** ($CDCl_3$, 300 MHz, 25.0 °C) δ_H 7.81 (d, J = 4.0 Hz, 2 *H*), 7.80 (s, 2 *H*), 7.16 (d, J = 4.0 Hz, 2 *H*). **UV-Vis** ($CHCl_3$) λ_{max} (nm) 455. **IR** $\bar{\nu}$ (cm^{-1}) 3089 (w, C-H str.). Due to the low solubility of 4,7-bis(5-bromothiophen-2-yl)benzo[*c*][1,2,5]thiadiazole, a ^{13}C NMR of sufficient quality could not be obtained.

4,7-Di([2,2'-bithiophen]-5-yl)benzo[*c*][1,2,5]thiadiazole (ThTh-BTZ)

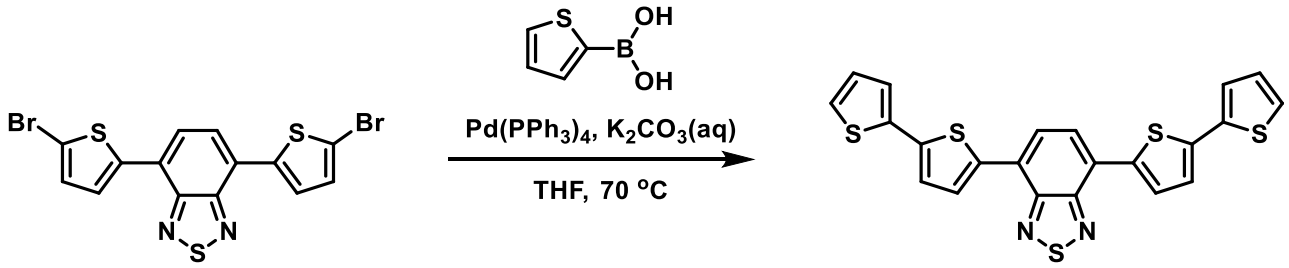

$C_{22}H_{12}N_2S_5$
464.65 g mol^{-1}

A dry 2-neck flask was charged with 4,7-bis(5-bromothiophen-2-yl)benzo[*c*][1,2,5]thiadiazole (229 mg, 0.5 mmol), thiophen-2-yl boronic acid (160 mg, 1.25 mmol), potassium carbonate (138 mg, 1.0 mmol) and $Pd(PPh_3)_4$ (29 mg, 0.025 mmol). The flask was connected to a Schlenk line then evacuated and backfilled with nitrogen three times. Degassed THF (40 mL) and degassed deionised water (5 mL) were added and the

reaction heated to 70 °C for overnight. Following this time, the mixture was allowed to cool to room temperature, poured onto deionised water and extracted with DCM (3 x 25 mL). The combined organic phases were washed with deionised water (50 mL), dried over $MgSO_4$ and the solvent removed under reduced pressure. The crude product was then washed with hot methylated spirits to give a metallic purple coloured powder (160 mg, 69%). **^{1}H NMR** ($CDCl_3$, 300 MHz, 25.0 °C) δ_H 8.06 (d, J = 4.0 Hz, 2 *H*), 7.87 (s, 2 *H*), 7.31 (dd, J = 3.6, 1.1 Hz, 2 *H*), 7.28 (d, J = 4.0 Hz, 2 *H*), 7.28 (m, 2 *H*), 7.07 (dd, J = 5.1, 3.6 Hz, 2 *H*). **^{13}C NMR** ($CDCl_3$, 75.5 MHz, 25.0 °C) δ_C 139.0 (C), 138.1 (C), 137.3 (C), 128.3 (C), 128.0 (C), 125.6 (C), 125.2 (CH), 124.9 (CH), 124.6 (CH), 124.1 (CH). **UV-Vis** ($CHCl_3$) λ_{max} (nm) 505. **IR** $\bar{\nu}$ (cm^{-1}) 3100 (w, C-H str.). **HRMS** (ES+, MeCN) m/z = 454.9651 $[M+H]^+$, calc. 464.9682.

4,7-Bis(benzo[*b*]thiophen-2-yl)benzo[*c*][1,2,5]thiadiazole (BTh-BTZ)

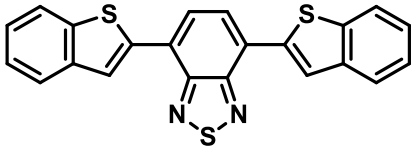

$C_{22}H_{12}N_2S_3$
400.53 g mol^{-1}

General procedure A for Suzuki-Miyaura coupling using 2-benzo[*b*]thiophen-2-ylboronic acid (445 mg, 2.5 mmol), 4,7-dibromobenzo[*c*][1,2,5]thiadiazole (294 mg, 1.0 mmol), potassium carbonate (276 mg, 2.0 mmol) and $Pd(PPh_3)_4$ (58 mg, 0.05 mmol). Crude product was washed with hot methylated spirits to give a red powder (273 mg, 69%). **^{1}H NMR** ($CDCl_3$, 300 MHz, 25.0 °C) δ_H 8.59 (d, J = 0.4 Hz, 2 *H*), 7.99 (s, 2 *H*), 7.90 (m, 4 *H*), 7.39 (m, 4 *H*). **^{13}C NMR** ($CDCl_3$, 75.5 MHz, 25.0 °C) δ_C 152.9 (C), 140.6 (C), 139.7 (C), 127.1 (CH), 126.7 (C), 125.5 (CH), 125.3 (CH), 124.7 (CH), 124.4 (CH), 122.1 (CH). **UV-Vis** ($CHCl_3$) λ_{max} (nm) 450. **IR** $\bar{\nu}$ (cm^{-1}) 3046 (w, C-H str.). **HRMS** (ES+, MeCN) m/z = 401.0236 $[M+H]^+$, calc. 401.0163.

4,7-Di(thiazol-2-yl)benzo[*c*][1,2,5]thiadiazole (Tz-BTZ)

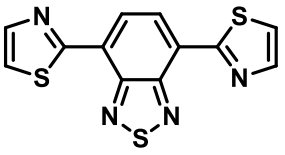

$C_{11}H_6N_4S_3$
302.39 g mol^{-1}

General procedure B for Suzuki-Miyaura coupling using 2-bromothiazole (246 mg, 1.5 mmol), 4,7-bis(4,4,5,5-tetramethyl-1,3,2-dioxaborolan-2-yl)benzo[*c*][1,2,5]thiadiazole (233 mg, 0.6 mmol), potassium carbonate (207 mg, 1.5 mmol) and $Pd(PPh_3)_4$ (58 mg, 0.05 mmol). The crude product was washed with hot methylated spirits to yield a red powder (43 mg, 24%). **^{1}H NMR** ($CDCl_3$, 300 MHz, 25.0 °C) δ_H 8.76 (s, 2*H*), 8.08 (d, 2*H*), 7.64 (d, J = 3.2 Hz, 2*H*). **UV-Vis** ($CHCl_3$) λ_{max} (nm) 428. **IR** $\bar{\nu}$ (cm^{-1}) 3110 (w, C-H str.). **HRMS** (ES+, MeCN) m/z = 302.9830 $[M+H]^+$, calc. 302.9833. Due to the low solubility of 4,7-di(thiazol-2-yl)benzo[*c*][1,2,5]thiadiazole, a ^{13}C NMR of sufficient quality could not be obtained.

Di-tert-butyl 2,2'-(benzo[*c*][1,2,5]thiadiazole-4,7-diyl)bis(1*H*-pyrrole-1-carboxylate) (Pyr-BTZ)

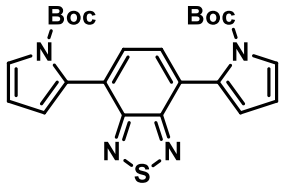

$C_{24}H_{26}N_4O_4S$
466.56 g mol^{-1}

General procedure A for Suzuki-Miyaura coupling using 1*H*-pyrrole-2-boronic acid, *N*-boc protected (464 mg, 2.2 mmol), 4,7-dibromobenzo[*c*][1,2,5]thiadiazole (294 mg, 1.0 mmol), potassium carbonate (276 mg, 2.0 mmol) and $Pd(PPh_3)_4$ (58 mg, 0.05 mmol). Crude product was a brown oil that was crystallised using hot methylated spirits to give yellow-brown crystals (200 mg, 43%). **^{1}H NMR** ($CDCl_3$, 300 MHz, 25.0 °C) δ_H 7.57 (s, 2 *H*), 7.49 (dd, J = 3.4, 1.8 Hz, 2 *H*), 6.41 (dd, J = 3.3, 1.8 Hz, 2 *H*), 6.33 (t, J = 3.3 Hz, 2 *H*), 1.19 (s, 18 *H*). **^{13}C NMR** ($CDCl_3$, 75.5 MHz, 25.0 °C) δ_C 154.4 (C), 149.1 (C), 130.3 (C), 127.5 (C), 127.5 (CH), 123.4 (CH), 115.7 (CH), 110.8 (CH), 83.5 (C), 27.5 (CH). **UV-Vis** ($CHCl_3$) λ_{max} (nm) 397. **IR** $\bar{\nu}$ (cm^{-1}) 2975 (w, C-H str.), 1739 (s, C=O str.). **HRMS** (ES+, MeCN) m/z = 467.1753 $[M+H]^+$, calc. 467.1753.

4,7-Di(pyridin-4-yl)benzo[*c*][1,2,5]thiadiazole (4N-BTZ)

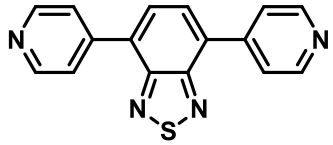

$C_{16}H_{10}N_4S$
290.34 g mol^{-1}

General procedure B for Suzuki-Miyaura coupling using 4-bromopyridine hydrochloride (292 mg, 1.5 mmol), 4,7-bis(4,4,5,5-tetramethyl-1,3,2-dioxaborolan-2-yl)benzo[*c*][1,2,5]thiadiazole (233 mg, 0.6 mmol), potassium carbonate (415 mg, 3.0 mmol) and $Pd(PPh_3)_4$ (35 mg, 0.03 mmol). The crude product was washed with hot methylated spirits to yield a light yellow-brown powder (86 mg, 50%). **^{1}H NMR** ($CDCl_3$, 300 MHz, 25.0 °C) δ_H 8.82 (m, 4*H*), 7.95 (s, 2*H*), 7.94 (m, 4*H*). **^{13}C NMR** ($CDCl_3$, 75.5 MHz, 25.0 °C) δ_C 153.5 (C), 150.3 (CH), 144.2 (C), 132.0 (C), 128.5 (CH), 123.6 (CH). **UV-Vis** ($CHCl_3$) λ_{max} (nm) 359. **IR** $\bar{\nu}$ (cm^{-1}) 3336 (w, O-H str.), 3019 (w, C-H str.). **HRMS** (ES+, MeCN) m/z = 291.0711 $[M+H]^+$, calc. 291.0704.

4,7-Di([1,1'-biphenyl]-2-yl)benzo[*c*][1,2,5]thiadiazole (oPh-BTZ)

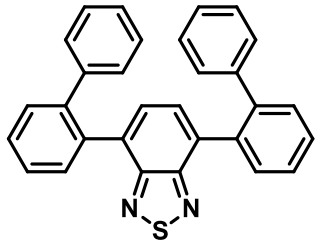

$C_{30}H_{20}N_2S$
440.56 g mol^{-1}

General procedure A for Suzuki-Miyaura coupling using 2-biphenyl boronic acid (495 mg, 2.5 mmol), 4,7-dibromobenzo[*c*][1,2,5]thiadiazole (294 mg, 1.0 mmol), potassium carbonate (276 mg, 2.0 mmol) and $Pd(PPh_3)_4$ (58 mg, 0.05 mmol). Crude product was washed with hot methylated spirits to yield a yellow powder (280 mg, 64%). **^{1}H NMR** ($CDCl_3$, 300 MHz, 25.0 °C) δ_H 7.60 (m, 2 *H*), 7.52 (m, 4 *H*), 7.48 (m, 2 *H*), 7.14 (s, 2 *H*), 7.09 (m, 10 *H*). **UV-Vis** ($CHCl_3$) λ_{max} (nm) 373. **IR** $\bar{\nu}$ (cm^{-1}) 3060 (w, C-H str.). **HRMS** (ES+, MeCN) m/z = 441.1425 $[M+H]^+$, calc. 441.1425. Due to the low solubility

of 4,7-di([1,1'-biphenyl]-2-yl)benzo[*c*][1,2,5]thiadiazole), a ^{13}C NMR of sufficient quality could not be obtained.

4,7-Di([1,1'-biphenyl]-3-yl)benzo[*c*][1,2,5]thiadiazole (mPh-BTZ)

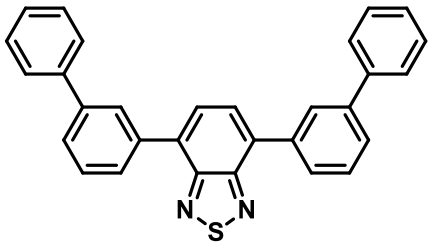

$C_{30}H_{20}N_2S$
440.56 g mol^{-1}

General procedure A for Suzuki-Miyaura coupling using 3-biphenyl boronic acid (495 mg, 2.5 mmol), 4,7-dibromobenzo[*c*][1,2,5]thiadiazole (294 mg, 1.0 mmol), potassium carbonate (276 mg, 2.0 mmol) and $Pd(PPh_3)_4$ (58 mg, 0.05 mmol). Crude product was washed with hot methylated spirits to yield a yellow powder (190 mg, 43%). **^{1}H NMR** ($CDCl_3$, 300 MHz, 25.0 °C) δ_H 8.15 (m, 2 *H*), 7.89 (m, 2 *H*), 7.74 (s, 2 *H*), 7.64 (m, 4 *H*), 7.64 (m, 2 *H*), 7.54 (m, 2 *H*), 7.42 (m, 4 *H*), 7.32 (m, 2 *H*). **^{13}C NMR** ($CDCl_3$, 75.5 MHz, 25.0 °C) δ_C 154.2 (C), 141.7 (C), 141.1 (C), 137.9 (C), 133.5 (C), 129.1 (CH), 128.9 (CH), 128.2 (CH), 128.2 (CH), 127.5 (CH), 127.4 (CH), 127.3 (CH). **UV-Vis** ($CHCl_3$) λ_{max} (nm) 381. **IR** $\bar{\nu}$ (cm^{-1}) 3028 (w, C-H str.). **HRMS** (ES+, MeCN) m/z = 441.1423 $[M+H]^+$, calc. 441.1425.

4,7-Di([1,1'-biphenyl]-4-yl)benzo[*c*][1,2,5]thiadiazole (pPh-BTZ)

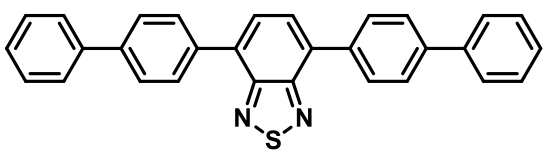

$C_{30}H_{20}N_2S$
440.56 g mol^{-1}

General procedure A for Suzuki-Miyaura coupling using 4-biphenyl boronic acid (495 mg, 2.5 mmol), 4,7-dibromobenzo[*c*][1,2,5]thiadiazole (294 mg, 1.0 mmol), potassium carbonate (276 mg, 2.0 mmol) and $Pd(PPh_3)_4$ (58 mg, 0.05 mmol). The crude product was washed with hot methylated spirits to yield bright yellow crystals (223 mg, 51%). **^{1}H NMR** ($CDCl_3$, 300 MHz, 25.0 °C) δ_H 8.09 (m, 4 *H*), 7.88 (s, 2 *H*), 7.80 (m, 4 *H*), 7.70 (m, 4 *H*), 7.49 (m, 4 *H*), 7.39 (m, 2 *H*). **^{13}C NMR** ($CDCl_3$, 75.5 MHz, 25.0 °C) δ_C 154.2 (C), 141.3 (C), 140.7 (C), 136.4 (C), 133.0 (C), 129.7 (C), 128.9 (C), 128.0 (C), 127.6 (C), 127.4 (C), 127.2 (C). **UV-Vis** ($CHCl_3$) λ_{max} (nm) 399. **IR** $\bar{\nu}$ (cm^{-1}) 3030 (w, C-H str.). **HRMS** (ES+, MeCN) m/z = 441.1430 $[M+H]^+$, calc. 441.1425.

4,7-Di(naphthalen-1-yl)benzo[*c*][1,2,5]thiadiazole (1Nap-BTZ)

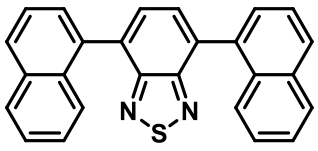

$C_{26}H_{16}N_2S$
388.49 g mol^{-1}

General procedure A for Suzuki-Miyaura coupling using napthalen-1-ylboronic acid (375 mg, 2.5 mmol), 4,7-dibromobenzo[*c*][1,2,5]thiadiazole (294 mg, 1.0 mmol), potassium carbonate (276 mg, 2.0 mmol) and $Pd(PPh_3)_4$ (58 mg, 0.05 mmol). The crude product was then washed with methylated spirits to

yield a bright yellow powder (340 mg, 87%). **^{1}H NMR** ($CDCl_3$, 300 MHz, 25.0 °C) δ_H 8.00 (m, 2 *H*), 8.00 (m, 2 *H*), 7.84 (s, 2 *H*), 7.73 (m, 2 *H*), 7.73 (m, 2 *H*), 7.66 (m, 2 *H*), 7.55 (m, 2 *H*), 7.44 (m, 2 *H*). **^{13}C NMR** ($CDCl_3$, 75.5 MHz, 25.0 °C) δ_C 154.8 (C), 135.5 (C), 133.9 (C), 133.4 (C), 131.9 (C), 130.3 (CH), 129.0 (CH), 128.6 (CH), 128.1 (CH), 126.3 (CH), 126.1 (CH), 125.9 (CH), 125.4 (CH). **UV-Vis** ($CHCl_3$) λ_{max} (nm) 376. **IR** $\bar{\nu}$ (cm^{-1}) 3050 (w, C-H str.). **HRMS** (ES+, MeCN) m/*z* = 389.1116 $[M+H]^+$, calc. 389.1112.

4,7-Di(naphthalen-2-yl)benzo[*c*][1,2,5]thiadiazole (2Nap-BTZ)

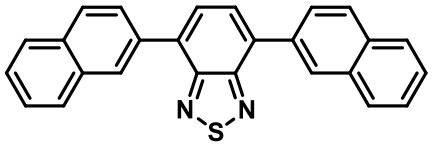

$C_{26}H_{16}N_2S$
388.49 g mol^{-1}

General procedure A for Suzuki-Miyaura coupling using napthalen-2-ylboronic acid (430 mg, 2.5 mmol), 4,7-dibromobenzo[*c*][1,2,5]thiadiazole (294 mg, 1.0 mmol), potassium carbonate (276 mg, 2.0 mmol) and $Pd(PPh_3)_4$ (58 mg, 0.05 mmol). Crude product was washed with warm methylated spirits to yield a yellow powder (336 mg, 86%). **^{1}H NMR** ($CDCl_3$, 300 MHz, 25.0 °C) δ_H 8.51 (d, J = 1.3 Hz, 2 *H*), 8.12 (dd, J = 8.8, 1.8 Hz, 2 *H*), 8.03 (d, J = 8.8 Hz, 2 *H*), 7.99 (m, 2 *H*), 7.97 (s, 2 *H*), 7.93 (m, 2 *H*), 7.56 (m, 2 *H*), 7.56 (m, 2 *H*). **^{13}C NMR** ($CDCl_3$, 75.5 MHz, 25.0 °C) δ_C 135.5 (C), 133.4 (C), 133.2 (C), 128.7 (CH), 128.6 (CH), 128.5 (CH), 128.2 (CH), 127.7 (CH), 127.0 (CH), 126.6 (CH), 126.4 (CH). **UV-Vis** ($CHCl_3$) λ_{max} (nm) 396. **IR** $\bar{\nu}$ (cm^{-1}) 3050 (w, C-H str.). **HRMS** (ES+, MeCN) m/*z* = 389.1112 $[M+H]^+$, calc. 389.1112.

4,7-Bis(9,9-dioctyl-9*H*-fluoren-2-yl)benzo[*c*][1,2,5]thiadiazole (Flu-BTZ)

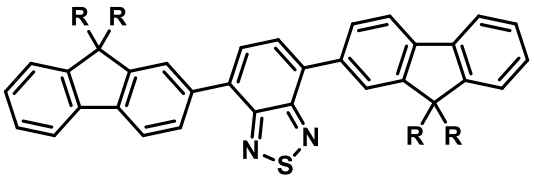

R = n-C_8H_{17}
$C_{64}H_{84}N_2S$
913.45 g mol^{-1}

General procedure A for Suzuki-Miyaura coupling using 9,9-dioctylfluorene-2-boronic acid pinacol ester (341 mg, 0.66 mmol), 4,7-dibromobenzo[*c*][1,2,5]thiadiazole (88 mg, 0.3 mmol), potassium carbonate (83 mg, 0.6 mmol) and $Pd(PPh_3)_4$ (17 mg, 0.015 mmol). The crude product was purified *via* silica-gel column chromatography using DCM: Pet. Ether 40-60 °C 1:10 (v:v) as the eluent. This yielded a yellow oil that when left for one week gave a yellow powder (187 mg, 68%). **^{1}H NMR** ($CDCl_3$, 300 MHz, 25.0 °C) δ_H 8.05 (dd, J = 7.9, 1.6 Hz, 2 *H*), 7.99 (d, J = 1.2 Hz, 2 *H*), 7.91 (s, 2 *H*), 7.89 (d, J = 7.5 Hz, 2 *H*), 7.80 (m, 2 *H*), 7.39 (m, 6 *H*), 2.07 (m, 8 *H*), 1.12 (m, 48 *H*), 0.82 (t, J = 6.8 Hz, 12 *H*). **^{13}C NMR** ($CDCl_3$, 75.5 MHz, 25.0 °C) δ_C 154.4 (C), 151.4 (C), 151.1 (C), 141.4 (C), 140.7 (C), 136.2 (C), 133.6 (C), 128.2 (CH), 127.9 (CH), 127.3 (CH) 126.8 (CH), 123.9 (CH), 123.0 (CH), 120.0 (CH), 119.7 (CH), 55.3 (C), 40.3 (CH_2), 31.8 (CH_2), 30.1 (CH_2), 29.3 (CH_2), 29.3 (CH_2), 23.9 (CH_2), 22.6 (CH_2), 14.1 (CH_3). **UV-Vis** ($CHCl_3$) λ_{max} (nm) 420. **IR** $\bar{\nu}$ (cm^{-1}) 3034

(w, C-H str.), 2923 (s, C-H str.). **HRMS** (ES+, MeCN) m/z = 913.6439 $[M+H]^+$, calc. 913.6433.

4,7-Di-*p*-tolylbenzo[*c*][1,2,5]thiadiazole (pMe-BTZ)

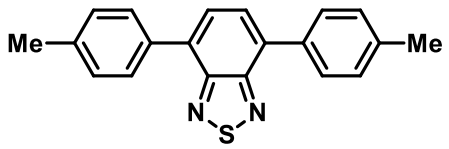

$C_{20}H_{16}N_2S$
316.42 g mol^{-1}

General procedure A for Suzuki-Miyaura coupling using 4,4,5,5-tetramethyl-2-(*p*-tolyl)-1,3,2-dioxaborolane (545 mg, 2.5 mmol), 4,7-dibromobenzo[*c*][1,2,5]thiadiazole (294 mg, 1.0 mmol), potassium carbonate (276 mg, 2.0 mmol) and $Pd(PPh_3)_4$ (58 mg, 0.05 mmol). Crude product was recrystallised from hot methylated spirits to yield yellow crystals (195 mg, 62%). **^{1}H NMR** ($CDCl_3$, 300 MHz, 25.0 °C) δ_H 7.86 (m, 4 *H*), 7.75 (s, 2 *H*), 7.36 (m, 4 *H*), 2.46 (s, 6 *H*). **^{13}C NMR** ($CDCl_3$, 75.5 MHz, 25.0 °C) δ_C 154.2 (C), 138.3 (C), 134.7 (C), 133.1 (C), 129.4 (CH), 129.1 (CH), 127.8 (CH), 21.3 (CH_3). **UV-Vis** ($CHCl_3$) λ_{max} (nm) 391. **IR** $\bar{\nu}$ (cm^{-1}) 3030 (w, C-H str.), 2920 (w, C-H str.). **HRMS** (ES+, MeCN) m/z = 317.1112 $[M+H]^+$, calc. 317.1112.

4,4'-(Benzo[*c*][1,2,5]thiadiazole-4,7-diyl)diphenol (pOH-BTZ)

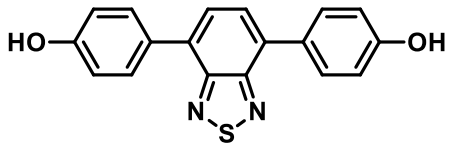

$C_{18}H_{12}N_2O_2S$
320.37 g mol^{-1}

General procedure A for Suzuki-Miyaura coupling using 4-hydroxyphenyl boronic acid (345 mg, 2.5 mmol), 4,7-dibromobenzo[*c*][1,2,5]thiadiazole (294 mg, 1.0 mmol), potassium carbonate (276 mg, 2.0 mmol) and $Pd(PPh_3)_4$ (58 mg, 0.05 mmol). The crude product was recrystallised from hot methylated spirits to yield bright yellow crystals (170 mg, 55%). **^{1}H NMR** ($CDCl_3$, 300 MHz, 25.0 °C) δ_H 7.88 (m, 4 *H*), 7.72 (s, 2 *H*), 7.01 (m, 4 *H*), 4.88 (s, 2 *H*). **UV-Vis** ($CHCl_3$) λ_{max} (nm) 404. **IR** $\bar{\nu}$ (cm^{-1}) 3336 (w, O-H str.), 3019 (w, C-H str.). **HRMS** (ES+, MeCN) m/z = 321.0699 $[M+H]^+$, calc. 321.0698. Due to the low solubility of 4,4'-(benzo[*c*][1,2,5]thiadiazole-4,7-diyl)diphenol, a ^{13}C NMR of sufficient quality could not be obtained.

4,7-Bis(4-methoxyphenyl)benzo[*c*][1,2,5]thiadiazole (pOMe-BTZ)

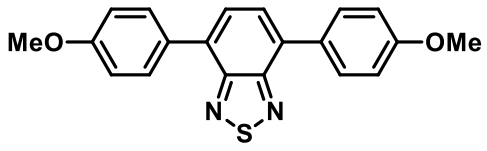

$C_{20}H_{16}N_2O_2S$
348.42 g mol^{-1}

General procedure A for Suzuki-Miyaura coupling using 4-methoxyphenyl boronic acid (380 mg, 2.5 mmol), 4,7-dibromobenzo[*c*][1,2,5]thiadiazole (294 mg, 1.0 mmol), potassium carbonate (276 mg, 2.0 mmol) and $Pd(PPh_3)_4$ (58 mg, 0.05 mmol). The crude product was recrystallised from hot methylated spirits to yield bright yellow crystals (170 mg, 49%). **^{1}H NMR** ($CDCl_3$, 300 MHz, 25.0 °C) δ_H 7.93 (m, 4 *H*), 7.72 (s, 2 *H*), 7.09 (m, 4 *H*), 3.90 (s, 6

H). **^{13}C NMR** ($CDCl_3$, 75.5 MHz, 25.0 °C) δ_C 159.8 (C), 154.2 (C), 132.4 (C), 130.4 (CH), 130.0 (C), 127.4 (CH), 114.1 (CH), 55.4 (CH_3). **UV-Vis** ($CHCl_3$) λ_{max} (nm) 409. **IR** $\bar{\nu}$ (cm^{-1}) 3010 (w, C-H str.), 2930 (w, C-H str.). **HRMS** (ES+, MeCN) m/z = 349.1004 $[M+H]^+$, calc. 349.1011.

4,4'-(benzo[*c*][1,2,5]thiadiazole-4,7-diyl)dibenzaldehyde (pCHO-BTZ)

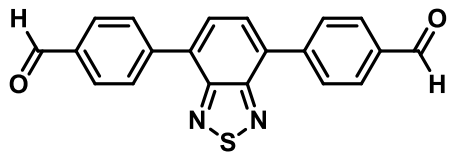

$C_{20}H_{12}N_2O_2S$
344.39 g mol^{-1}

General procedure A for Suzuki-Miyaura coupling using 4-formyl boronic acid (375 mg, 2.5 mmol), 4,7-dibromobenzo[*c*][1,2,5]thiadiazole (294 mg, 1.0 mmol), potassium carbonate (276 mg, 2.0 mmol) and $Pd(PPh_3)_4$ (58 mg, 0.05 mmol). The crude product was washed with hot methylated spirits to yield a yellow powder (215 mg, 63%). **^{1}H NMR** ($CDCl_3$, 300 MHz, 25.0 °C) δ_H 10.13 (s, 2*H*), 8.18 (m, 4*H*), 8.08 (m, 4*H*), 7.91 (s, 2*H*). **^{13}C NMR** ($CDCl_3$, 75.5 MHz, 25.0 °C) δ_C 191.8 (C), 153.8 (C), 143.0 (C), 136.1 (C), 133.0 (C), 130.0 (CH), 129.9 (CH), 128.7 (CH). **UV-Vis** ($CHCl_3$) λ_{max} (nm) 377. **IR** $\bar{\nu}$ (cm^{-1}) 1701 (m, C=O str.). **HRMS** (ES+, MeCN) m/z = 345.0695 $[M+H]^+$, calc. 345.0698.

4,4'-(Benzo[*c*][1,2,5]thiadiazole-4,7-diyl)dibenzonitrile (pCN-BTZ)

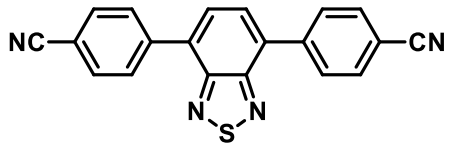

$C_{20}H_{10}N_4S$
338.39 g mol^{-1}

General procedure B for Suzuki-Miyaura coupling using 4-bromobenzonitrile (273 mg, 1.5 mmol), 4,7-bis(4,4,5,5-tetramethyl-1,3,2-dioxaborolan-2-yl)benzo[*c*][1,2,5]thiadiazole (233 mg, 0.6 mmol), potassium carbonate (166 mg, 1.2 mmol) and $Pd(PPh_3)_4$ (35 mg, 0.03 mmol). The crude product was washed with hot methylated spirits to yield a yellow powder (87 mg, 43%). **^{1}H NMR** ($CDCl_3$, 300 MHz, 25.0 °C) δ_H 8.12 (m, 4*H*), 7.88 (s, 2*H*), 7.86 (m, 4*H*). **UV-Vis** ($CHCl_3$) λ_{max} (nm) 372. **IR** $\bar{\nu}$ (cm^{-1}) 3050 (w, C-H str.), 2220 (m, C≡N str.). **HRMS** (ES+, MeCN) m/z = 339.0689 $[M+H]^+$, calc. 339.0704. Due to the low solubility of 4,4'-(benzo[*c*][1,2,5]thiadiazole-4,7-diyl)dibenzonitrile, a ^{13}C NMR of sufficient quality could not be obtained.

4,7-Bis(4-(trifluoromethyl)phenyl)benzo[*c*][1,2,5]thiadiazole (pCF$_3$-BTZ)

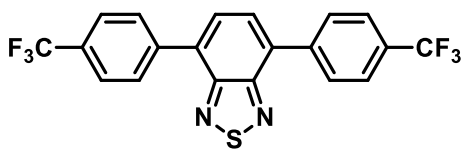

$C_{20}H_{10}F_6N_2S$
424.36 g mol^{-1}

General procedure B for Suzuki-Miyaura coupling using 4-bromobenzotrifluoride (338 mg, 1.5 mmol), 4,7-bis(4,4,5,5-tetramethyl-1,3,2-dioxaborolan-2-yl)benzo[*c*][1,2,5]thiadiazole (233 mg, 0.6 mmol), potassium carbonate (166 mg, 1.2 mmol) and $Pd(PPh_3)_4$ (35 mg, 0.03 mmol). The crude product was recrystallised from hot methylated spirits to

yield bright yellow crystals (140 mg, 55%). **^{1}H NMR** ($CDCl_3$, 300 MHz, 25.0 °C) δ_H 8.10 (m, 4*H*), 7.86 (s, 2*H*), 7.82 (m, 4*H*). **^{19}F NMR** ($CDCl_3$, 282 MHz, 25.0 °C) δ_F -62.6 (s, 3 *F*). **UV-Vis** ($CHCl_3$) λ_{max} (nm) 369. **HRMS** (ES+, MeCN) m/*z* = 425.0544 $[M+H]^+$, calc. 425.0547. Due to the low solubility of 4,7-bis(4-(trifluoromethyl)phenyl)benzo[*c*][1,2,5]thiadiazole, a ^{13}C NMR of sufficient quality could not be obtained.

4,7-Bis(4-nitrophenyl)benzo[*c*][1,2,5]thiadiazole (pNO_2-BTZ)

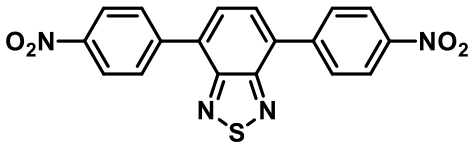

$C_{18}H_{10}N_4O_4S$
378.36 g mol^{-1}

General procedure B for Suzuki-Miyaura coupling using 4-iodonitrobenzene (374 mg, 1.5 mmol), 4,7-bis(4,4,5,5-tetramethyl-1,3,2-dioxaborolan-2-yl)benzo[*c*][1,2,5]thiadiazole (233 mg, 0.6 mmol), potassium carbonate (166 mg, 1.2 mmol) and $Pd(PPh_3)_4$ (35 mg, 0.03 mmol). The crude product was washed with hot methylated spirits to yield a bright yellow powder (95 mg, 42%). **^{1}H NMR** ($CDCl_3$, 300 MHz, 25.0 °C) δ_H 8.43 (m, 4 *H*), 8.19 (m, 4 *H*), 7.94 (s, 2 *H*). **UV-Vis** ($CHCl_3$) λ_{max} (nm) 377. **IR** $\bar{\nu}$ (cm^{-1}) 3110 (w, C-H str.), 1510 (s, N-O str.), 1340 (N-O, str.). Due to the low solubility of 4,7-bis(4-nitrophenyl)benzo[*c*][1,2,5]thiadiazole, a ^{13}C NMR of sufficient quality could not be obtained.

3. Single Crystal X-Ray Structures

Crystal data for pF-BTZ (CCDC Deposition Number – 2179275)

Grown by slow evaporation from DCM. Crystal data for $C_{18}H_{10}F_2N_2S$ (M =324.34 g/mol): triclinic, space group P-1 (no. 2), a = 9.3311(7) Å, b = 9.4843(10) Å, c = 16.4631(12) Å, α = 90.981(6)°, β = 94.978(3)°, γ = 106.929(5)°, V = 1387.2(2) Å^3, Z = 4, T = 100.0 K, μ(CuKα) = 2.289 mm^{-1}, *Dcalc* = 1.553 g/cm^3, 44066 reflections measured (5.394° ≤ 2Θ ≤ 149.238°), 5605 unique (R_{int} = 0.0421, R_{sigma} = 0.0265) which were used in all calculations. The final R1 was 0.0556 (I > 2σ(I)) and wR2 was 0.1731 (all data). The crystal was not single therefore an HKLF 5 compiled by OLEX2 twinning routine was employed. Twin law applied: -1 0 0 ; 0 -1 0; 0.354 0.161 1

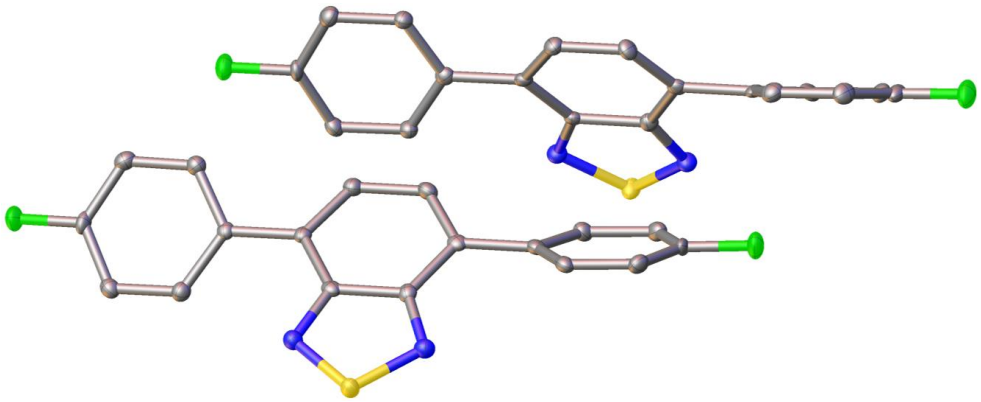

Figure S2 X-ray crystal structure of **pF-BTZ**. The atoms are shown as ellipsoids at 50% probability. H atoms omitted for clarity.

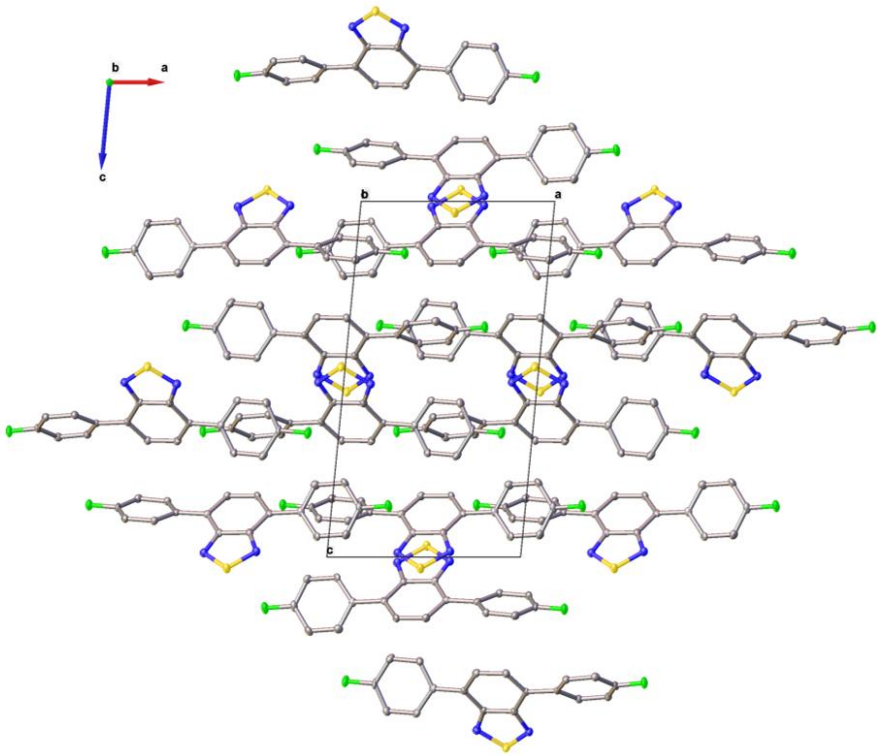

Figure S3 X-ray crystal structure of **pF-BTZ** showing the packing of molecules as viewed down the b-axis [010]. Hydrogen atoms omitted for clarity.

Crystal data for pCl-BTZ (CCDC Deposition Number - 2179278)

Grown by cooling a saturated solution in hot toluene. Crystal data for $C_{18}H_{10}Cl_2N_2S$ (M =357.24 g/mol): triclinic, space group P-1 (no. 2), a = 9.4442(4) Å, b = 9.5031(4) Å, c = 17.4731(6) Å, α = 90.2759(19)°, β = 94.3850(18)°, γ = 108.3803(18)°, V = 1483.14(10) Å^3, Z = 4, T = 100(2) K, μ(MoKα) = 0.577 mm^{-1}, $Dcalc$ = 1.600 g/cm^3, 35268 reflections measured (4.678° ≤ 2Θ ≤ 60.972°), 9001 unique (R_{int} = 0.0752, R_{sigma} = 0.0782) which were used in all calculations. The final R1 was 0.0566 (I > 2σ(I)) and wR2 was 0.1289 (all data).

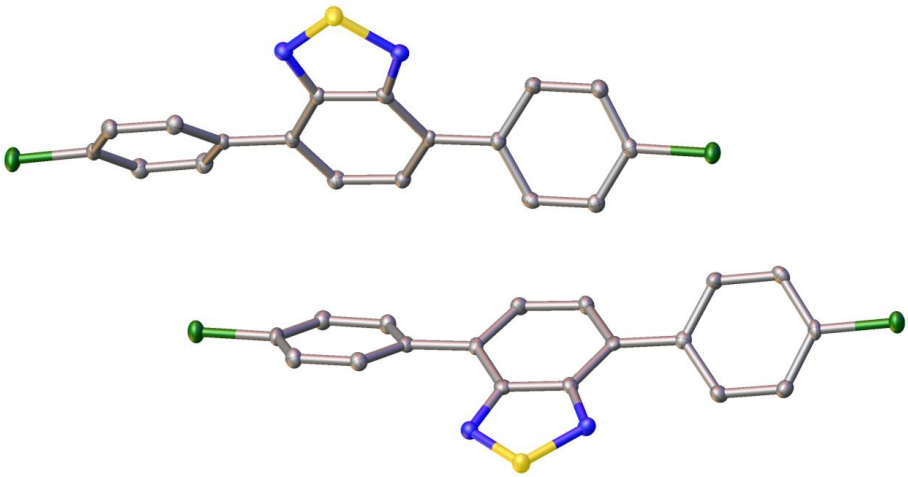

Figure S4 X-ray crystal structure of **pCl-BTZ**. The atoms are shown as ellipsoids at 50% probability. H atoms omitted for clarity.

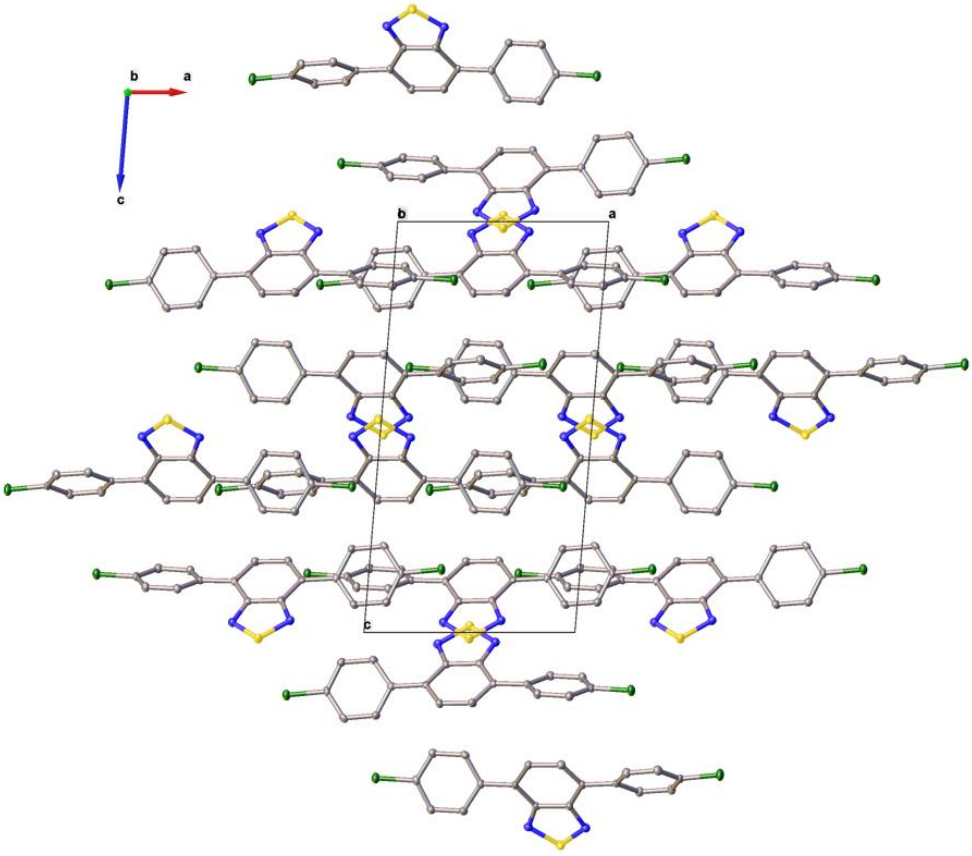

Figure S5 X-ray crystal structure of **pCl-BTZ** showing the packing of molecules as viewed down the b-axis [010]. Hydrogen atoms omitted for clarity.

Crystal data for pI-BTZ (CCDC Deposition Number - 2179277)

Grown by slow evaporation from DCM. Crystal data for $C_{18}H_{10}I_2N_2S$ (M =540.14 g/mol): orthorhombic, space group $P2_12_12_1$ (no. 19), a = 4.00180(10) Å, b = 11.2976(3) Å, c = 36.3004(11) Å, V = 1641.17(8) Å^3, Z = 4, T = 100(2) K, μ(CuKα) = 31.280 mm^{-1}, *Dcalc* = 2.186 g/cm^3, 22058 reflections measured (4.868° ≤ 2Θ ≤ 149.296°), 3329 unique (R_{int} = 0.0633, R_{sigma} = 0.0397) which were used in all calculations. The final R_1 was 0.0371 (I > 2σ(I)) and ωR_2 was 0.0962 (all data).

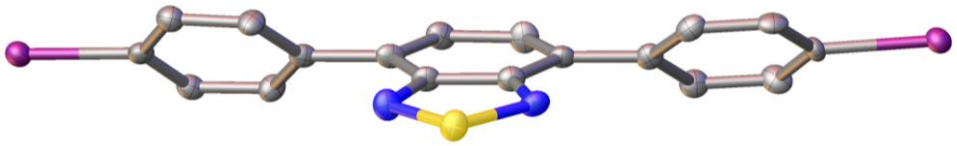

Figure S6 X-ray crystal structure of **pI-BTZ**. The atoms are shown as ellipsoids at 50% probability. H atoms omitted for clarity.

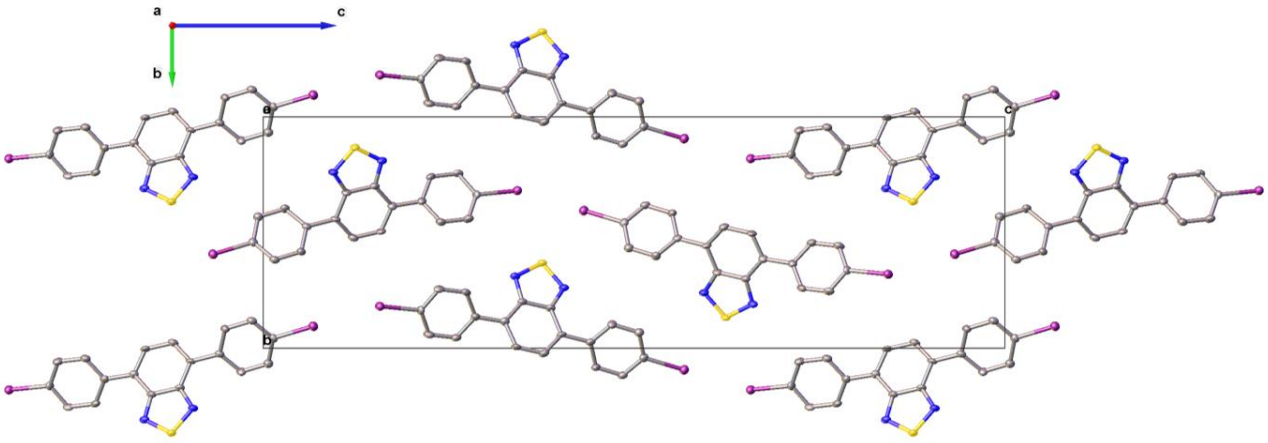

Figure S7 X-ray crystal structure of **pI-BTZ** showing the packing of molecules as viewed down the a-axis [100]. Hydrogen atoms omitted for clarity.

Crystal data for ThTh-BTZ (CCDC Deposition Number - 2179280)

Grown by slow evaporation from DCM. Crystal data for $C_{110}H_{60}N_{10}S_{25}$ (M =2323.18 g/mol): monoclinic, space group $P2_1/n$ (no. 14), a = 5.6980(2) Å, b = 31.4674(15) Å, c = 26.9001(11) Å, β = 92.599(3)°, V = 4818.3(3) Å^3, Z = 2, T = 100.0 K, μ(CuKα) = 5.641 mm^{-1}, *Dcalc* = 1.601 g/cm^3, 118988 reflections measured (4.324° ≤ 2Θ ≤ 140.668°), 9129 unique (R_{int} = 0.1359, R_{sigma} = 0.0509) which were used in all calculations. The final R1 was 0.0839 (I > 2σ(I)) and wR2 was 0.1827 (all data). C-S and C-C distances restrained and displacement parameters of substitutionally disordered C and S atoms constrained in disordered 5 membered rings.

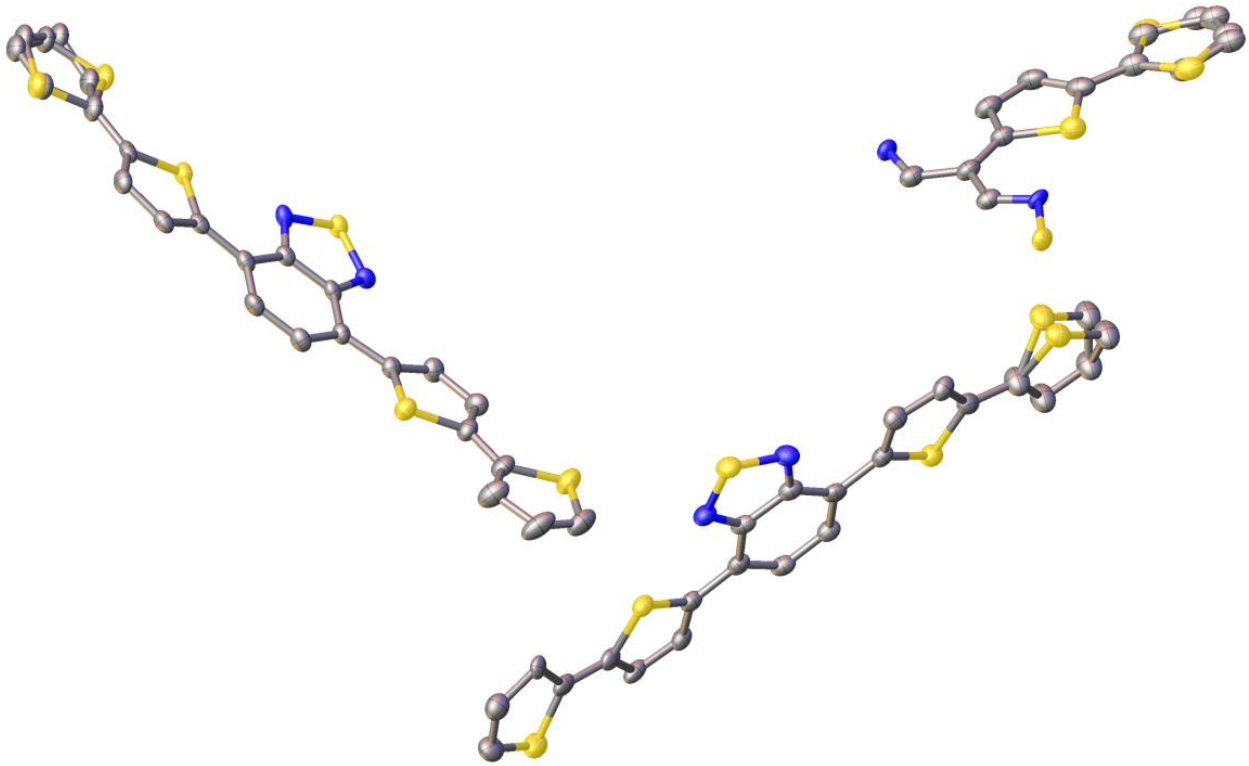

Figure S8 X-ray crystal structure of **ThTh-BTZ**. The atoms are shown as ellipsoids at 50% probability. H atoms omitted for clarity.

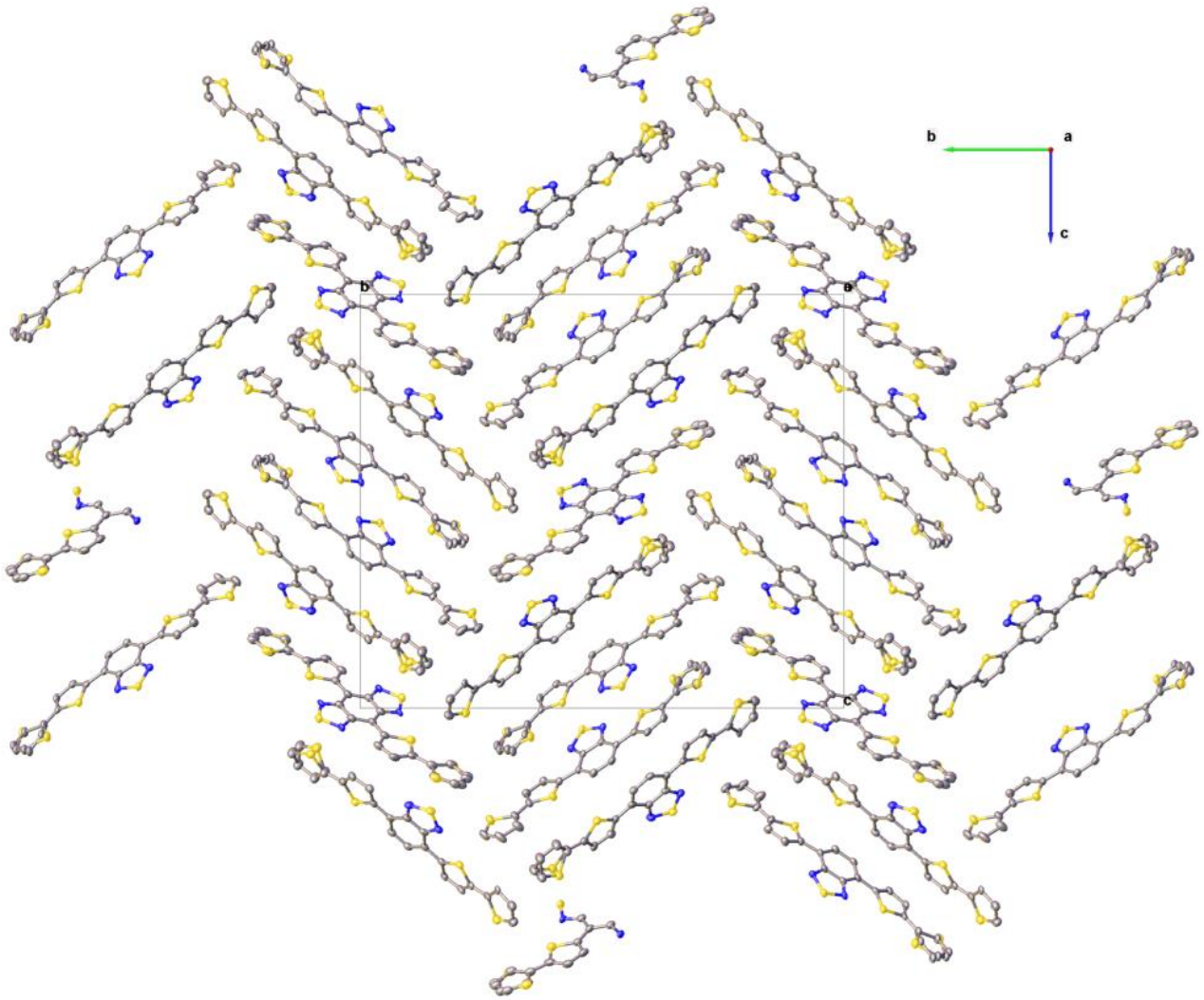

Figure S9 X-ray crystal structure of **ThTh-BTZ** showing the packing of molecules as viewed down the a-axis [100]. Hydrogen atoms omitted for clarity.

Crystal data for BTh-BTZ (CCDC Deposition Number - 2179273)

Grown by slow evaporation from DCM. Crystal data for $C_{22}H_{12}N_2S_3$ (M =400.52 g/mol): orthorhombic, space group $P2_12_12_1$ (no. 19), a = 3.8527(3) Å, b = 18.2496(11) Å, c = 24.0476(16) Å, V = 1690.8(2) Å^3, Z = 4, T = 100(2) K, μ(CuKα) = 4.079 mm^{-1}, $Dcalc$ = 1.573 g/cm^3, 11269 reflections measured (6.08° ≤ 2Θ ≤ 149.248°), 3403 unique (R_{int} = 0.0732, R_{sigma} = 0.0672) which were used in all calculations. The final R_1 was 0.0567 (I > 2σ(I)) and wR_2 was 0.1408 (all data). C/S substitutional disorder in five membered rings treated with same Uiso and same coordinate constraints (EADP and EXYZ).

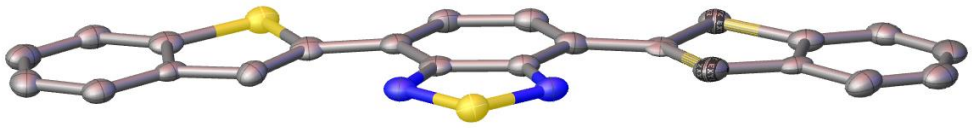

Figure S10 X-ray crystal structure of **BTh-BTZ**. The atoms are shown as ellipsoids at 50% probability. H atoms omitted for clarity.

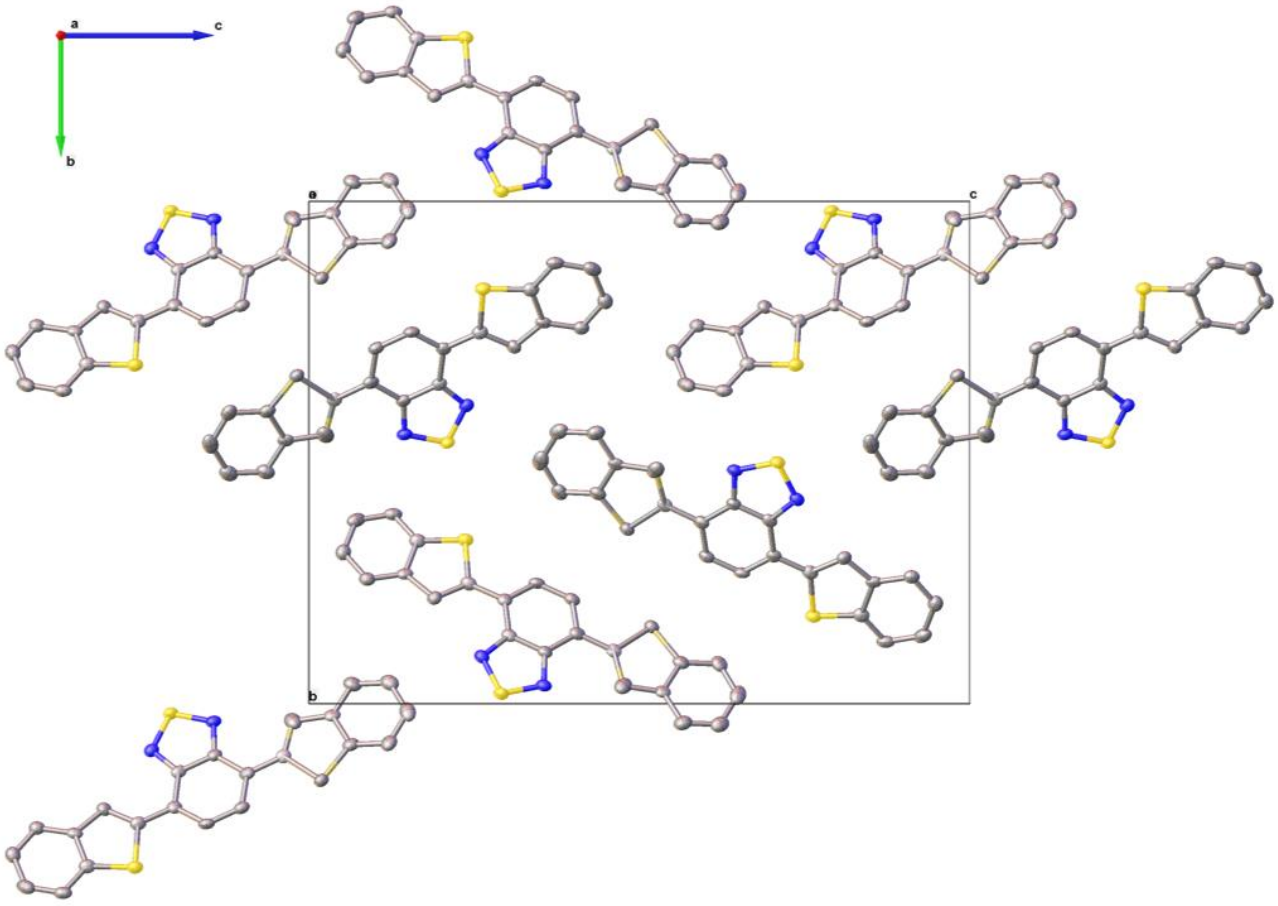

Figure S11 X-ray crystal structure of **BTh-BTZ** showing the packing of molecules as viewed down the a-axis [100]. Hydrogen atoms omitted for clarity.

Crystal data for oPh-BTZ (CCDC Deposition Number - 2179270)

Grown by slow evaporation from DCM. Crystal data for $C_{30}H_{20}N_2S$ (M =440.54 g/mol): monoclinic, space group C2/c (no. 15), a = 14.0869(2) Å, b = 13.0076(2) Å, c = 12.0906(2) Å, β = 105.0421(5)°, V = 2139.53(6) Å^3, Z = 4, T = 100(2) K, μ(CuKα) = 1.501 mm^{-1}, *Dcalc* = 1.368 g/cm^3, 17484 reflections measured (9.406° ≤ 2Θ ≤ 148.884°), 2160 unique (R_{int} = 0.0264, R_{sigma} = 0.0157) which were used in all calculations. The final R_1 was 0.0317 (I > 2σ(I)) and wR_2 was 0.0811 (all data).

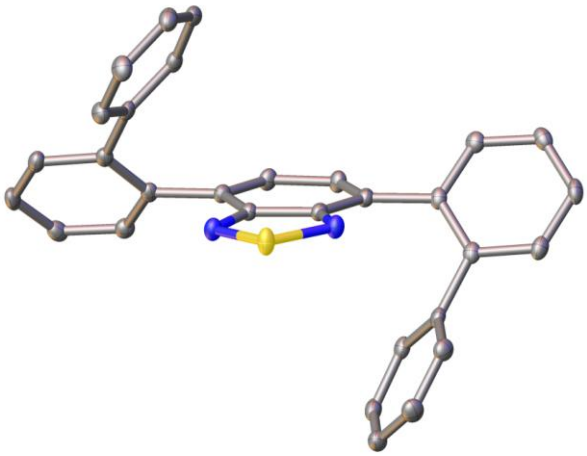

Figure S12 X-ray crystal structure of **oPh-BTZ**. The atoms are shown as ellipsoids at 50% probability. H atoms omitted for clarity.

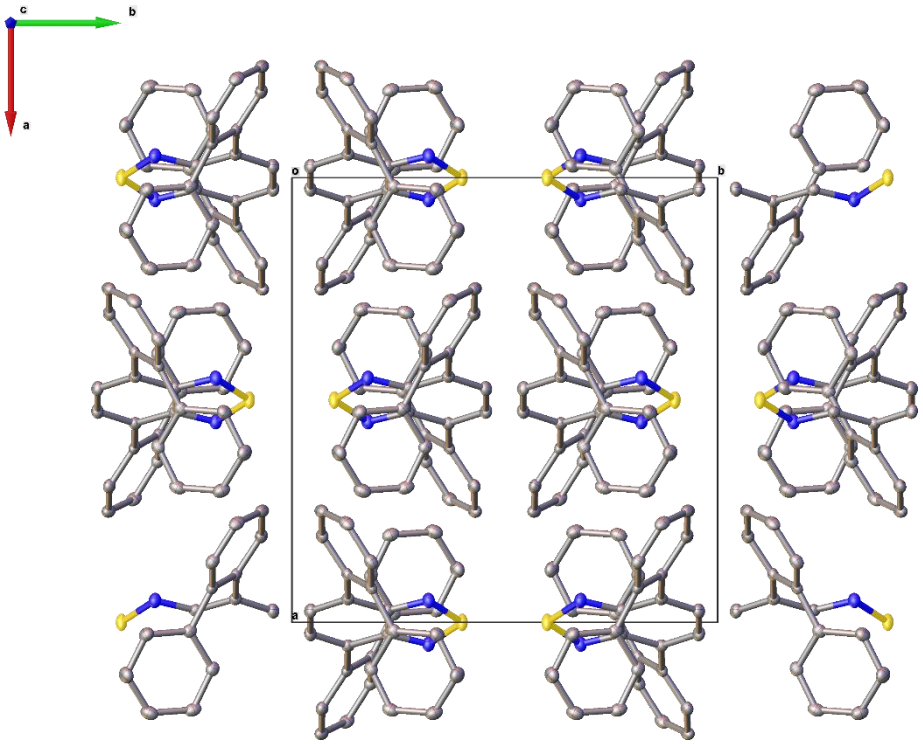

Figure S13 X-ray crystal structure of **oPh-BTZ** showing the packing of molecules as viewed down the c-axis [001]. Hydrogen atoms omitted for clarity.

Crystal data for mPh-BTZ (CCDC Deposition Number – 2179274)

Grown by slow evaporation from DCM. Crystal Data for $C_{30}H_{20}N_2S$ (M =440.54 g/mol): monoclinic, space group $P2_1/n$ (no. 14), a = 16.0078(3) Å, b = 7.33120(10) Å, c = 17.9268(3) Å, β = 90.6553(6)°, V = 2103.69(6) Å^3, Z = 4, T = 101(2) K, μ(CuKα) = 1.526 mm^{-1}, *Dcalc* = 1.391 g/cm^3, 74879 reflections measured (7.362° ≤ 2Θ ≤ 148.96°), 4284 unique (R_{int} = 0.0391, R_{sigma} = 0.0138) which were used in all calculations. The final R_1 was 0.0306 (I > 2σ(I)) and wR_2 was 0.0852 (all data).

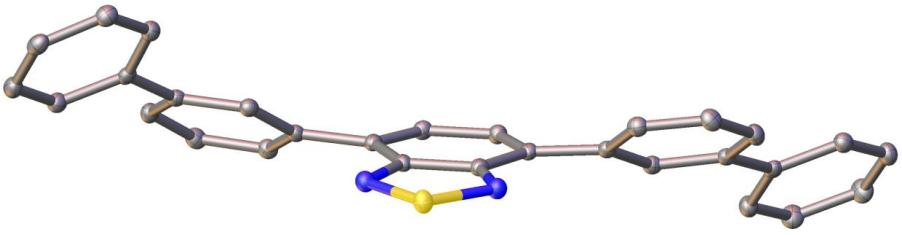

Figure S14 X-ray crystal structure of **mPh-BTZ**. The atoms are shown as ellipsoids at 50% probability. H atoms omitted for clarity.

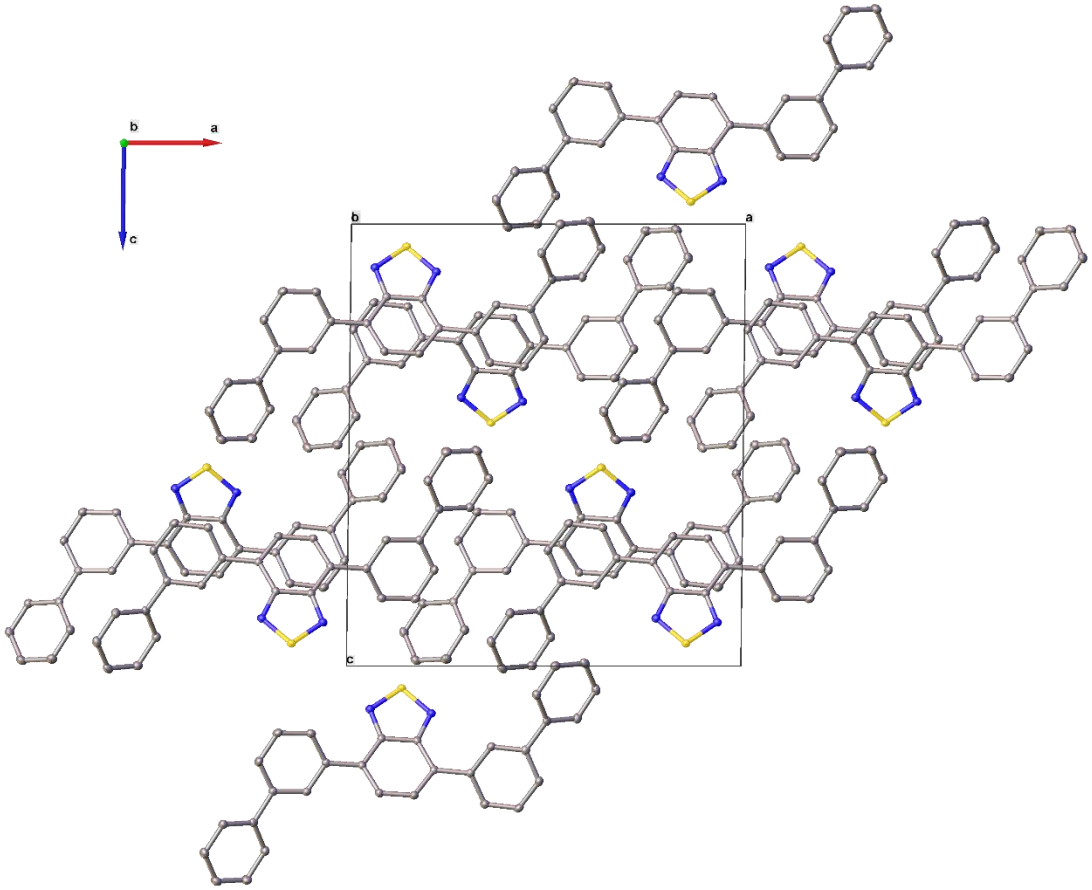

Figure S15 X-ray crystal structure of **mPh-BTZ** showing the packing of molecules as viewed down the b-axis [010]. Hydrogen atoms omitted for clarity.

Crystal data for pPh-BTZ (CCDC Deposition Number – 2179271)

Grown by slow evaporation from DCM. Crystal Data for $C_{30}H_{20}N_2S$ (M =440.54 g/mol): triclinic, space group P-1 (no. 2), a = 10.0161(2) Å, b = 10.5126(2) Å, c = 10.5965(2) Å, α = 90.8070(10)°, β = 98.9060(10)°, γ = 104.3010(10)°, V = 1066.55(4) Å^3, Z = 2, T = 100.0 K, μ(CuKα) = 1.505 mm^{-1}, *Dcalc* = 1.372 g/cm^3, 47343 reflections measured (8.458° ≤ 2Θ ≤ 144.494°), 4204 unique (R_{int} = 0.0561, R_{sigma} = 0.0258) which were used in all calculations. The final R_1 was 0.0385 (I > 2σ(I)) and ωR_2 was 0.0993 (all data).

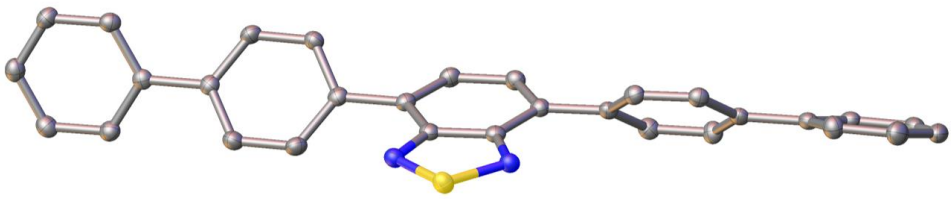

Figure S16 X-ray crystal structure of **pPh-BTZ**. The atoms are shown as ellipsoids at 50% probability. H atoms omitted for clarity.

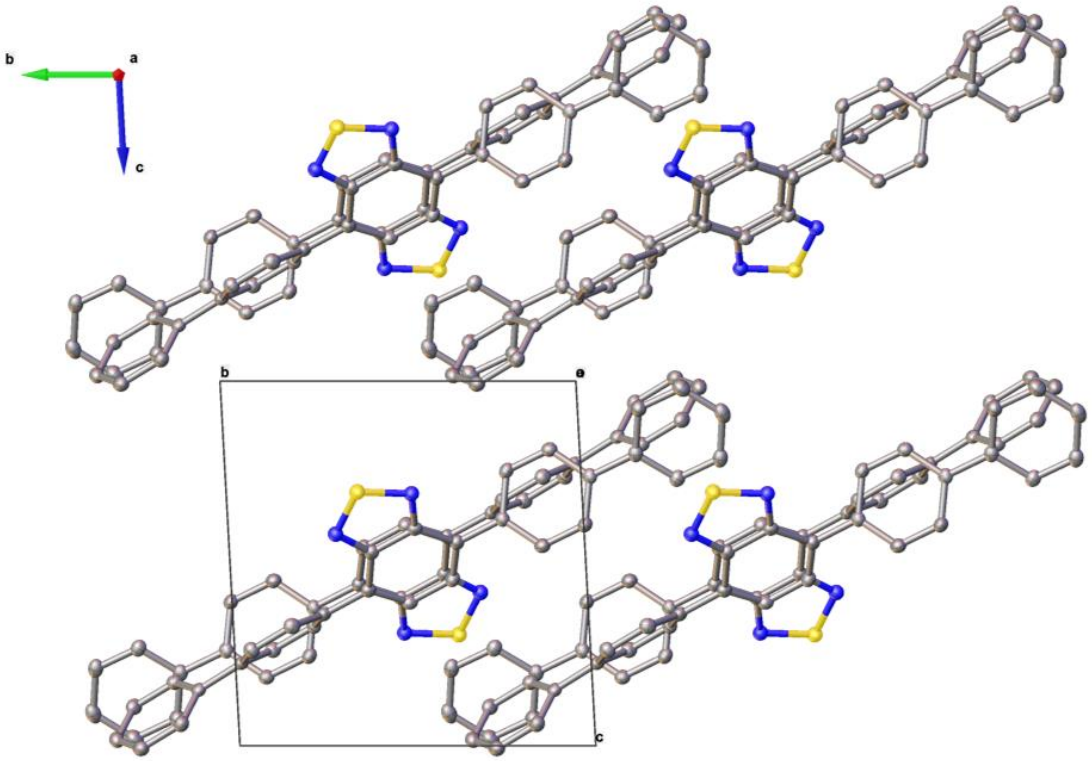

Figure S17 X-ray crystal structure of **pPh-BTZ** showing the packing of molecules as viewed down the a-axis [100]. Hydrogen atoms omitted for clarity.

Crystal data for 1Nap-BTZ (CCDC Number – 2179276)

Grown by slow evaporation from DCM. Crystal data for $C_{26}H_{16}N_2S$ (M =388.47 g/mol): orthorhombic, space group Pnma (no. 62), a = 15.0206(3) Å, b = 29.3812(6) Å, c = 3.98040(10) Å, V = 1756.64(7) Å^3, Z = 4, T = 100(2) K, μ(CuKα) = 1.745 mm^{-1}, $Dcalc$ = 1.469 g/cm^3, 16310 reflections measured (6.016° ≤ 2Θ ≤ 148.744°), 1812 unique (R_{int} = 0.0413, R_{sigma} = 0.0221) which were used in all calculations. The final R_1 was 0.0389 (I > 2σ(I)) and ωR_2 was 0.1026 (all data).

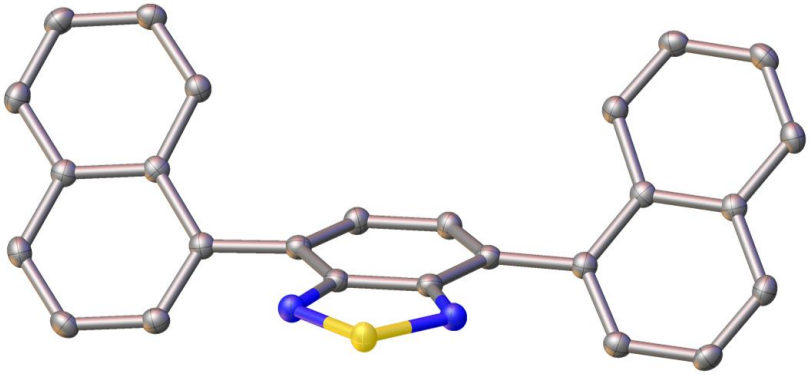

Figure S18 X-ray crystal structure of **1Nap-BTZ**. The atoms are shown as ellipsoids at 50% probability. H atoms omitted for clarity.

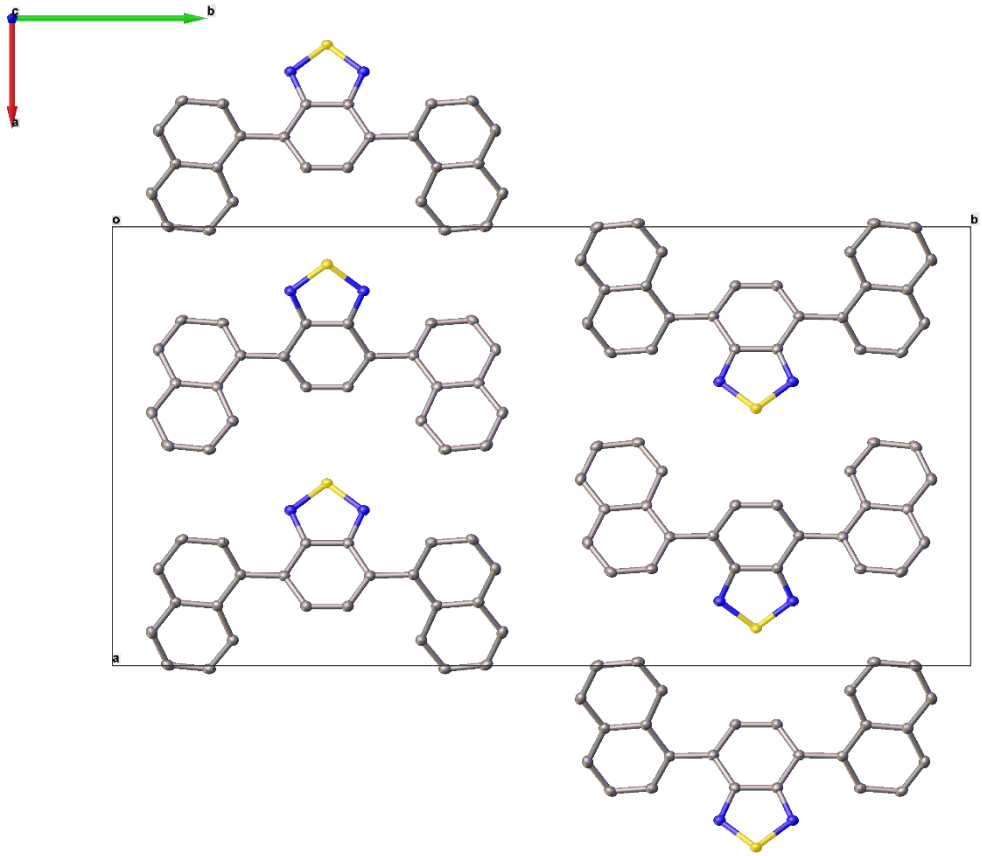

Figure S19 X-ray crystal structure of **1Nap-BTZ** showing the packing of molecules as viewed down the c-axis [001]. Hydrogen atoms omitted for clarity.

Crystal data for 2Nap-BTZ (CCDC Deposition Number - 2179272)

Grown by slow evaporation from DCM. Crystal Data for $C_{26}H_{16}N_2S$ (M =388.47 g/mol): monoclinic, space group $P2_1/c$ (no. 14), a = 5.83690(10) Å, b = 24.3284(6) Å, c = 13.1740(3) Å, β = 98.6190(10)°, V = 1849.61(7) Å^3, Z = 4, T = 100(2) K, μ(CuKα) = 1.657 mm^{-1}, *Dcalc* = 1.395 g/cm^3, 25819 reflections measured (7.266° ≤ 2Θ ≤ 159.566°), 3978 unique (R_{int} = 0.1062, R_{sigma} = 0.0568) which were used in all calculations. The final R_1 was 0.0498 (I > 2σ(I)) and wR_2 was 0.1358 (all data).

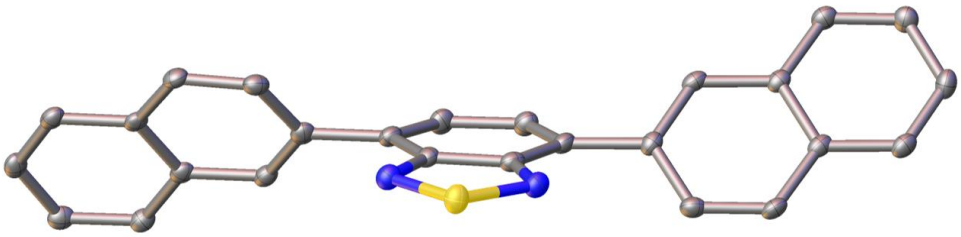

Figure S20 X-ray crystal structure of **2Nap-BTZ**. The atoms are shown as ellipsoids at 50% probability. H atoms omitted for clarity.

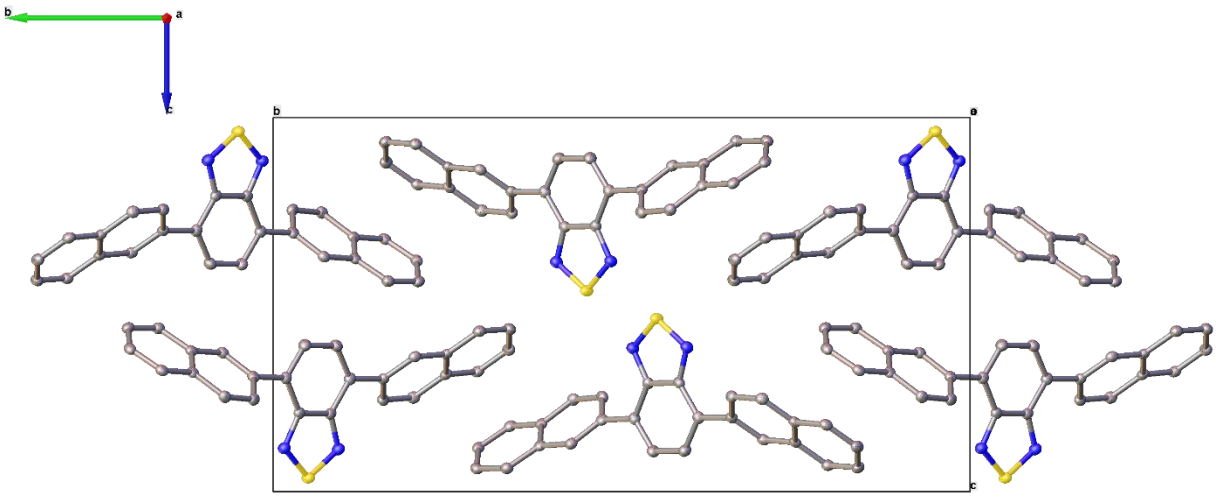

Figure S21 X-ray crystal structure of **2Nap-BTZ** showing the packing of molecules as viewed down the a-axis [100]. Hydrogen atoms omitted for clarity.

Crystal data for pMe-BTZ (CCDC Deposition Number – 2179269)

Grown by slow evaporation from DCM. Crystal data for $C_{20}H_{16}N_2S$ (M =316.41 g/mol): triclinic, space group P-1 (no. 2), a = 5.7484(4) Å, b = 10.8200(12) Å, c = 12.3382(11) Å, α = 88.148(5)°, β = 87.502(3)°, γ = 89.861(3)°, V = 766.28(12) Å^3, Z = 2, T = 100(2) K, μ(CuKα) = 1.860 mm^{-1}, *Dcalc* = 1.371 g/cm^3, 11410 reflections measured (10.71° ≤ 2Θ ≤ 149.722°), 3082 unique (R_{int} = 0.0323, R_{sigma} = 0.0300) which were used in all calculations. The final R_1 was 0.0341 (I > 2σ(I)) and ωR_2 was 0.0944 (all data).

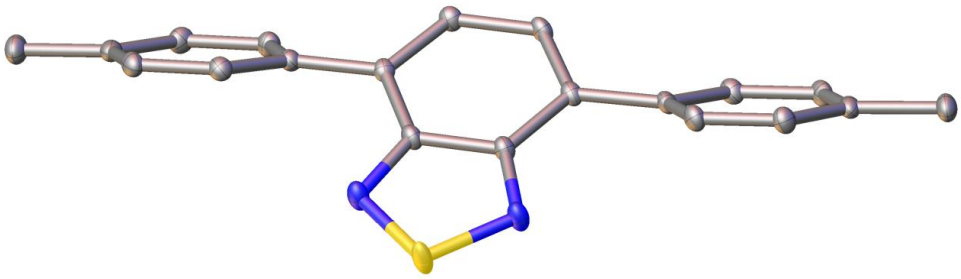

Figure S22 X-ray crystal structure of **pMe-BTZ**. The atoms are shown as ellipsoids at 50% probability. H atoms omitted for clarity.

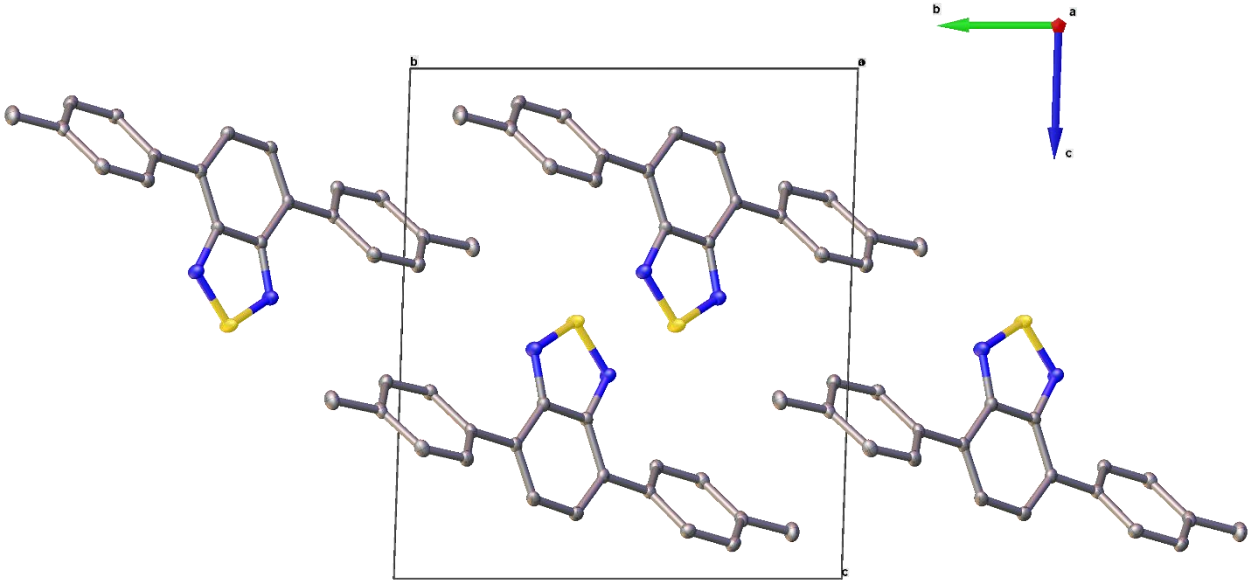

Figure S23 X-ray crystal structure of **pMe-BTZ** showing the packing of molecules as viewed down the a-axis [100]. Hydrogen atoms omitted for clarity.

Crystal Data for pOH-BTZ (CCDC Deposition Number – 2179279)

Grown by slow evaporation of THF. Crystal Data for $C_{20}H_{16}N_2O_{2.5}S$ (M =356.41 g/mol): triclinic, space group P-1 (no. 2), a = 7.47480(10) Å, b = 14.5894(2) Å, c = 15.1674(2) Å, α = 91.5980(10)°, β = 101.6100(10)°, γ = 96.6260(10)°, V = 1607.16(4) Å^3, Z = 4, T = 100.0 K, μ(CuKα) = 1.962 mm^{-1}, D_{calc} = 1.473 g/cm^3, 53419 reflections measured (5.956° ≤ 2Θ ≤ 149.222°), 6586 unique (R_{int} = 0.0338, R_{sigma} = 0.0179) which were used in all calculations. The final R1 was 0.0342 (I > 2σ(I)) and wR2 was 0.0924 (all data). The THF solvent and H atoms on the OH groups are disordered. THF C-O distances and C-C distances restrained and some THF displacement parameters restrained with ISOR and others constrained with EADP.

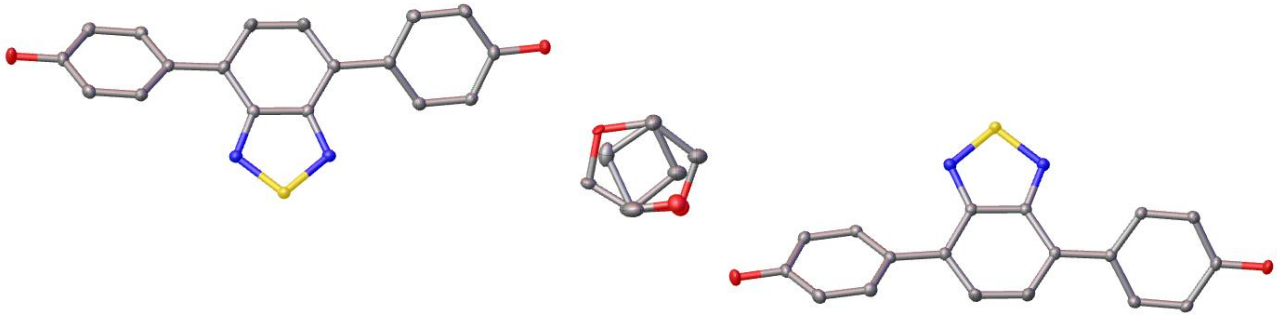

Figure S24 X-ray crystal structure of **pOH-BTZ**. The atoms are shown as ellipsoids at 50% probability. H atoms omitted for clarity.

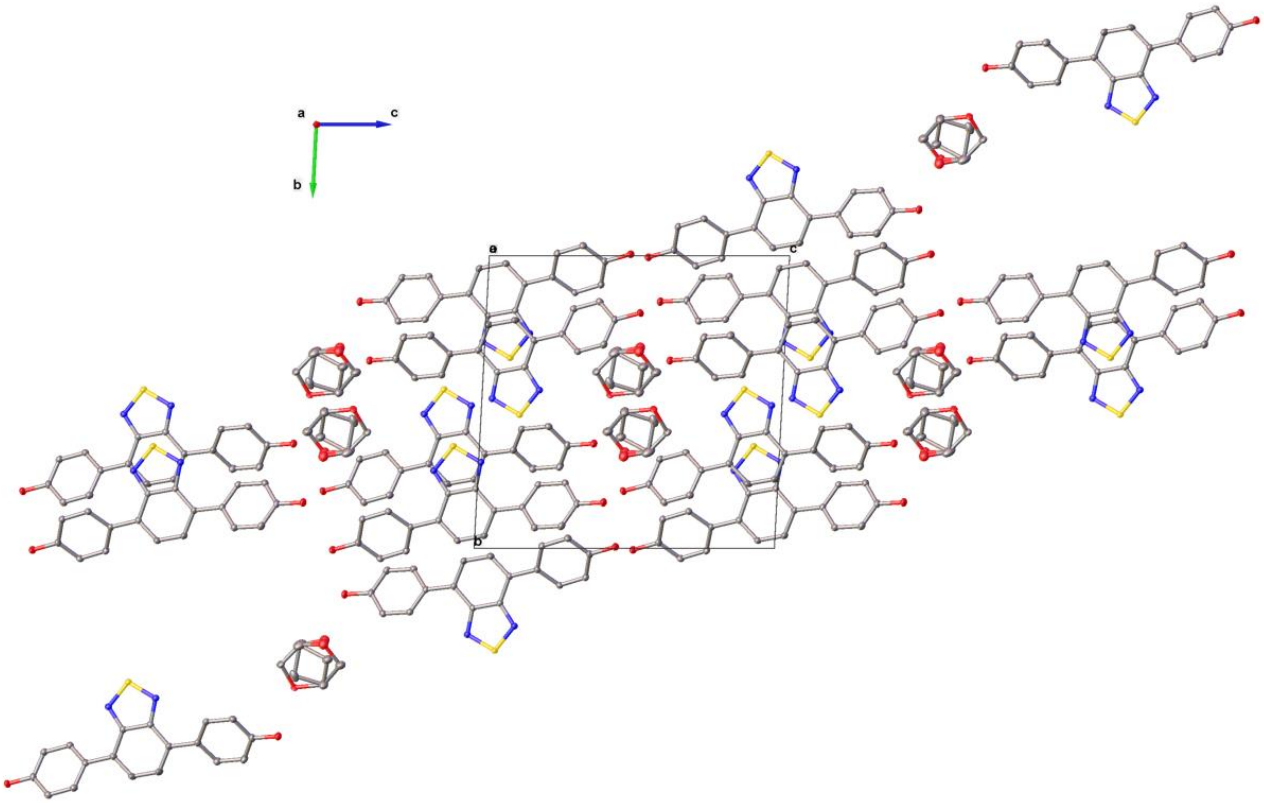

Figure S25 X-ray crystal structure of **pOH-BTZ** showing the packing of molecules as viewed down the a-axis [100]. Hydrogen atoms omitted for clarity.

Crystal data for pCF_3-BTZ (CCDC Deposition Number – 2179281)

Grown by slow evaporation from DCM. Crystal data for $C_{20}H_{10}N_2F_6S$ (M =424.36 g/mol): triclinic, space group P-1 (no. 2), a = 9.6001(3) Å, b = 9.7278(3) Å, c = 10.4526(3) Å, α = 90.6038(9)°, β = 117.0952(9)°, γ = 99.9999(9)°, V = 851.33(5) Å^3, Z = 2, T = 100(2) K, μ(CuKα) = 2.375 mm^{-1}, *Dcalc* = 1.655 g/cm^3, 15906 reflections measured (9.28° ≤ 2Θ ≤ 149.462°), 3444 unique (R_{int} = 0.0290, R_{sigma} = 0.0235) which were used in all calculations. The final R_1 was 0.0294 (I > 2σ(I)) and ωR_2 was 0.0794 (all data).

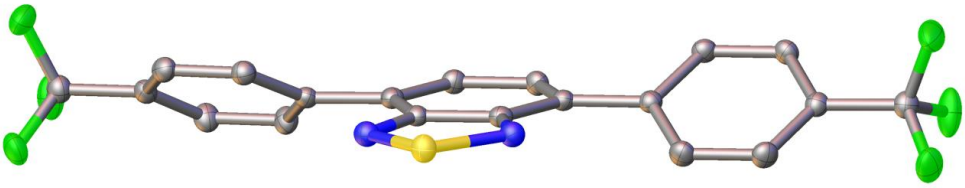

Figure S26 X-ray crystal structure of **pCF_3-BTZ**. The atoms are shown as ellipsoids at 50% probability. H atoms omitted for clarity.

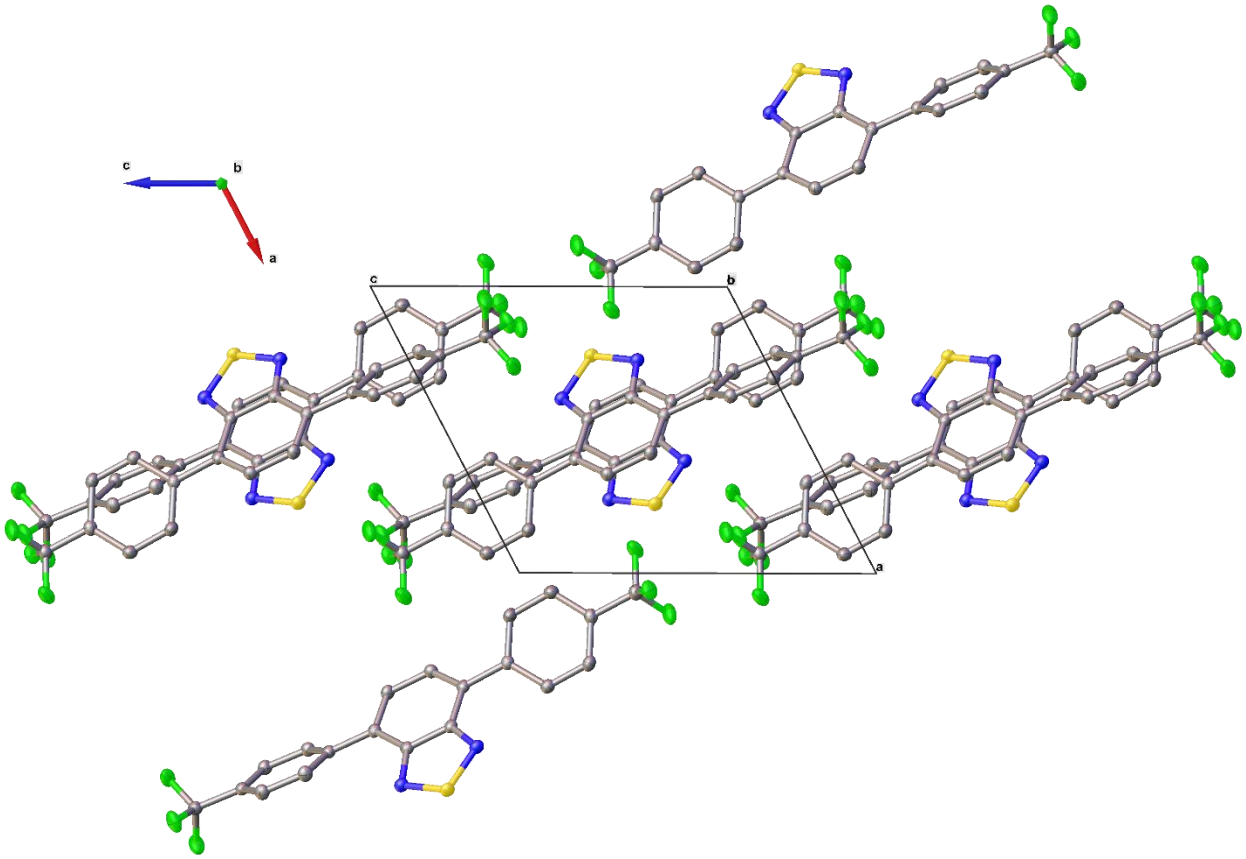

Figure S27 X-ray crystal structure of **pCF_3-BTZ** showing the packing of molecules as viewed down the b-axis [010]. Hydrogen atoms omitted for clarity.

Crystal Data for 7 (CCDC Deposition Number – 2179284)

Grown by slow evaporation from DCM. Grown by Crystal data for $C_{20}H_{23}N$ (M =277.39 g/mol): triclinic, space group P-1 (no. 2), a = 6.5737(2) Å, b = 10.6100(3) Å, c = 11.3773(3) Å, α = 73.1270(10)°, β = 88.4100(10)°, γ = 77.2260(10)°, V = 740.01(4) Å^3, Z = 2, T = 100(2) K, μ(CuKα) = 0.537 mm^{-1}, *Dcalc* = 1.245 g/cm^3, 15951 reflections measured (8.126° ≤ 2Θ ≤ 144.108°), 2881 unique (R_{int} = 0.0351, R_{sigma} = 0.0223) which were used in all calculations. The final R_1 was 0.0387 (I > 2σ(I)) and wR_2 was 0.1090 (all data).

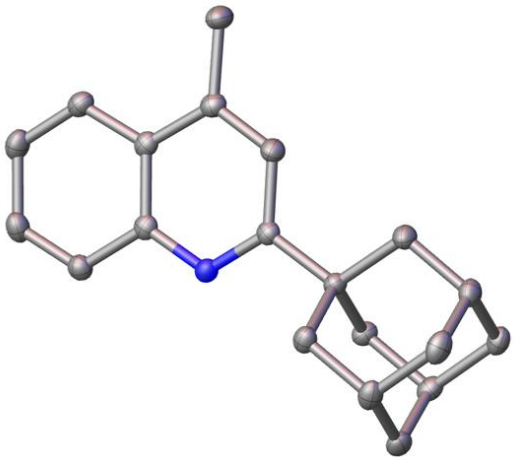

Figure S28 X-ray crystal structure of **7**. The atoms are shown as ellipsoids at 50% probability. H atoms omitted for clarity.

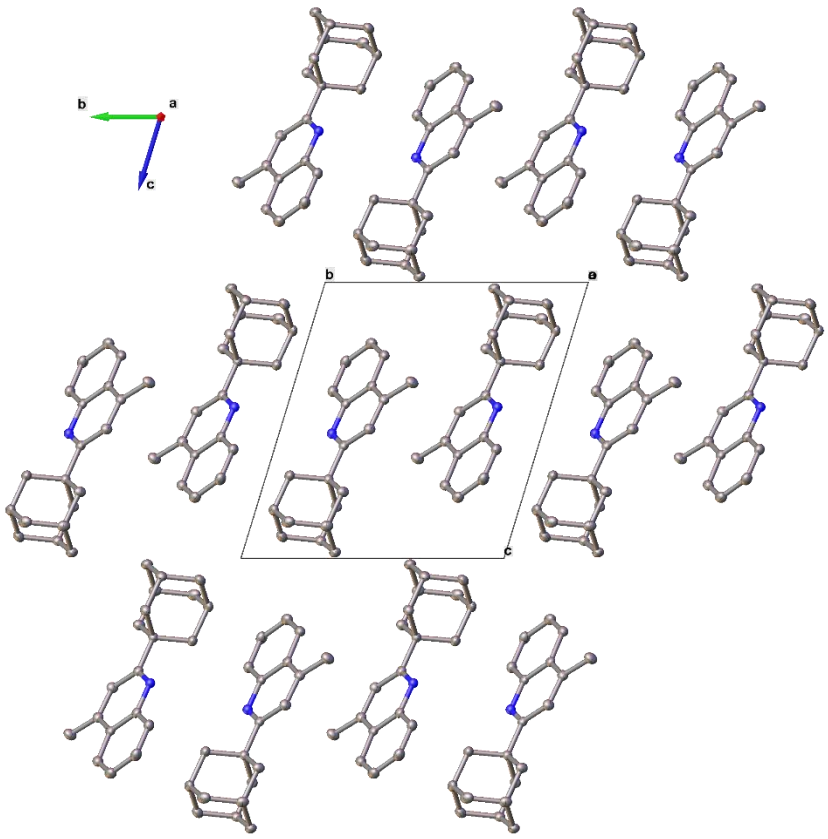

Figure S29 X-ray crystal structure of **7** showing the packing of molecules as viewed down the a-axis [100]. Hydrogen atoms omitted for clarity.

4. Photophysical Properties of the Photocatalysts

4.1 UV-Vis Absorption and Emission Spectra

UV-Vis absorption spectra for the synthesised photocatalysts were obtained using a Perkin-Elmer Lambda 35 in chloroform solution in quartz cuvettes. For comparison between different spectra, each set of data was normalised to the maximum absorbance observed in the region of 350 – 800 nm.

Emission spectra in the visible region were recorded using a Perkin Elmer LS 55 fluorescence spectrometer in chloroform solution using quartz cuvettes. The excitation wavelength (λ_{ex}) used was the wavelength of maximum absorption for each photocatalyst. Data was collected in the region of 400 – 800 nm. Reflection of the excitation wavelengths were removed by subtracting blank spectra recorded as the same excitation wavelength.

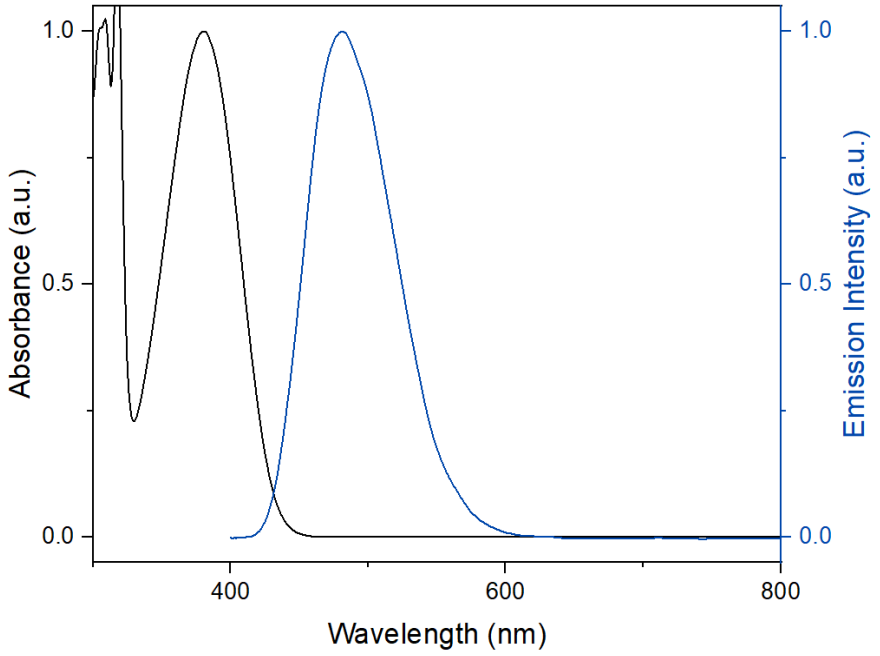

Figure S30 Normalised absorption (black) and emission spectra (blue, λ_{ex} = 380 nm) of **pH-BTZ** in $CHCl_3$.

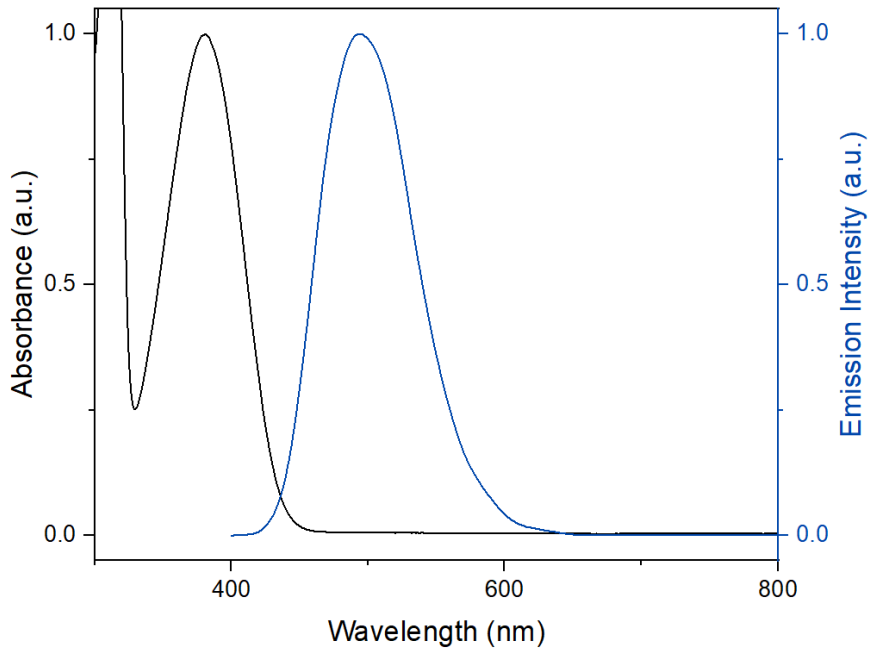

Figure S31 Normalised absorption (black) and emission spectra (blue, λ_{ex} = 381 nm) of **pF-BTZ** in $CHCl_3$.

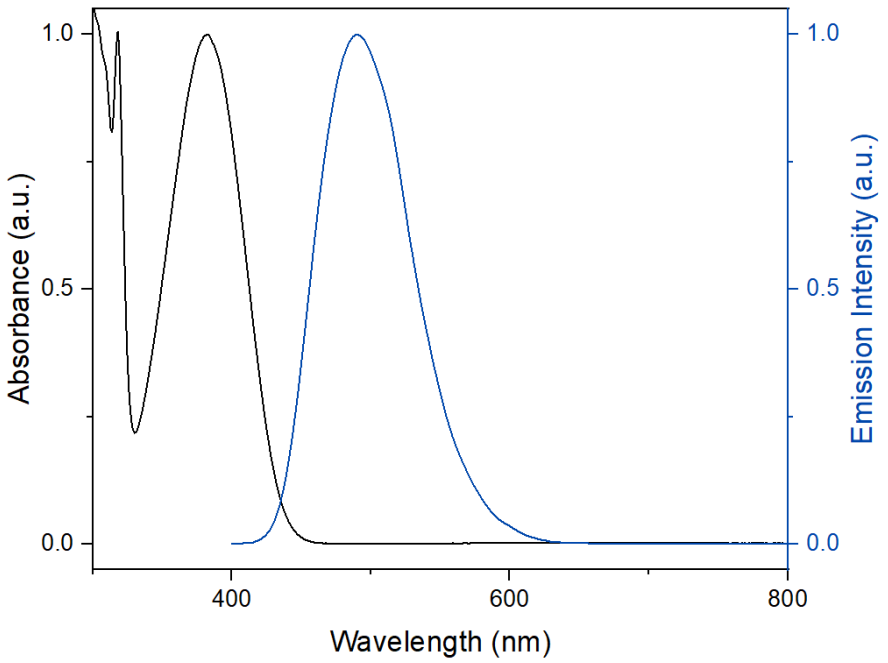

Figure S32 Normalised absorption (black) and emission spectra (blue, λ_{ex} = 383 nm) of **pCl-BTZ** in $CHCl_3$.

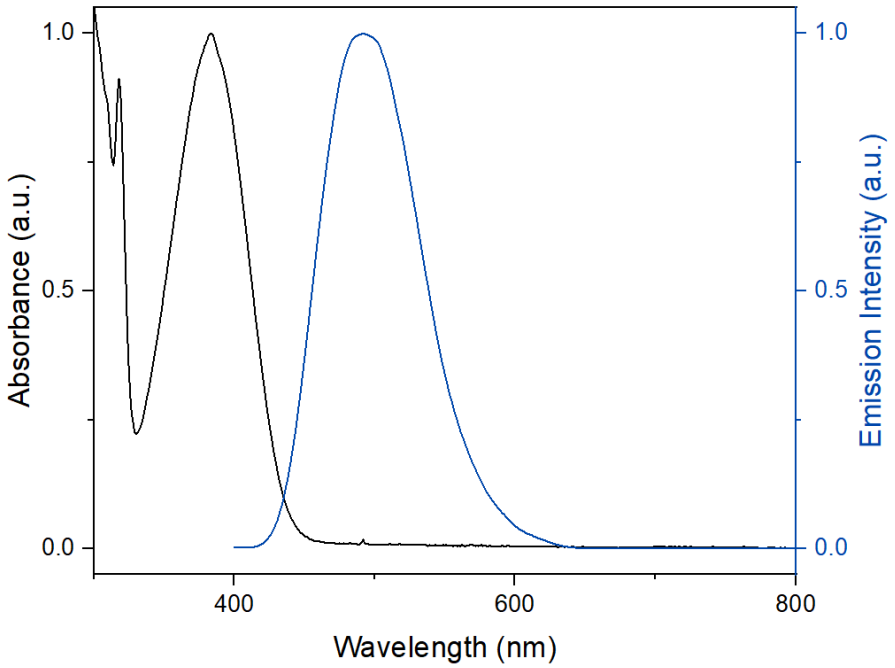

Figure S33 Normalised absorption (black) and emission spectra (blue, λ_{ex} = 381 nm) of **pBr-BTZ** in $CHCl_3$.

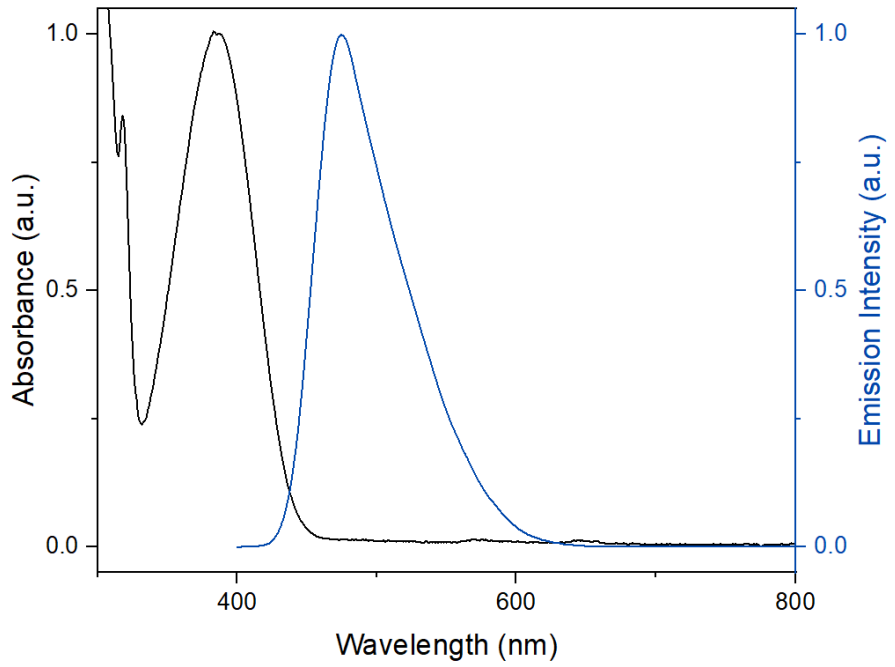

Figure S34 Normalised absorption (black) and emission spectra (blue, λ_{ex} = 384 nm) of **pI-BTZ** in $CHCl_3$.

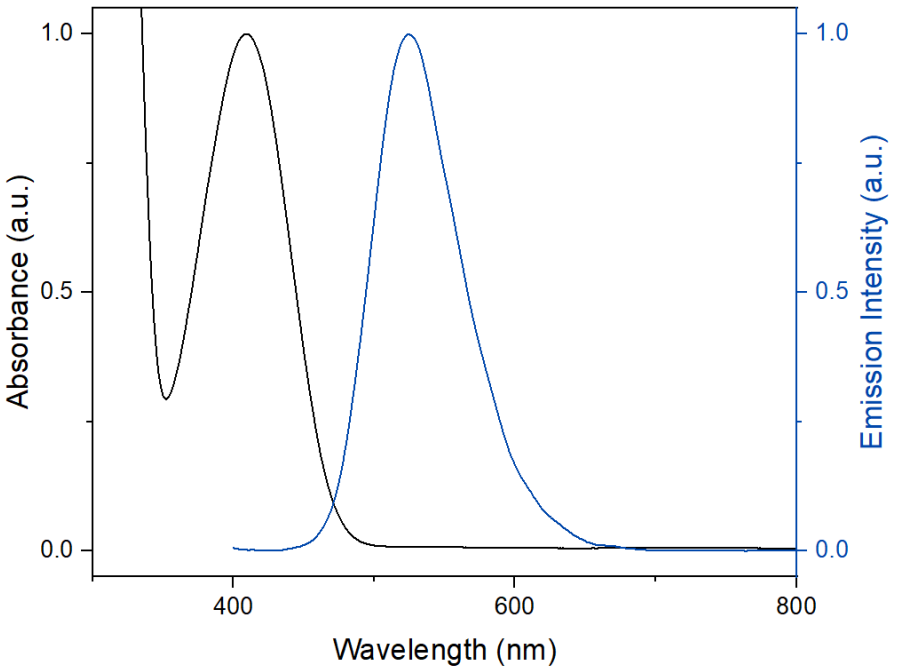

Figure S35 Normalised absorption (black) and emission spectra (blue, λ_{ex} = 409 nm) of **pTh-BTZ** in $CHCl_3$.

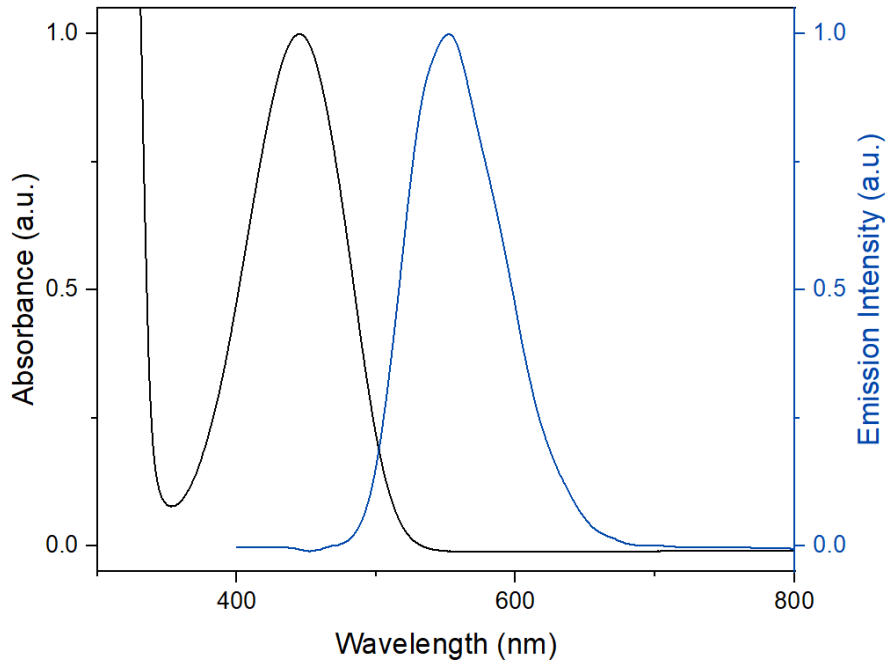

Figure S36 Normalised absorption (black) and emission spectra (blue, λ_{ex} = 446 nm) of **Th-BTZ** in $CHCl_3$.

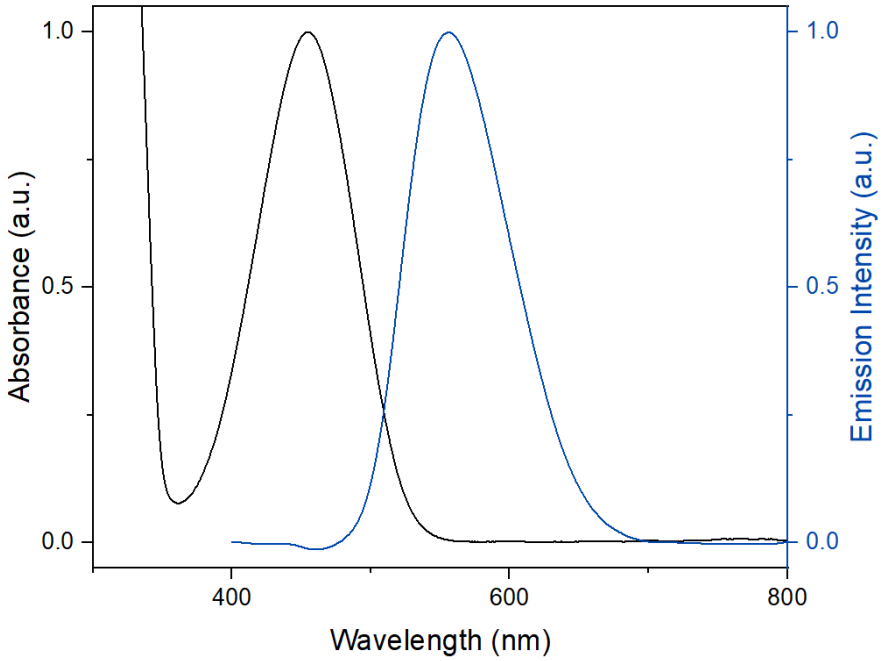

Figure S37 Normalised absorption (black) and emission spectra (blue, λ_{ex} = 455 nm) of **ThBr-BTZ** in $CHCl_3$.

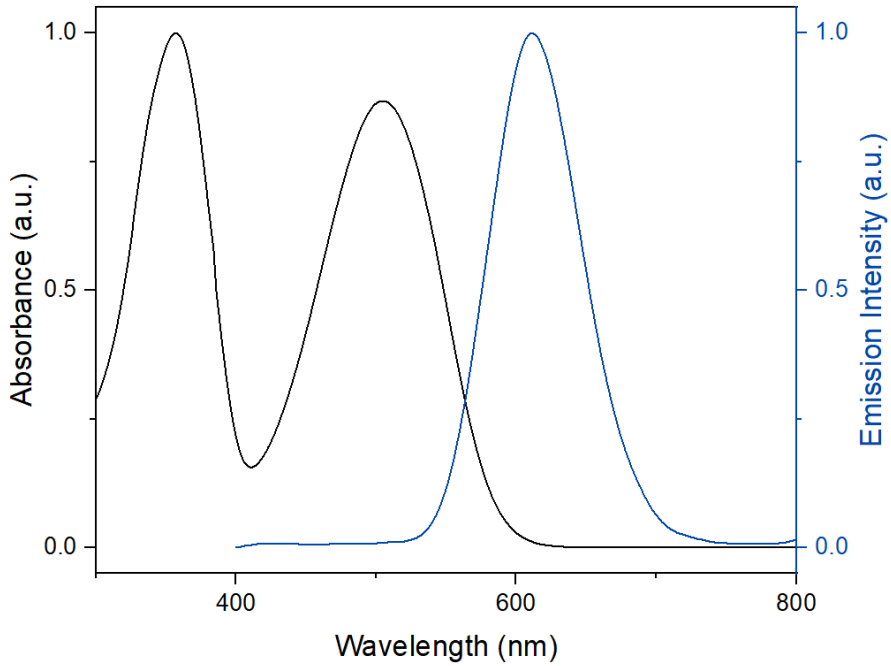

Figure S38 Normalised absorption (black) and emission spectra (blue, λ_{ex} = 505 nm) of **ThTh-BTZ** in $CHCl_3$.

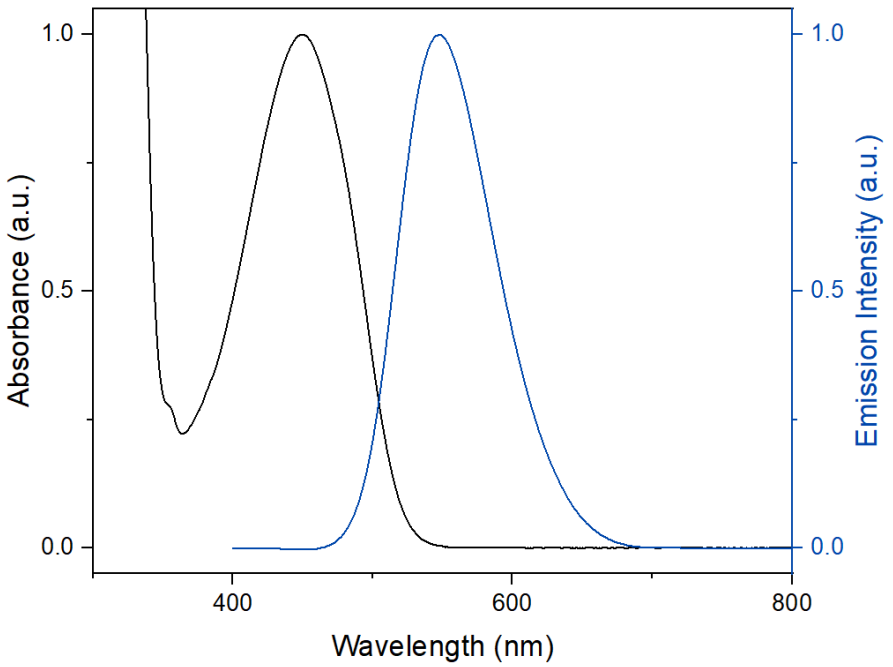

Figure S39 Normalised absorption (black) and emission spectra (blue, λ_{ex} = 450 nm) of **BTh-BTZ** in $CHCl_3$.

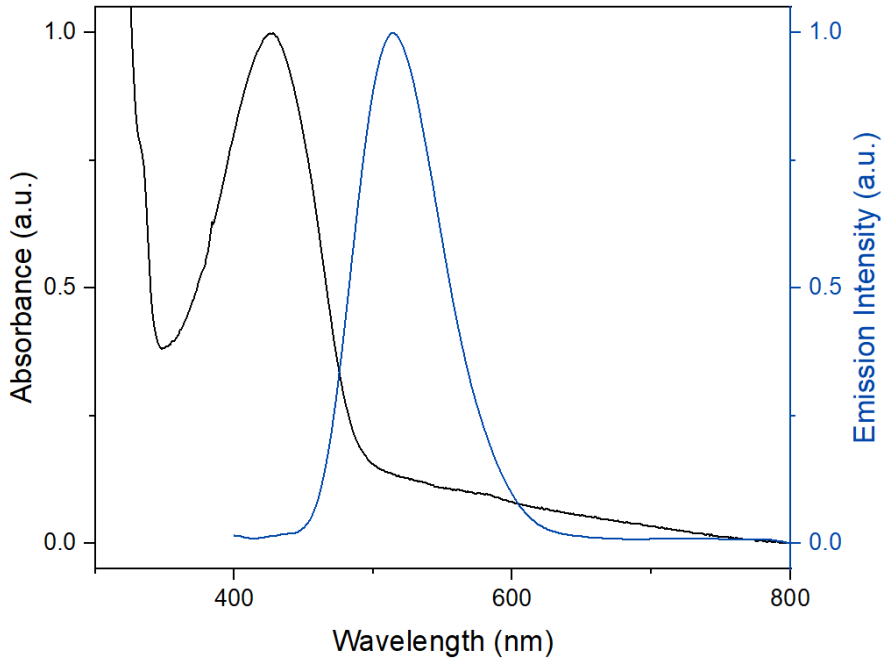

Figure S40 Normalised absorption (black) and emission spectra (blue, λ_{ex} = 428 nm) of **Tz-BTZ** in $CHCl_3$.

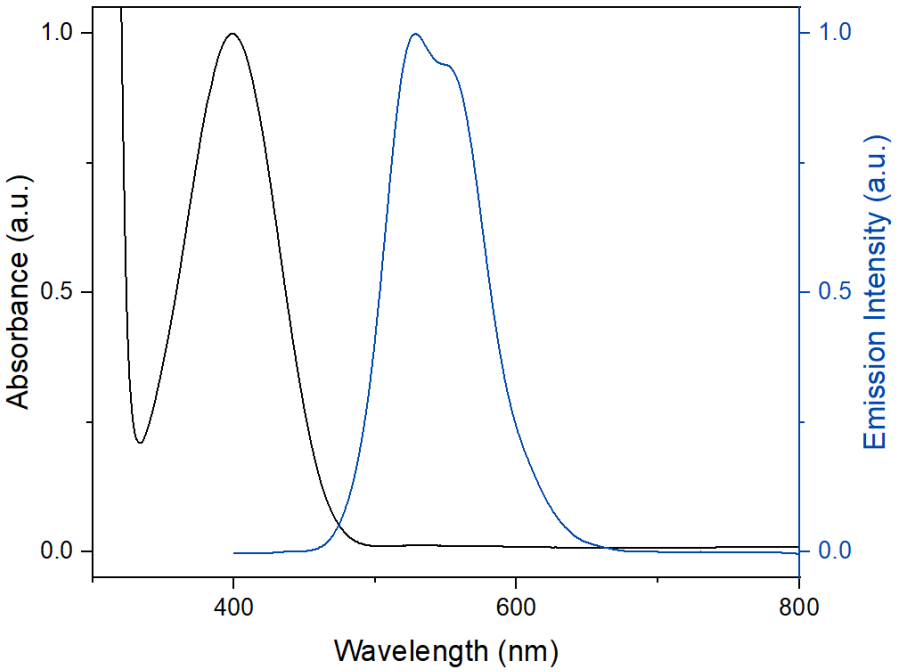

Figure S41 Normalised absorption (black) and emission spectra (blue, λ_{ex} = 397 nm) of **Pyr-BTZ** in $CHCl_3$.

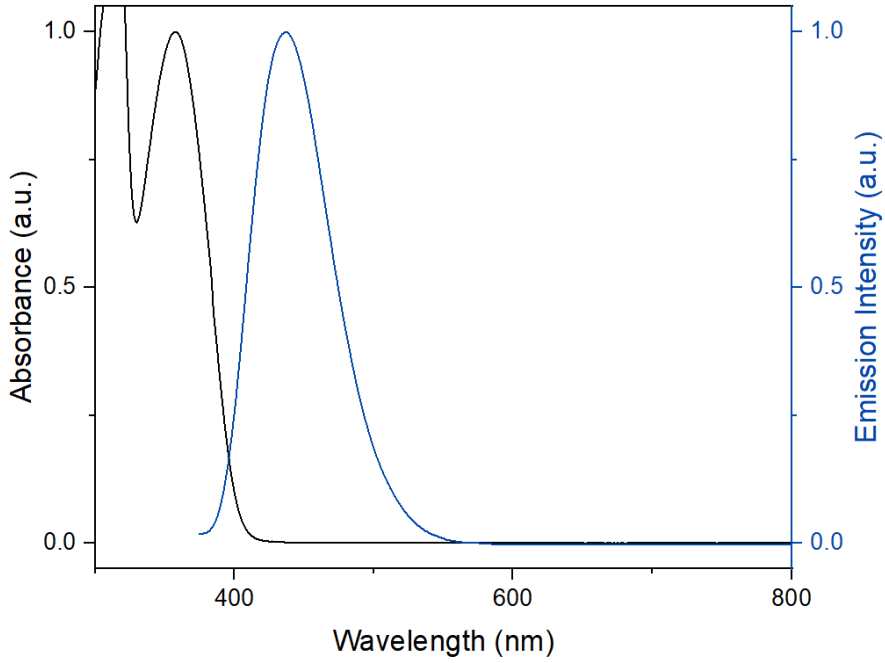

Figure S42 Normalised absorption (black) and emission spectra (blue, λ_{ex} = 359 nm) of **4N-BTZ** in $CHCl_3$.

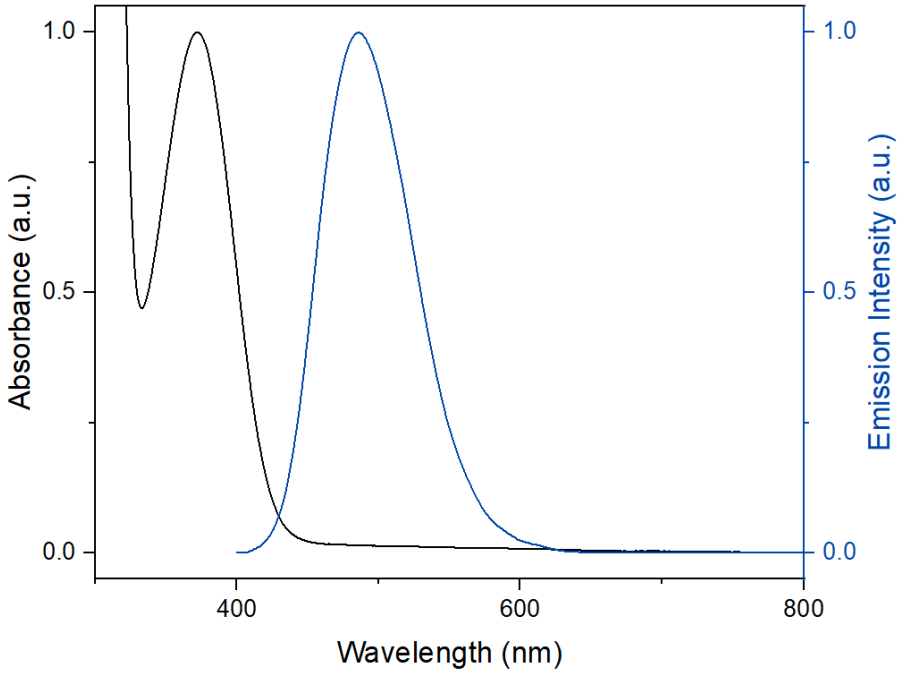

Figure S43 Normalised absorption (black) and emission spectra (blue, λ_{ex} = 373 nm) of **oPh-BTZ** in $CHCl_3$.

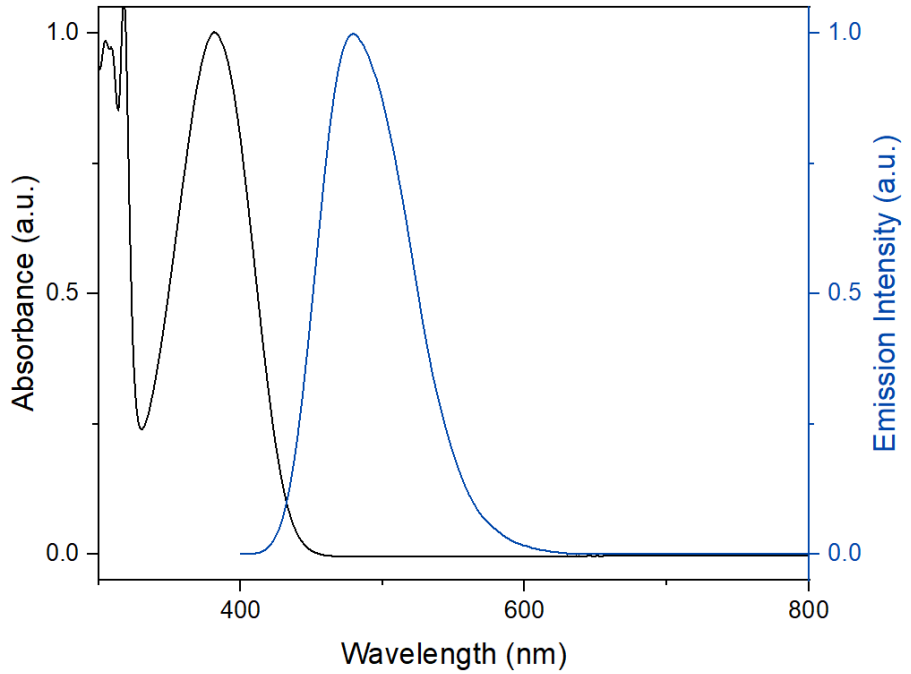

Figure S44 Normalised absorption (black) and emission spectra (blue, λ_{ex} = 381 nm) of **mPh-BTZ** in $CHCl_3$.

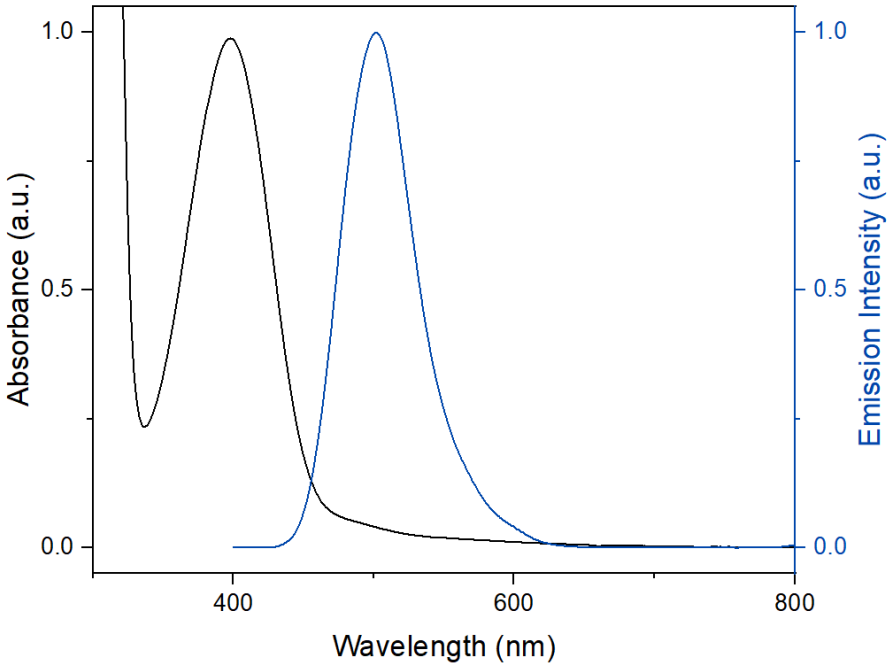

Figure S45 Normalised absorption (black) and emission spectra (blue, λ_{ex} = 398 nm) of **pPh-BTZ** in $CHCl_3$.

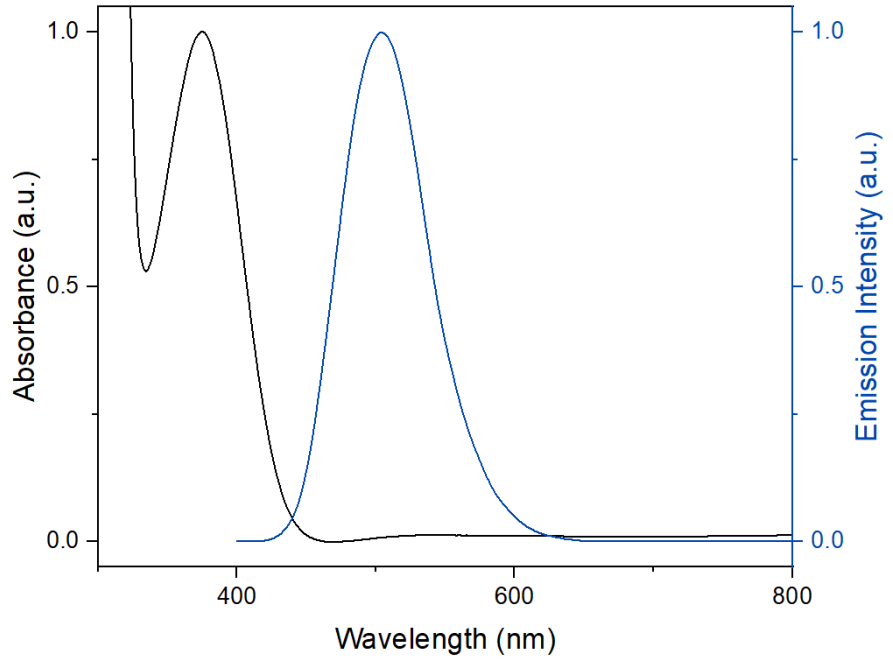

Figure S46 Normalised absorption (black) and emission spectra (blue, λ_{ex} = 376 nm) of **1Nap-BTZ** in $CHCl_3$.

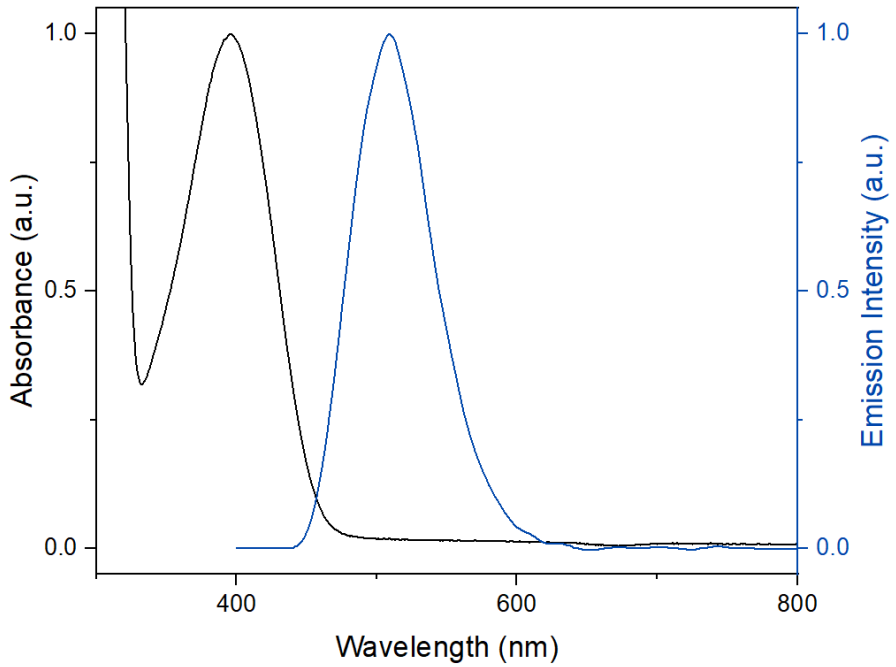

Figure S47 Normalised absorption (black) and emission spectra (blue, λ_{ex} = 396 nm) of **2Nap-BTZ** in $CHCl_3$.

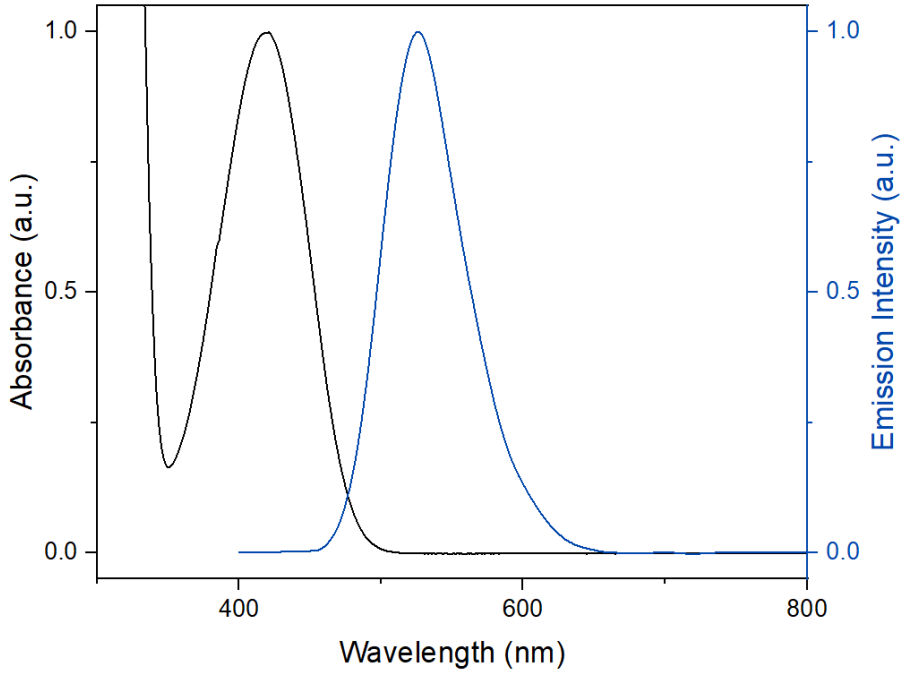

Figure S48 Normalised absorption (black) and emission spectra (blue, λ_{ex} = 420 nm) of **Flu-BTZ** in $CHCl_3$.

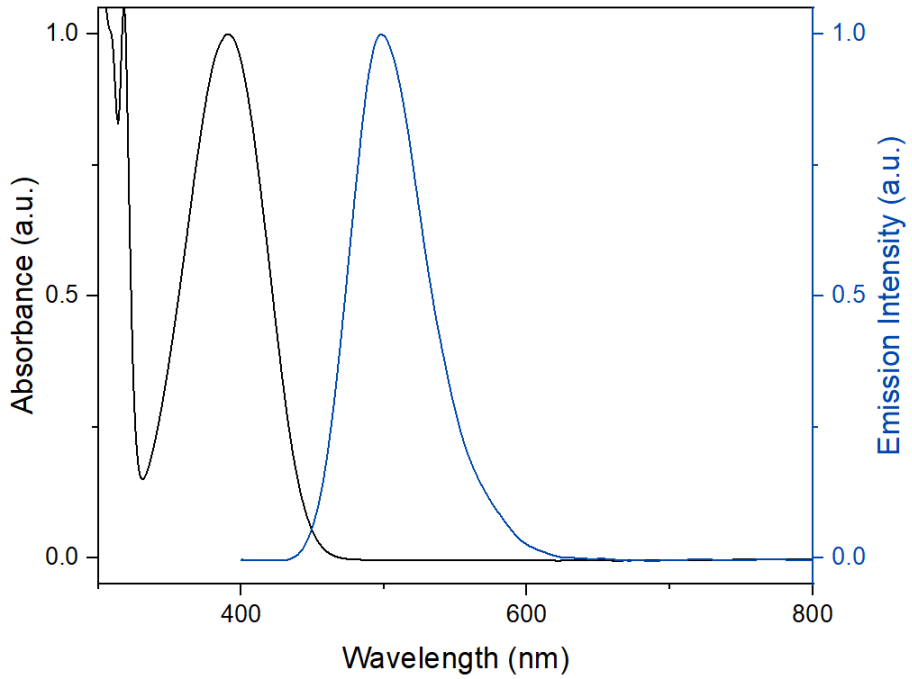

Figure S49 Normalised absorption (black) and emission spectra (blue, λ_{ex} = 391 nm) of **pMe-BTZ** in $CHCl_3$.

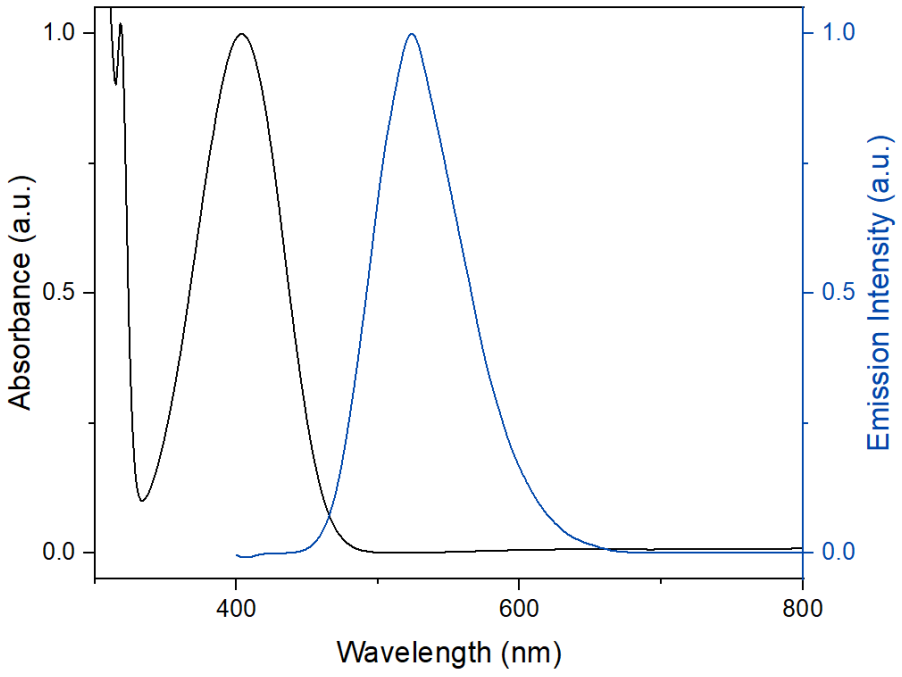

Figure S50 Normalised absorption (black) and emission spectra (blue, λ_{ex} = 404 nm) of **pOH-BTZ** in $CHCl_3$.

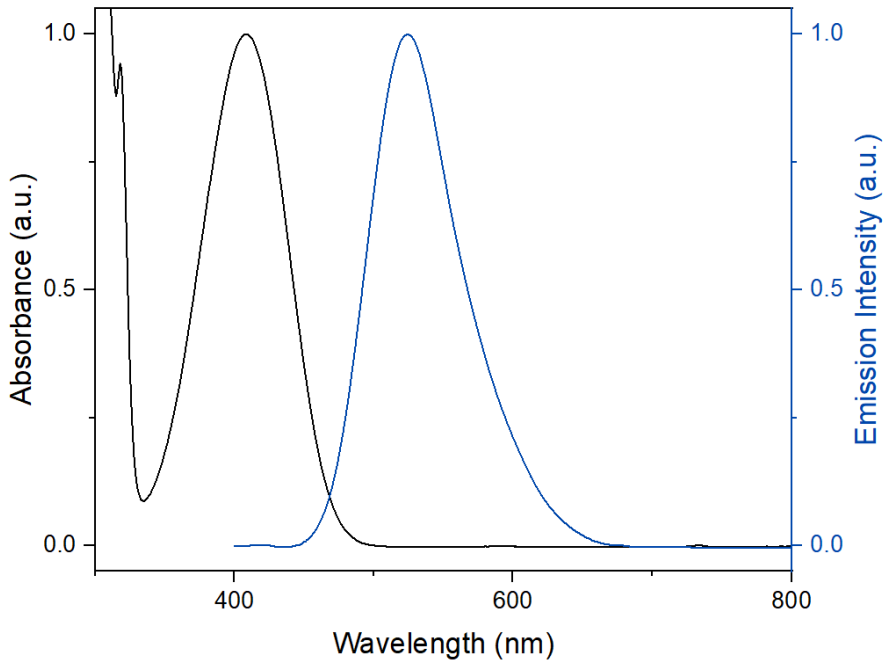

Figure S51 Normalised absorption (black) and emission spectra (blue, λ_{ex} = 409 nm) of **pOMe-BTZ** in $CHCl_3$.

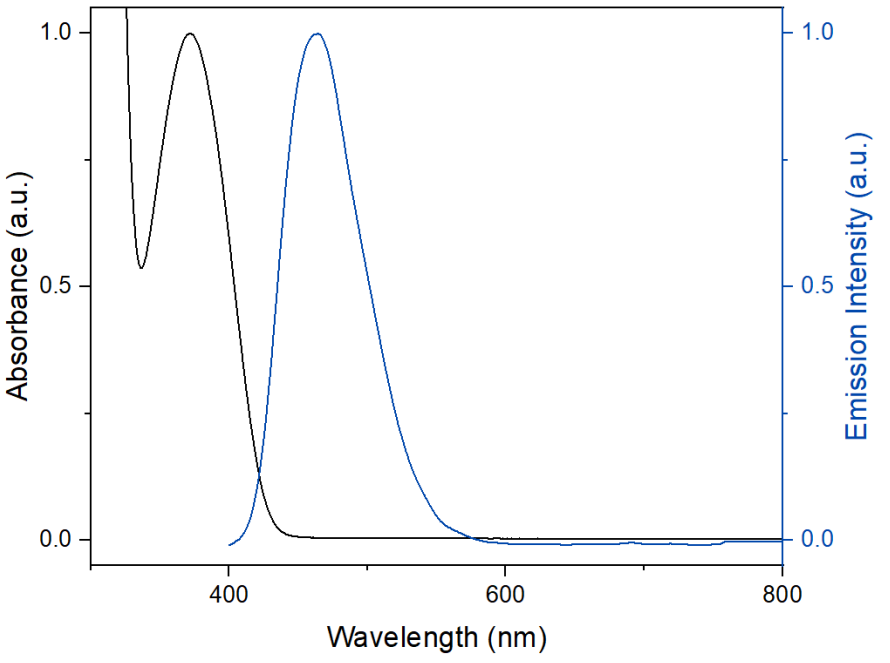

Figure S52 Normalised absorption (black) and emission spectra (blue, λ_{ex} = 377 nm) of **pCHO-BTZ** in $CHCl_3$.

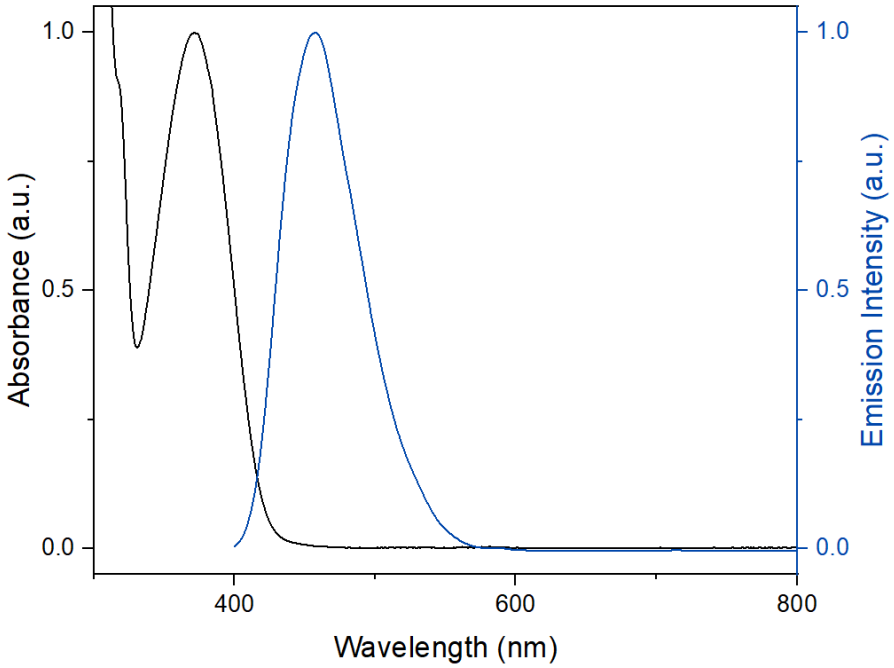

Figure S53 Normalised absorption (black) and emission spectra (blue, λ_{ex} = 372 nm) of **pCN-BTZ** in $CHCl_3$.

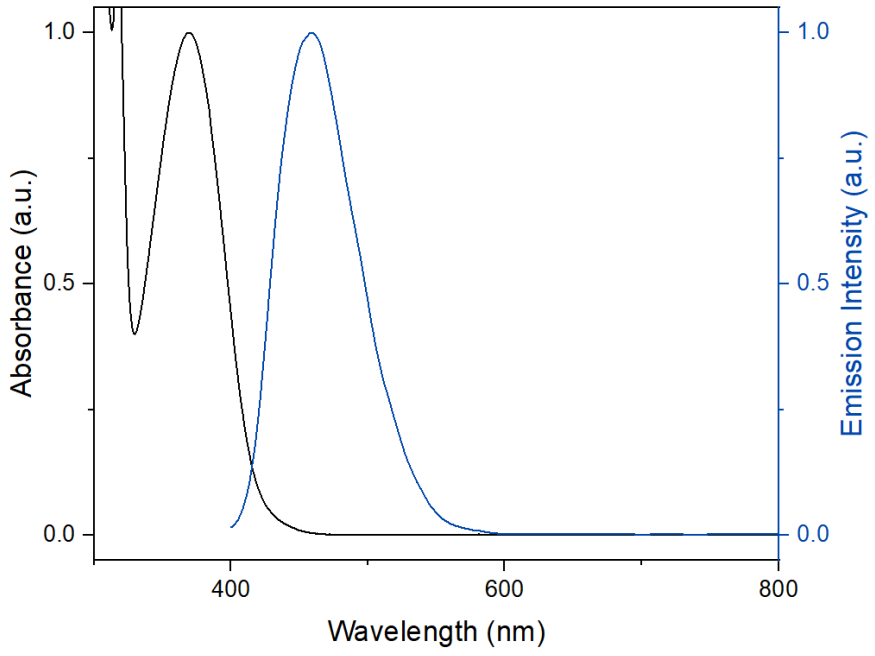

Figure S54 Normalised absorption (black) and emission spectra (blue, λ_{ex} = 369 nm) of **pCF$_3$-BTZ** in $CHCl_3$.

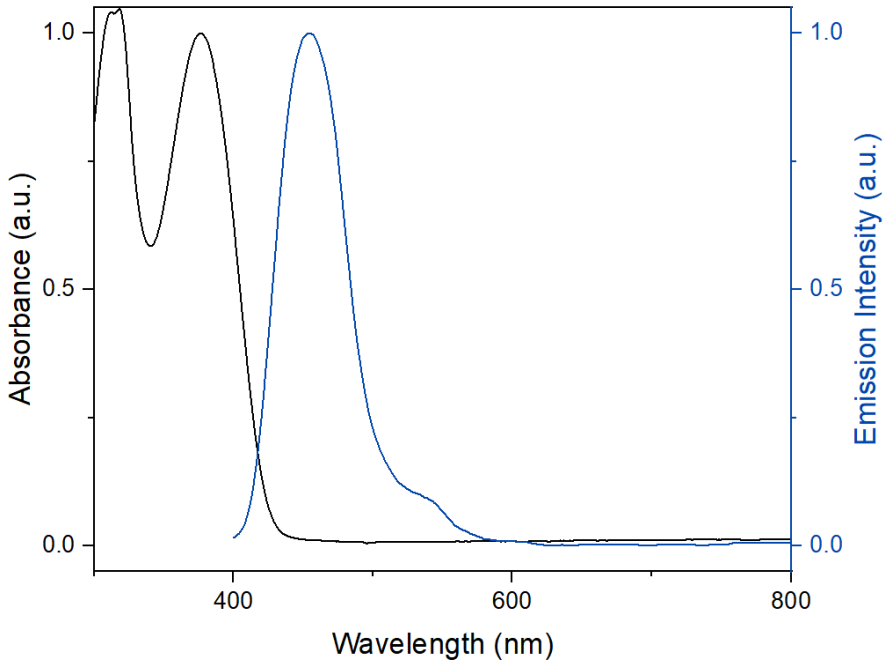

Figure S55 Normalised absorption (black) and emission spectra (blue, λ_{ex} = 377 nm) of **pNO$_2$-BTZ** in $CHCl_3$.

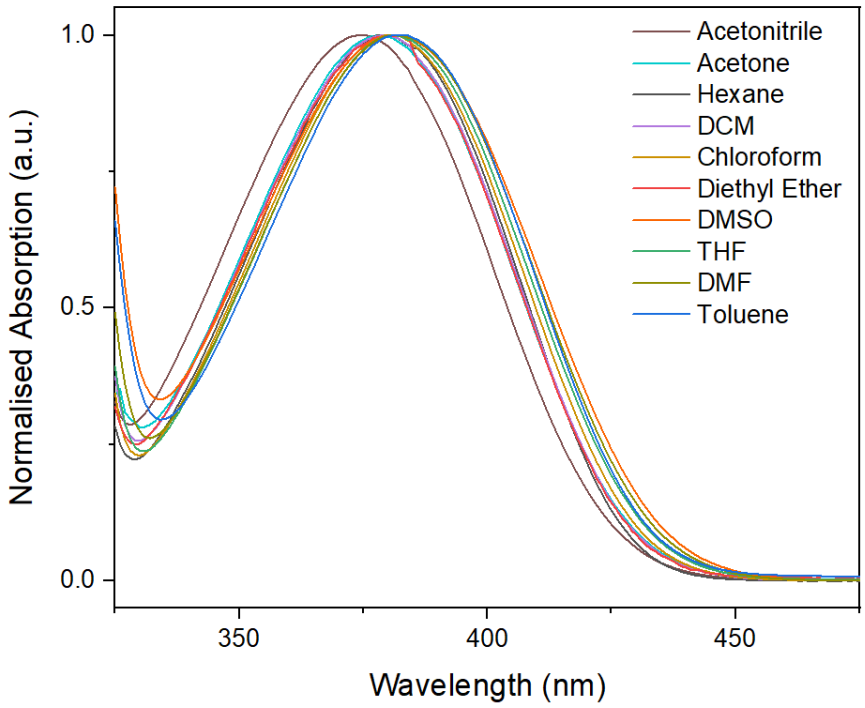

Figure S56 Normalised absorption spectra of **pH-BTZ** in various solvents. Legend is ordered from top to bottom in order of increasing wavelength of maximum absorption.

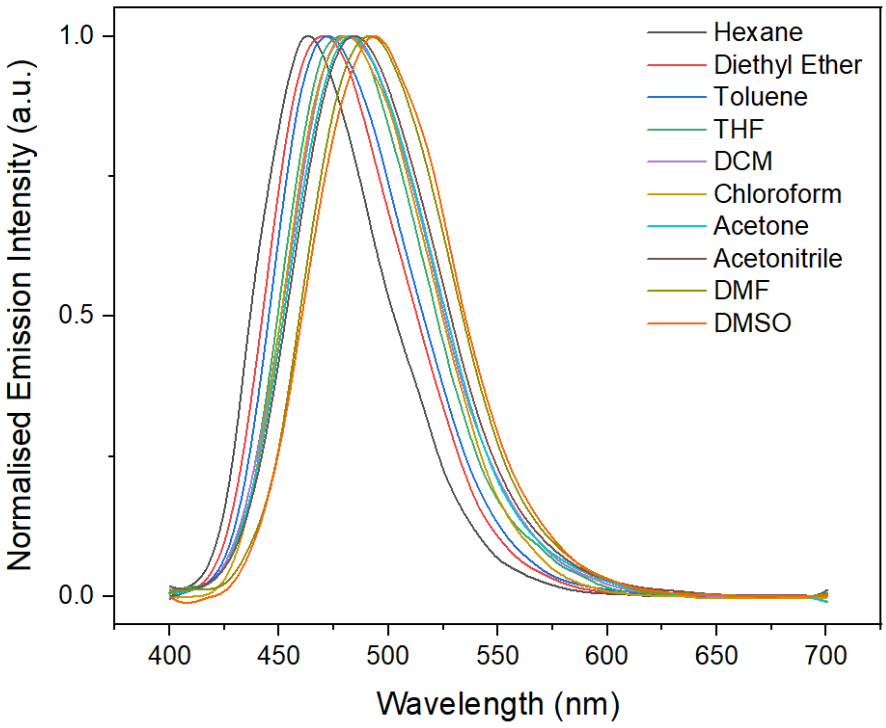

Figure S57 Normalised emission spectra (λ_{ex} = 380 nm) of **pH-BTZ** in various solvents. Legend is ordered from top to bottom in order of increasing wavelength of emission.

Table S1 Summary of the solvatochromic properties of the **pH-BTZ** used to construct Figures S58 and S59. [a]Excitation wavelength was the wavelength of maximum absorption of the photocatalyst. [b]Calculated from equation (1). [c]Values for n and ε from reference S10. [d]Reichardt parameters ($E_T(30)$) from reference S11.

Solvent	**λ_{abs}/nm**	**λ_{em}/nm[a]**	**Stokes Shift (Δν)/ x 10^3 cm^{-1}**	**Δf[b,c]**	**$E_T(30)$[d]**
Hexane	380	463	4.72	0.00	30.90
Diethyl Ether	380	470	5.04	0.17	34.60
Toluene	382	472	4.99	0.02	33.90
THF	381	479	5.37	0.21	37.40
DCM	379	481	5.60	0.22	41.10
Chloroform	380	482	5.57	0.15	39.10
Acetone	378	483	5.75	0.28	42.20
Acetonitrile	375	485	6.01	0.31	46.00
DMF	380	491	5.95	0.27	43.80
DMSO	380	494	6.07	0.26	45.10

The orientation polarisability function, Δf, is defined as:

$$\Delta f(\varepsilon, n) = \left(\frac{\varepsilon-1}{2\varepsilon+1}\right) - \left(\frac{n^2-1}{2n^2+1}\right) \qquad (1)$$

where ε and n are the dielectric constant and refractive index of each solvent respectively.

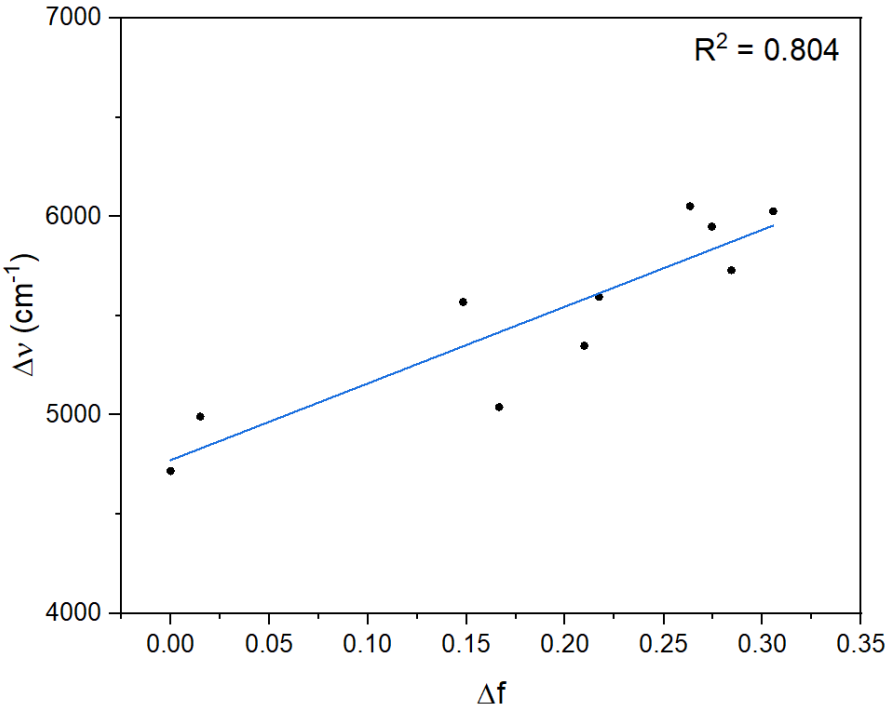

Figure S58 Lippert-Mataga plot for **pH-BTZ**.

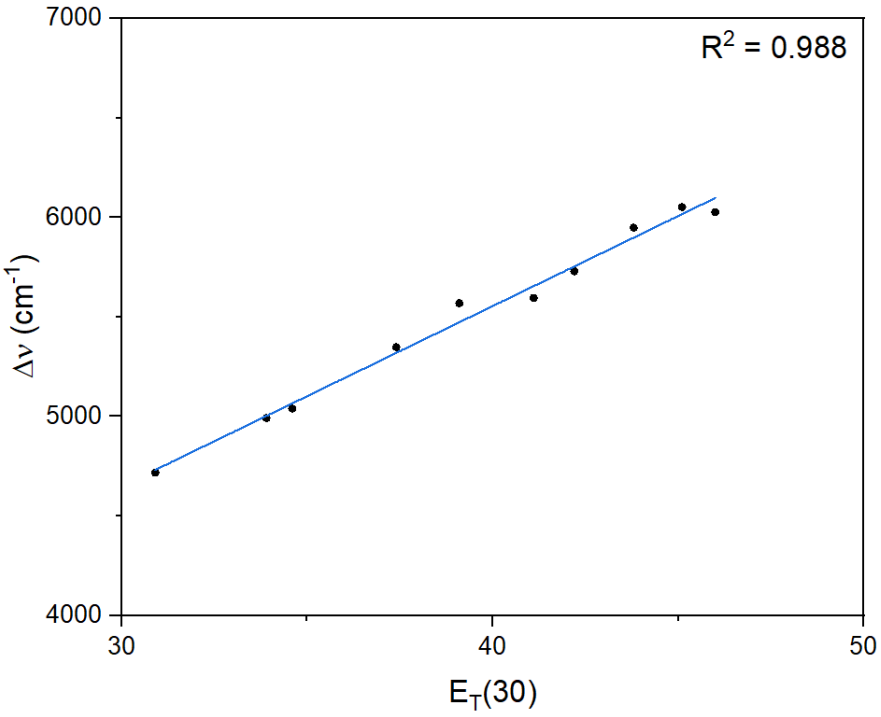

Figure S59 Plot of Stokes' shift against the solvent Reichardt $E_T(30)$ parameters for **pH-BTZ**.

4.2 Molar Attenuation Coefficient Measurements

For measuring the molar attenuation coefficient (ε_M), stock solutions of each photocatalyst in chloroform were prepared with concentrations in the range of 0 - 20 μM. The absorbance of each of these solutions was then measured. Plotting absorbance against concentration gave a Beer-Lambert-Bouguer plot, with a gradient equal to the attenuation coefficient. The error quoted in the attenuation coefficient was taken as the error in the line fitting. The results are summarised in Table S2.

4.3 Summary of Photophysical Results

Table S2 Summary of the photophysical properties of the **BTZ** photocatalysts. [a]In $CHCl_3$ solution. [b]Excitation wavelength was the wavelength of maximum absorption of the photocatalyst. [c]Absolute PLQY.

Entry	Compound	λ_{abs}/ nm[a]	Shift from pH-BTZ/ nm	λ_{em}/ nm[a,b]	Stokes' Shift/ nm	ϵ_M / x 10^3 M^{-1} cm^{-1}	PLQY[a,c]/ %
1	**pH-BTZ**	380	NA	482	102	7.5 ± 0.1	86.4
2	**pF-BTZ**	381	1	495	114	7.5 ± 0.3	93.3
3	**pCl-BTZ**	383	3	490	107	10.4 ± 0.2	94.3
4	**pBr-BTZ**	381	1	492	111	9.8 ± 0.4	93.4
5	**pI-BTZ**	384	4	475	91	13.7 ± 0.2	91.9
6	**pTh-BTZ**	409	29	525	116	17.9 ± 0.6	86.9
7	**Th-BTZ**	446	66	552	106	12.1 ± 0.4	88.1
8	**ThBr-BTZ**	455	75	556	101	17.4 ± 0.5	91.4
9	**ThTh-BTZ**	505	125	611	106	22.8 ± 0.2	58.0
10	**BTh-BTZ**	450	70	548	98	16.6 ± 0.3	96.2
11	**Tz-BTZ**	428	48	514	86	17.3 ± 0.6	92.7
12	**Pyr-BTZ**	397	17	529	132	5.6 ± 0.1	73.4
13	**4N-BTZ**	359	-21	437	78	12.3 ± 0.3	66.1
14	**oPh-BTZ**	373	-7	486	113	6.5 ± 0.2	100
15	**mPh-BTZ**	381	1	479	98	10.2 ± 0.4	92.3
16	**pPh-BTZ**	398	18	502	104	18.2 ± 0.3	97.3
17	**1Nap-BTZ**	376	-4	504	128	5.6 ± 0.1	23.6
18	**2Nap-BTZ**	396	16	509	113	15.5 ± 0.3	66.2
19	**Flu-BTZ**	420	40	526	106	19.9 ± 0.1	96.8
20	**pMe-BTZ**	391	11	499	108	13.0 ± 0.4	92.7
21	**pOH-BTZ**	404	24	524	120	11.3 ± 0.1	89.1
22	**pOMe-BTZ**	409	29	525	116	9.8 ± 0.4	94.0
23	**pCHO-BTZ**	377	-3	464	87	25.2 ± 0.2	85.2
24	**pCN-BTZ**	372	-8	457	85	18.3 ± 0.3	93.9
25	**pCF_3-BTZ**	369	-11	459	90	9.4 ± 0.3	88.2
26	**pNO_2-BTZ**	377	-3	455	78	23.1 ± 1.0	4.87

4.4 Photobleaching Studies

Photocatalyst (0.01 mmol) was dissolved in $CDCl_3$ (0.7 mL). The solution was then oxygenated for 1 minute using an oxygen stream of 20 mL min^{-1}, following which the solution was transferred to a NMR tube and ^1H NMR spectra recorded. The NMR tube was then irradiated with a 420 nm light for 18 hours. Following this another ^1H NMR spectra was obtained and compared to the original. The photocatalysts were then classified as:

- stable under the conditions described above if no change were observed between the initial and final spectra.
- moderately stable if only small changes were observed, corresponding to only minor photocatalyst decomposition.
- unstable if significant changes were observed, indicating significant bleaching had occurred.

Table S3 Summary of the photostability studies of the **BTZ** photocatalysts.

Entry	Compound	Photostable	Moderately Stable	Photounstable
1	**pH-BTZ**	✓		
2	**pF-BTZ**	✓		
3	**pCl-BTZ**	✓		
4	**pBr-BTZ**	✓		
5	**pI-BTZ**	✓		
6	**pTh-BTZ**		✓	
7	**Th-BTZ**		✓	
8	**ThBr-BTZ**	✓		
9	**ThTh-BTZ**		✓	
10	**BTh-BTZ**	✓		
11	**Tz-BTZ**		✓	
12	**Pyr-BTZ**			✓
13	**4N-BTZ**	✓		
14	**oPh-BTZ**	✓		
15	**mPh-BTZ**	✓		
16	**pPh-BTZ**	✓		
17	**1Nap-BTZ**		✓	
18	**2Nap-BTZ**			✓
19	**Flu-BTZ**	✓		
20	**pMe-BTZ**	✓		
21	**pOH-BTZ**	✓		
22	**pOMe-BTZ**	✓		
23	**pCHO-BTZ**			✓
24	**pCN-BTZ**	✓		
25	**pCF$_3$-BTZ**	✓		
26	**pNO$_2$-BTZ**	✓		

5. Computational Studies

5.1 General Information

All calculations were carried out utilizing the Gaussian16 software,[12] and visualised using GaussView6.[13] Geometry optimisations were conducted utilising the B3LYP[14-18]//cc-pVTZ[19] model chemistry incorporating the SMD solvent model to model a dichloromethane solvent environment; structural minima were verified through the presence of only positive curvature upon vibrational frequency analysis.[20] TD-DFT calculations of the absorption and emission spectra where generated utilising the CAM-B3LYP[21]//cc-pVTZ model chemistry, again incorporating the SMD solvent model through. Calculation of the first 50 excited states (S_1-S_{50}) and the application of a phenomenological broadening factor of 0.15 eV to represent the half width at half height was used to produce each spectra reported here. Additionally, NTO analysis was conducted on states deemed to provide a significant contribution to each absorption peak (oscillator strength of > 0.4); for the absorption range reported here, peaks are comprised primarily of contributions from S_1. The second peak, observed at approx. 275 nm of the absorption spectra but within the reported range of the emission spectra are in turn comprised primarily of S_2 and/or S_3 contributions, which are also reported here. CAM-B3LYP was selected at the functional of choice due to both its agreement with experimentally derived spectra within this work, and its strong performance in similar systems.[22-26] A comparison between the theoretical optimised geometry and reported crystal structures of **pH-BTZ**, **Th-BTZ** and **Tz-BTZ** as representative examples of the entire **BTZ** library is provided in section 5.7. In general, good agreement between the theoretical and experimental structures was observed.

5.2 Theoretical Absorption and Emission Spectra

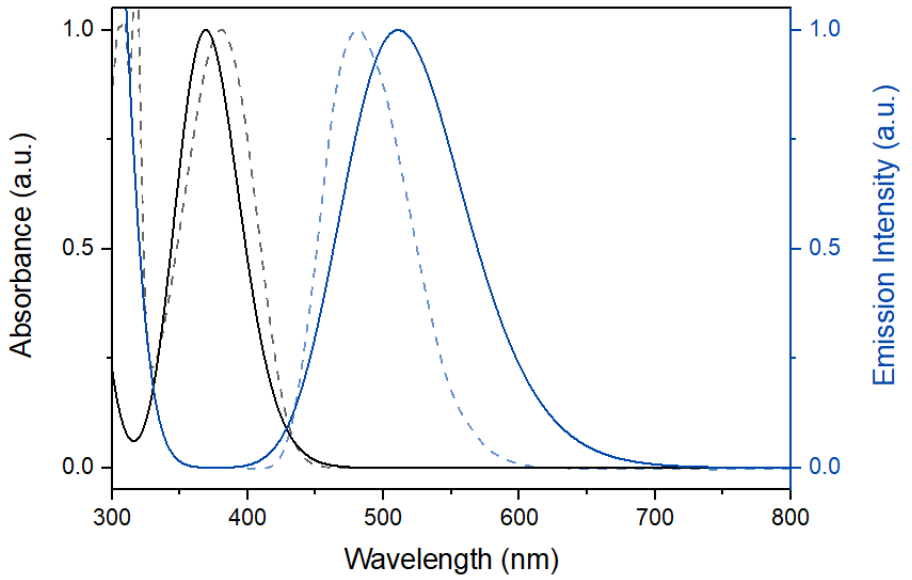

Figure S60 Normalised theoretical absorption (solid black) and emission spectra (solid blue) of **pH-BTZ**. Experimental adsorption and emission spectra are displayed using dashed lines.

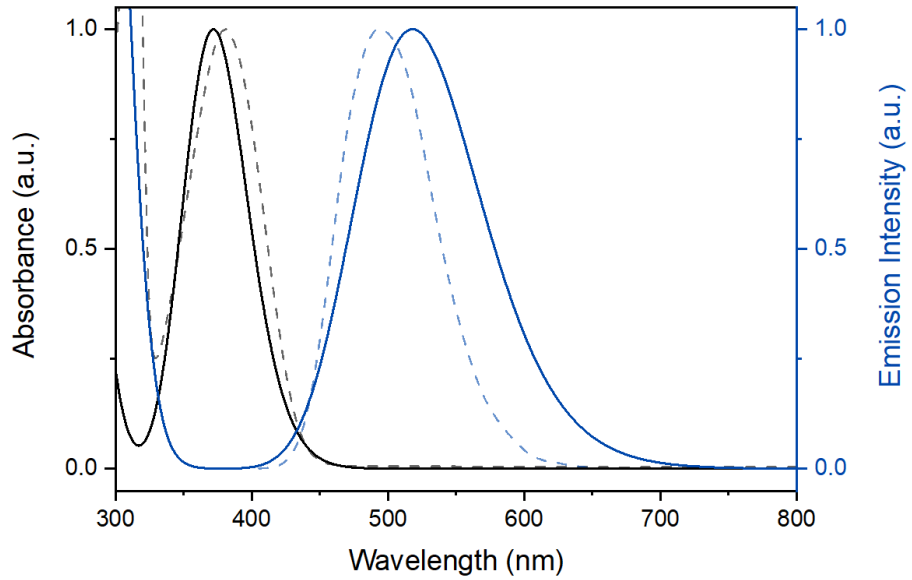

Figure S61 Normalised theoretical absorption (solid black) and emission spectra (solid blue) of **pF-BTZ**. Experimental adsorption and emission spectra are displayed using dashed lines.

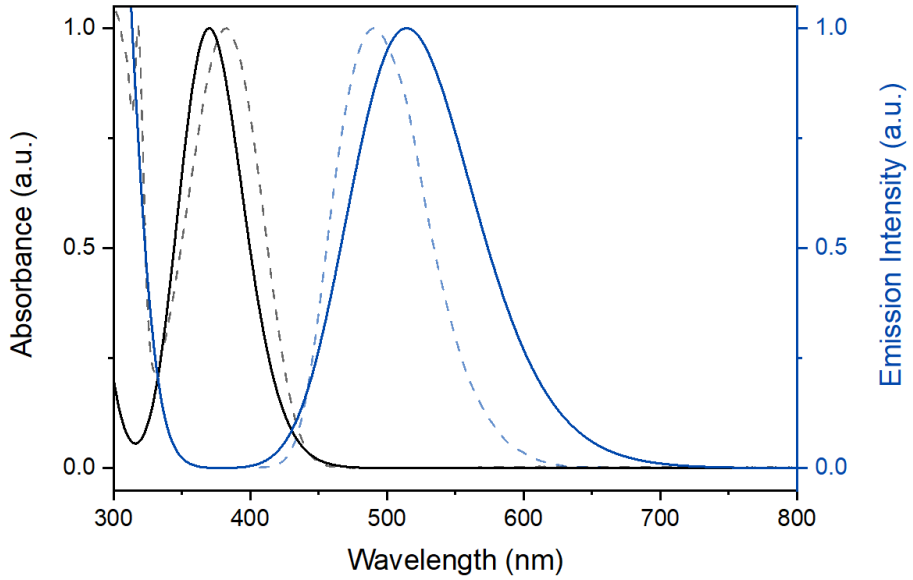

Figure S62 Normalised theoretical absorption (solid black) and emission spectra (solid blue) of **pCl-BTZ**. Experimental adsorption and emission spectra are displayed using dashed lines.

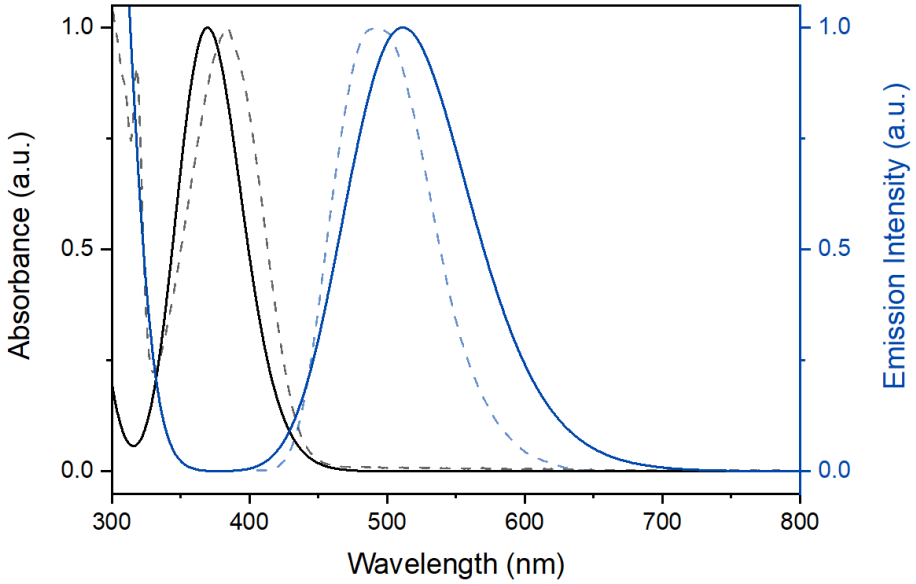

Figure S63 Normalised theoretical absorption (solid black) and emission spectra (solid blue) of **pBr-BTZ**. Experimental adsorption and emission spectra are displayed using dashed lines.

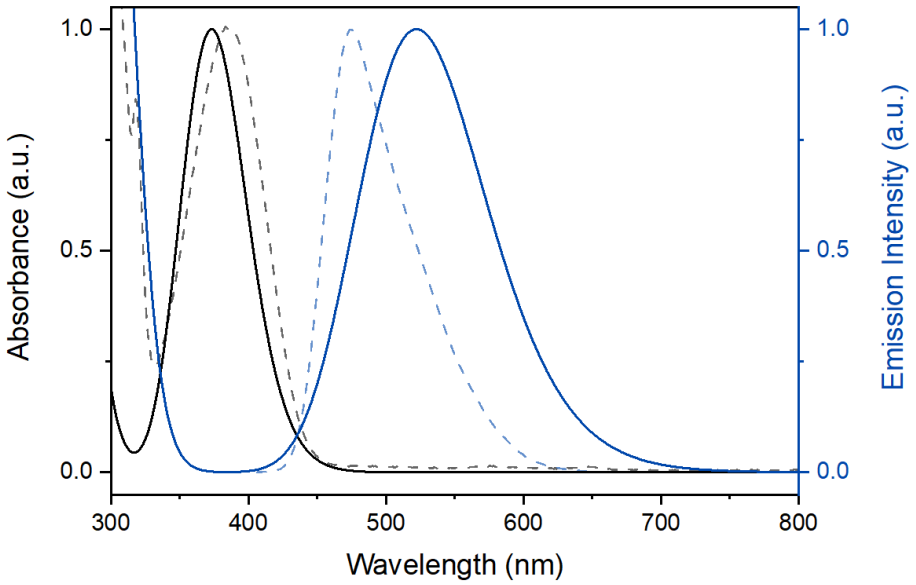

Figure S64 Normalised theoretical absorption (solid black) and emission spectra (solid blue) of **pI-BTZ**. Experimental adsorption and emission spectra are displayed using dashed lines.

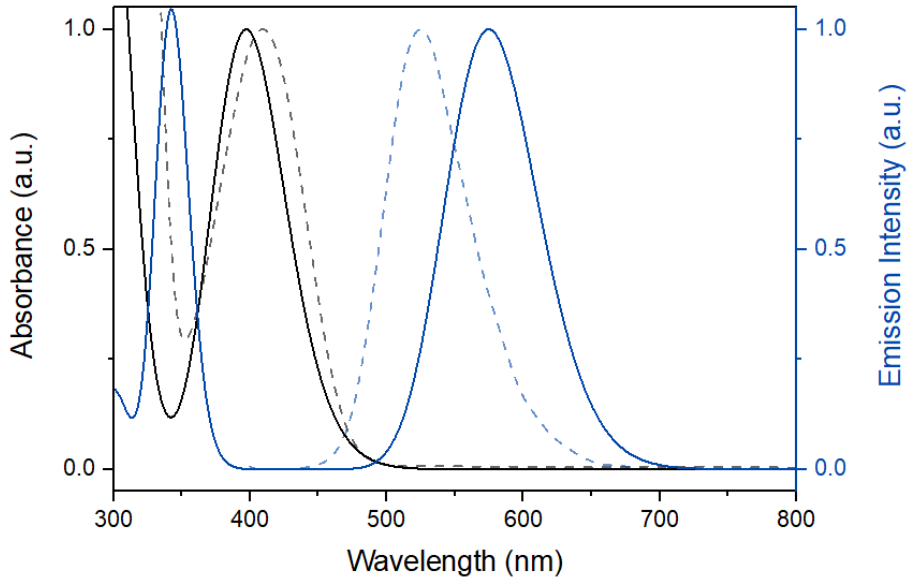

Figure S65 Normalised theoretical absorption (solid black) and emission spectra (solid blue) of **pTh-BTZ**. Experimental adsorption and emission spectra are displayed using dashed lines.

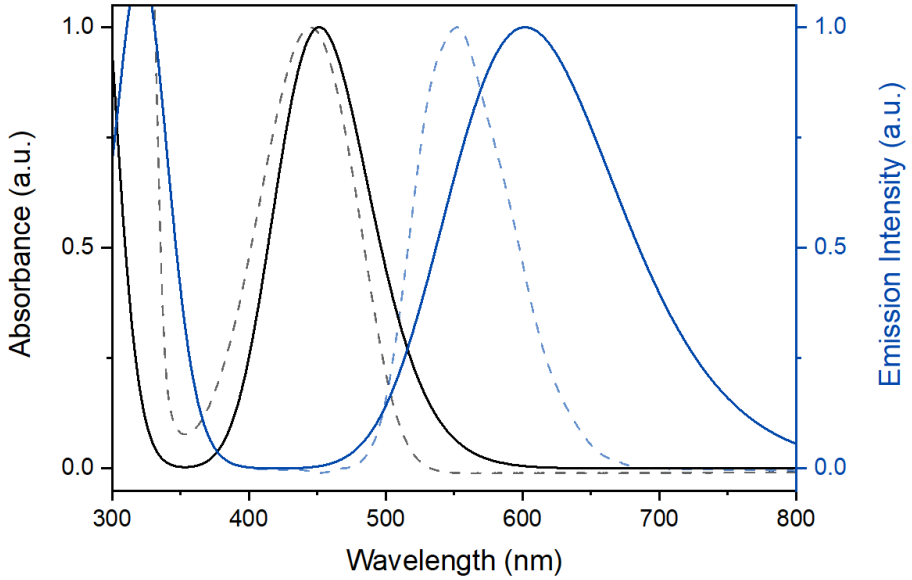

Figure S66 Normalised theoretical absorption (solid black) and emission spectra (solid blue) of **Th-BTZ**. Experimental adsorption and emission spectra are displayed using dashed lines.

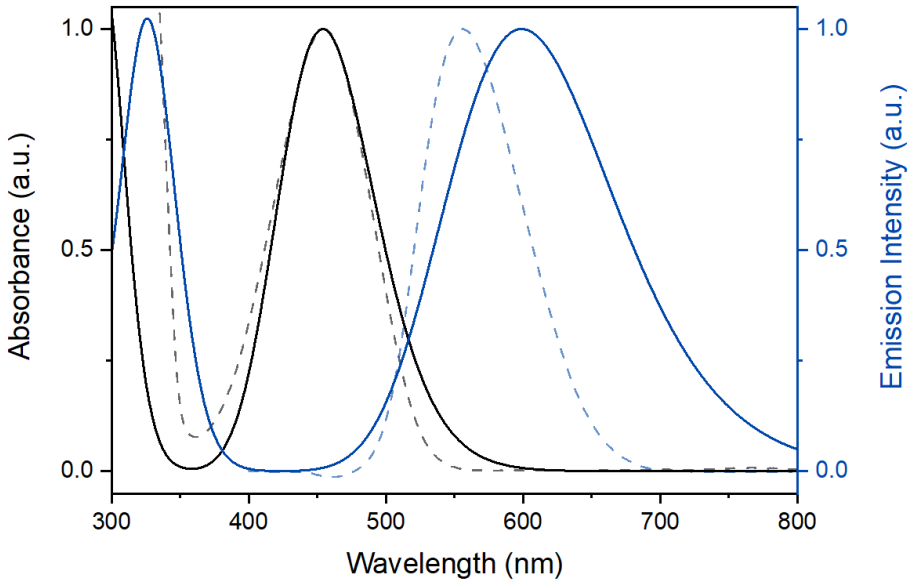

Figure S67 Normalised theoretical absorption (solid black) and emission spectra (solid blue) of **ThBr-BTZ**. Experimental adsorption and emission spectra are displayed using dashed lines.

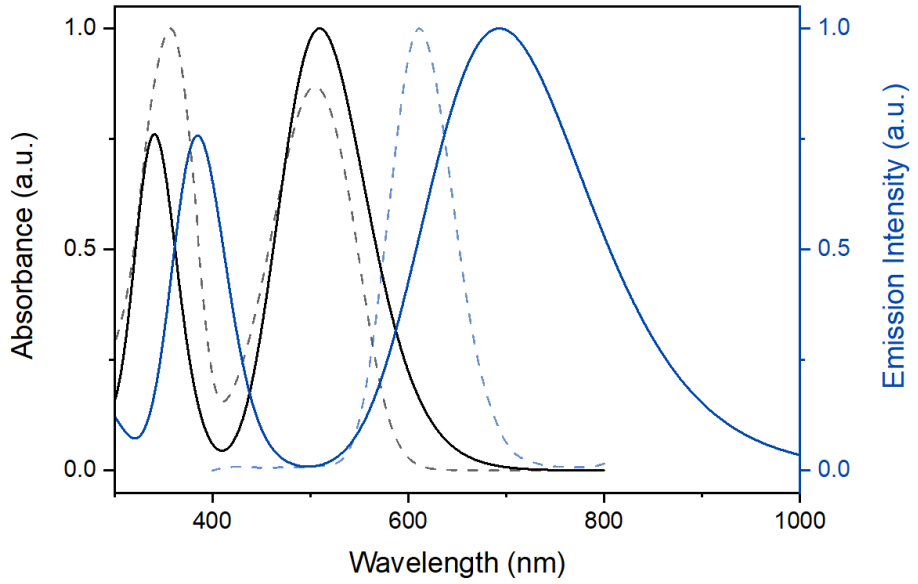

Figure S68 Normalised theoretical absorption (solid black) and emission spectra (solid blue) of **ThTh-BTZ**. Experimental adsorption and emission spectra are displayed using dashed lines.

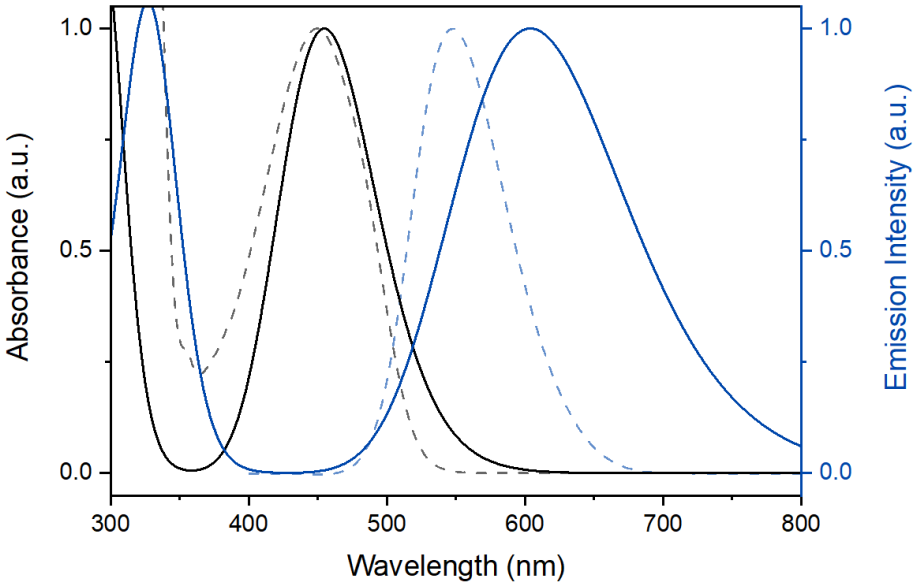

Figure S69 Normalised theoretical absorption (solid black) and emission spectra (solid blue) of **BTh-BTZ**. Experimental adsorption and emission spectra are displayed using dashed lines.

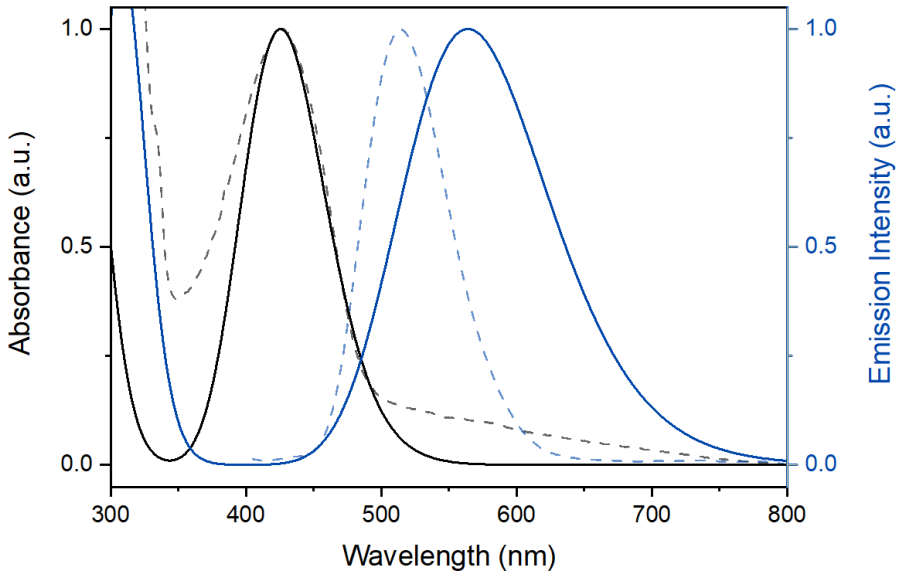

Figure S70 Normalised theoretical absorption (solid black) and emission spectra (solid blue) of **Tz-BTZ**. Experimental adsorption and emission spectra are displayed using dashed lines.

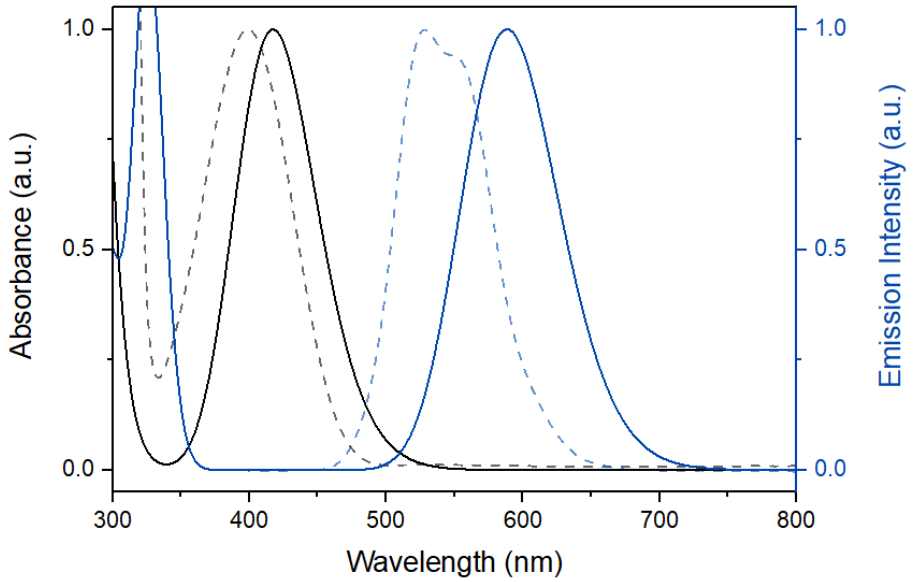

Figure S71 Normalised theoretical absorption (solid black) and emission spectra (solid blue) of **Pyr-BTZ**. Experimental adsorption and emission spectra are displayed using dashed lines.

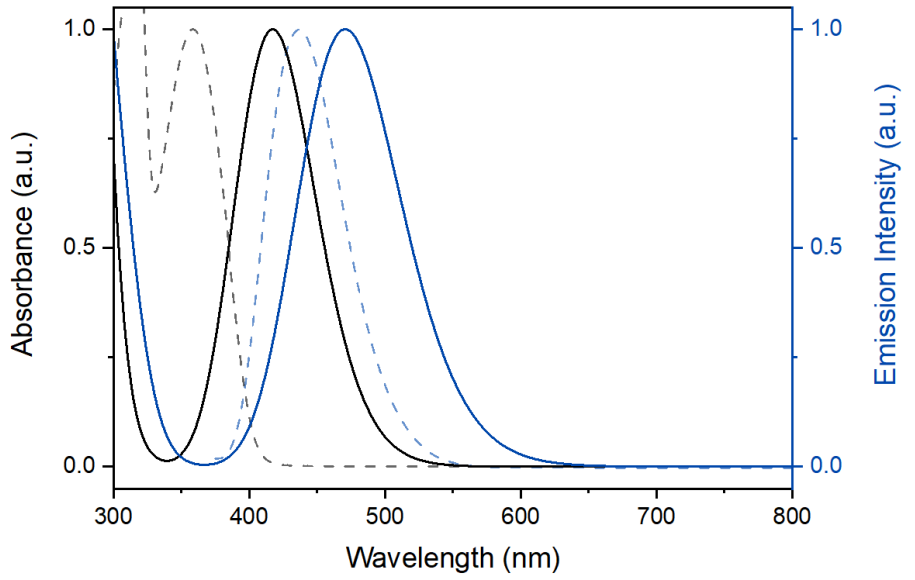

Figure S72 Normalised theoretical absorption (solid black) and emission spectra (solid blue) of **4N-BTZ**. Experimental adsorption and emission spectra are displayed using dashed lines.

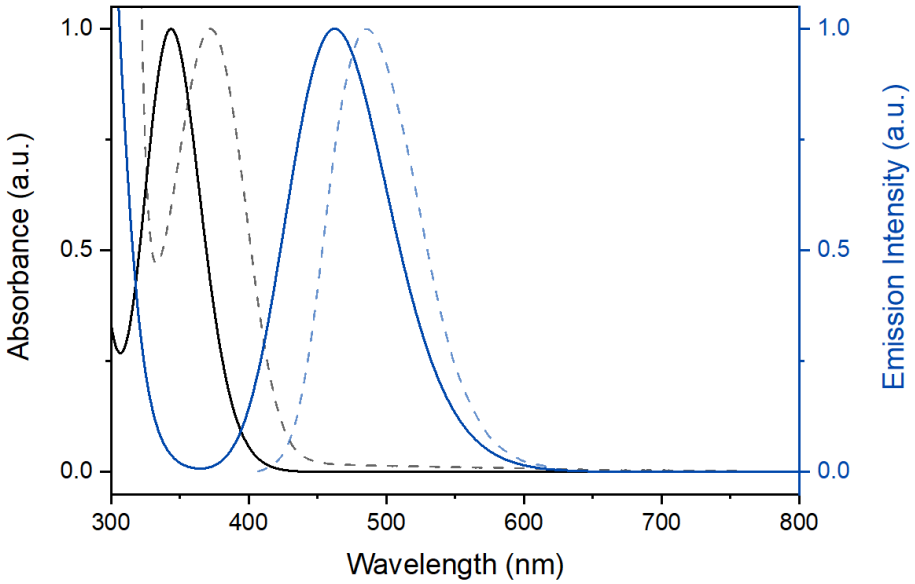

Figure S73 Normalised theoretical absorption (solid black) and emission spectra (solid blue) of **oPh-BTZ**. Experimental adsorption and emission spectra are displayed using dashed lines.

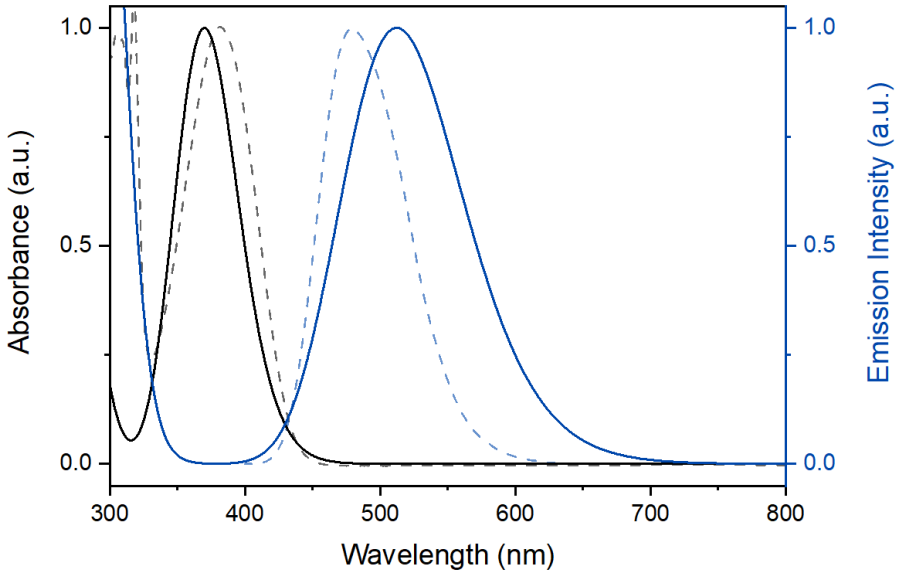

Figure S74 Normalised theoretical absorption (solid black) and emission spectra (solid blue) of **mPh-BTZ**. Experimental adsorption and emission spectra are displayed using dashed lines.

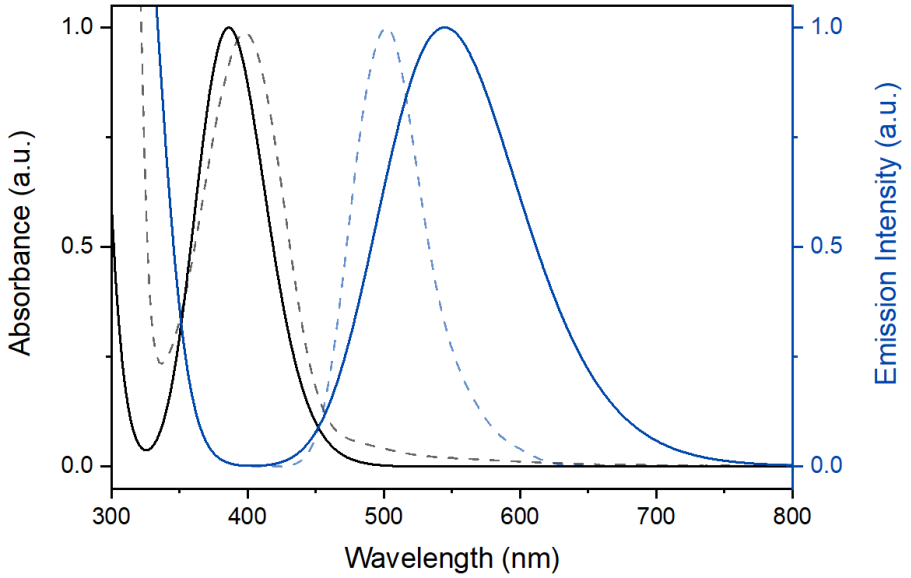

Figure S75 Normalised theoretical absorption (solid black) and emission spectra (solid blue) of **pPh-BTZ**. Experimental adsorption and emission spectra are displayed using dashed lines.

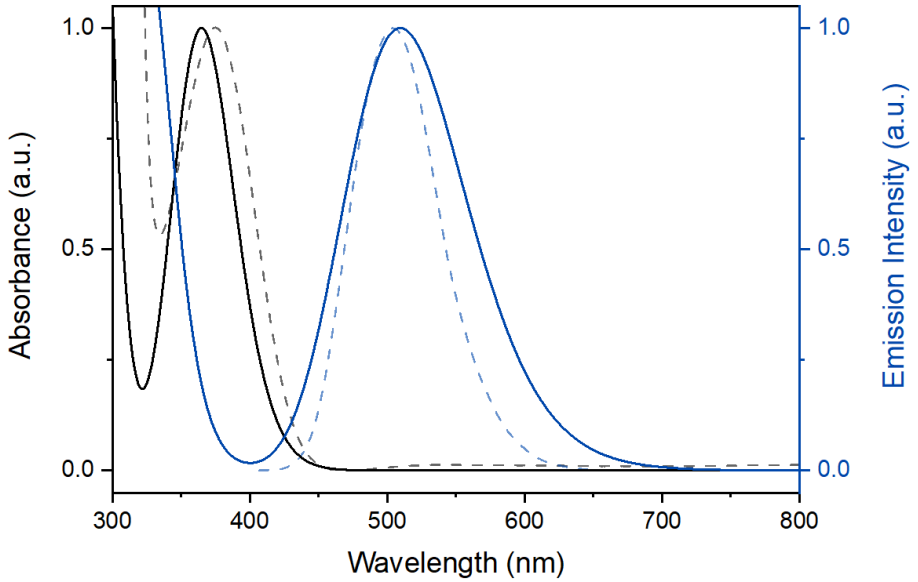

Figure S76 Normalised theoretical absorption (solid black) and emission spectra (solid blue) of **1Nap-BTZ**. Experimental adsorption and emission spectra are displayed using dashed lines.

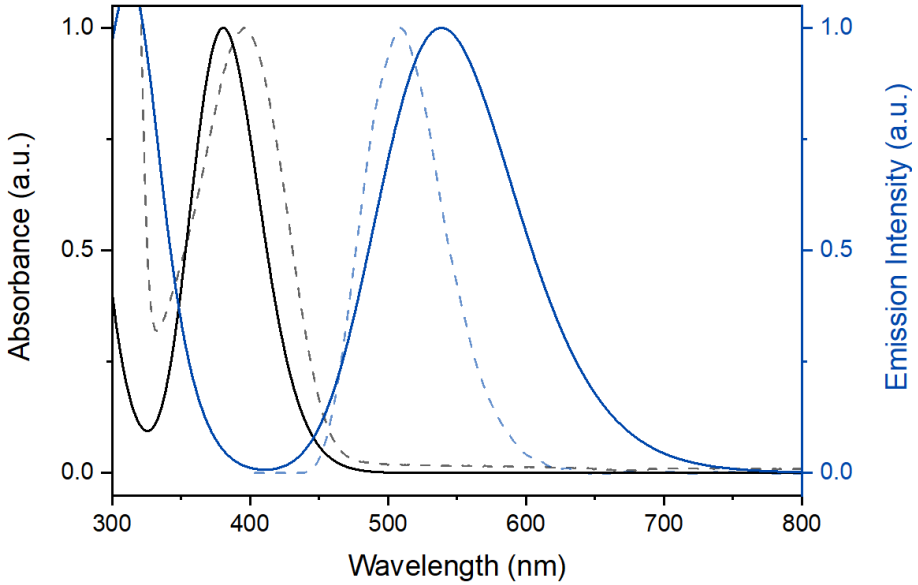

Figure S77 Normalised theoretical absorption (solid black) and emission spectra (solid blue) of **2Nap-BTZ**. Experimental adsorption and emission spectra are displayed using dashed lines.

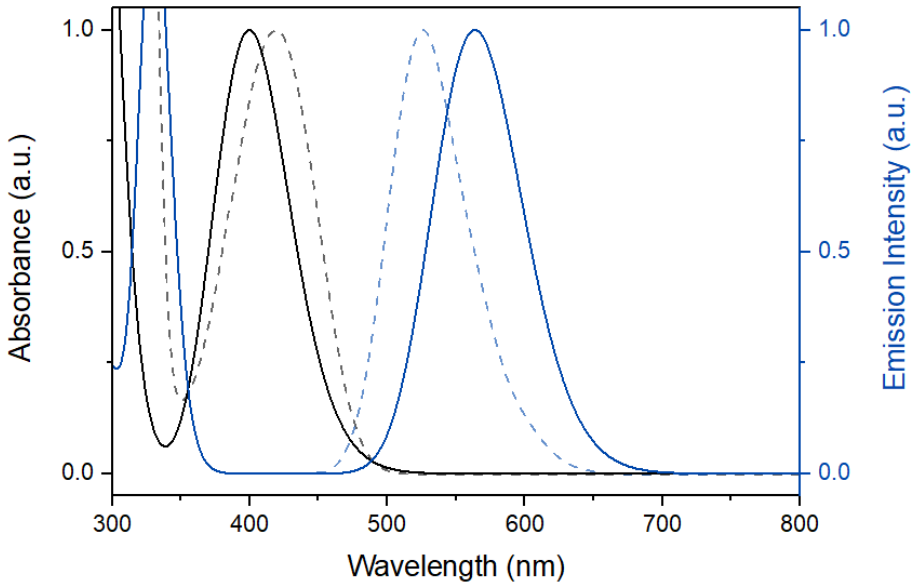

Figure S78 Normalised theoretical absorption (solid black) and emission (solid blue) spectra of **Flu-BTZ**. Experimental adsorption and emission spectra are displayed using dashed lines.

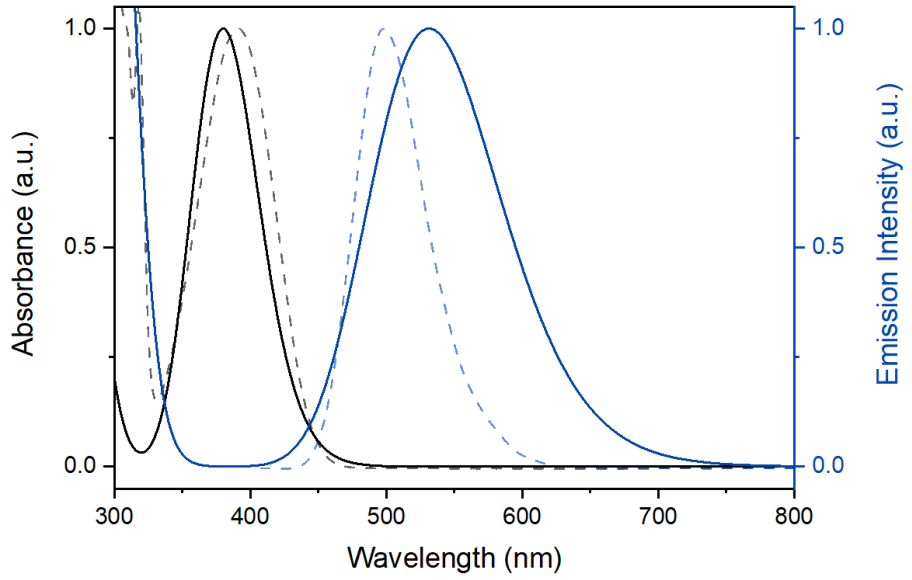

Figure S79 Normalised theoretical absorption (solid black) and emission spectra (solid blue) of **pMe-BTZ**. Experimental adsorption and emission spectra are displayed using dashed lines.

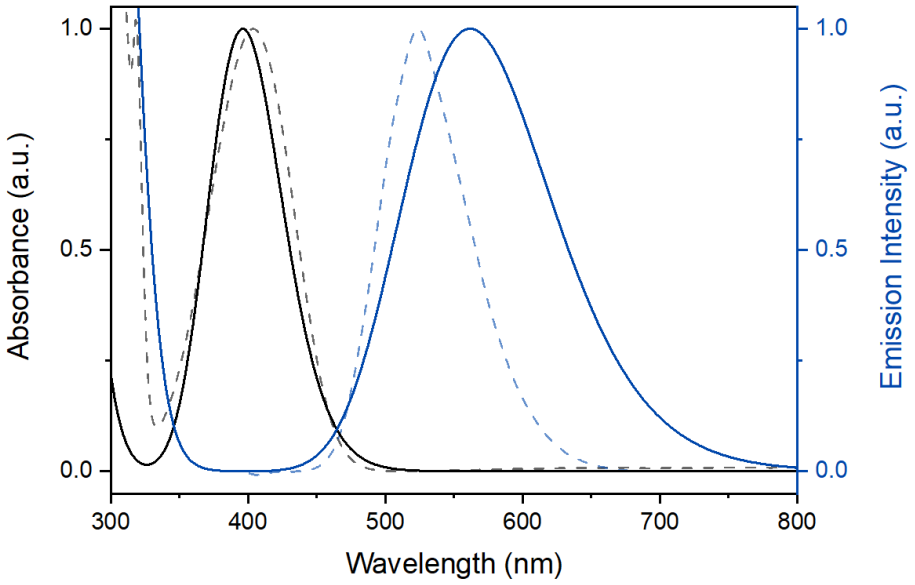

Figure S80 Normalised theoretical absorption (solid black) and emission spectra (solid blue) of **pOH-BTZ**. Experimental adsorption and emission spectra are displayed using dashed lines.

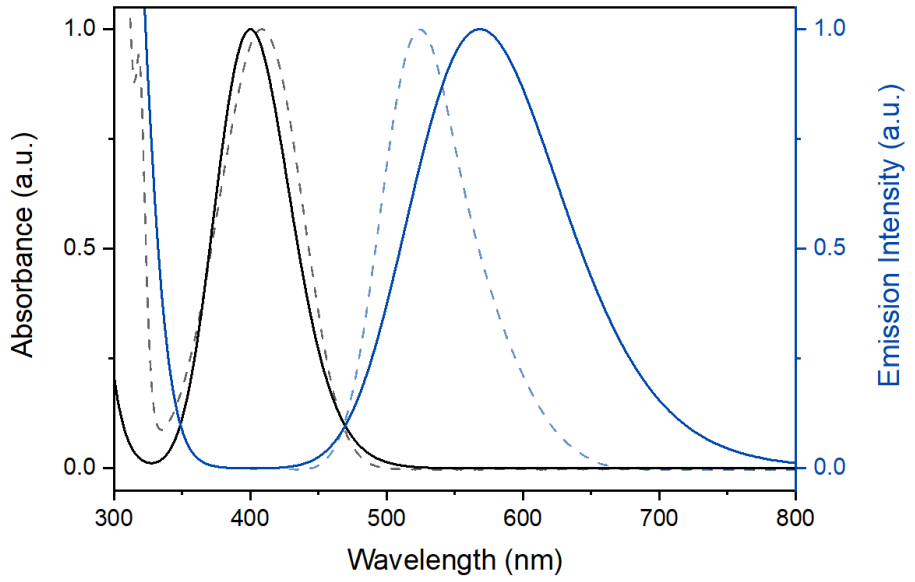

Figure S81 Normalised theoretical absorption (solid black) and emission spectra (solid blue) of **pOMe-BTZ**. Experimental adsorption and emission spectra are displayed using dashed lines.

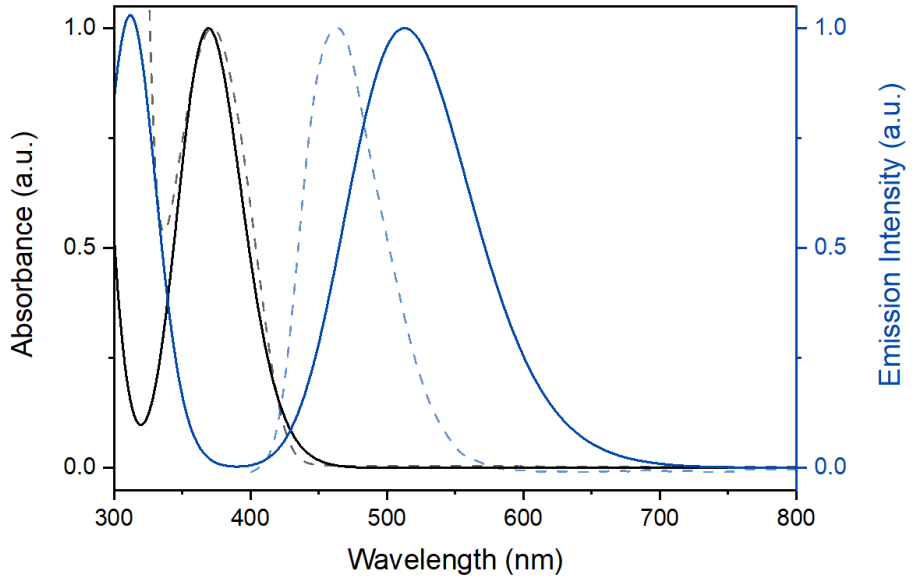

Figure S82 Normalised theoretical absorption (solid black) and emission spectra (solid blue) of **pCHO-BTZ**. Experimental adsorption and emission spectra are displayed using dashed lines.

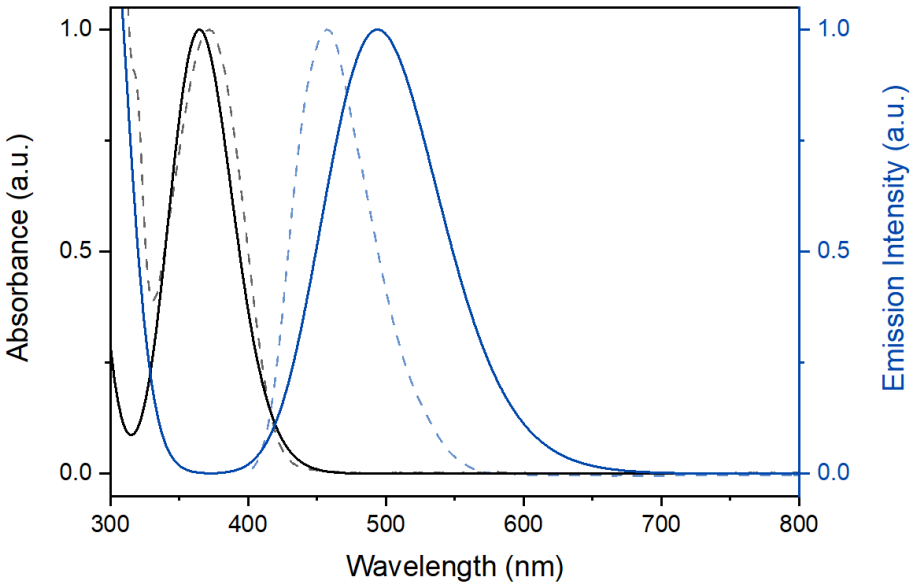

Figure S83 Normalised theoretical absorption (solid black) and emission spectra (solid blue) of **pCN-BTZ**. Experimental adsorption and emission spectra are displayed using dashed lines.

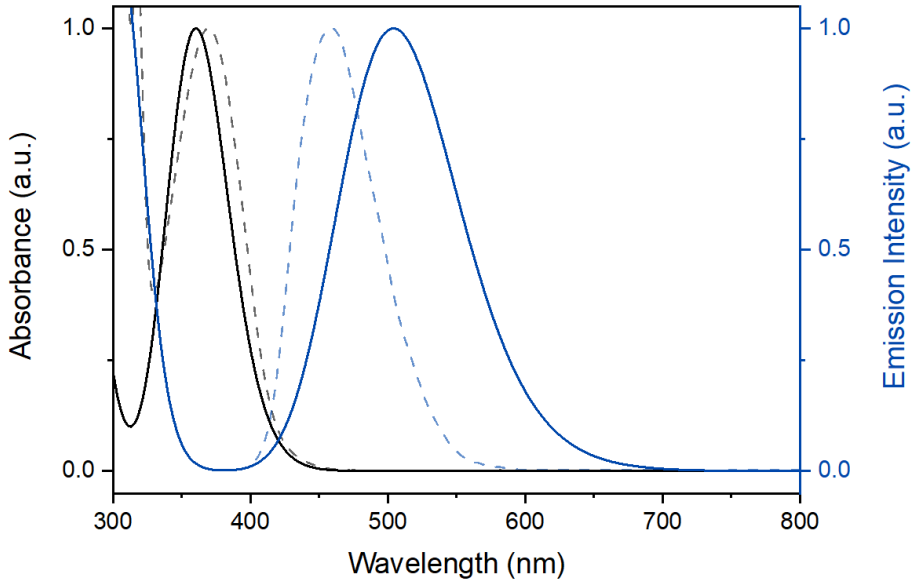

Figure S84 Normalised theoretical absorption (solid black) and emission spectra (solid blue) of **pCF$_3$-BTZ**. Experimental adsorption and emission spectra are displayed using dashed lines.

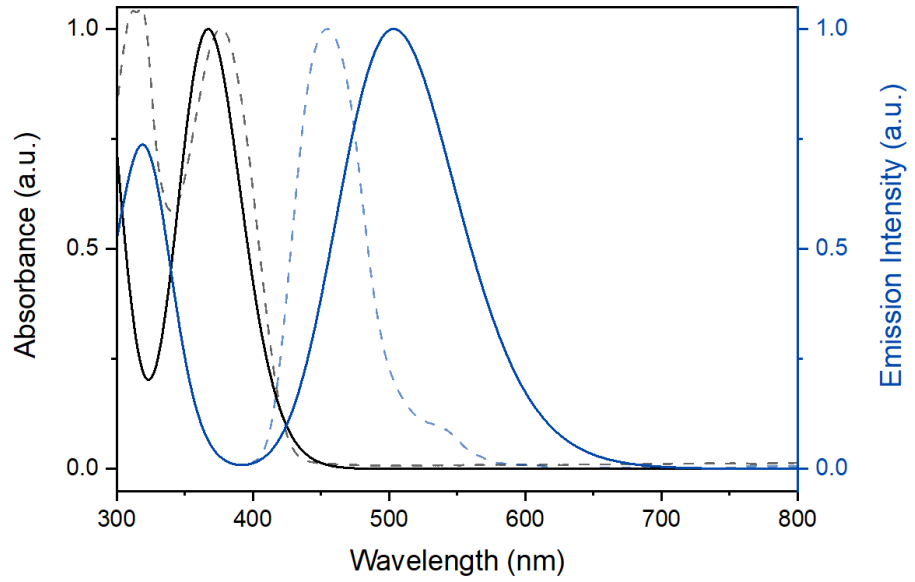

Figure S85 Normalised theoretical absorption (solid black) and emission spectra (solid blue) of **pNO$_2$-BTZ**. Experimental adsorption and emission spectra are displayed using dashed lines.

5.3 Summary of Results

Table S4 Summary of the theoretical absorption and emission properties of the **BTZ** photocatalysts.

Entry	Compound	λ_{abs}/ nm	λ_{em}/ nm	Stokes Shift/ nm
1	**pH-BTZ**	369	511	142
2	**pF-BTZ**	372	518	146
3	**pCl-BTZ**	370	514	144
4	**pBr-BTZ**	370	511	141
5	**pI-BTZ**	373	522	149
6	**pTh-BTZ**	397	575	178
7	**Th-BTZ**	451	602	151
8	**ThBr-BTZ**	454	599	145
9	**ThTh-BTZ**	510	693	183
10	**BTh-BTZ**	455	604	149
11	**Tz-BTZ**	426	564	138
12	**Pyr-BTZ**	417	588	171
13	**4N-BTZ**	351	471	120
14	**oPh-BTZ**	344	463	119
15	**mPh-BTZ**	370	512	142
16	**pPh-BTZ**	386	545	159
17	**1Nap-BTZ**	365	510	145
18	**2Nap-BTZ**	381	539	158
19	**Flu-BTZ**	400	564	164
20	**pMe-BTZ**	380	531	151
21	**pOH-BTZ**	396	562	166
22	**pOMe-BTZ**	400	568	168
23	**pCHO-BTZ**	369	513	144
24	**pCN-BTZ**	365	494	129
25	**pCF$_3$-BTZ**	360	504	144
26	**pNO$_2$-BTZ**	367	503	136

5.4 Excited State Orbitals

Table S5 Hole and particle natural transition orbitals calculated for **pH-BTZ**.

State	Energy (nm) [contribution]	Hole Orbital	Particle Orbital
S_1	371 [0.98888]	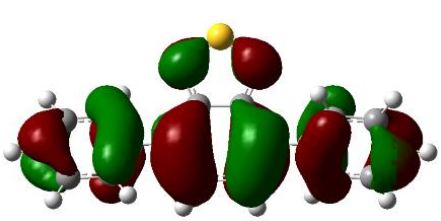	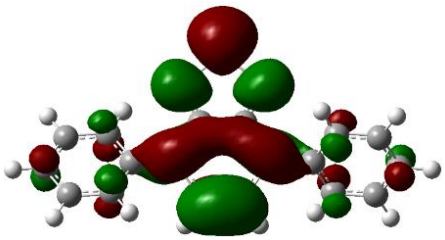
S_2	279 [0.90336]	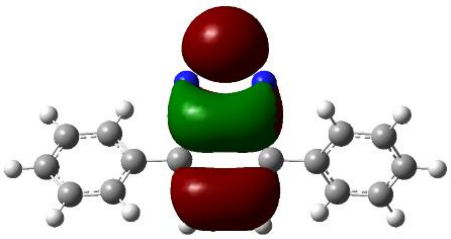	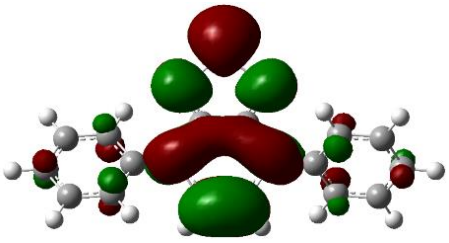
S_6	252 [0.63181]	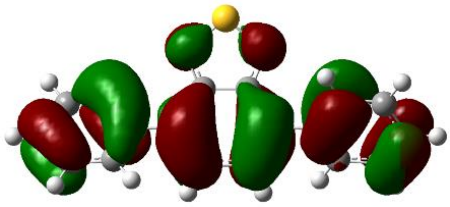	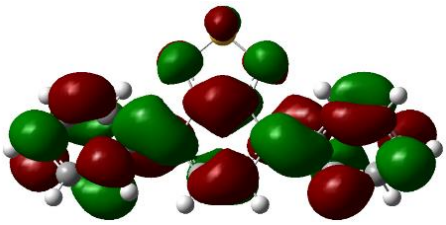

Table S6 Hole and particle natural transition orbitals calculated for **pF-BTZ**.

State	Energy (nm) [contribution]	Hole Orbital	Particle Orbital
S_1	375 [0.98950]	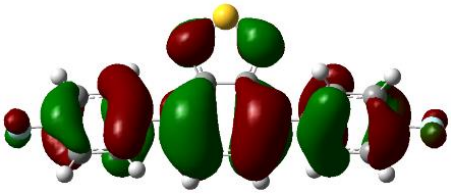	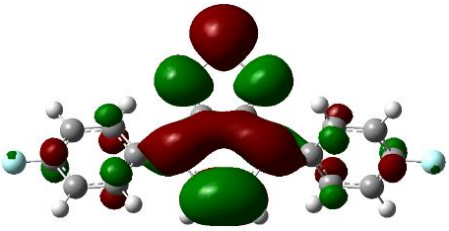
S_2	279 [0.90172]	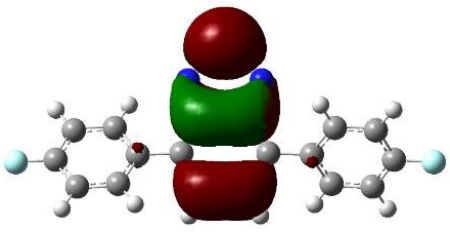	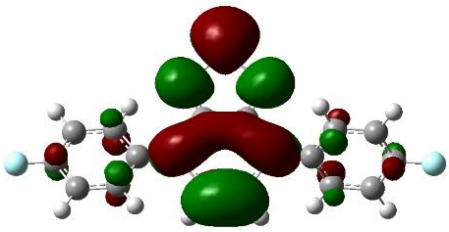
S_4	252 [0.85149]	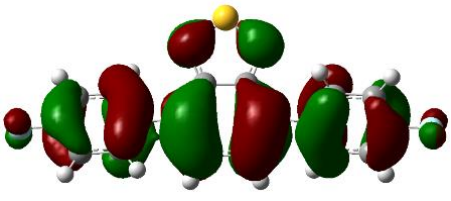	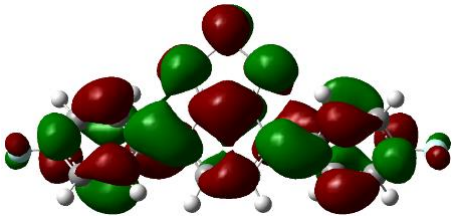

Table S7 Hole and particle natural transition orbitals calculated for **pCl-BTZ**.

State	Energy (nm) [contribution]	Hole Orbital	Particle Orbital
S_1	373 [0.98749]	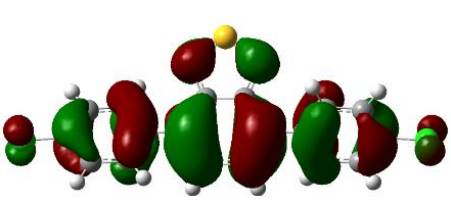	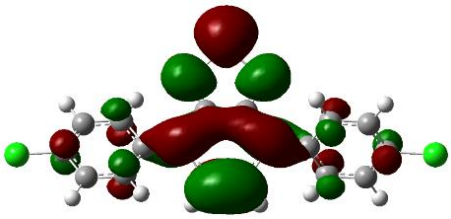
S_2	280 [0.90270]	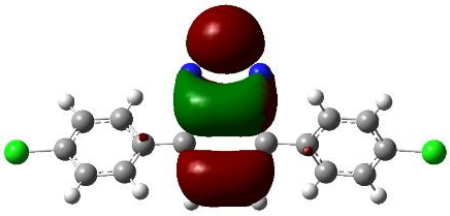	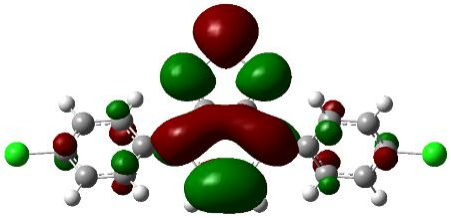
S_4	258 [0.86568]	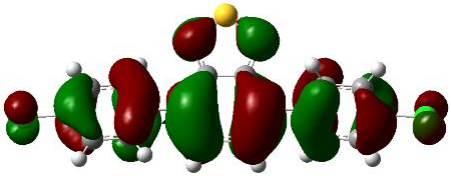	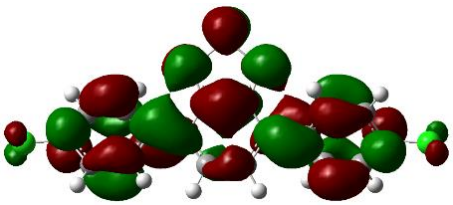

Table S8 Hole and particle natural transition orbitals calculated for **pBr-BTZ**.

State	Energy (nm) [contribution]	Hole Orbital	Particle Orbital
S_1	373 [0.98695]	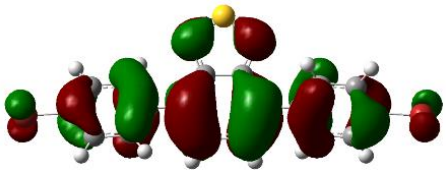	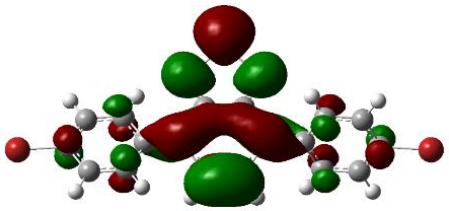
S_2	280 [0.90281]	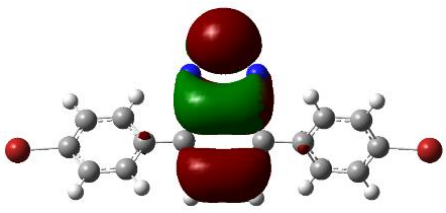	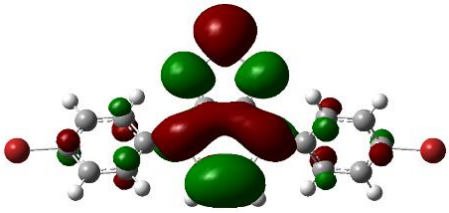
S_4	258 [0.85349]	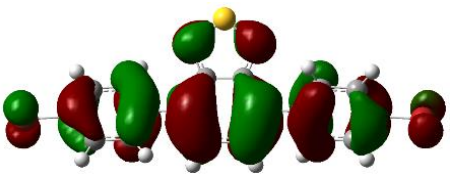	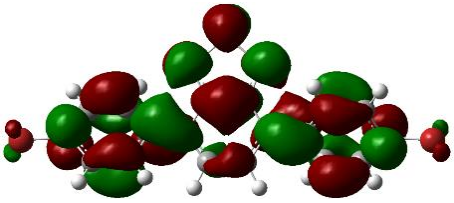

Table S9 Hole and particle natural transition orbitals calculated for **pI-BTZ**.

State	Energy (nm) [contribution]	Hole Orbital	Particle Orbital
S_1	376 [0.98527]	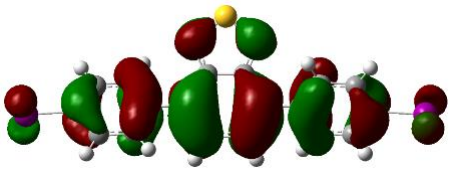	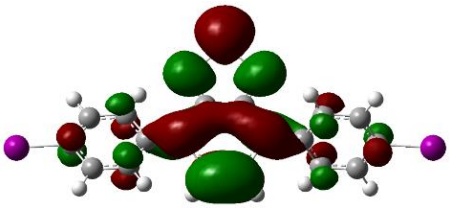
S_2	281 [0.90121]	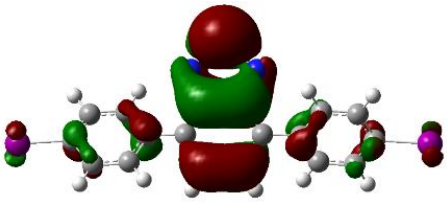	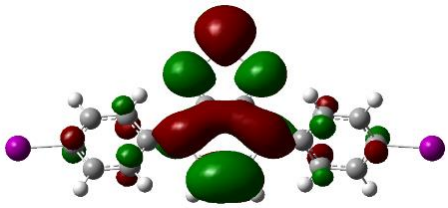
S_6	261 [0.55618]	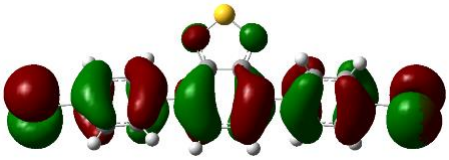	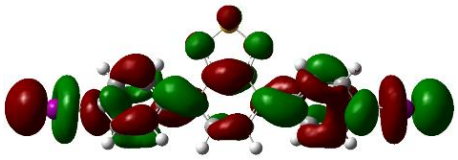

Table S10 Hole and particle natural transition orbitals calculated for **pTh-BTZ**.

State	Energy (nm) [contribution]	Hole Orbital	Particle Orbital
S_1	400 [0.96780]	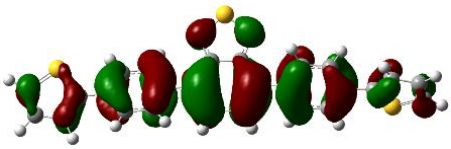	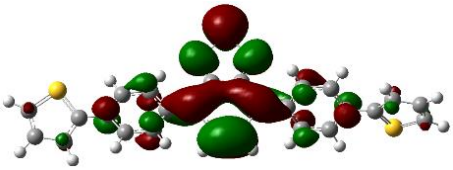
S_3	297 [0.65703]	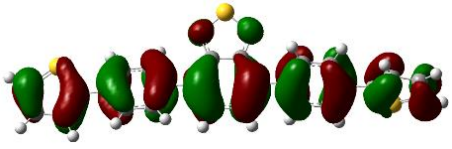	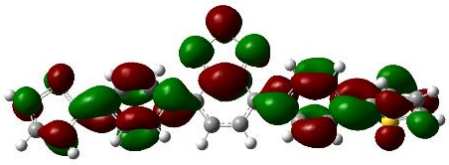

Table S11 Hole and particle natural transition orbitals calculated for **Th-BTZ**.

State	Energy (nm) [contribution]	Hole Orbital	Particle Orbital
S_1	452 [0.98710]	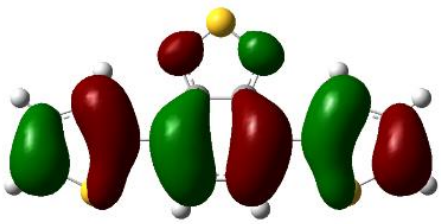	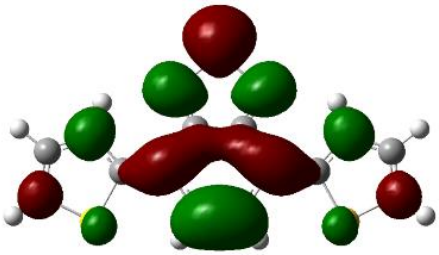
S_3	288 [0.91296]	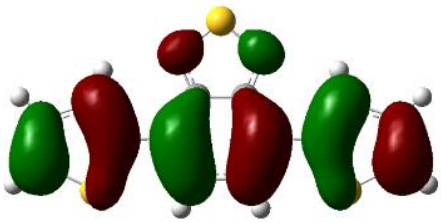	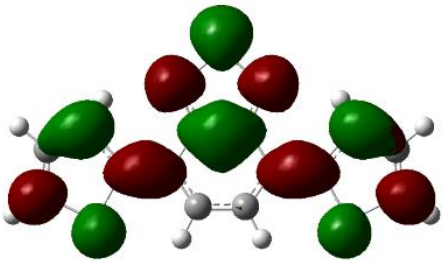

Table S12 Hole and particle natural transition orbitals calculated for **ThBr-BTZ**.

State	Energy (nm) [contribution]	Hole Orbital	Particle Orbital
S_1	455 [0.98426]	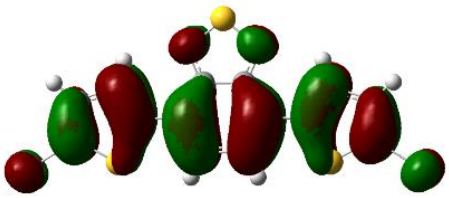	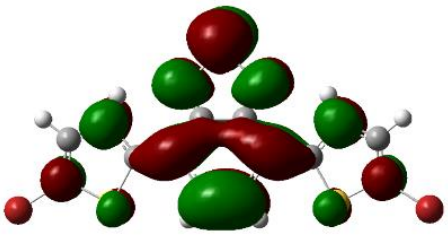
S_3	294 [0.91953]	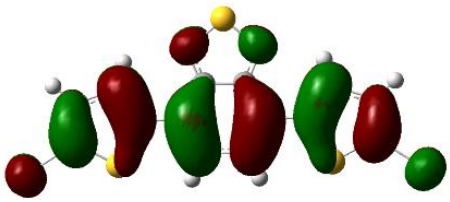	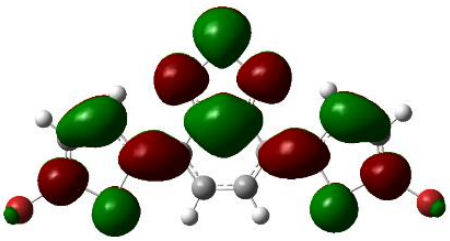

Table S13 Hole and particle natural transition orbitals calculated for **ThTh-BTZ**.

State	Energy (nm) [contribution]	Hole Orbital	Particle Orbital
S_1	518 [0.96385]	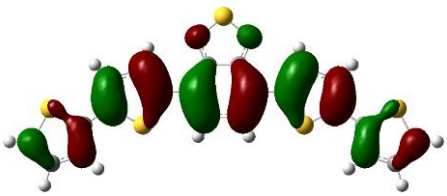	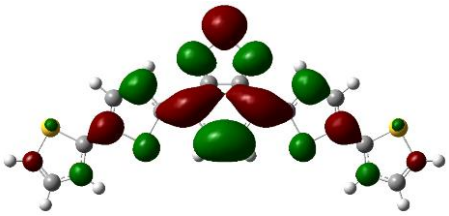
S_3	343 [0.81966]	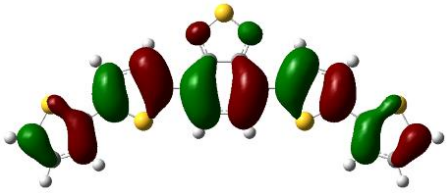	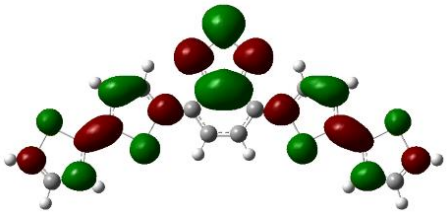

Table S14 Hole and particle natural transition orbitals calculated for **BTh-BTZ**.

State	Energy (nm) [contribution]	Hole Orbital	Particle Orbital
S_1	455 [0.98316]	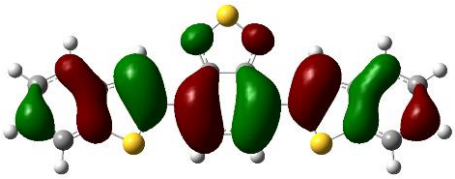	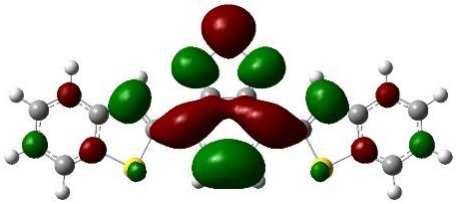
S_5	295 [0.90550]	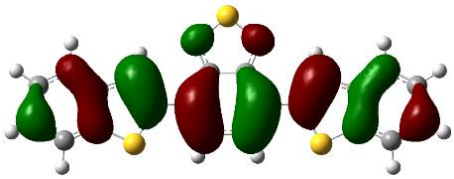	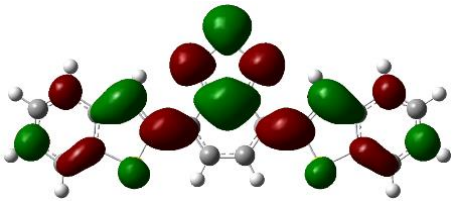

Table S15 Hole and particle natural transition orbitals calculated for **Tz-BTZ**.

State	Energy (nm) [contribution]	Hole Orbital	Particle Orbital
S_1	426 [0.98507]	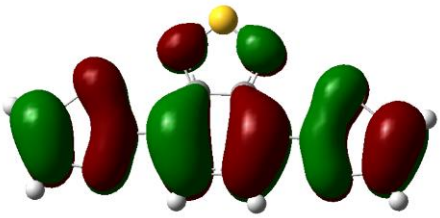	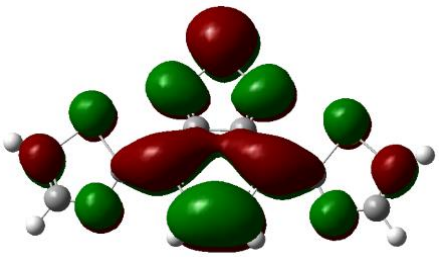
S_4	278 [0.87194]	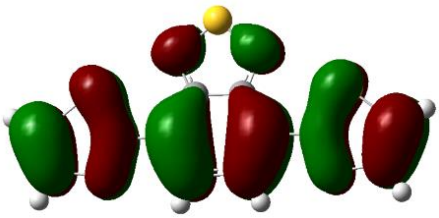	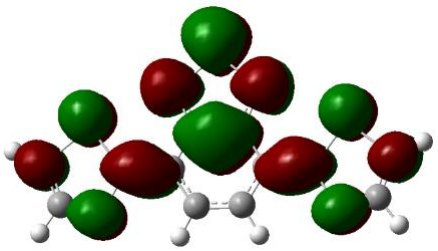

Table S16 Hole and particle natural transition orbitals calculated for **Pyr-BTZ**.

State	Energy (nm) [contribution]	Hole Orbital	Particle Orbital
S_1	419 [0.98796]	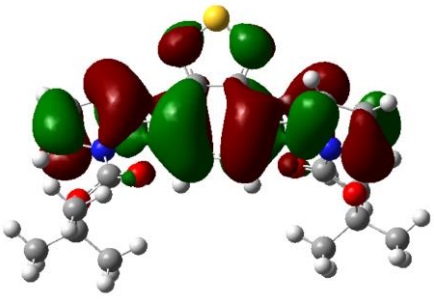	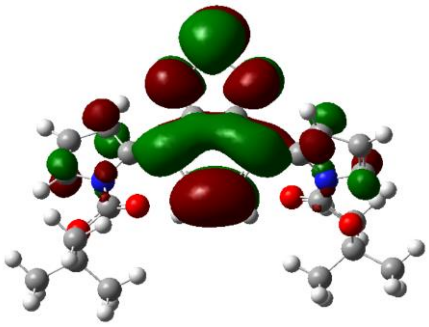
S_3	283 [0.88202]	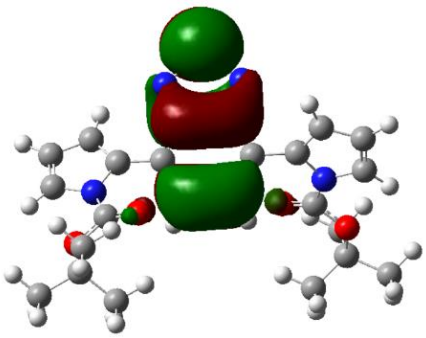	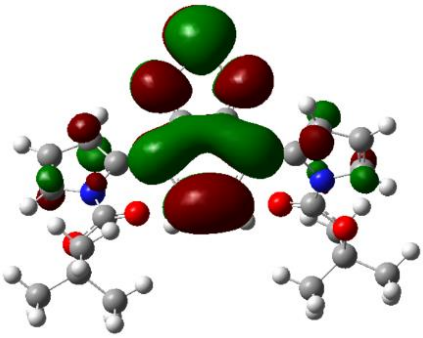
S_4	281 [0.88290]	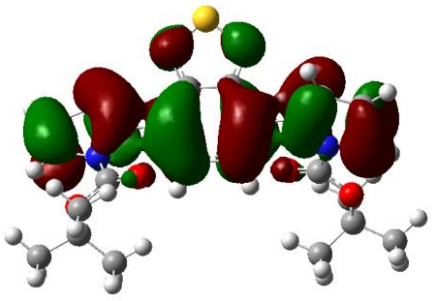	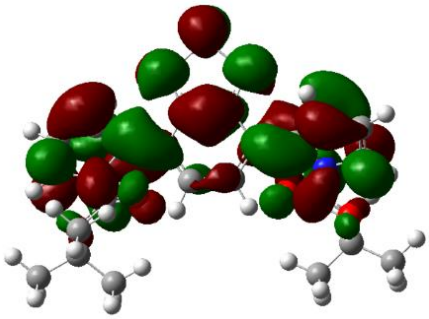

Table S17 Hole and particle natural transition orbitals calculated for **4N-BTZ**.

State	Energy (nm) [contribution]	Hole Orbital	Particle Orbital
S_1	351 [0.98742]	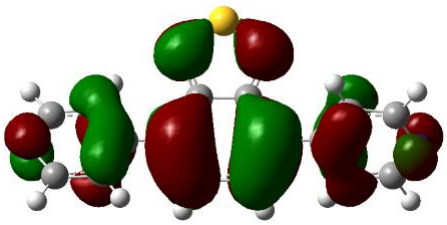	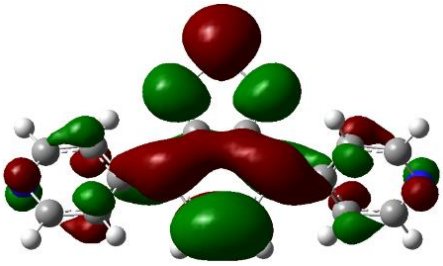
S_2	265 [0.91486]	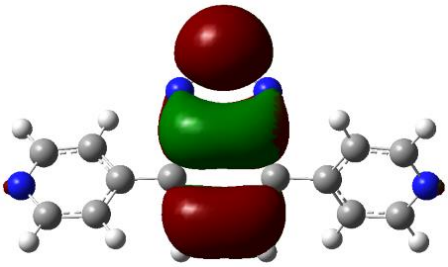	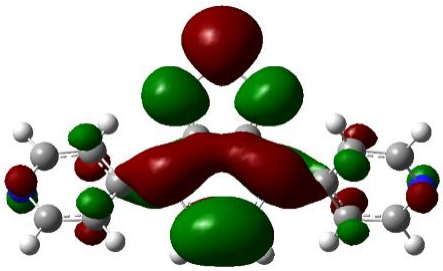
S_7	250 [0.83431]	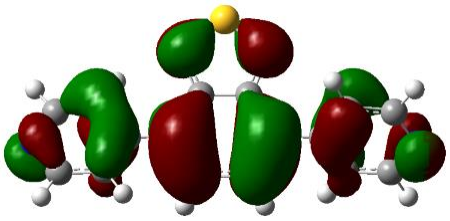	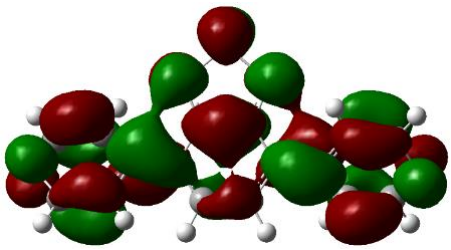

Table S18 Hole and particle natural transition orbitals calculated for **oPh-BTZ**.

State	Energy (nm) [contribution]	Hole Orbital	Particle Orbital
S_1	346 [0.98655]	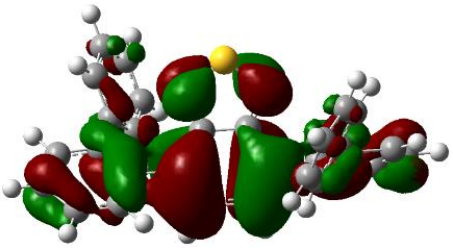	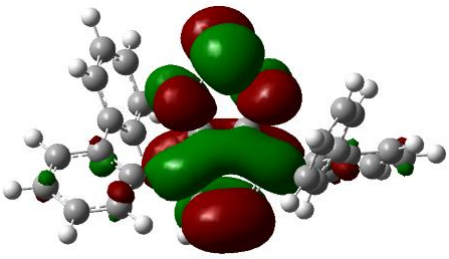
S_2	287 [0.95319]	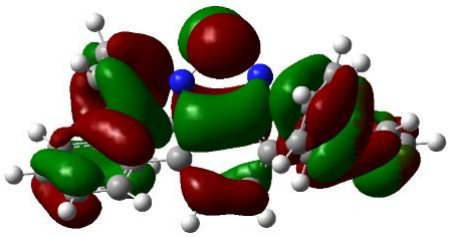	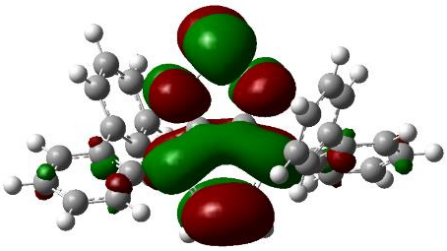
S_4	275 [0.92758]	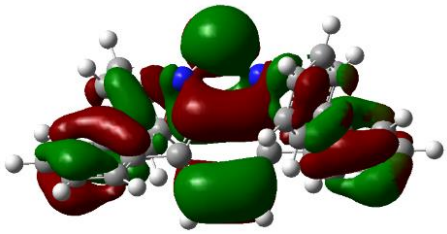	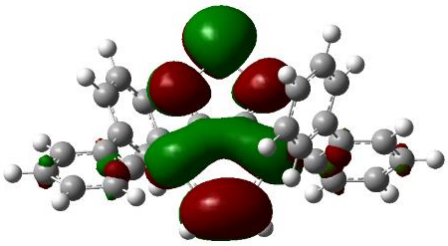

Table S19 Hole and particle natural transition orbitals calculated for **mPh-BTZ**.

State	Energy (nm) [contribution]	Hole Orbital	Particle Orbital
S_1	371 [0.98725]	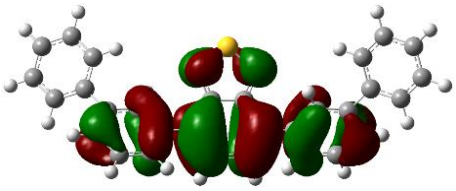	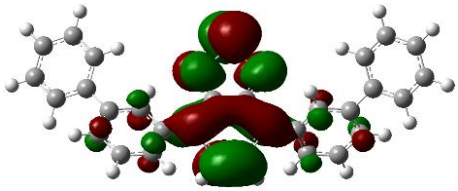
S_4	279 [0.91579]	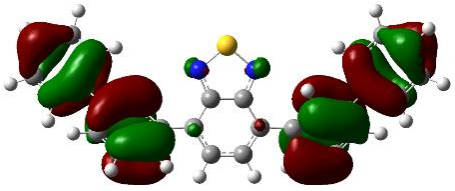	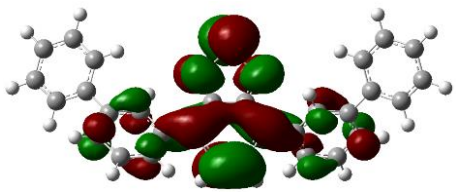
S_6	253 [0.85144]	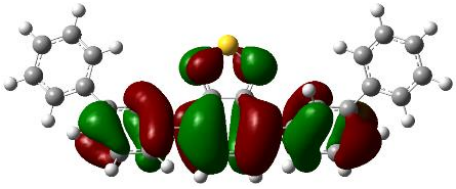	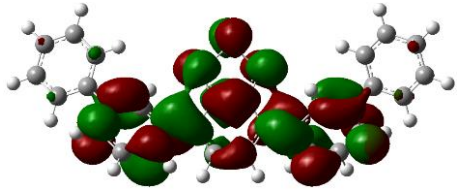
S_8	245 [0.58482]	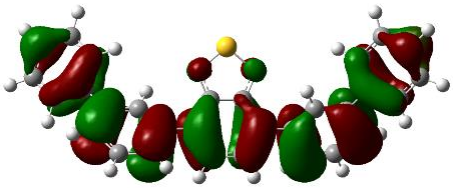	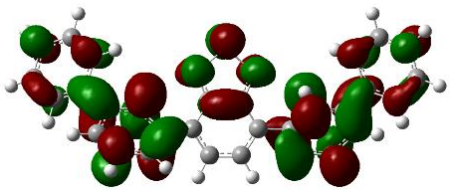
S_{10}	240 [0.47136]	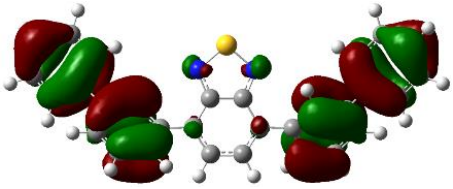	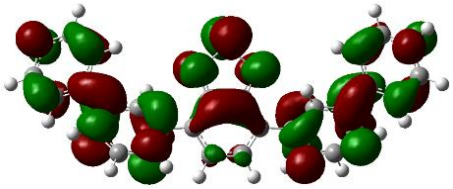

Table S20 Hole and particle natural transition orbitals calculated for **pPh-BTZ**.

State	Energy (nm) [contribution]	Hole Orbital	Particle Orbital
S_1	386. [0.97952]	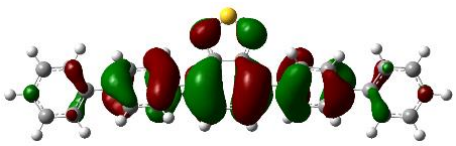	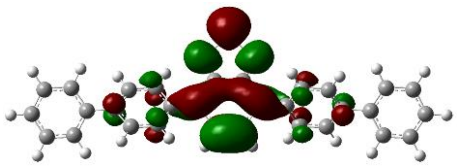
S_4	276 [0.72245]	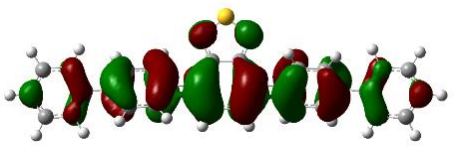	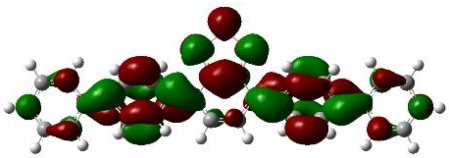

Table S21 Hole and particle natural transition orbitals calculated for **1Nap-BTZ**.

State	Energy (nm) [contribution]	Hole Orbital	Particle Orbital
S_1	370 [0.98283]	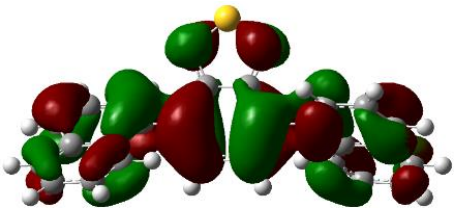	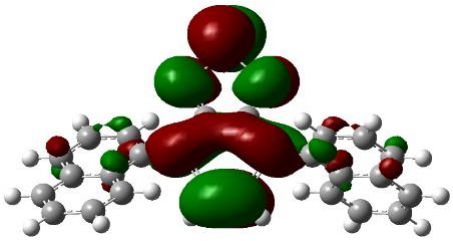
S_3	286 [0.57896]	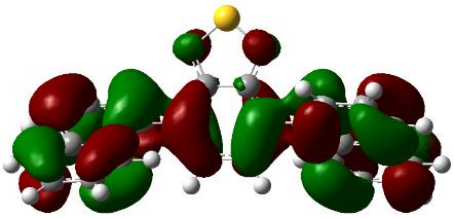	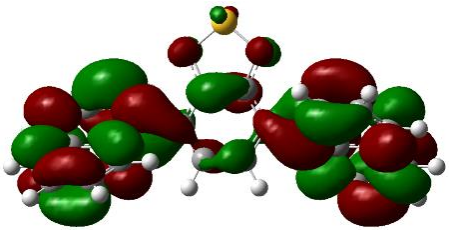
S_4	281 [0.51573]	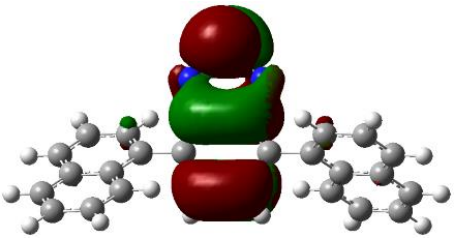	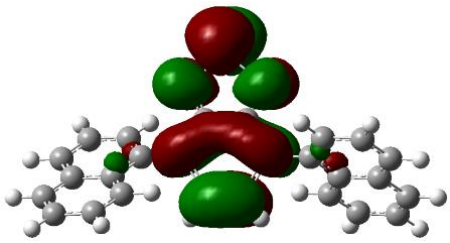
S_5	276 [0.84560]	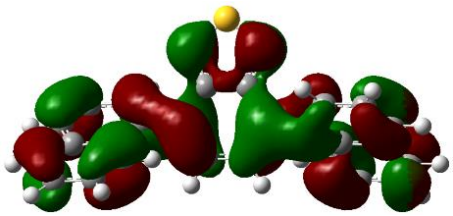	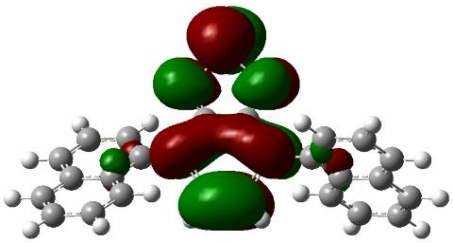

Table S22 Hole and particle natural transition orbitals calculated for **2Nap-BTZ**.

State	Energy (nm) [contribution]	Hole Orbital	Particle Orbital
S_1	382 [0.98144]	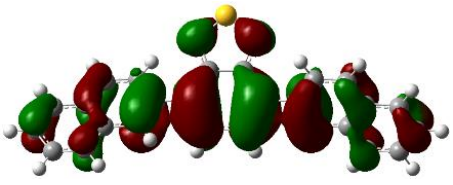	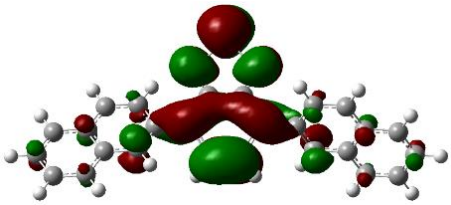
S_{10}	250 [0.44266]	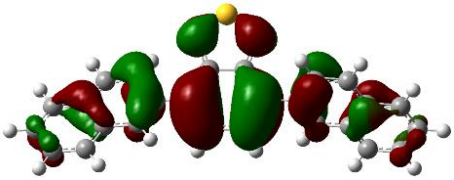	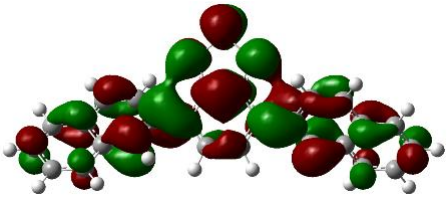

Table S23 Hole and particle natural transition orbitals calculated for **Flu-BTZ**. Note, **Flu-BTZ** was modelled with ethyl groups instead of *n*-octyl groups to reduce the cost of the computational calculation.

State	Energy (nm) [contribution]	Hole Orbital	Particle Orbital
S_1	403 [0.97537]	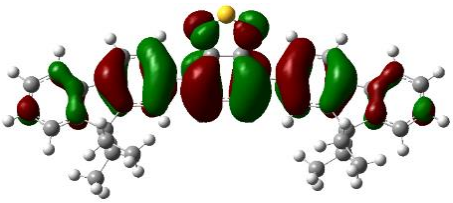	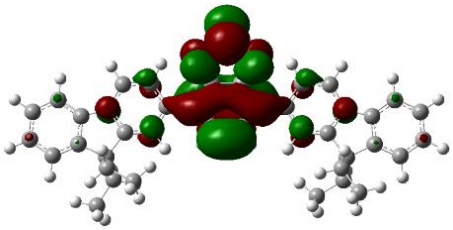
S_{10}	290 [0.70843]	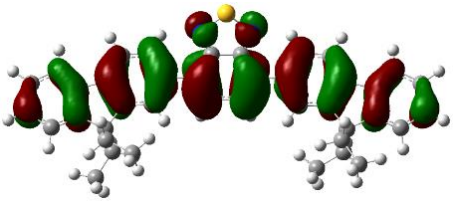	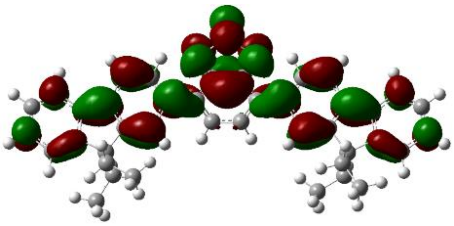

Table S24 Hole and particle natural transition orbitals calculated for **pMe-BTZ**.

State	Energy (nm) [contribution]	Hole Orbital	Particle Orbital
S_1	382 [0.98883]	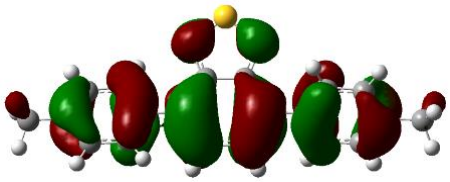	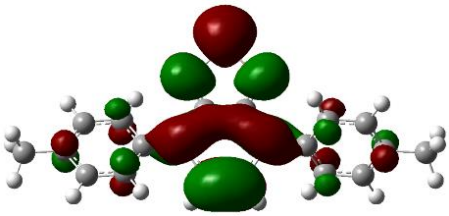
S_5	257 [0.78635]	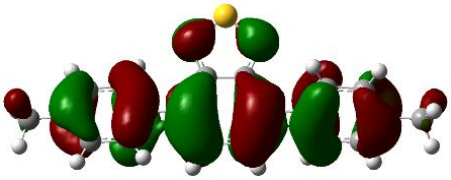	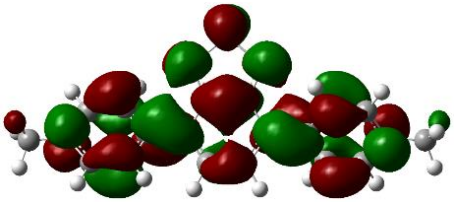

Table S25 Hole and particle natural transition orbitals calculated for **pOH-BTZ**.

State	Energy (nm) [contribution]	Hole Orbital	Particle Orbital
S_1	399 [0.99014]	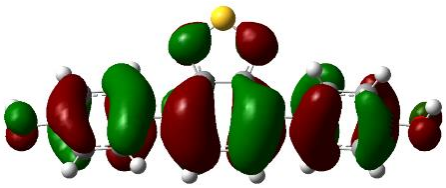	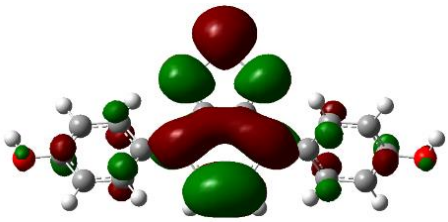
S_4	260 [0.74570]	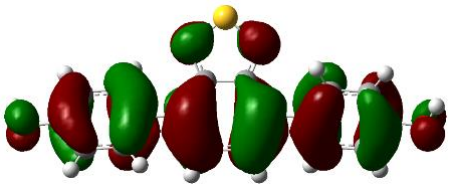	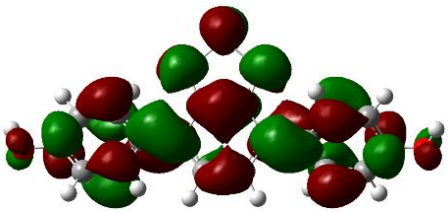

Table S26 Hole and particle natural transition orbitals calculated for **pOMe-BTZ**.

State	Energy (nm) [contribution]	Hole Orbital	Particle Orbital
S_1	402 [0.98951]	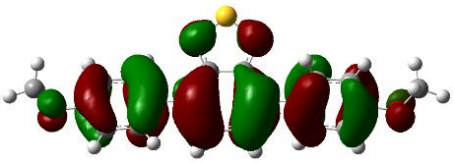	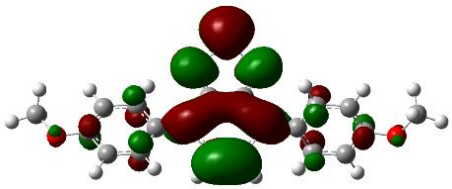
S_4	263 [0.72998]	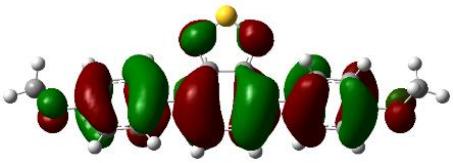	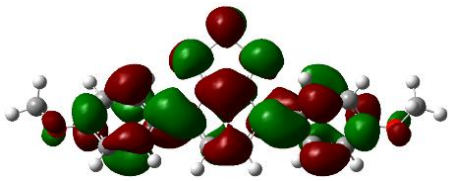

Table S27 Hole and particle natural transition orbitals calculated for **pCHO-BTZ**.

State	Energy (nm) [contribution]	Hole Orbital	Particle Orbital
S_1	370 [0.97808]	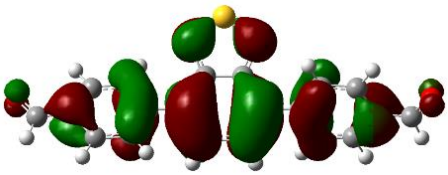	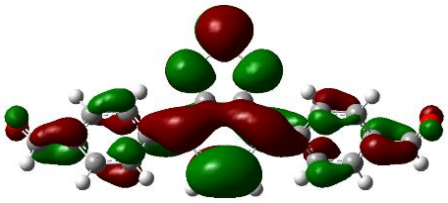
S_5	278 [0.88710]	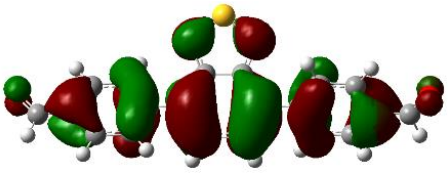	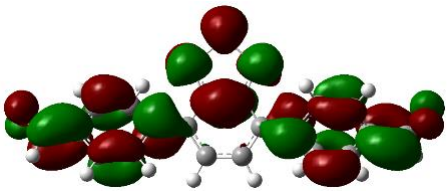

Table S28 Hole and particle natural transition orbitals calculated for **pCN-BTZ**.

State	Energy (nm) [contribution]	Hole Orbital	Particle Orbital
S_1	362 [0.98697]	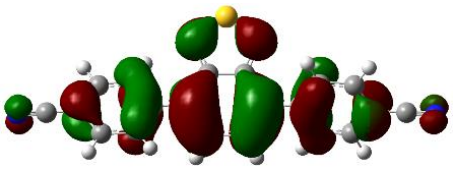	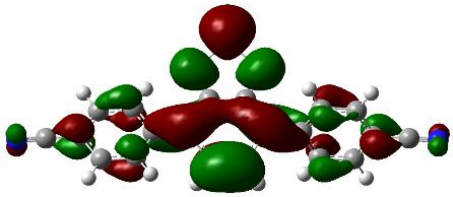
S_2	281 [0.90820]	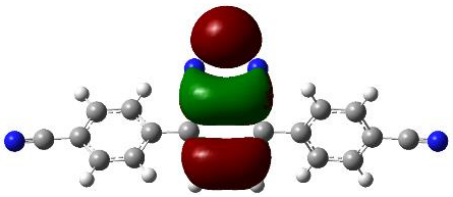	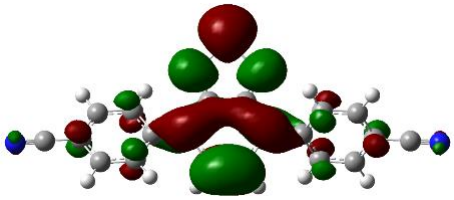
S_3	257 [0.91524]	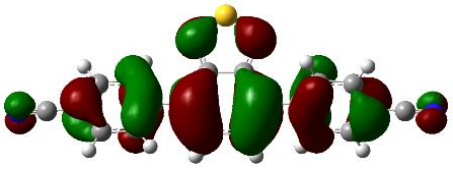	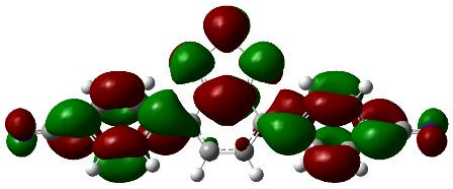

Table S29 Hole and particle natural transition orbitals calculated for **pCF$_3$-BTZ**.

State	Energy (nm) [contribution]	Hole Orbital	Particle Orbital
S$_1$	362 [0.98697]	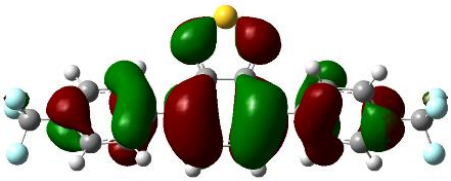	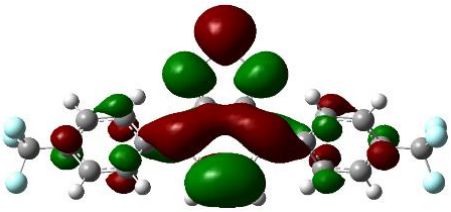
S$_2$	281 [0.90820]	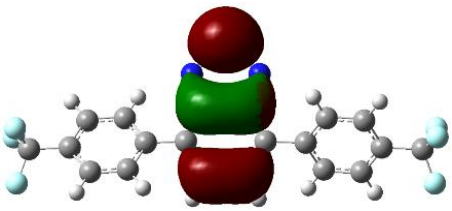	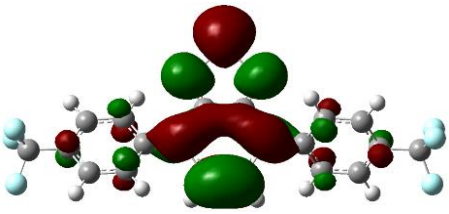
S4	257 [0.91524]	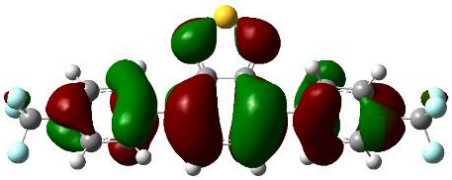	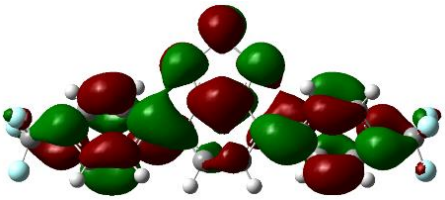

Table S30 Hole and particular natural transition orbitals calculated for **pNO$_2$-BTZ**.

State	Energy (nm) [contribution]	Hole Orbital	Particle Orbital
S$_1$	367 [0.96930]	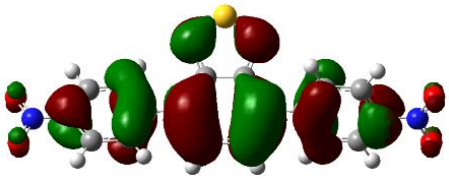	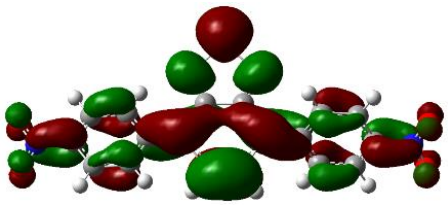
S$_3$	290 [0.86332]	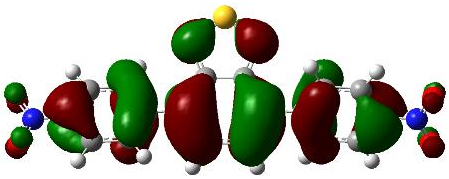	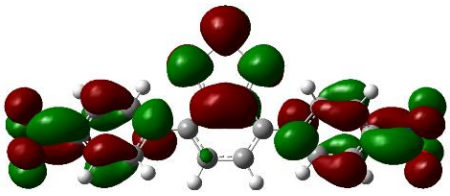

5.5 Theoretical Analysis of Selenophene and Tellurophene Analogues of Th-BTZ

Although they were not synthesised as part of the library of photocatalysts, a theoretical analysis was performed the selenophene and tellurophene analogues of **Th-BTZ**, designated as **Se-BTZ** and **Te-BTZ**.

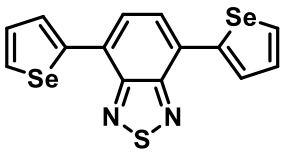

Se-BTZ

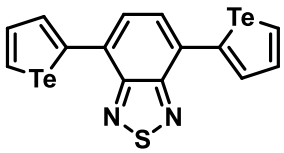

Te-BTZ

Table S31 Summary of the theoretical absorption and emission properties of the **Se-BTZ** and **Te-BTZ**.

Entry	Compound	λ_{abs}/ nm	λ_{em}/ nm	Stokes Shift/ nm
1	**Se-BTZ**	462	627	165
2	**Te-BTZ**	495	697	202

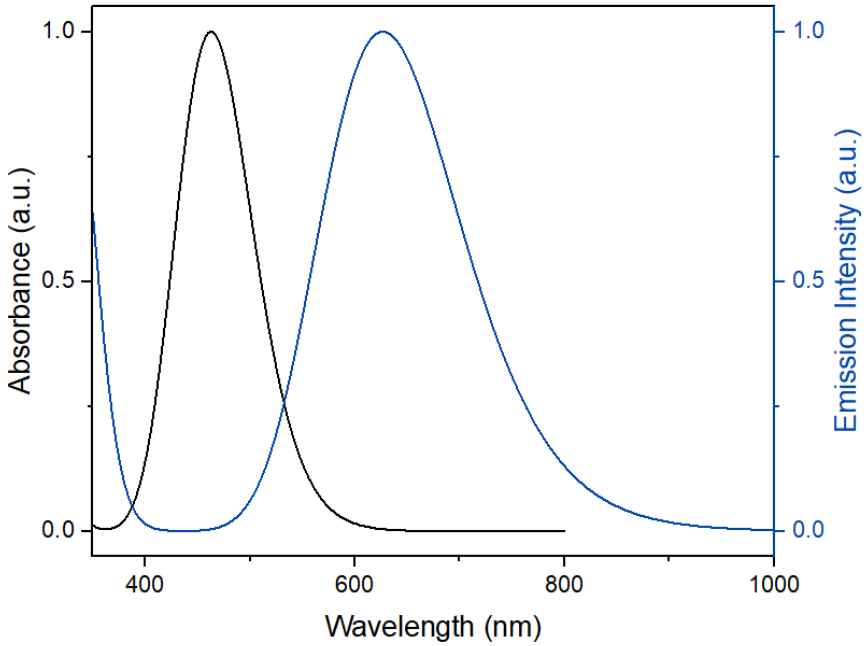

Figure S86 Normalised theoretical absorption (black) and emission spectra (blue) of **Se-BTZ**.

Table S32 Hole and particle natural transition orbitals calculated for **Se-BTZ**.

State	Energy (nm) [contribution]	Hole Orbital	Particle Orbital
S_1	462 [0.98410]	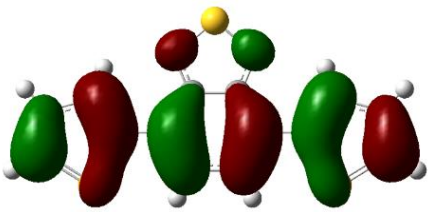	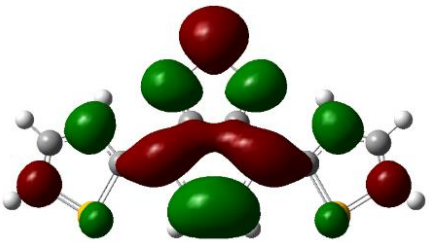
S_3	300 [0.54116]	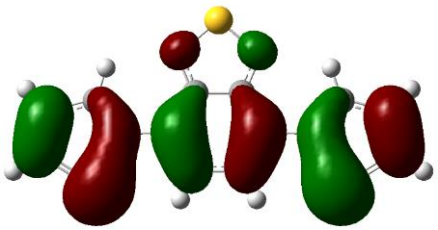	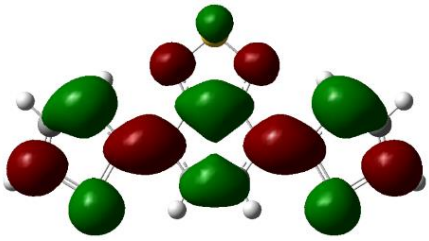
S_5	290 [0.57027]	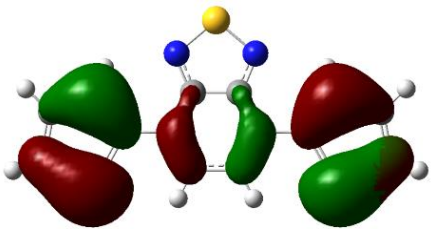	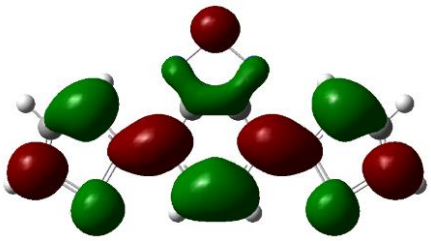
S_6	280 [0.86501]	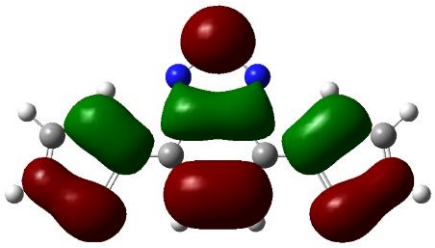	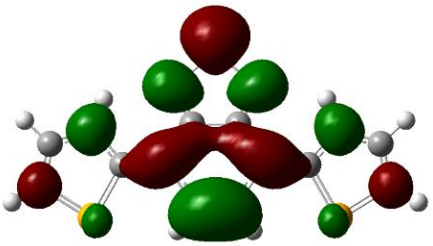

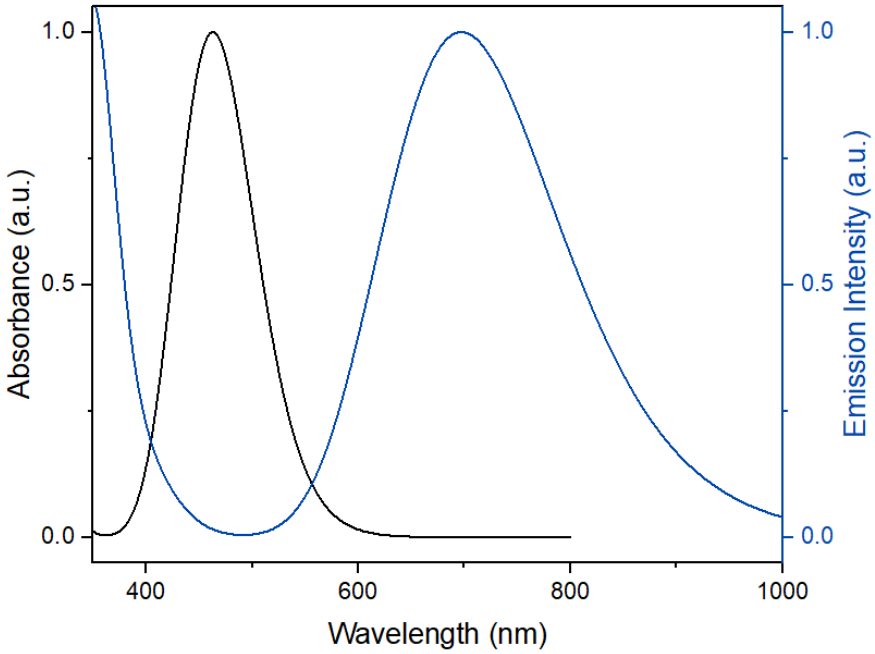

Figure S87 Normalised theoretical absorption (black) and emission spectra (blue) of **Te-BTZ**.

Table S33 Hole and particle natural transition orbitals calculated for **Te-BTZ**.

State	Energy (nm) [contribution]	Hole Orbital	Particle Orbital
S_1	495 [0.98605]	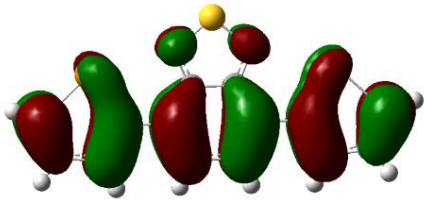	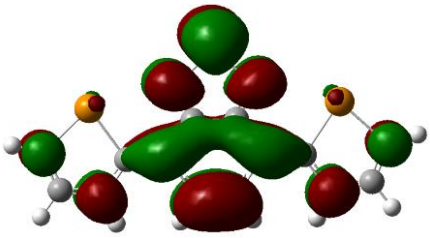
S_3	364 [0.96222]	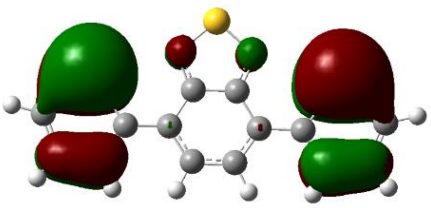	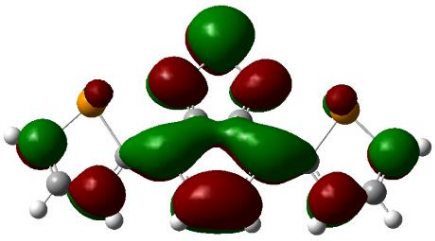

5.6 Energy Barriers to Bond Rotation of Selected Photocatalysts

Figures S88 – S91 show the rotational energy barriers to rotation around the highlighted donor-acceptor bonds in selected photocatalysts.

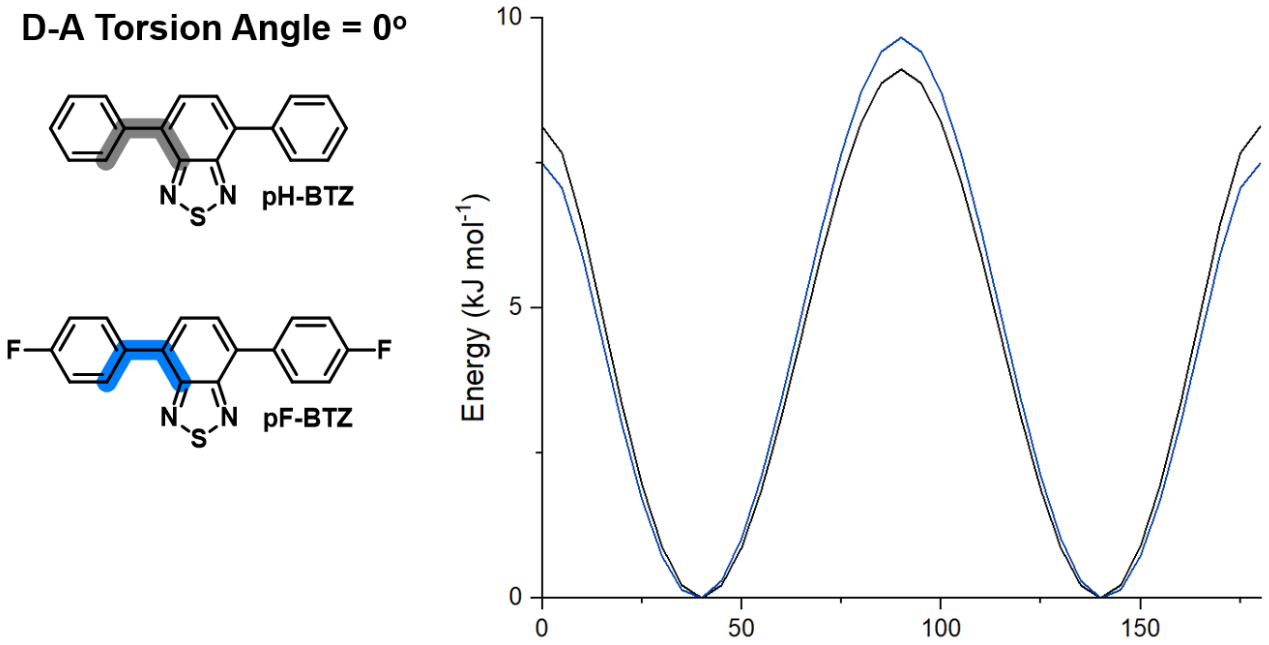

Figure S88 Energy against donor-acceptor dihedral angle plots for **pH-BTZ** (black) and **pF-BTZ** (blue). The structures corresponding to a donor-acceptor torsion angle (highlighted) of 0° are shown on the left.

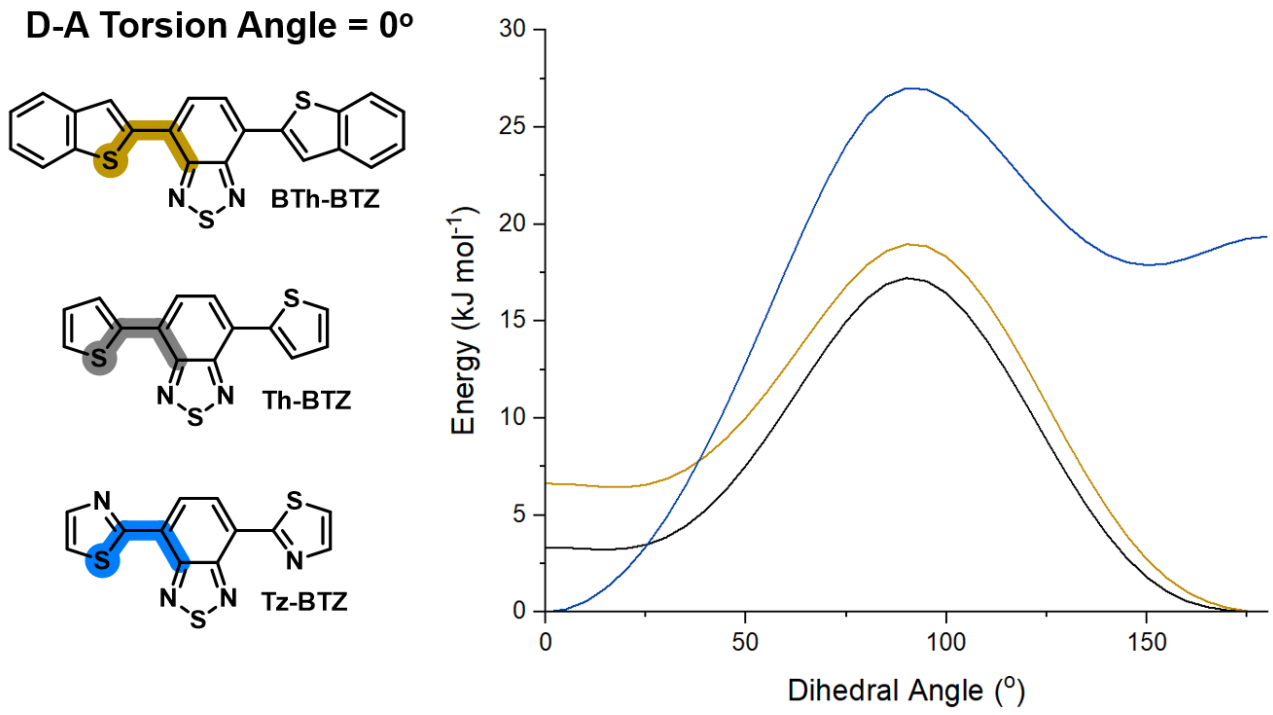

Figure S89 Energy against donor-acceptor dihedral angle plots for **Th-BTZ** (black), **BTh-BTZ** (yellow) and **Tz-BTZ** (blue). The structures corresponding to a donor-acceptor torsion angle (highlighted) of 0° are shown on the left.

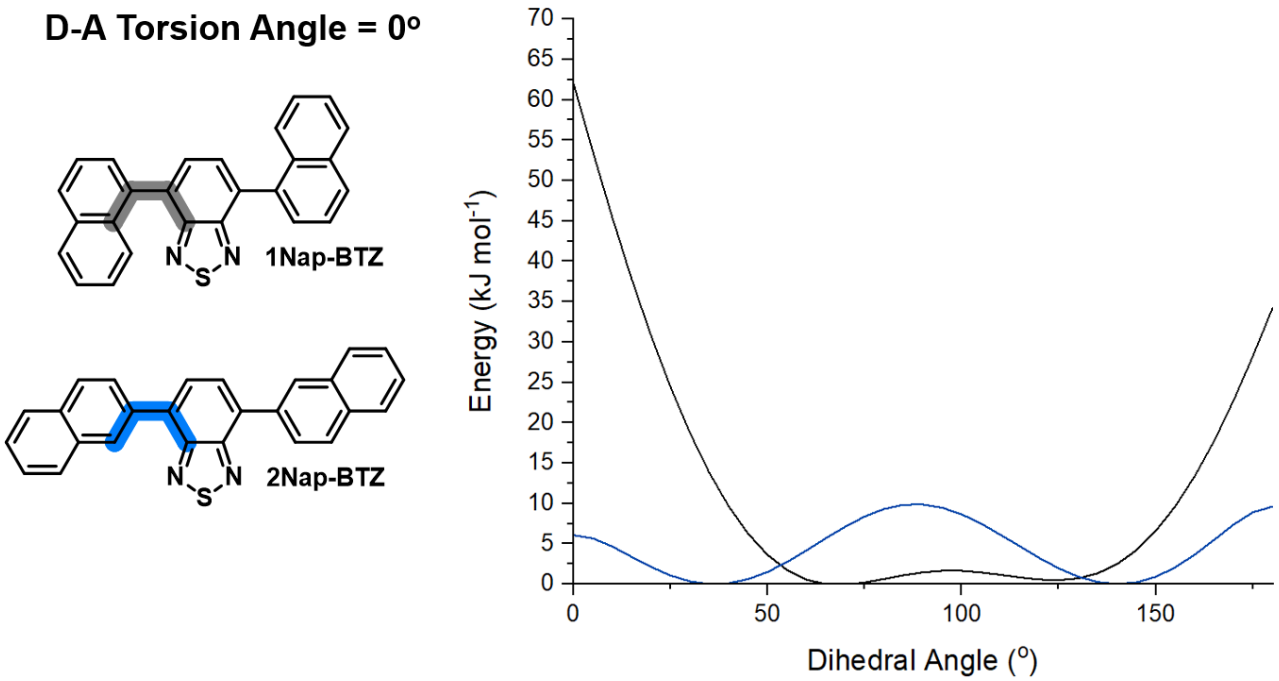

Figure S90 Energy against donor-acceptor dihedral angle plots for **1Nap-BTZ** (black) and **2Nap-BTZ** (blue). The structures corresponding to a donor-acceptor torsion angle (highlighted) of 0° are shown on the left.

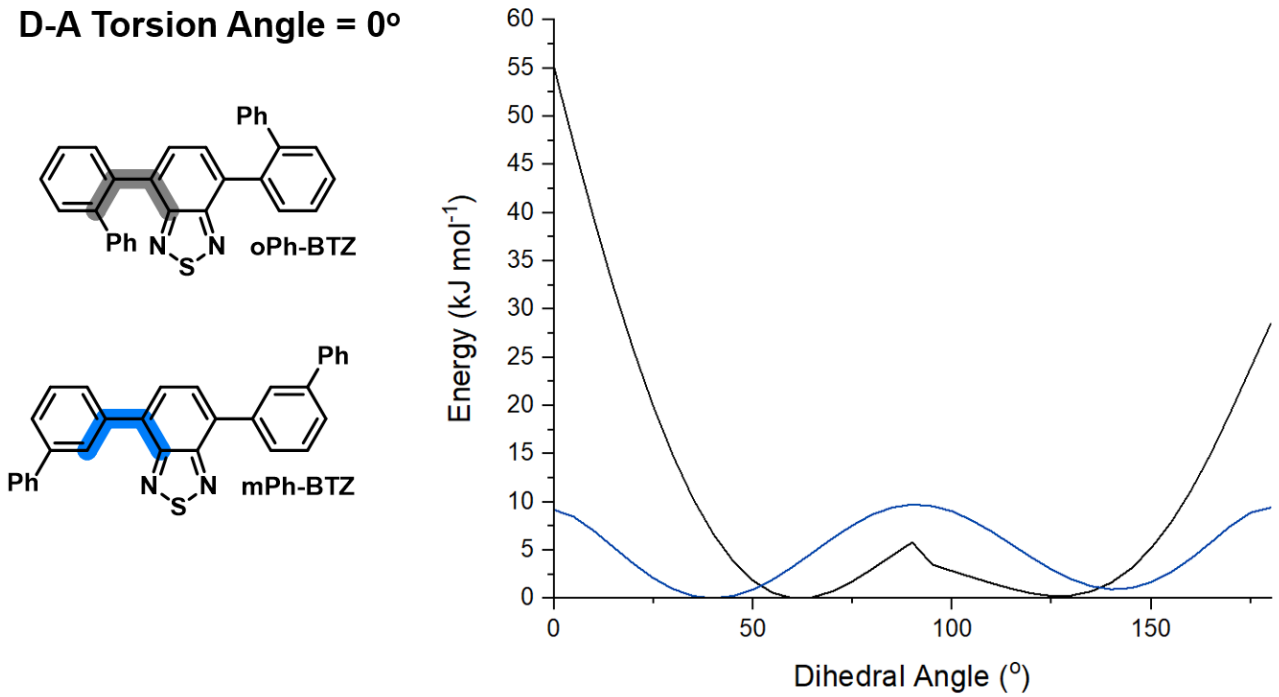

Figure S91 Energy against donor-acceptor dihedral angle plots for **oPh-BTZ** (black) and **mPh-BTZ** (blue). The structures corresponding to a donor-acceptor torsion angle (highlighted) of 0° are shown on the left.

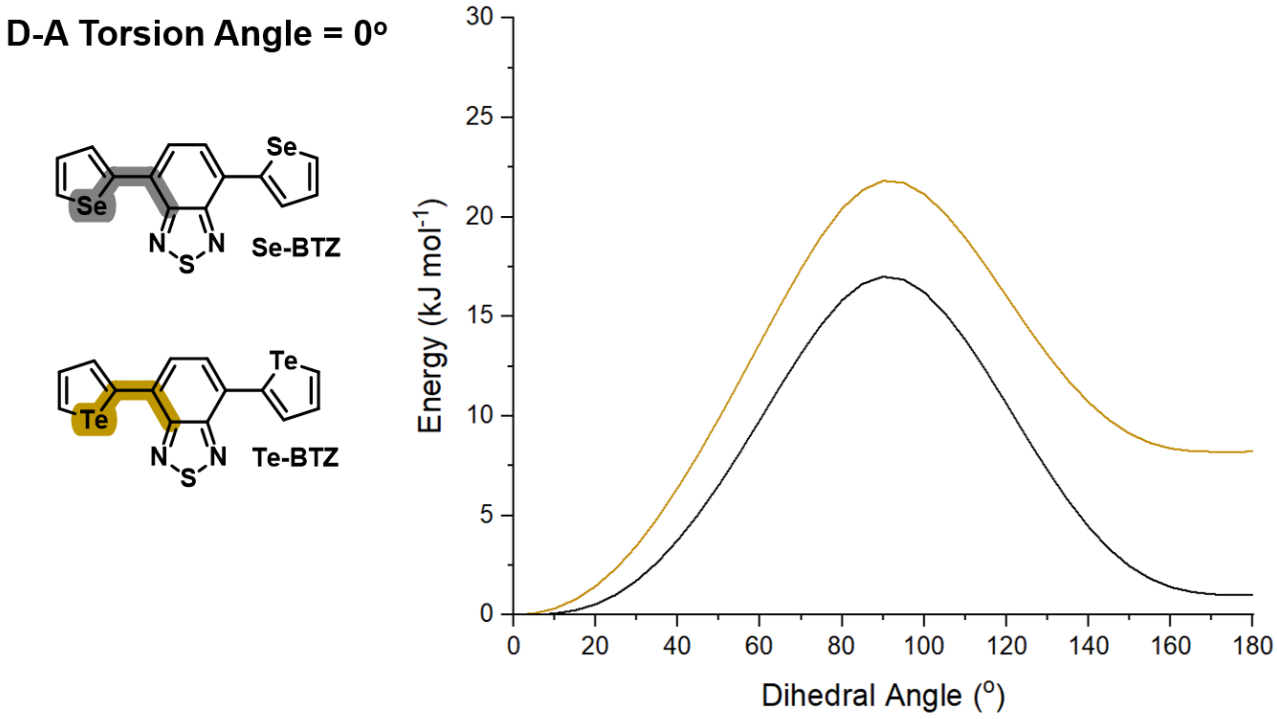

Figure S92 Energy against donor-acceptor dihedral angle plots for **Se-BTZ** (black) and **Te-BTZ** (yellow). The structures corresponding to a donor-acceptor torsion angle (highlighted) of 0° are shown on the left.

5.7 Geometry Comparison Table

Table S34 Comparison between the optimised computational geometry and literature crystal structures for **pH-BTZ**, **Th-BTZ** and **Tz-BTZ**. Experimental data from reported crystal structure.[27-29]

Geometric Feature	pH-BTZ		Th-BTZ		Tz-BTZ	
	Theoretical	Experimental	Theoretical	Experimental	Theoretical	Experimental
Bond Lengths/Å						
S-N (1)	1.62554	1.6273	1.6249	1.6096	1.62685	1.6162
N-C (2)	1.33713	1.3594	1.33506	1.3462	1.33453	1.3434
C-C (3)	1.45205	1.4514	1.45479	1.4442	1.4477	1.4333
D-A (4)	1.47843	1.4994	1.45532	1.4330	1.45862	1.4523
Angles/°						
N-S-N (5)	100.2613	101.45	99.87949	101.509	99.87911	101.1312
S-N-C (6)	106.9086	106.32	107.3116	106.3613	107.0678	106.2816
C-C-C (7)	123.0716	123.03	123.0282	123.04	123.7952	123.23
Dihedral Angles/°						
N-C-C-C (8)	-141.352	-142.53	-	-	-	-
N-C-C-S (9)	-	-	-179.97	-175.711	-	-
N-C-C-N (10)	-	-	-	-	179.9963	-175.82

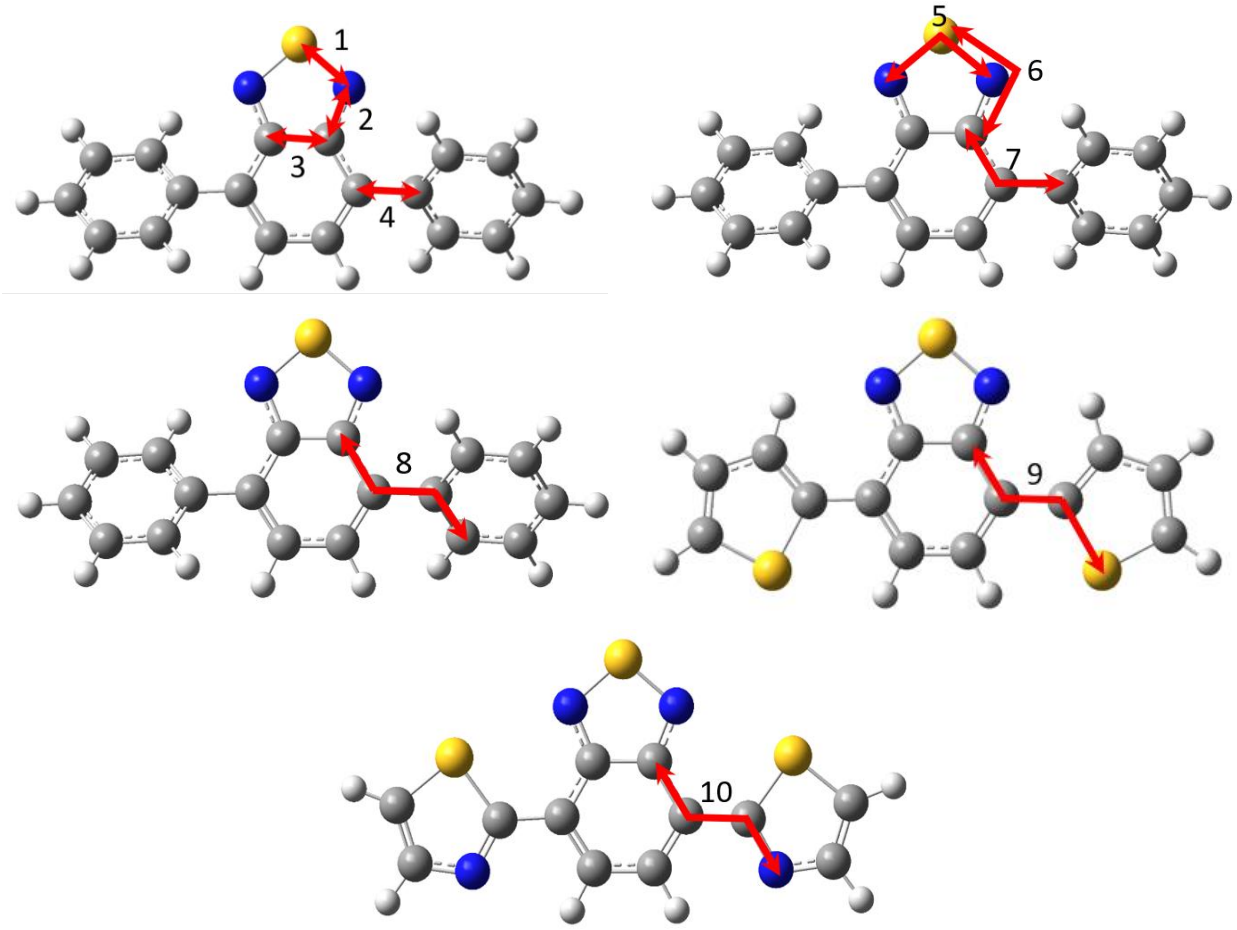

Figure S93 Naming scheme for geometric features compared in table S34. Colour legend: carbon (grey), hydrogen (white), nitrogen (blue) and sulfur (yellow).

6. Cyclic Voltammetry Studies

6.1 Cyclic Voltammograms

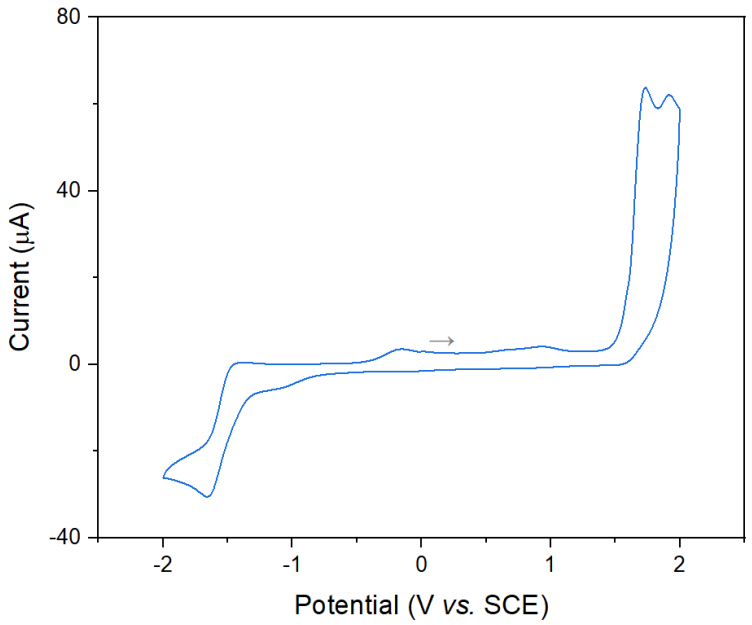

Figure S94 Cyclic voltammogram of **pH-BTZ** in DCM.

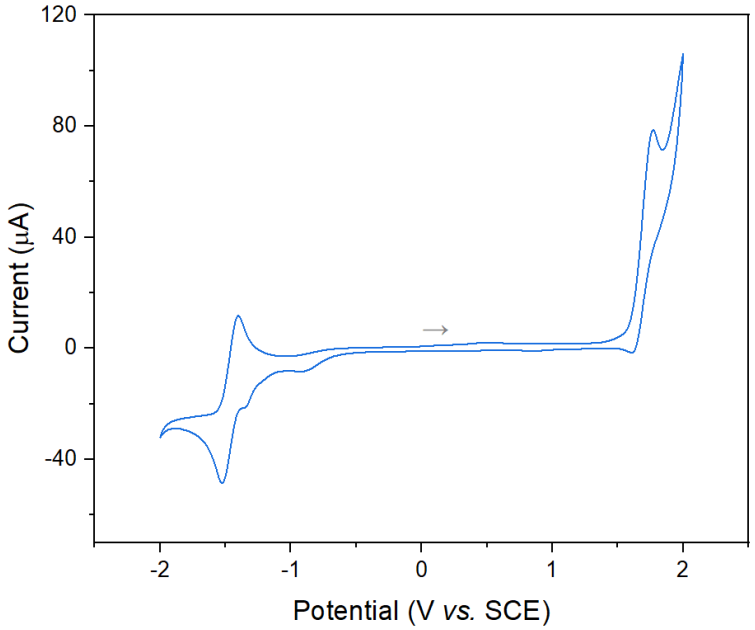

Figure S95 Cyclic voltammogram of **pF-BTZ** in DCM.

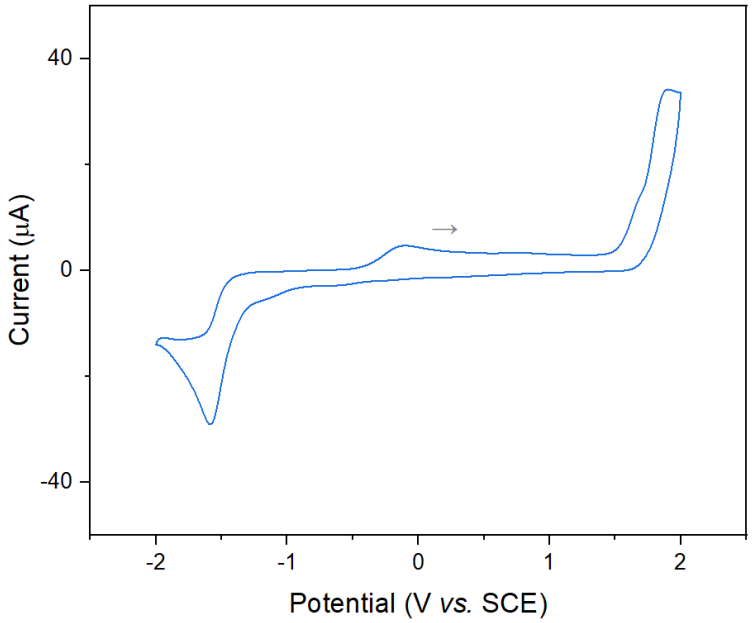

Figure S96 Cyclic voltammogram of **pCl-BTZ** in DCM.

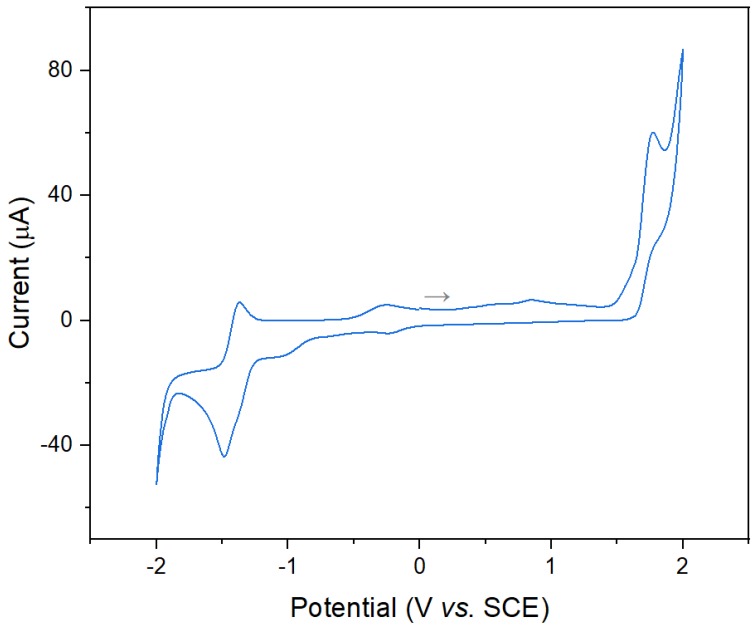

Figure S97 Cyclic voltammogram of **pBr-BTZ** in DCM.

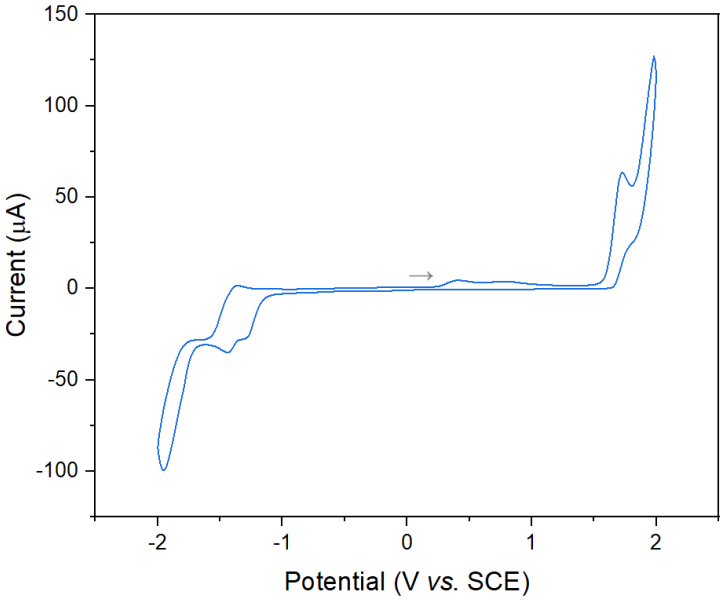

Figure S98 Cyclic voltammogram of **pI-BTZ** in DCM.

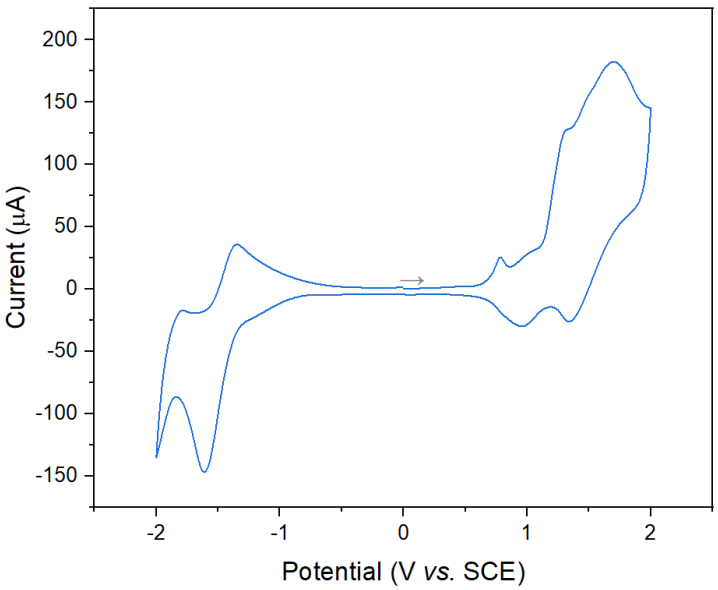

Figure S99 Cyclic voltammogram of **pTh-BTZ** in DCM.

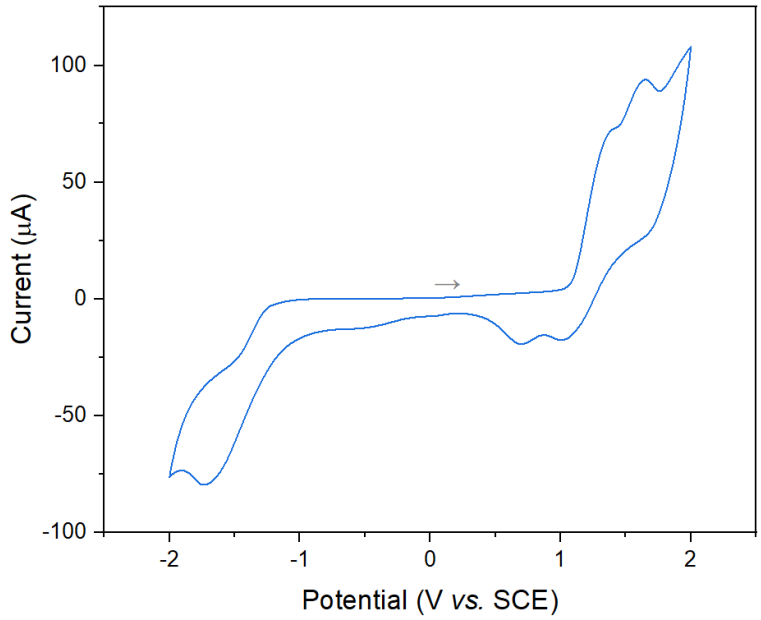

Figure S100 Cyclic voltammogram of **Th-BTZ** in DCM.

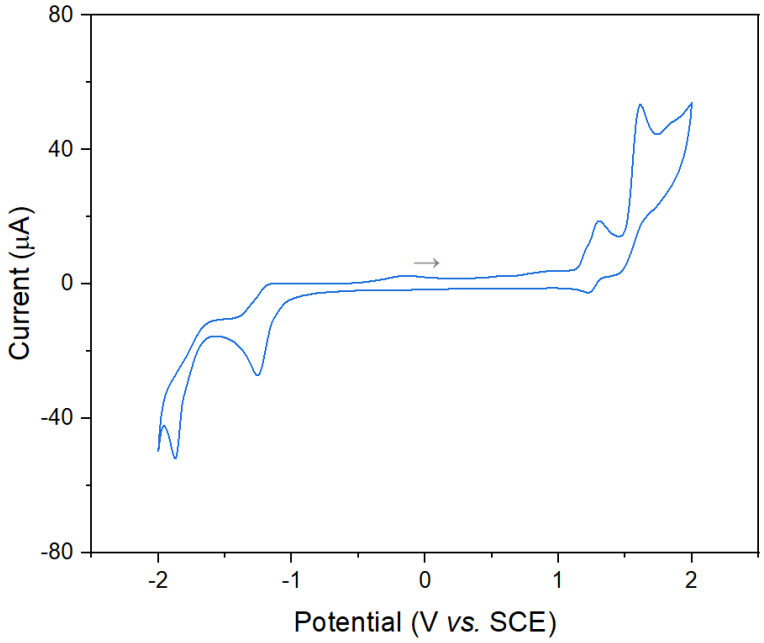

Figure S101 Cyclic voltammogram of **ThBr-BTZ** in DCM.

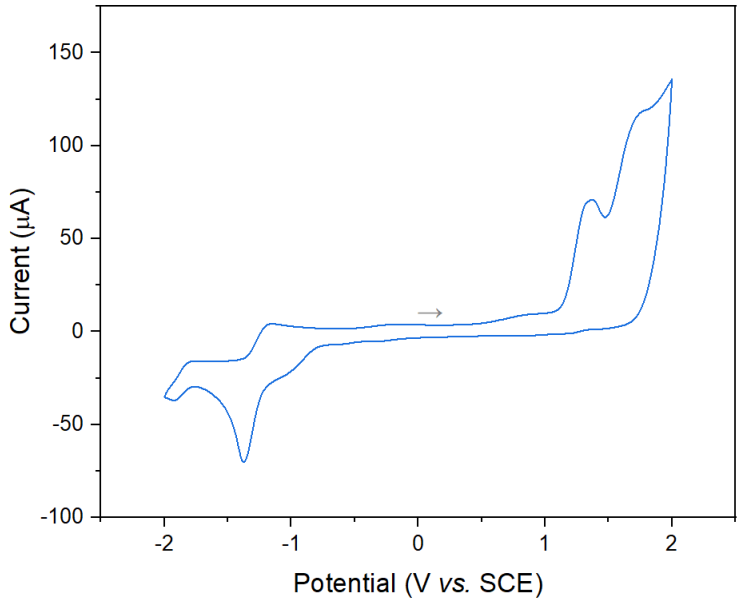

Figure S102 Cyclic voltammogram of **BTh-BTZ** in DCM.

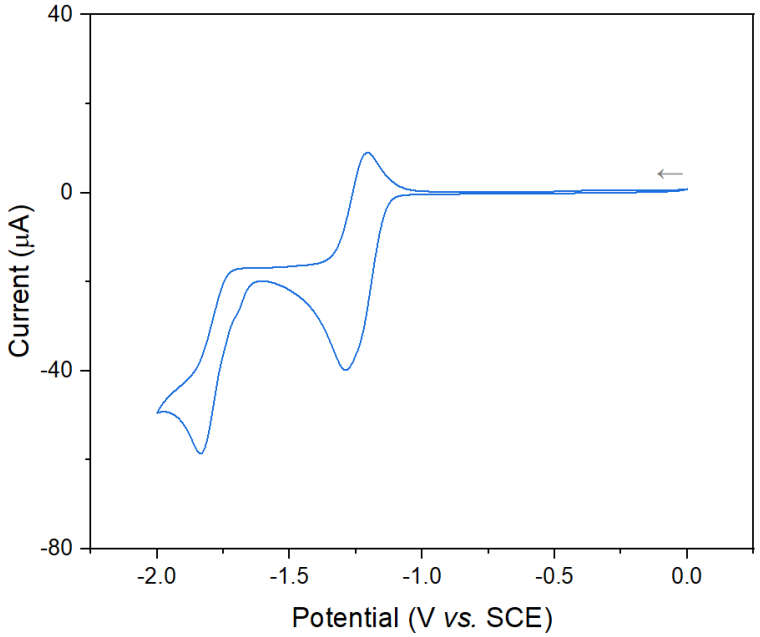

Figure S103 Cyclic voltammogram of **ThTh-BTZ** in DCM.

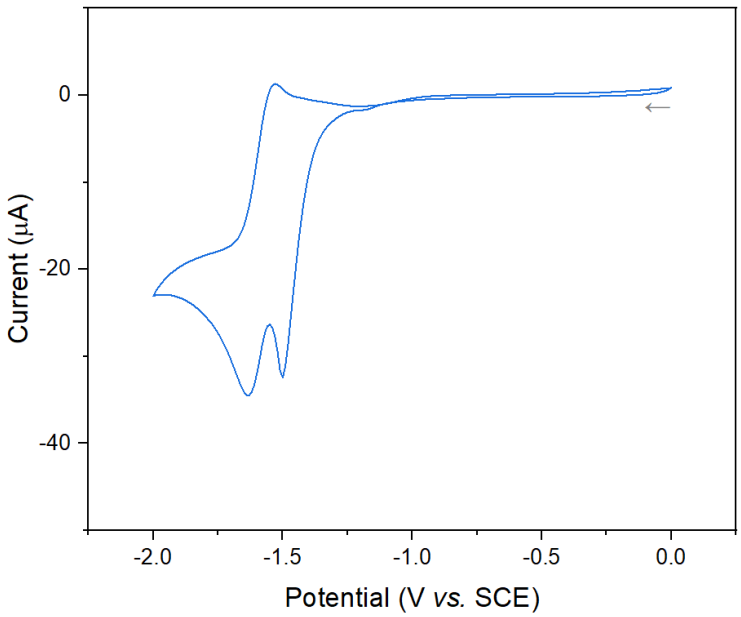

Figure S104 Cyclic voltammogram of **Pyr-BTZ** in DCM.

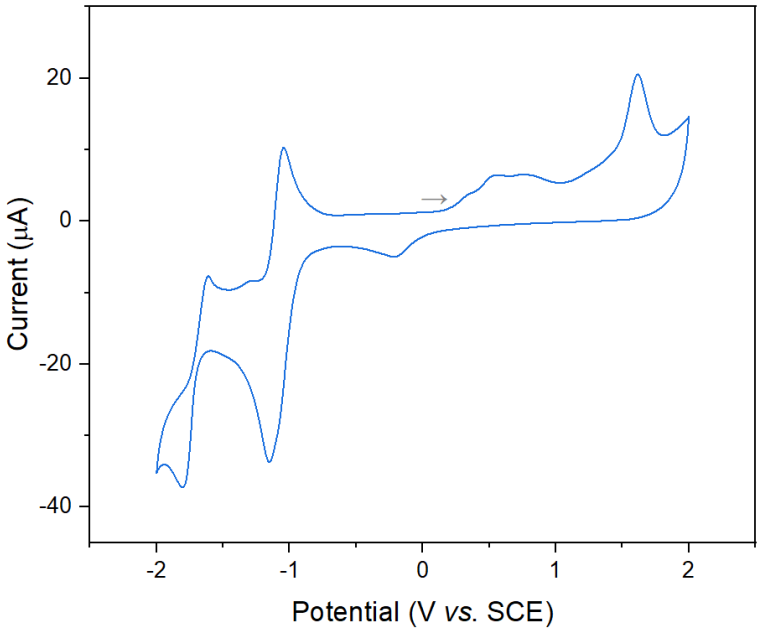

Figure S105 Cyclic voltammogram of **Tz-BTZ** in DCM.

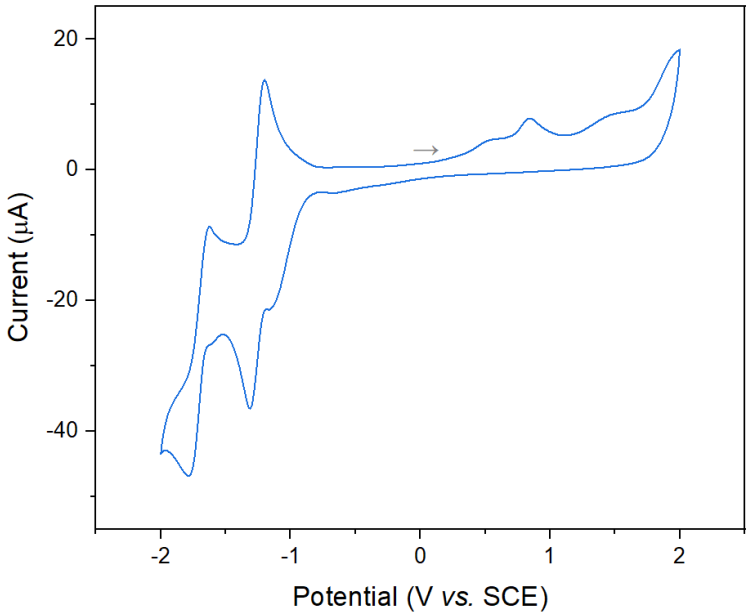

Figure S106 Cyclic voltammogram of **4N-BTZ** in DCM.

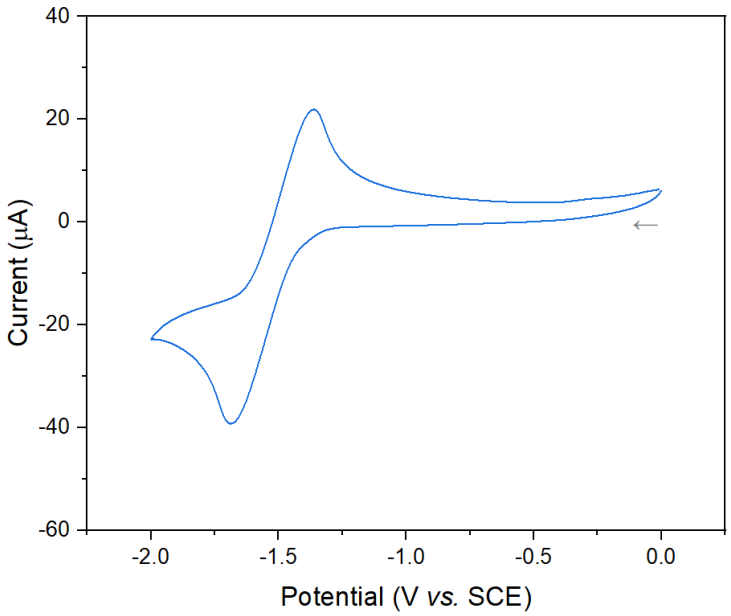

Figure S107 Cyclic voltammogram of **1Nap-BTZ** in DCM.

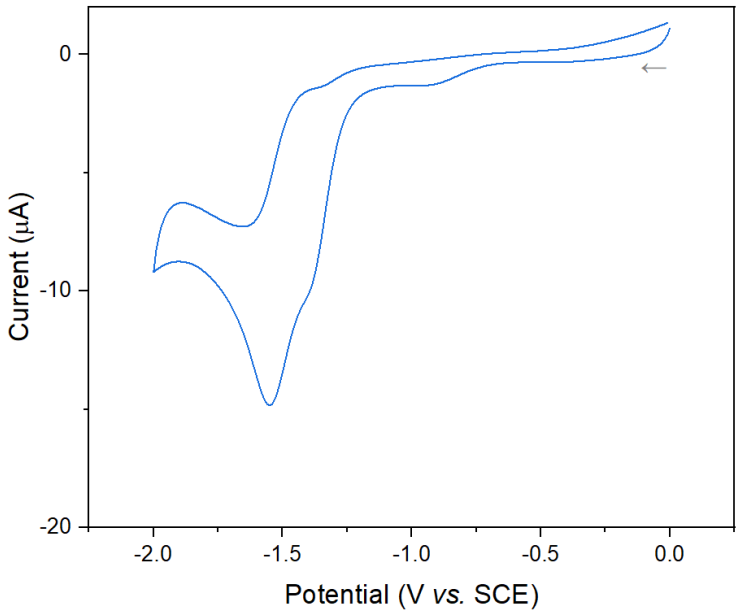

Figure S108 Cyclic voltammogram of **2Nap-BTZ** in DCM.

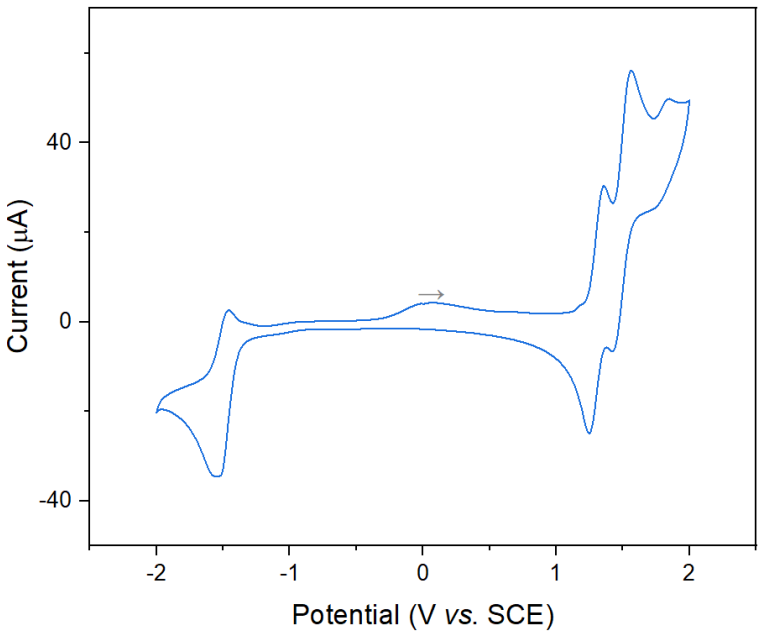

Figure S109 Cyclic voltammogram of **Flu-BTZ** in DCM.

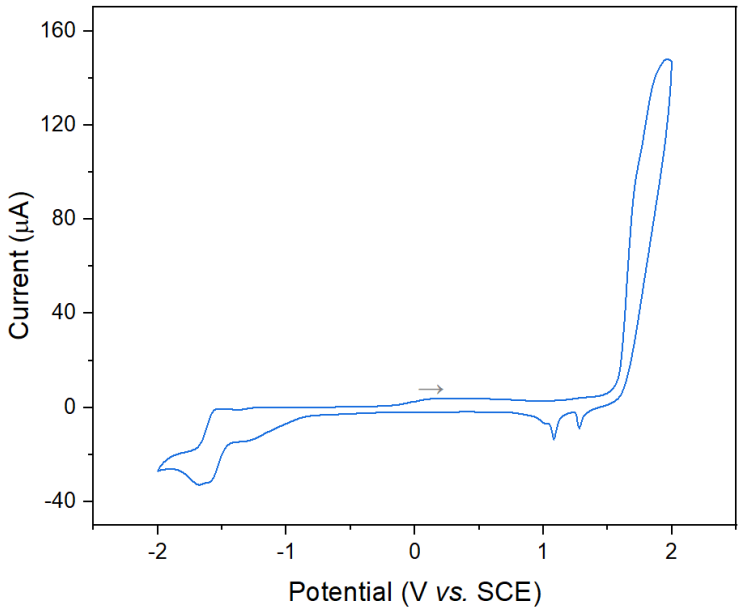

Figure S110 Cyclic voltammogram of **oPh-BTZ** in DCM.

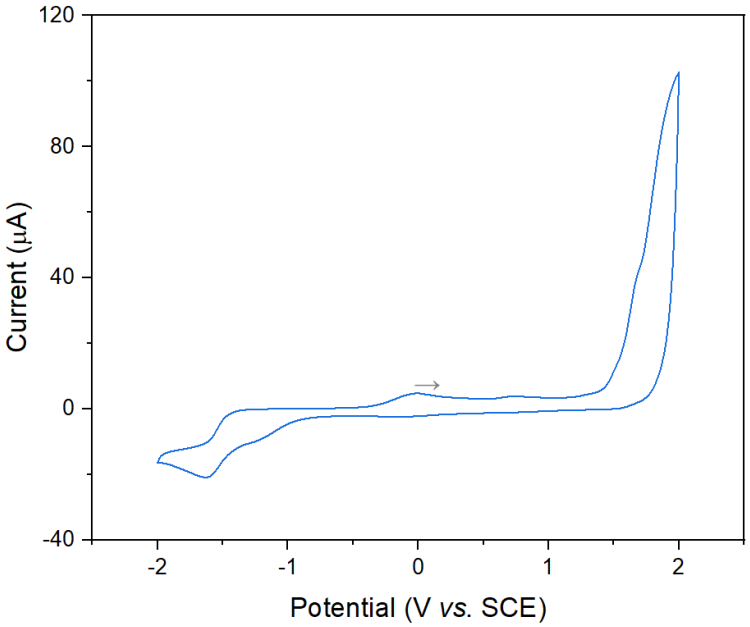

Figure S111 Cyclic voltammogram of **mPh-BTZ** in DCM.

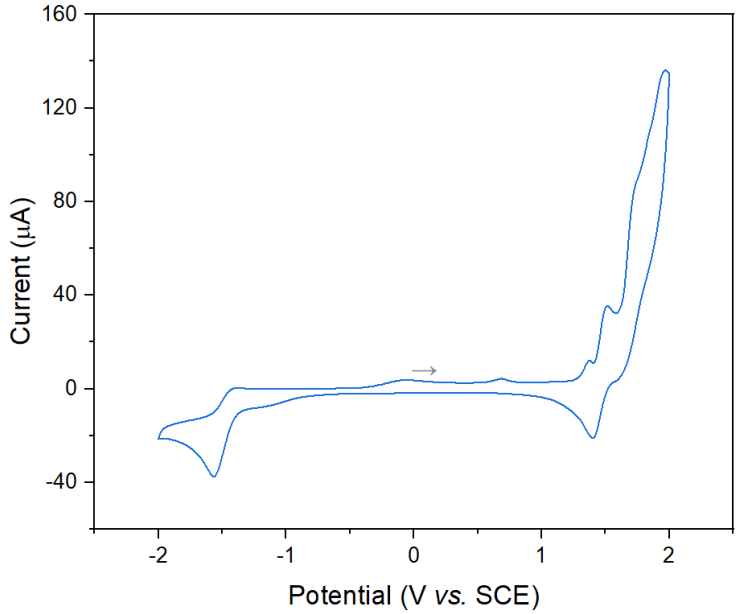

Figure S112 Cyclic voltammogram of **pPh-BTZ** in DCM.

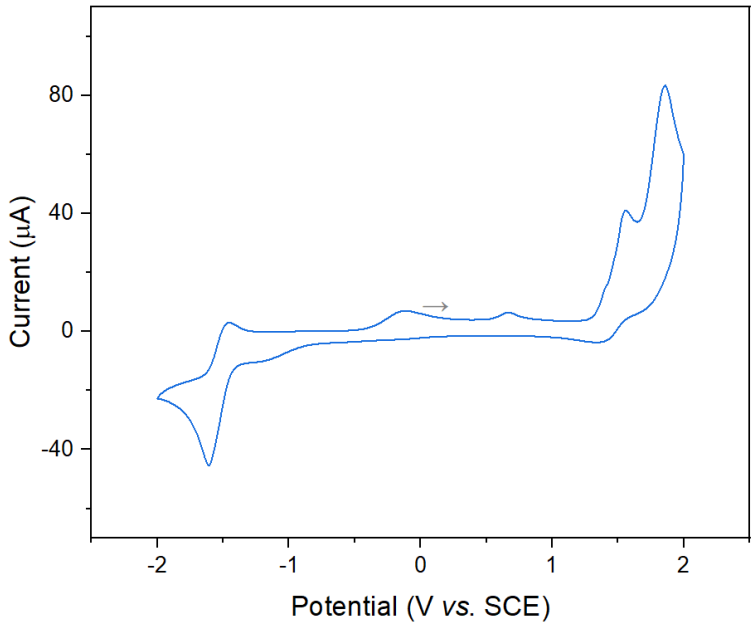

Figure S113 Cyclic voltammogram of **pMe-BTZ** in DCM.

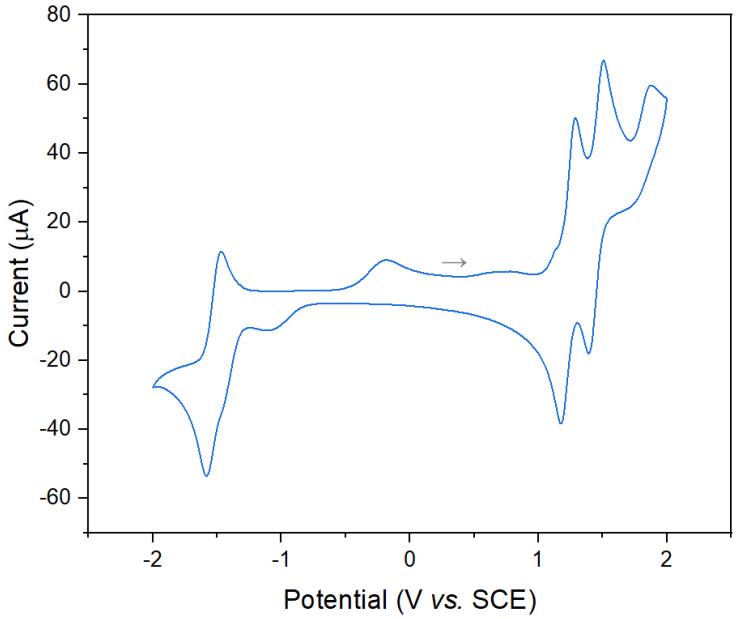

Figure S114 Cyclic voltammogram of **pOMe-BTZ** in DCM.

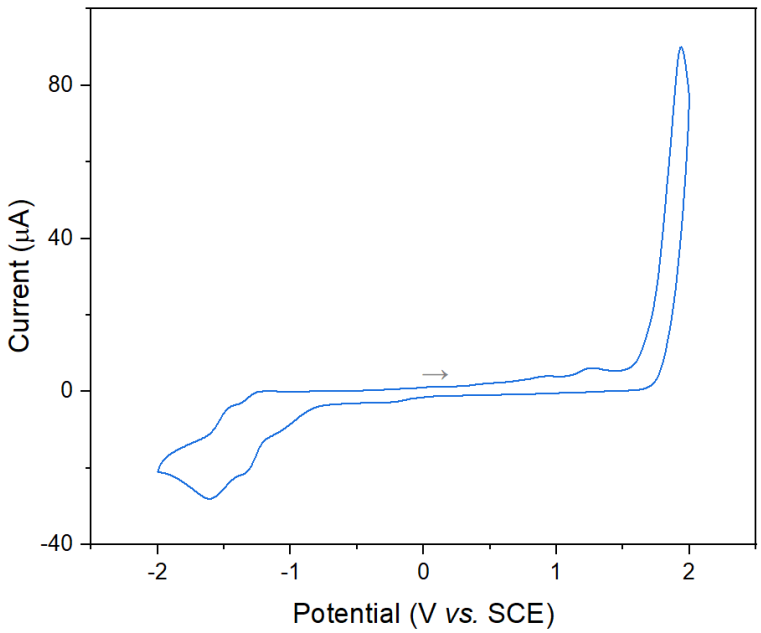

Figure S115 Cyclic voltammogram of **pCHO-BTZ** in DCM.

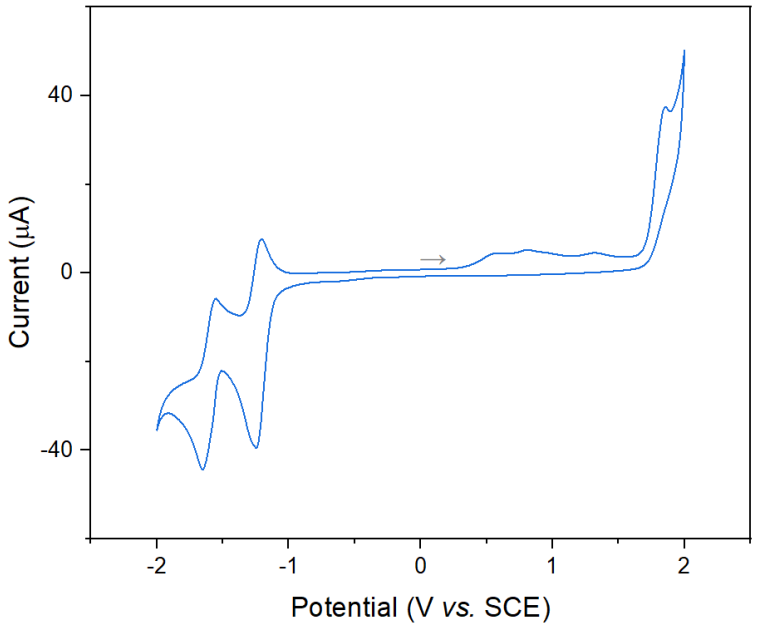

Figure S116 Cyclic voltammogram of **pCN-BTZ** in DCM.

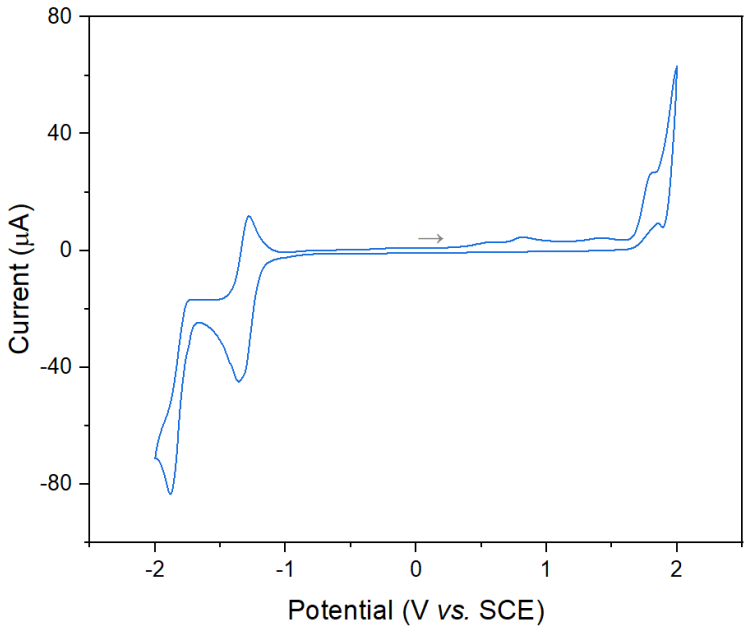

Figure S117 Cyclic voltammogram of **pCF$_3$-BTZ** in DCM.

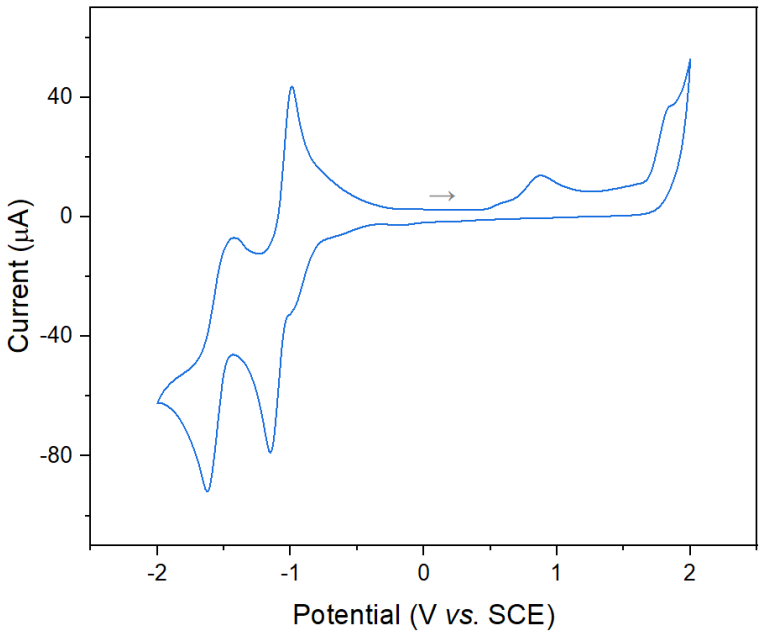

Figure S118 Cyclic voltammogram of **pNO$_2$-BTZ** in DCM.

6.2 Summary of Results

Table S35 Summary of the electrochemical properties of the **BTZ** photocatalysts. [a]Measured using 2 mM of photocatalyst dissolved in 250 mM NBu_4PF_6 in dry and degassed DCM solution using a glassy carbon working electrode, platinum wire counterelectrode, standard calomel electrode (SCE) and a scan rate of 100 mV s^{-1}. [b]Quoted E_{ox} or E_{red} is the half-wave potential ($E_{1/2}$) for all reversible transformations. For irreversible or quasi-reversible transformations half-peak potential ($E_{p/2}$) is quoted instead. [c]Estimated from the intersection of normalised absorption and emission spectra.[30,31] [d]Calculated from E_{ox}, E_{red} and $E_{0,0}$.[32] [e]Compound decomposed under both separate positive and negative potential sweeps.

Entry	Compound	E_{ox} /V[a,b]	E_{red} /V[a,b]	$E_{0,0}$ /eV[c]	E_{ox}*/V[d]	E_{red}*/V[d]
1	**pH-BTZ**	1.64	-1.46	2.88	-1.24	1.42
2	**pF-BTZ**	1.70	-1.47	2.84	-1.14	1.38
3	**pCl-BTZ**	-	-1.45	2.85	-	1.40
4	**pBr-BTZ**	1.68	-1.43	2.85	-1.17	1.42
5	**pI-BTZ**	1.66	-1.40	2.83	-1.17	1.43
6	**pTh-BTZ**	1.14	-1.48	2.63	-1.49	1.16
7	**Th-BTZ**	1.05	-1.39	2.47	-1.43	1.08
8	**ThBr-BTZ**	1.27	-1.21	2.43	-1.17	1.22
9	**ThTh-BTZ**	-	-1.25	2.20	-	0.95
10	**BTh-BTZ**	1.23	-1.26	2.46	-1.23	1.20
11	**Tz-BTZ**	1.50	-1.10	2.61	-1.11	1.51
12	**Pyr-BTZ**	-	-1.43	2.61	-	1.18
13	**4N-BTZ**	-	-1.25	3.13	-	1.88
14	**oPh-BTZ**	-	-1.53	2.89	-	1.36
15	**mPh-BTZ**	-	-1.46	2.87	-	1.41
16	**pPh-BTZ**	1.46	-1.46	2.72	-1.24	1.24
17	**1Nap-BTZ**	-	-1.52	2.82	-	1.30
18	**2Nap-BTZ**	-	-1.35	2.71	-	1.36
19	**Flu-BTZ**	1.30	-1.51	2.60	-1.30	1.09
20	**pMe-BTZ**	1.47	-1.53	2.76	-1.29	1.23
21	**pOH-BTZ**	-	-	2.66	-	-
22	**pOMe-BTZ**	1.24	-1.54	2.65	-1.41	1.11
23	**pCHO-BTZ**	-	-1.44	2.94	-	1.50
24	**pCN-BTZ**	1.76	-1.23	2.98	-1.22	1.75
25	**pCF$_3$-BTZ**	1.72	-1.32	2.99	-1.27	1.67
26	**pNO$_2$-BTZ**	-	-1.07	2.97	-	1.91

7. Decarboxylative C-H Functionalisation of Heteroarenes

7.1 Procedures for Batch Photocatalysis

General Procedure For Photocatalysis Under Batch Conditions

Heteroarene (0.3 mmol), photocatalyst (0.015 mmol, 5 mol%), oxidant (0.6 mmol) and cyclohexane carboxylic acid (385 mg, 3.0 mmol) were added to an oven dried vial. Anhydrous DMSO (3 mL) was added and the mixture degassed using nitrogen for 10 minutes. The mixture was then irradiated using a 12 W 420 nm LED for 16 h. Following this time, the mixture was then diluted with DCM (10 mL) then washed with saturated aqueous sodium carbonate solution (15 mL). The aqueous phase was extracted with DCM (3 x 10 mL) and the combined organic phases were washed with brine (30 mL). The combined organic phases were dried over $MgSO_4$ then the solvent removed under reduced pressure. The residue was then dissolved in $CDCl_3$ for quantitative analysis using ^1H NMR.

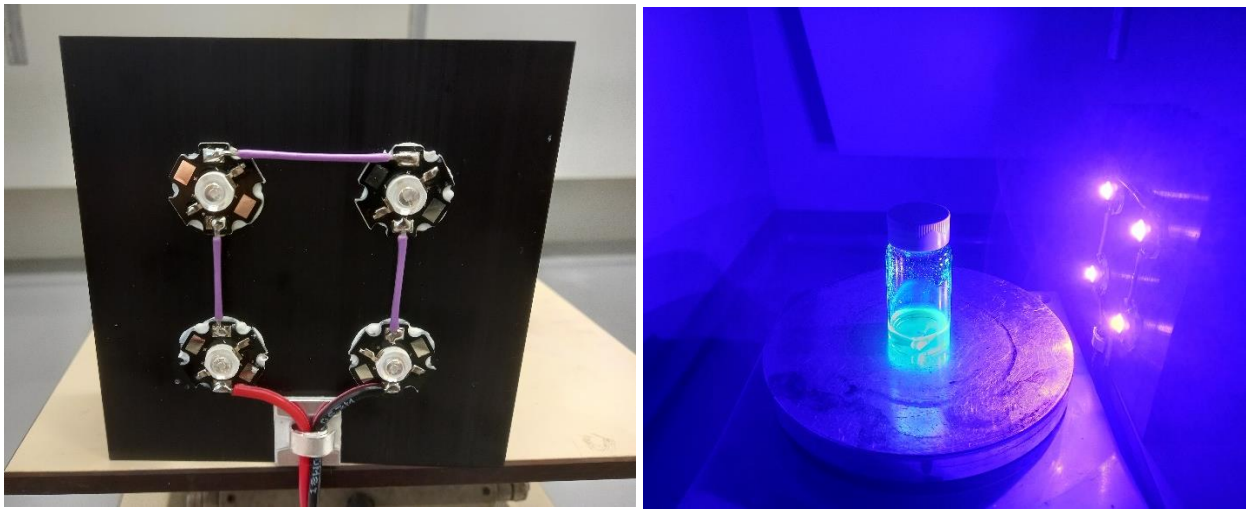

Figure S119 Pictures of the apparatus set up used for carrying out the photocatalytic reactions showing the LED module (left) and the reaction set up with irradiation (right). The LED module was constructed by mounting four individual LEDs onto an aluminium heat sink using thermal paste and connecting to an LED driver. In each experiment, the glass vial was placed at the centre of a stirrer plate, a distance of 7 cm away from the LED, then the set up covered with a reflective box (not shown).

Radical Trapping Using TEMPO

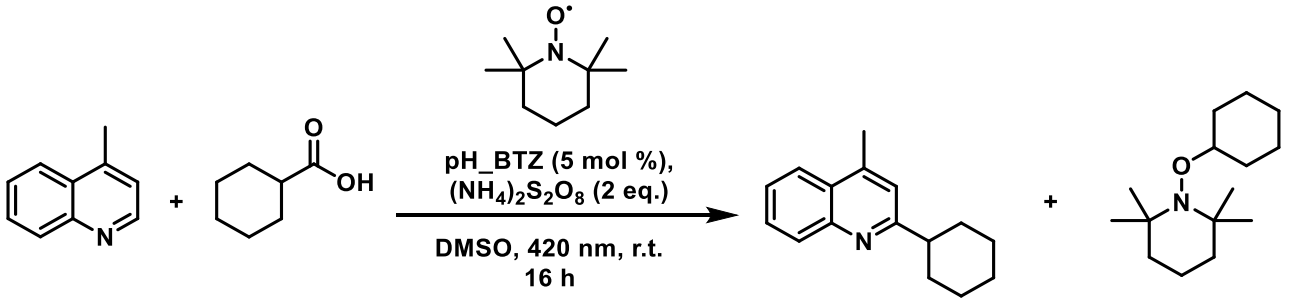

Lepidine (0.3 mmol), **pH-BTZ** (4.3 mg, 0.015 mmol, 5 mol%), ammonium persulfate (137 mg, 0.6 mmol), cyclohexane carboxylic acid (385 mg, 3.0 mmol) and (2,2,6,6-tetramethylpiperidiny-1-yl)oxyl (94 mg, 0.6 mmol) were added to an oven dried vial. Anhydrous DMSO (3 mL) was then added and the mixture degassed using nitrogen for 10 minutes. The mixture was then irradiated using a 12 W 420 nm LED for 16 h. Following this time, the mixture was diluted with DCM (10 mL) then washed with saturated aqueous sodium carbonate solution (15 mL). The aqueous phase was extracted with DCM (3 x 10 mL) and the combined organic phases were washed with brine (30 mL). The combined organic phases were dried over $MgSO_4$ then the solvent removed under reduced pressure. The residue was then analysed *via* ^1H NMR spectroscopy in $CDCl_3$ showing no signs of the product 2-cyclohexyl-4-methylquinoline.

Radical Trapping Using Cerium (III) Chloride Hydrate ($CeCl_3.xH_2O$)

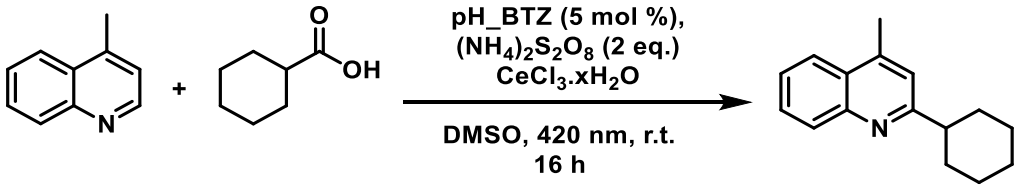

Lepidine (0.3 mmol), **pH-BTZ** (4.3 mg, 0.015 mmol, 5 mol%), ammonium persulfate (137 mg, 0.6 mmol), cyclohexane carboxylic acid (385 mg, 3.0 mmol) and cerium (III) chloride hydrate (224 mg) were added to an oven dried vial. Anhydrous DMSO (3 mL) was then added and the mixture degassed using nitrogen for 10 minutes. The mixture was then irradiated using a 12 W 420 nm LED for 16 h. Following this time, the mixture was diluted with DCM (10 mL) then washed with saturated aqueous sodium carbonate solution (15 mL). The aqueous phase was extracted with DCM (3 x 10 mL) and the combined organic phases were washed with brine (30 mL). The combined organic phases were dried over $MgSO_4$ then the solvent removed under reduced pressure. The residue was then analysed *via* ^1H NMR spectroscopy in $CDCl_3$, showing only 6% conversion.

7.2 Optimisation of Reaction Conditions

Table S36 Optimisation of reaction conditions for the decarboxylative C-H functionalisation of lepidine using cyclohexanecarboxylic acid. [a]Reaction conditions: Lepidine (0.3 mmol), oxidant (0.6 mmol), cyclohexane carboxylic acid (3 mmol), photocatalyst (0.015 mmol), solvent (3 mL), 12 W 410 – 420 nm LED, 16 h. [b]Conversion determined by ^{1}H NMR. [c]Reaction performed in the dark. [d]Reaction was performed without degassing the reaction mixture with nitrogen. [e]Reaction performed using a 505 nm light. [f]Reaction performed for 40 h. [g]Isolated yield in parenthesis. N.R. = No reaction.

Entry[a]	Photocatalyst	Oxidant	Solvent	Conversion (%)[b]
1	**pH-BTZ**	$(NH_4)_2S_2O_8$	DMSO	48
2	**pH-BTZ**	$K_2S_2O_8$	DMSO	15
3	**pH-BTZ**	$(NH_4)_2S_2O_8$	DMF	N.R.
4	**pH-BTZ**	$(NH_4)_2S_2O_8$	MeCN	4
5	**pH-BTZ**	$(NH_4)_2S_2O_8$	DMC	N.R.
6	**pH-BTZ**	$(NH_4)_2S_2O_8$	2-MeTHF	N.R.
7	**pH-BTZ**	-	DMSO	<1
8[c]	**pH-BTZ**	$(NH_4)_2S_2O_8$	DMSO	N.R.
9	**-**	$(NH_4)_2S_2O_8$	DMSO	N.R.
10[d]	**pH-BTZ**	$(NH_4)_2S_2O_8$	DMSO	4
11	**pF-BTZ**	$(NH_4)_2S_2O_8$	DMSO	19
12	**pCl-BTZ**	$(NH_4)_2S_2O_8$	DMSO	4
13	**pBr-BTZ**	$(NH_4)_2S_2O_8$	DMSO	N.R.
14	**pI-BTZ**	$(NH_4)_2S_2O_8$	DMSO	8
15	**pTh-BTZ**	$(NH_4)_2S_2O_8$	DMSO	7
16	**Th-BTZ**	$(NH_4)_2S_2O_8$	DMSO	7
17	**ThBr-BTZ**	$(NH_4)_2S_2O_8$	DMSO	N.R.
18	**ThTh-BTZ**	$(NH_4)_2S_2O_8$	DMSO	N.R.
19[e]	**ThTh-BTZ**	$(NH_4)_2S_2O_8$	DMSO	N.R.
20	**BTh-BTZ**	$(NH_4)_2S_2O_8$	DMSO	7
21	**Tz-BTZ**	$(NH_4)_2S_2O_8$	DMSO	2
22	**Py-BTZ**	$(NH_4)_2S_2O_8$	DMSO	N.R.
23	**oPh-BTZ**	$(NH_4)_2S_2O_8$	DMSO	53
24	**mPh-BTZ**	$(NH_4)_2S_2O_8$	DMSO	25
25	**pPh-BTZ**	$(NH_4)_2S_2O_8$	DMSO	N.R.
26	**1Nap-BTZ**	$(NH_4)_2S_2O_8$	DMSO	57
27	**2Nap-BTZ**	$(NH_4)_2S_2O_8$	DMSO	16
28	**Flu-BTZ**	$(NH_4)_2S_2O_8$	DMSO	1
29	**pMe-BTZ**	$(NH_4)_2S_2O_8$	DMSO	6
30	**pOH-BTZ**	$(NH_4)_2S_2O_8$	DMSO	N.R.
31	**pOMe-BTZ**	$(NH_4)_2S_2O_8$	DMSO	3
32	**pCHO-BTZ**	$(NH_4)_2S_2O_8$	DMSO	4
33	**pCN-BTZ**	$(NH_4)_2S_2O_8$	DMSO	6
34	**pCF_3-BTZ**	$(NH_4)_2S_2O_8$	DMSO	10
35	**pNO_2-BTZ**	$(NH_4)_2S_2O_8$	DMSO	11
36[f,g]	**1Nap-BTZ**	$(NH_4)_2S_2O_8$	DMSO	>99 (73)

7.3 Reaction Scope

2-Cyclohexyl-4-methylquinoline (1)

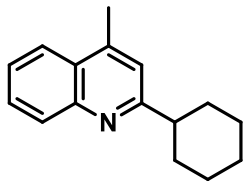

General procedure for photocatalysis under batch conditions using lepidine (43 mg, 0.3 mmol), cyclohexane carboxylic acid (385 mg, 3.0 mmol), ammonium persulfate (137 mg, 0.6 mmol), **1Nap-BTZ** (5.8 mg, 0.015 mmol) and DMSO (3 mL) for 40 h. Purification of the crude product was achieved by silica gel column chromatography using DCM:ethyl acetate 3:1 as the eluent to yield a yellow oil (50 mg, 73%). **^{1}H NMR** ($CDCl_3$, 300 MHz, 25.0 °C) δ_H 8.05 (dd, J = 8.5, 0.7 Hz, 1 *H*), 7.93 (dd, J = 8.4, 1.0 Hz, 1 *H*), 7.66 (ddd, J = 8.3, 6.8, 1.4 Hz, 1 *H*), 7.48 (ddd, J = 8.4, 6.8, 1.3 Hz, 1 *H*), 7.16 (d, J = 0.7 Hz, 1 *H*), 2.87 (tt, J = 11.9, 3.4 Hz, 3 *H*), 2.67 (d, J = 0.9 Hz, 3 *H*), 2.02 (m, 2 *H*), 1.89 (m, 2 *H*), 1.79 (m, 2 *H*), 1.63 (m, 2 *H*), 1.47 (m, 2 *H*), 1.31 (m, 1 *H*). **^{13}C NMR** ($CDCl_3$, 75.5 MHz, 25.0 °C) δ_C 166.5 (C), 147.7 (C), 144.2 (C), 129.5 (CH), 128.9 (CH), 127.1 (C), 125.4 (CH), 123.6 (CH), 120.3 (CH), 47.6 (CH_3), 32.9 (CH_2), 26.6 (CH_2), 26.2 (CH_2), 18.8 (CH_3).

4-Cyclohexyl-2-methylquinoline (2)

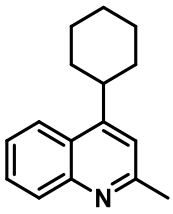

General procedure for photocatalysis under batch conditions using 2-methylquinoline (43 mg, 0.3 mmol), cyclohexane carboxylic acid (385 mg, 3.0 mmol), ammonium persulfate (137 mg, 0.6 mmol), **1Nap-BTZ** (5.8 mg, 0.015 mmol) and DMSO (3 mL) for 40 h. Purification of the crude product was achieved by silica gel column chromatography using ethyl acetate:hexane 1:3 as the eluent to yield a yellow oil (40 mg, 58%). **^{1}H NMR** ($CDCl_3$, 300 MHz, 25.0 °C) δ_H 8.03 (dt, J = 8.6, 1.7 Hz, 2 *H*), 7.64 (ddd, J = 8.3, 6.8, 1.5 Hz, 1 *H*), 7.47 (ddd, J = 8.4, 6.8, 1.3 Hz, 1 *H*), 7.16 (s, 1 *H*), 3.29 (m, 1 *H*), 3.10 (s, 3 *H*), 1.92 (m, 5 *H*), 1.54 (m, 4 *H*), 1.34 (m, 1 *H*). **^{13}C NMR** ($CDCl_3$, 75.5 MHz, 25.0 °C) δ_C 158.8 (C), 153.4 (C), 148.1 (C), 129.5 (CH), 128.8 (CH), 125.3 (C), 125.2 (CH), 122.8 (CH), 118.3 (CH), 38.8 (CH), 33.6 (CH_2), 26.9 (CH_2), 26.3 (CH_2), 25.5 (CH_3).

4-Cyclohexyl-2,6-dimethylpyridine (3)

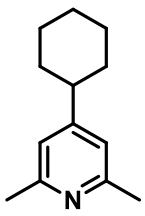

General procedure for photocatalysis under batch conditions using 2,6-dimethylpyridine (32 mg, 0.3 mmol), cyclohexane carboxylic acid (385 mg, 3.0 mmol), ammonium persulfate (137 mg, 0.6 mmol), **1Nap-BTZ** (5.8 mg, 0.015 mmol) and DMSO (3 mL) for 40 h. Purification of the crude product was achieved by silica gel column chromatography using DCM:ethyl acetate 1:2 as the eluent to yield a colourless oil (31 mg, 55%). **^{1}H NMR** ($CDCl_3$, 300 MHz, 25.0 °C) δ_H 6.79 (s, 2 *H*), 2.49 (s, 2 *H*), 2.41 (m, 1 *H*), 1.79 (m, 5 *H*), 1.33 (m, 5 *H*). **^{13}C NMR** ($CDCl_3$,

75.5 MHz, 25.0 °C) δ_C 157.5 (C), 157.3 (C), 119.0 (CH), 43.9 (C), 33.6 (CH_2), 26.6 (CH_2), 26.0 (CH_2), 24.4 (CH_3).

4-Cyclohexylquinazoline (4)

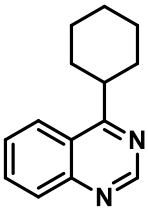

General procedure for photocatalysis under batch conditions using quinazoline (39 mg, 0.3 mmol), cyclohexane carboxylic acid (385 mg, 3.0 mmol), ammonium persulfate (137 mg, 0.6 mmol), **1Nap-BTZ** (5.8 mg, 0.015 mmol) and DMSO (3 mL) for 40 h. Purification of the crude product was achieved by silica gel column chromatography using ethyl acetate as the eluent to yield a yellow oil (41 mg, 64%). **^{1}H NMR** ($CDCl_3$, 300 MHz, 25.0 °C) δ_H 9.20 (s, 2 *H*), 8.15 (d, J = 8.6 Hz, 1 *H*), 8.00 (d, J = 8.3 Hz, 1 *H*), 7.83 (ddd, J = 8.5, 6.8, 1.5 Hz, 1 *H*), 7.60 (ddd, J = 8.5, 6.8, 1.2 Hz, 1 *H*), 3.52 (tt, J = 11.5, 3.3 Hz, 1 *H*), 1.91 (m, 4 *H*), 1.79 (m, 3 *H*), 1.40 (m, 3 *H*). **^{13}C NMR** ($CDCl_3$, 75.5 MHz, 25.0 °C) δ_C 175.1 (C), 154.8 (CH), 150.1 (C), 133.3 (CH), 129.3 (CH), 127.3 (CH), 124.2 (CH), 123.3 (C), 41.3 (CH), 32.0 (CH_2), 26.5 (CH_2), 26.0 (CH_2).

1-Cyclohexylisoquinoline (5)

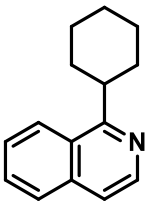

General procedure for photocatalysis under batch conditions using isoquinoline (39 mg, 0.3 mmol), cyclohexane carboxylic acid (385 mg, 3.0 mmol), ammonium persulfate (137 mg, 0.6 mmol), **1Nap-BTZ** (5.8 mg, 0.015 mmol) and DMSO (3 mL) for 40 h. Purification of the crude product was achieved by silica gel plug using DCM as the eluent to yield a yellow-brown oil (34 mg, 54%). **^{1}H NMR** ($CDCl_3$, 300 MHz, 25.0 °C) δ_H 8.48 (d, J = 6.7 Hz, 1 *H*), 8.22 (d, J = 8.4 Hz, 1 *H*), 7.80 (d, J = 5.7 Hz, 1 *H*), 7.64 (ddd, J = 8.3, 6.7, 1.3 Hz, 1 *H*), 7.57 (ddd, J = 8.6, 6.7, 1.6 Hz, 1 *H*), 7.47 (d, J = 6.0 Hz, 1 *H*), 3.56 (tt, J = 11.6, 3.5 Hz, 1 *H*), 1.94 (m, 4 *H*), 1.83 (m, 3 *H*), 1.56 (qt, J = 12.4, 3.0 Hz, 2 *H*), 1.41 (tt, J = 12.5, 3.6 Hz, 1 *H*). **^{13}C NMR** ($CDCl_3$, 75.5 MHz, 25.0 °C) δ_C 165.7 (C), 141.9 (CH), 136.4 (C), 129.6 (CH), 127.6 (CH), 126.8 (CH), 126.3 (C), 124.8 (CH), 118.9 (CH), 41.6 (CH), 32.6 (CH_2), 26.9 (CH_2), 26.3 (CH_2).

2-Cyclohexyl-1-methyl-1*H*-benzo[*d*]imidazole (6)

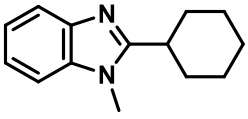

General procedure for photocatalysis under batch conditions using 1-methyl-1*H*-benzo[*d*]imidazole (40 mg, 0.3 mmol), cyclohexane carboxylic acid (385 mg, 3.0 mmol), ammonium persulfate (137 mg, 0.6 mmol), **1Nap-BTZ** (5.8 mg, 0.015 mmol) and DMSO (3 mL) for 40 h. Purification of the crude product was achieved by silica gel column chromatography using ethyl acetate as the eluent to yield a yellow-white powder (20 mg, 31%). **^{1}H NMR** ($CDCl_3$, 300 MHz, 25.0 °C) δ_H 7.73 (m, 1 *H*), 7.28 (m, 1 *H*), 7.22 (m, 2 *H*), 3.73 (s, 3 *H*), 2.84 (tt, J = 11.6, 3.5 Hz, 1

H), 1.94 (m, 4 *H*), 1.79 (m, 3 *H*), 1.40 (m, 3 *H*). **^{13}C NMR** ($CDCl_3$, 75.5 MHz, 25.0 °C) δ_C 159.0 (C), 142.5 (C), 135.6 (C), 121.9 (CH), 121.7 (CH), 119.3 (CH), 108.9 (CH), 36.4 (CH_3), 31.5 (CH_2), 29.6 (CH_3), 26.4 (CH_2), 25.8 (CH_2).

2-(Adamantan-1-yl)-4-methylquinoline (7)

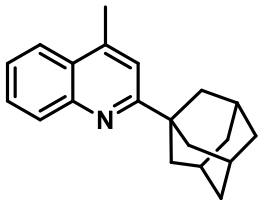

General procedure for photocatalysis under batch conditions using lepidine (43 mg, 0.3 mmol), adamantane-1-carboxylic acid (541 mg, 3.0 mmol), ammonium persulfate (137 mg, 0.6 mmol), **1Nap-BTZ** (5.8 mg, 0.015 mmol) and DMSO (3 mL) for 40 h. Purification of the crude product was achieved by silica gel column chromatography using DCM as the eluent to yield pale yellow crystals (44 mg, 53%). **^{1}H NMR** ($CDCl_3$, 300 MHz, 25.0 °C) δ_H 8.07 (d, J = 8.5 Hz, 1 *H*), 7.94 (dd, J = 8.3, 1.2 Hz, 1 *H*), 7.65 (ddd J = 8.4, 6.8, 1.6 Hz, 1 *H*,), 7.48 (ddd, J = 8.3, 6.9, 1.2 Hz, 1 *H*). 7.37 (d, J = 0.8 Hz, 1 *H*), 2.70 (s, 3 *H*), 2.14 (m, 9 *H*), 1.83 (m, 6 *H*). **^{13}C NMR** ($CDCl_3$, 75.5 MHz, 25.0 °C) δ_C 168.7 (C), 147.6 (C), 143.6 (C), 130.0 (CH), 128.6 (CH), 126.7 (C), 125.3 (CH), 123.4 (CH), 118.5 (CH), 41.6 (CH_2), 39.6 (CH_2), 36.9 (CH_2), 28.9 (CH_3), 19.0 (CH_3).

2-Isopentyl-4-methylquinoline (8)

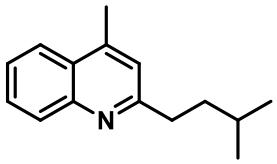

General procedure for photocatalysis under batch conditions using lepidine (43 mg, 0.3 mmol), 4-methylvaleric acid (385 mg, 3.0 mmol), ammonium persulfate (274 mg, 1.2 mmol), **1Nap-BTZ** (5.8 mg, 0.015 mmol) and DMSO (3 mL) for 40 h. Purification of the crude product was achieved by silica gel column chromatography using DCM:ethyl acetate 1:1 as the eluent to yield a yellow-brown oil (30 mg, 47%). **^{1}H NMR** ($CDCl_3$, 300 MHz, 25.0 °C) δ_H 8.04 (d, J = 8.6 Hz, 1 *H*), 7.94 (dd, J = 8.4, 1.5 Hz, 1 *H*), 7.66 (ddd, J = 8.7, 6.9, 1.4 Hz, 1 *H*), 7.49 (ddd, J = 8.4, 6.8, 1.3 Hz, 1 *H*), 7.14 (d, J = 0.8 Hz, 1 *H*), 2.92 (m, 2 *H*), 2.67 (s, 3 *H*), 1.69 (m, 3 *H*), 0.98 (d, J = 6.5 Hz, 6 *H*). **^{13}C NMR** ($CDCl_3$, 75.5 MHz, 25.0 °C) δ_C 163.0 (C), 147.7 (C), 144.2 (C), 129.3 (CH), 129.0 (CH), 126.8 (C), 125.4 (CH), 123.6 (CH), 122.0 (CH), 39.2 (CH_2), 37.2 (CH_2), 28.2 (CH_3), 22.6 (CH_3), 18.7 (CH).

N-((4-methylquinolin-2-yl)methyl)acetamide (9)

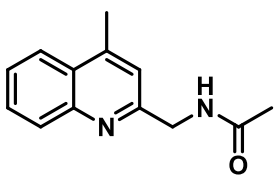

General procedure for photocatalysis under batch conditions using lepidine (43 mg, 0.3 mmol), *N*-acetylglycine (351 mg, 3.0 mmol), ammonium persulfate (137 mg, 0.6 mmol), **1Nap-BTZ** (5.8 mg, 0.015 mmol) and DMSO (3 mL) for 40 h. Purification of the crude product was achieved by silica gel column chromatography using DCM:ethyl acetate 1:1 to elute the photocatalyst before switching to ethyl acetate:methanol 10:1 to isolate the product as

a white powder (61 mg, 95%). **^{1}H NMR** ($CDCl_3$, 300 MHz, 25.0 °C) δ_H 8.03 (dd, J = 8.5, 0.6 Hz, 1 *H*,), 7.97 (d, J = 8.4, 0.6 Hz, 1 *H*), 7.70 (ddd, J = 8.3, 6.9, 1.5 Hz, 1 *H*), 7.54 (ddd, J = 8.3, 6.9, 1.5 Hz, 1 *H*), 7.22 (bs, 1 *H*), 7.15 (s, 1 *H*), 4.67 (d, J = 4.6 Hz, 2 *H*), 2.68 (d, J = 0.9 Hz, 2 *H*), 2.14 (s, 3 *H*). **^{13}C NMR** ($CDCl_3$, 75.5 MHz, 25.0 °C) δ_C 169.3 (C), 154.8 (C), 146.0 (C), 144.2 (C), 128.4 (CH), 128.2 (CH), 126.4 (C), 125.2 (CH), 122.8 (CH), 119.6 (CH), 43.9 (CH_2), 22.3 (CH_3), 17.7 (CH_3).

1-(3,4-Dimethoxybenzyl)isoquinoline (10)

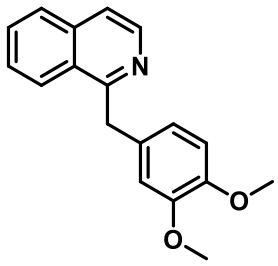

General procedure for photocatalysis under batch conditions using isoquinoline (39 mg, 0.3 mmol), 2-(3,4-dimethoxyphenyl)acetic acid (589 mg, 3.0 mmol), ammonium persulfate (137 mg, 0.6 mmol), **1Nap-BTZ** (5.8 mg, 0.015 mmol) and DMSO (3 mL) for 40 h. Purification of the crude product was achieved by silica gel column chromatography using DCM:ethyl acetate 2:1 as the eluent to yield a yellow oil (48 mg, 57%). **^{1}H NMR** ($CDCl_3$, 300 MHz, 25.0 °C) δ_H 8.48 (d, J = Hz, 1 *H*), 8.17 (d, J = Hz, 1 *H*), 7.79 (d, J = Hz, 1 *H*), 7.62 (ddd, J = Hz, 1 *H*), 7.5 (d, J = Hz, 1 *H*), 7.52 (ddd, J = Hz, 1 *H*), 6.79 (m, 3 *H*), 4.60 (s, 2 *H*), 3.79 (s, 3 *H*), 3.77 (s, 3 *H*). **^{13}C NMR** ($CDCl_3$, 75.5 MHz, 25.0 °C) δ_C 160.3 (C), 149.0 (C), 147.5 (C), 141.9 (CH), 136.6 (C), 130.0 (C), 129.9 (CH), 127.4 (CH), 127.2 (CH), 125.8 (CH), 120.6 (CH), 119.8 (CH), 112.0 (CH), 111.2 (CH), 55.8 (CH_3), 55.8 (CH_3), 41.6 (CH_2).

7.4 Photocatalysis In Flow

Procedure For Photocatalysis Under Flow Conditions

Heteroarene (0.6 mmol), **1Nap-BTZ** (11.6 mg, 0.03 mmol), ammonium persulfate (274 mg, 6.0 mmol) and cyclohexane carboxylic acid (769 mg, 30.0 mmol) were added to an oven dried round bottom flask equip with a septum. Anhydrous DMSO (6 mL) was then added and the mixture degassed using nitrogen for 10 minutes. The reaction mixture was then pumped using a Vaportec flow reactor through a 5 mL coil of fluorinated ethylene-propylene (FEP) tubing at a constant rate of 1 mL min^{-1} under an atmosphere of nitrogen (using a balloon filled with nitrogen). Irradiation was achieved either using an in-house manufactured 12 W LED (external light source) or by placing the coil into a UV-150 flow photoreactor (internal light source, 60 W). Following reaction, the reaction mixture was worked up using the same procedure utilised under batch conditions.

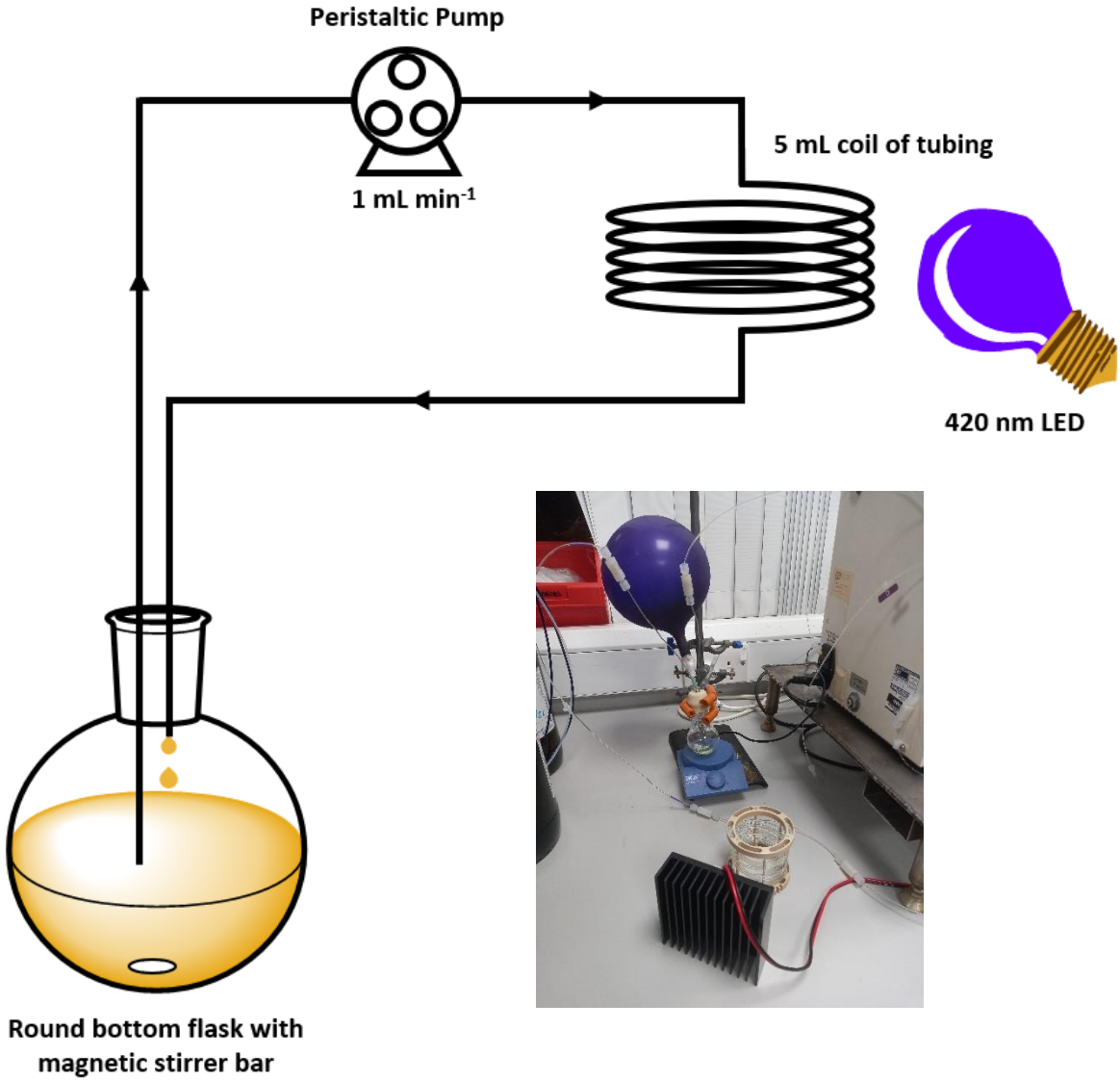

Figure S120 Schematic representation of the experimental setup used for flow photocatalysis. Inset photograph shows the set up for irradiating the coil of tubing. The reflective box normally used to house the LED and reaction vessel has been removed for clarity.

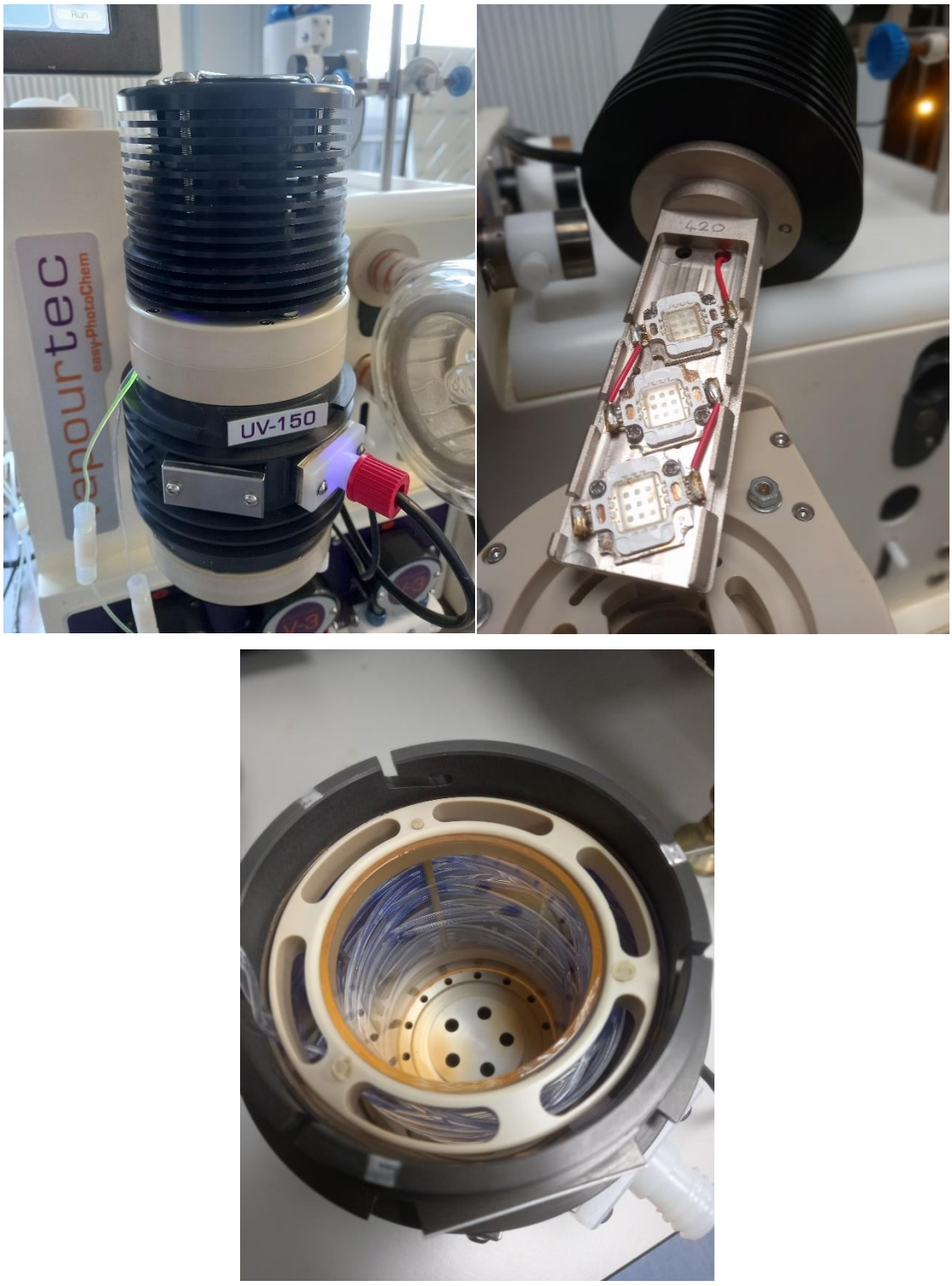

Figure S121 Easy-Photochem flow system from Vapourtec equipped with a UV-150 photoreactor. (A) UV-150 photoreactor in operation. Temperature is regulated by the thermocouple (red adaptor on the side of the reactor) linked to a fan on the top of the module (temperature maintained at 25 °C. (B) 420 nm LED shown separate to the reactor (three more LEDs are positioned on the reverse side of the module). (C) Disassembled UV-150 photoreactor showing the interior of the reactor with reflective coating on the walls. The LED shown in (B) sits in the centre and irradiates the tubing in 360°.

8. Characterisation of Photocatalysts

4,7-Diphenylbenzo[*c*][1,2,5]thiadiazole (pH-BTZ)

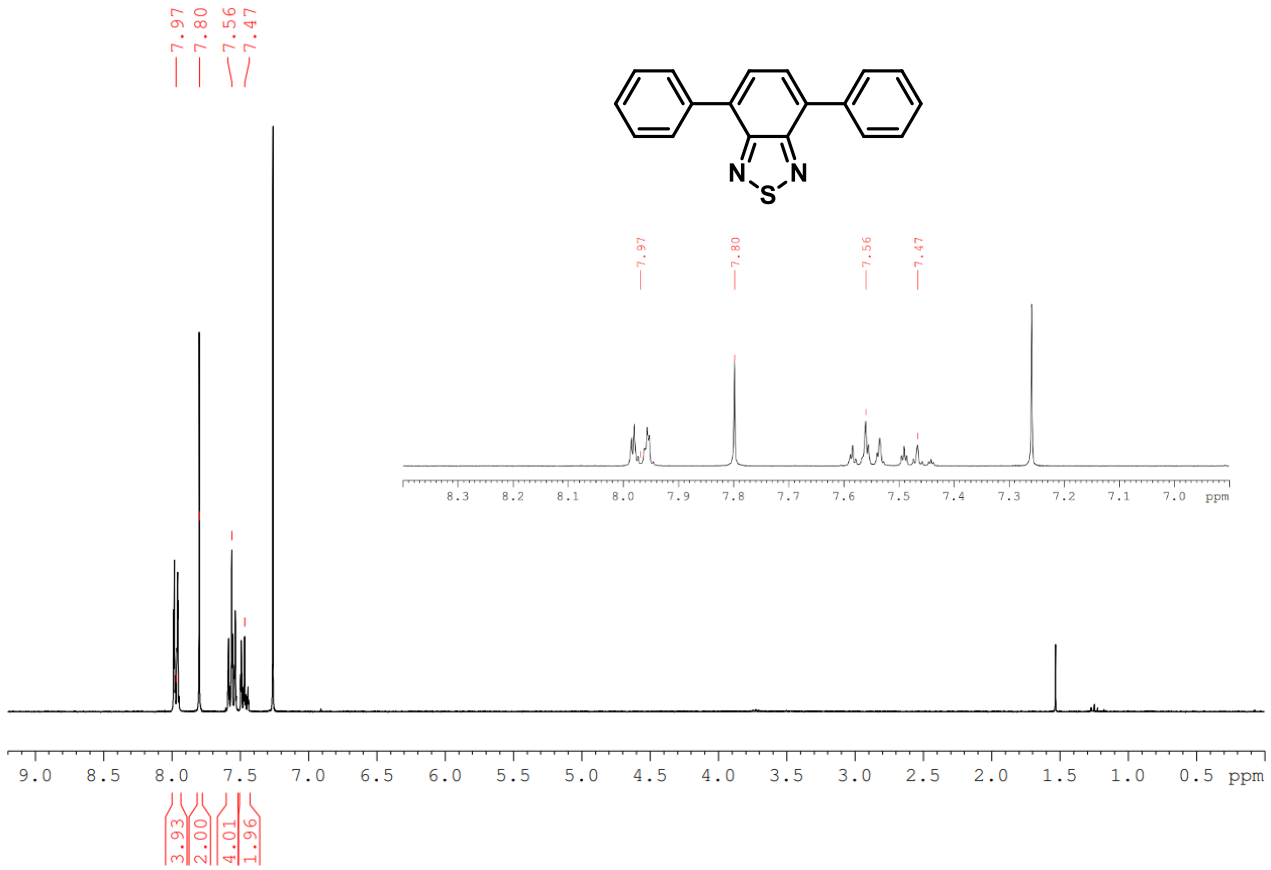

Figure S122 ^{1}H NMR of **pH-BTZ** in $CDCl_3$.

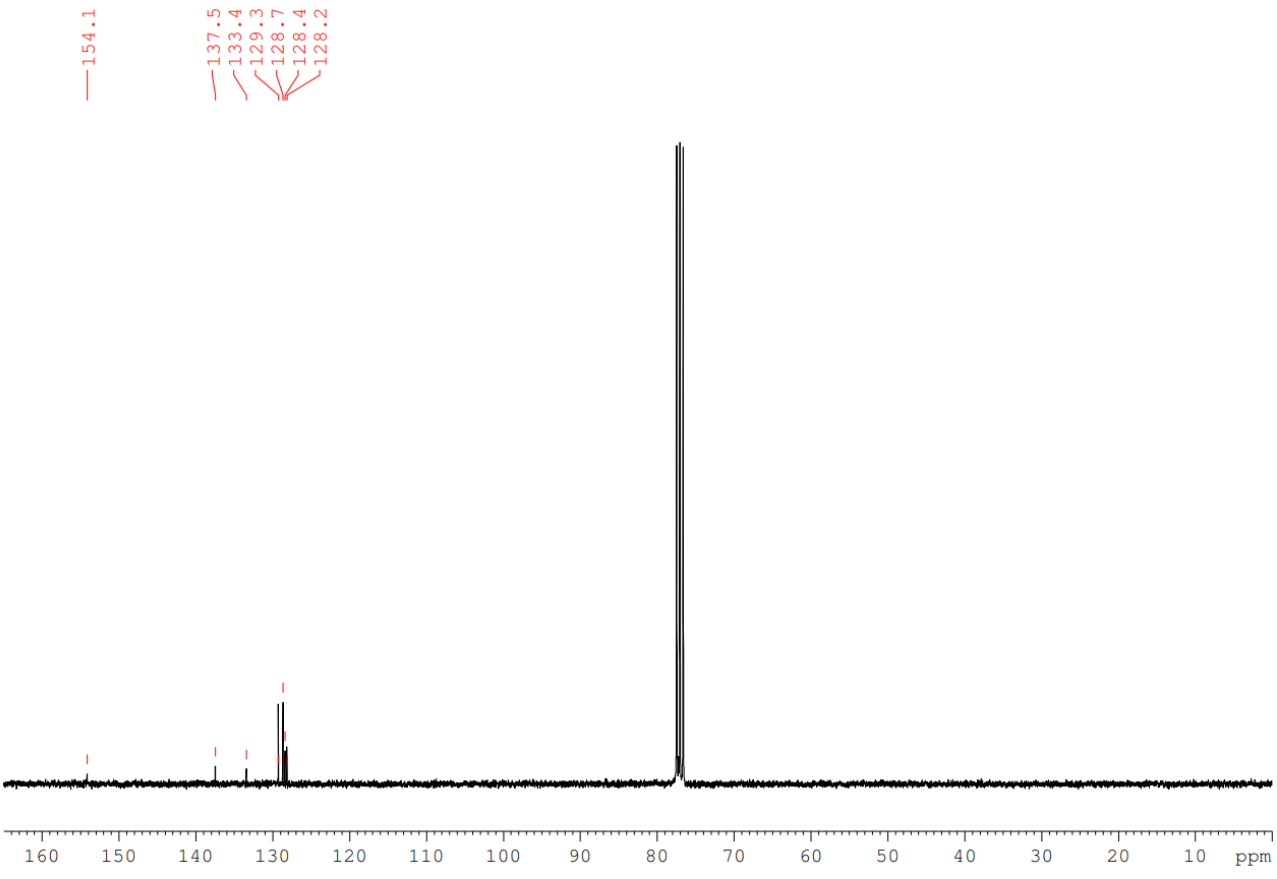

Figure S123 ^{13}C NMR of **pH-BTZ** in $CDCl_3$.

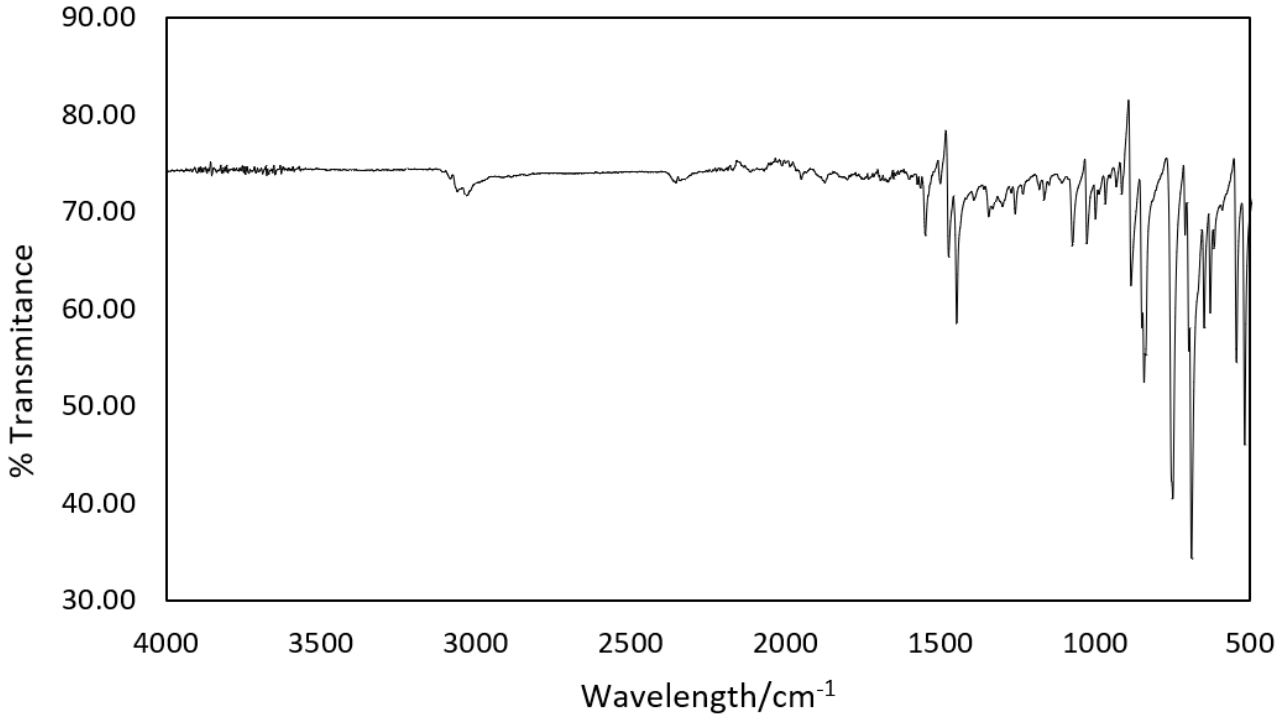

Figure S124 IR spectra of **pH-BTZ**.

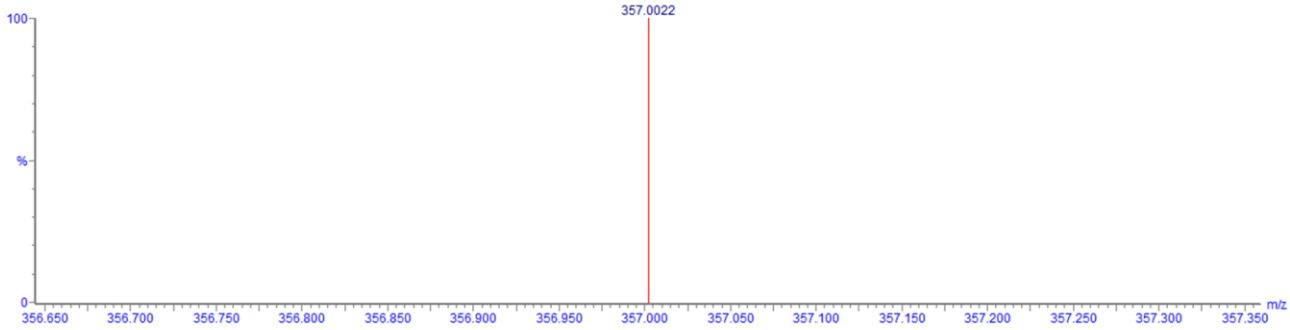

Figure S125 HRMS spectra of **pH-BTZ**.

4,7-Bis(4-fluorophenyl)benzo[*c*][1,2,5]thiadiazole (pF-BTZ)

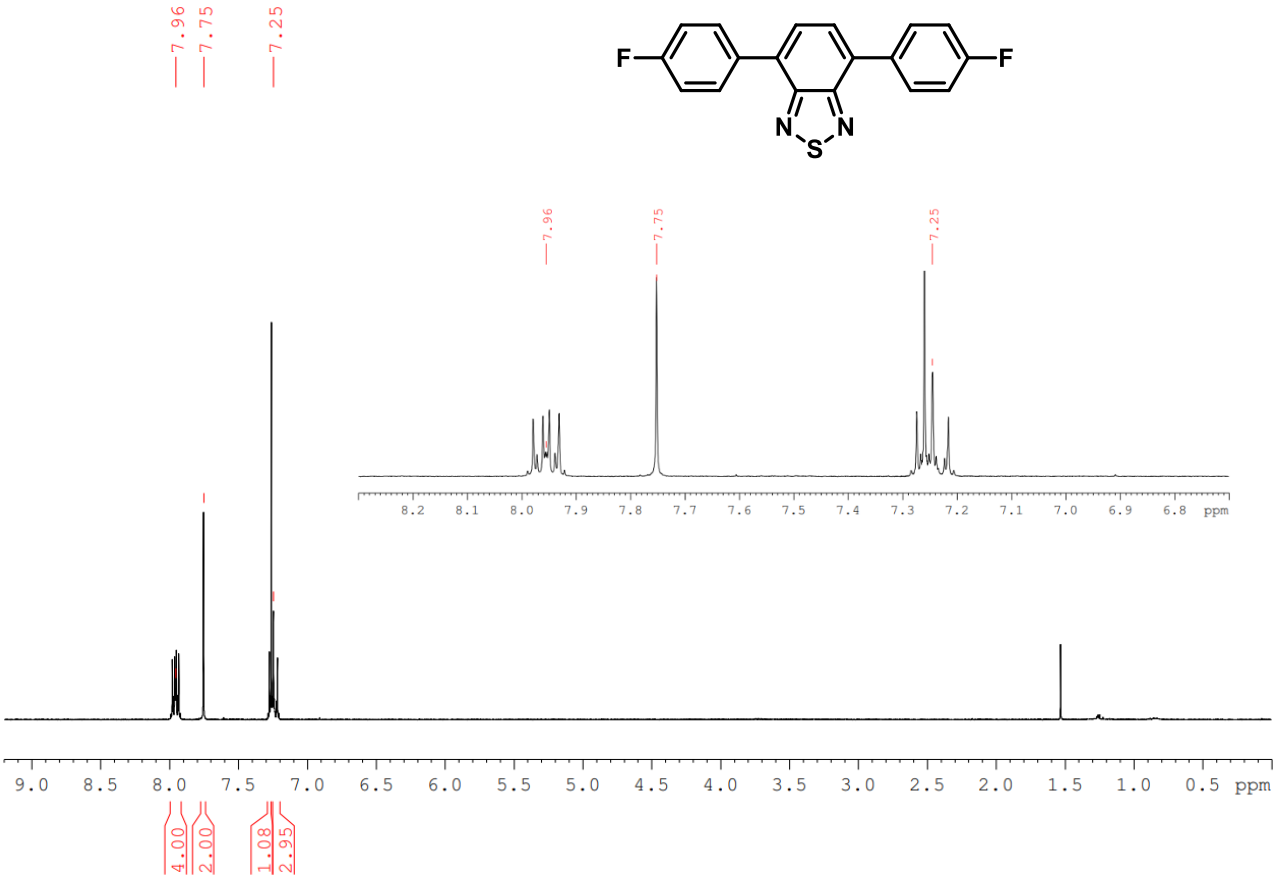

Figure S126 ^{1}H NMR of **pF-BTZ** in $CDCl_3$.

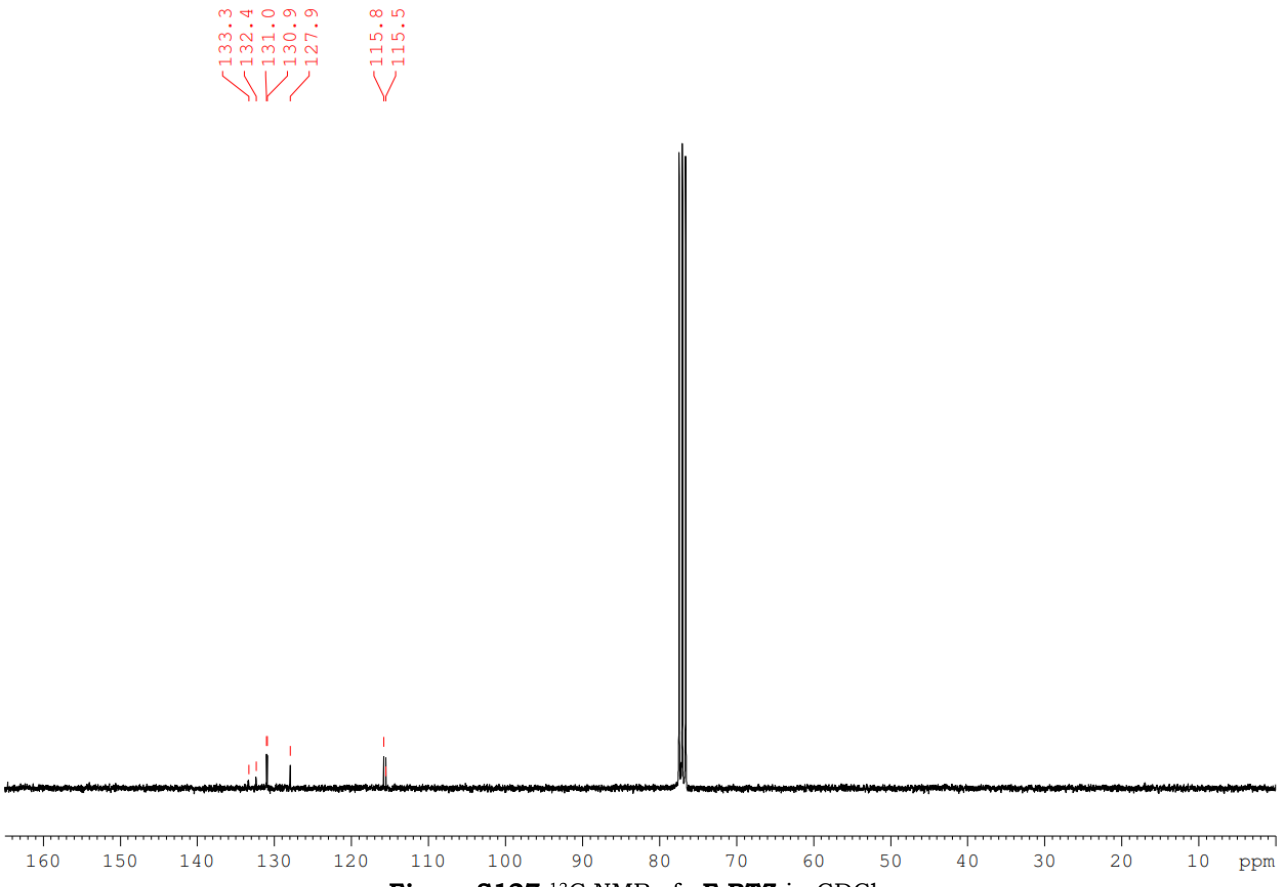

Figure S127 ^{13}C NMR of **pF-BTZ** in $CDCl_3$.

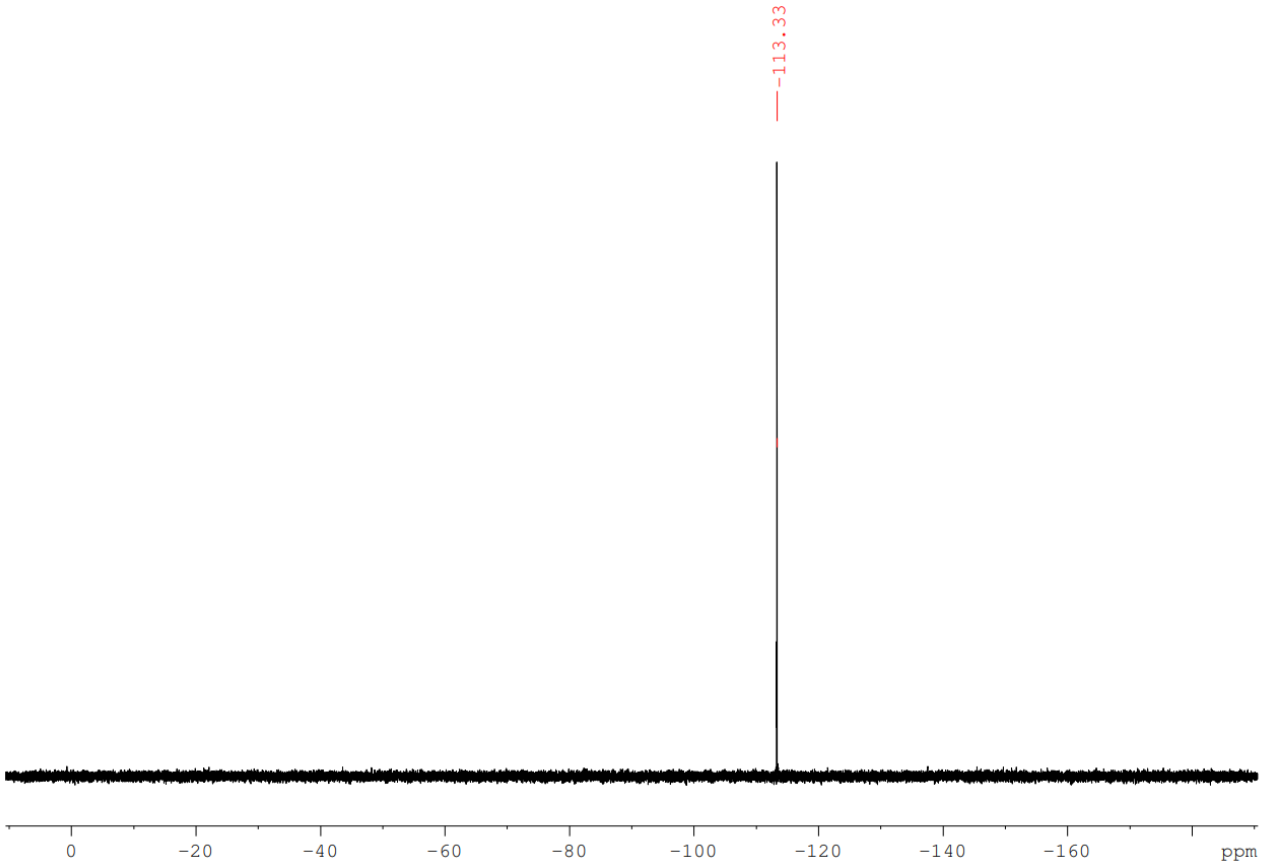

Figure S128 ^{19}F NMR of **pF-BTZ** in $CDCl_3$.

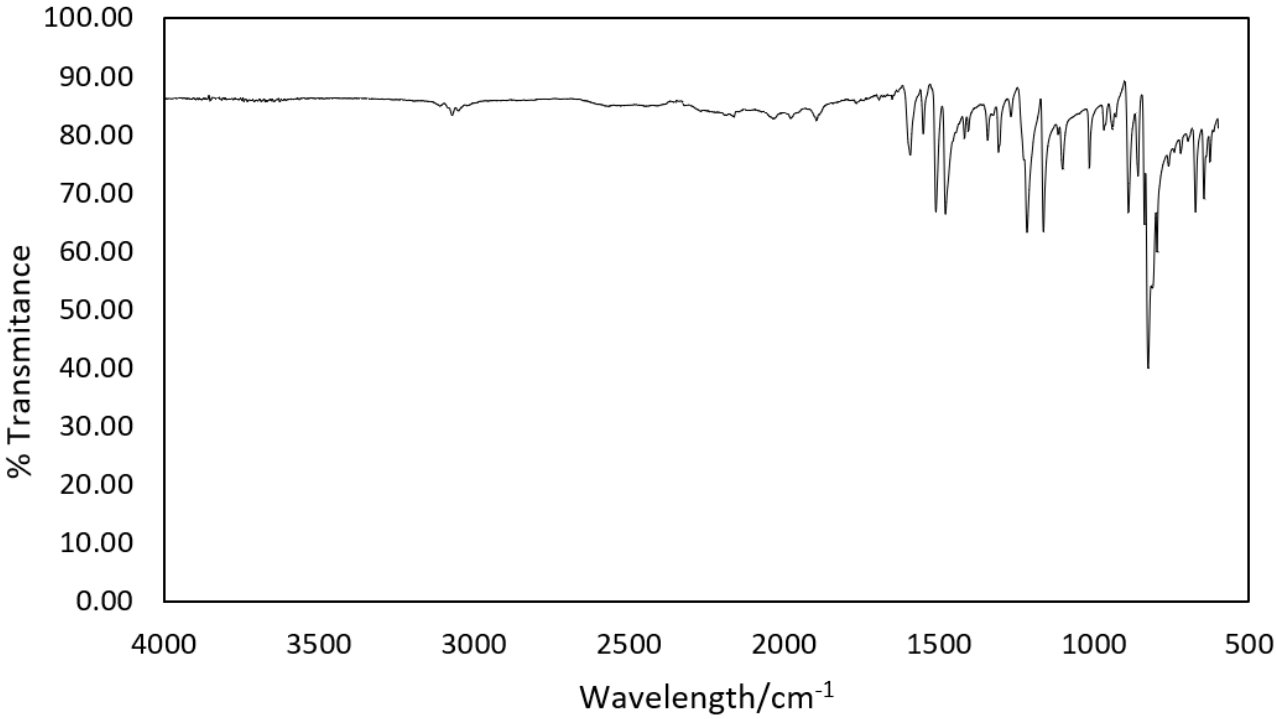

Figure S129 IR spectra of **pF-BTZ**.

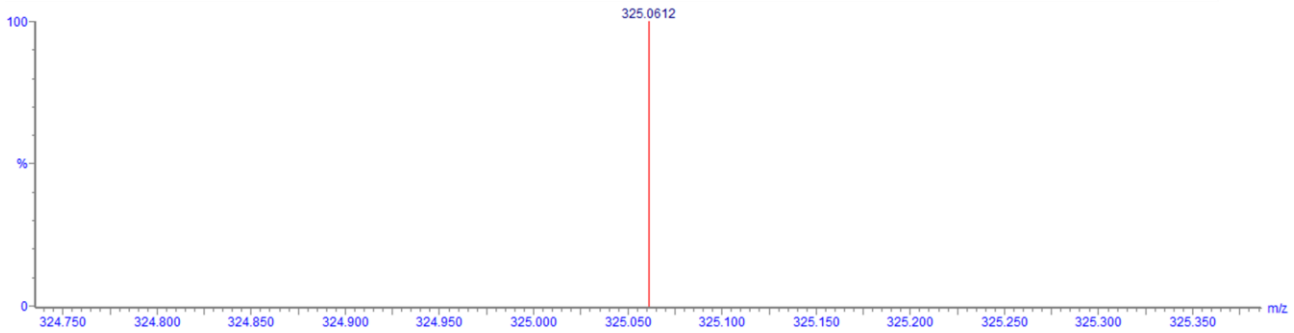

Figure S130 HRMS spectra of **pF-BTZ**.

4,7-Bis(4-chlorophenyl)benzo[*c*][1,2,5]thiadiazole (pCl-BTZ)

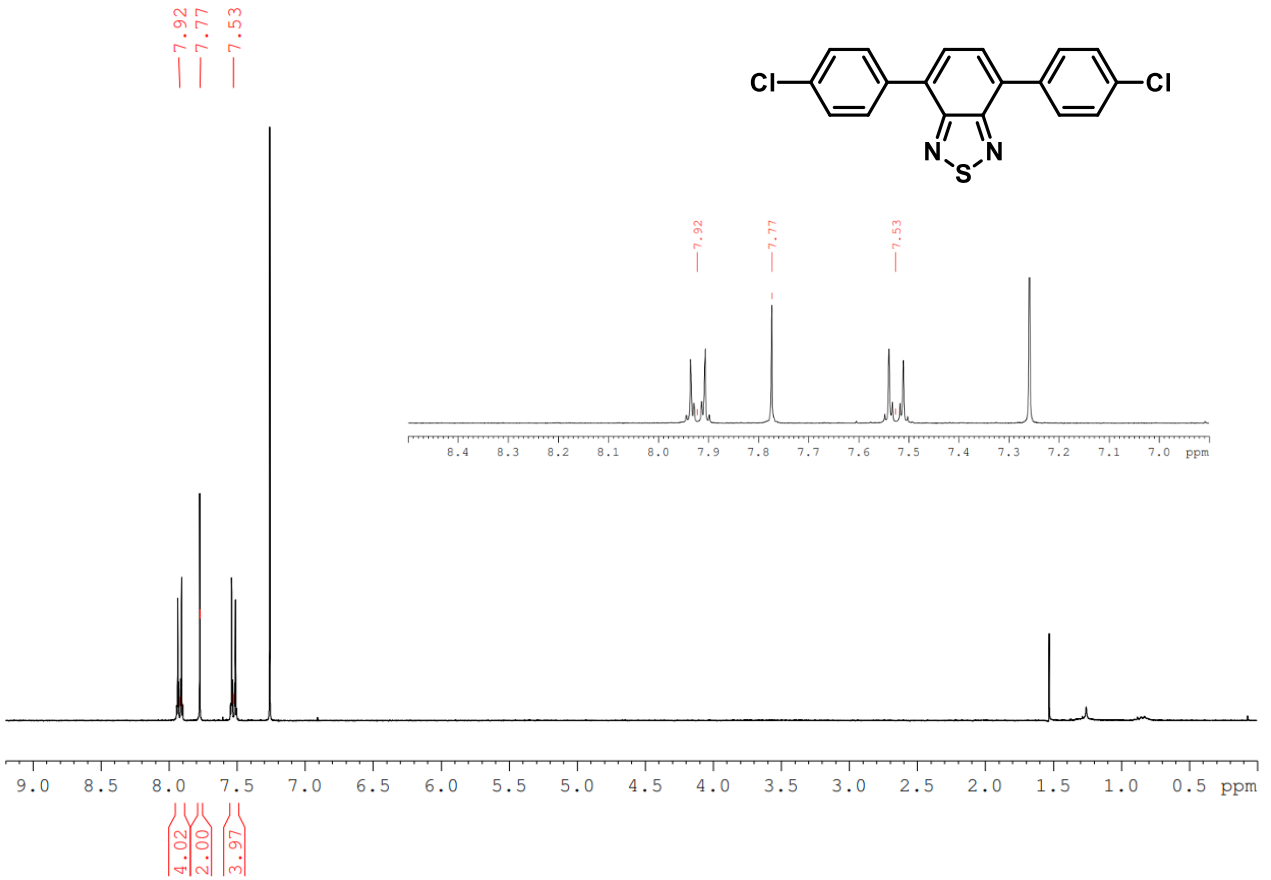

Figure S131 ^{1}H NMR spectra of **pCl-BTZ** in $CDCl_3$.

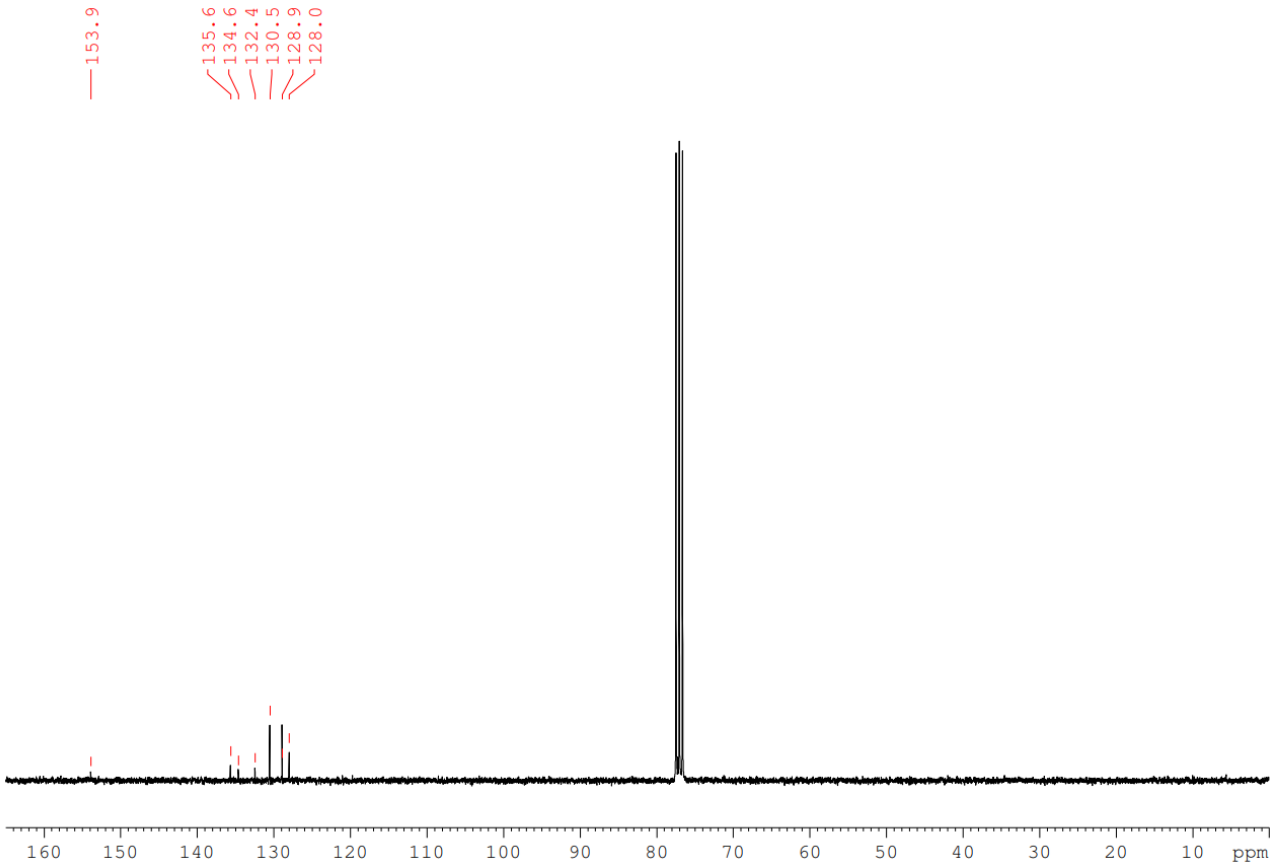

Figure S132 ^{13}C NMR spectra of **pCl-BTZ** in $CDCl_3$.

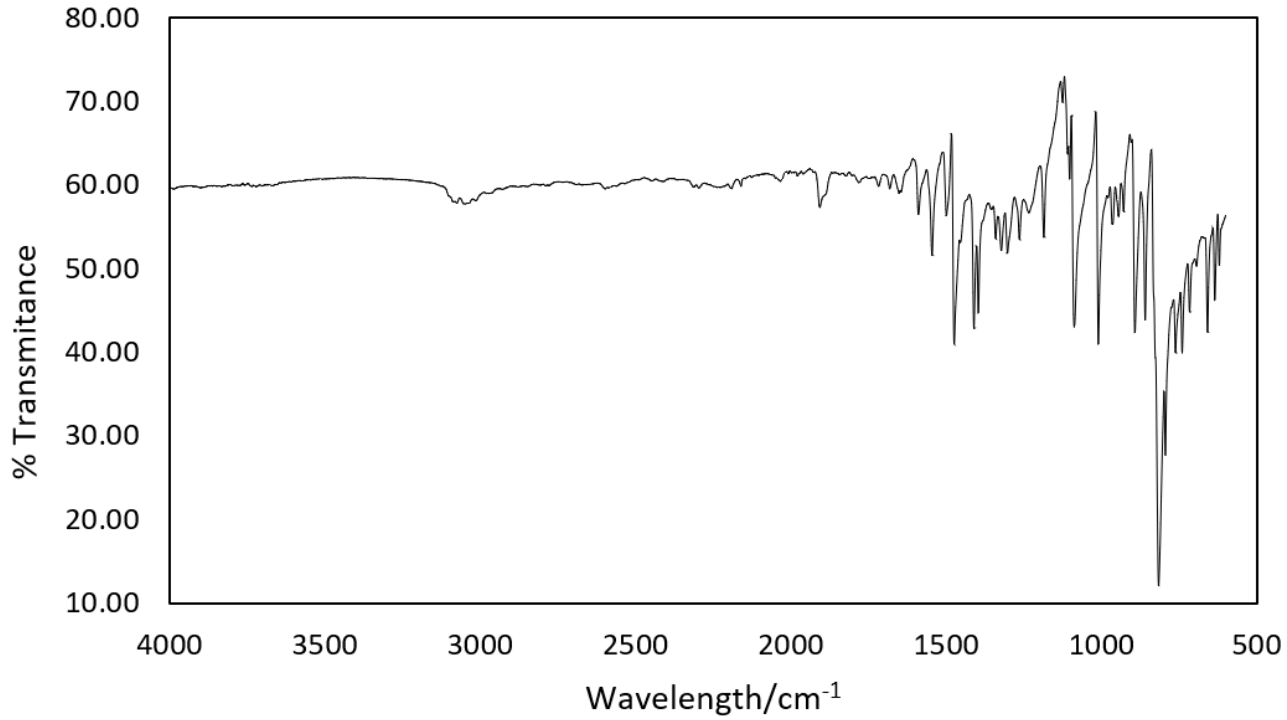

Figure S133 IR spectra of **pCl-BTZ**.

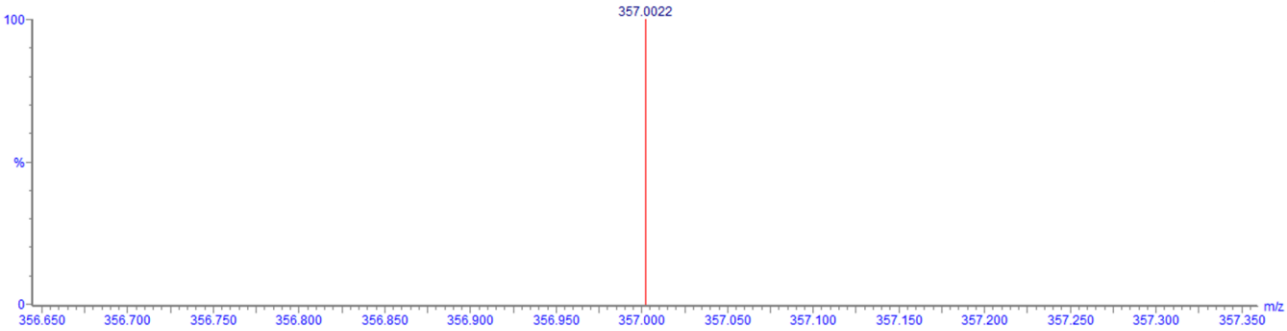

Figure S134 HRMS spectra of **pCl-BTZ**.

4,7-Bis(4-bromophenyl)benzo[*c*][1,2,5]thiadiazole (pBr-BTZ)

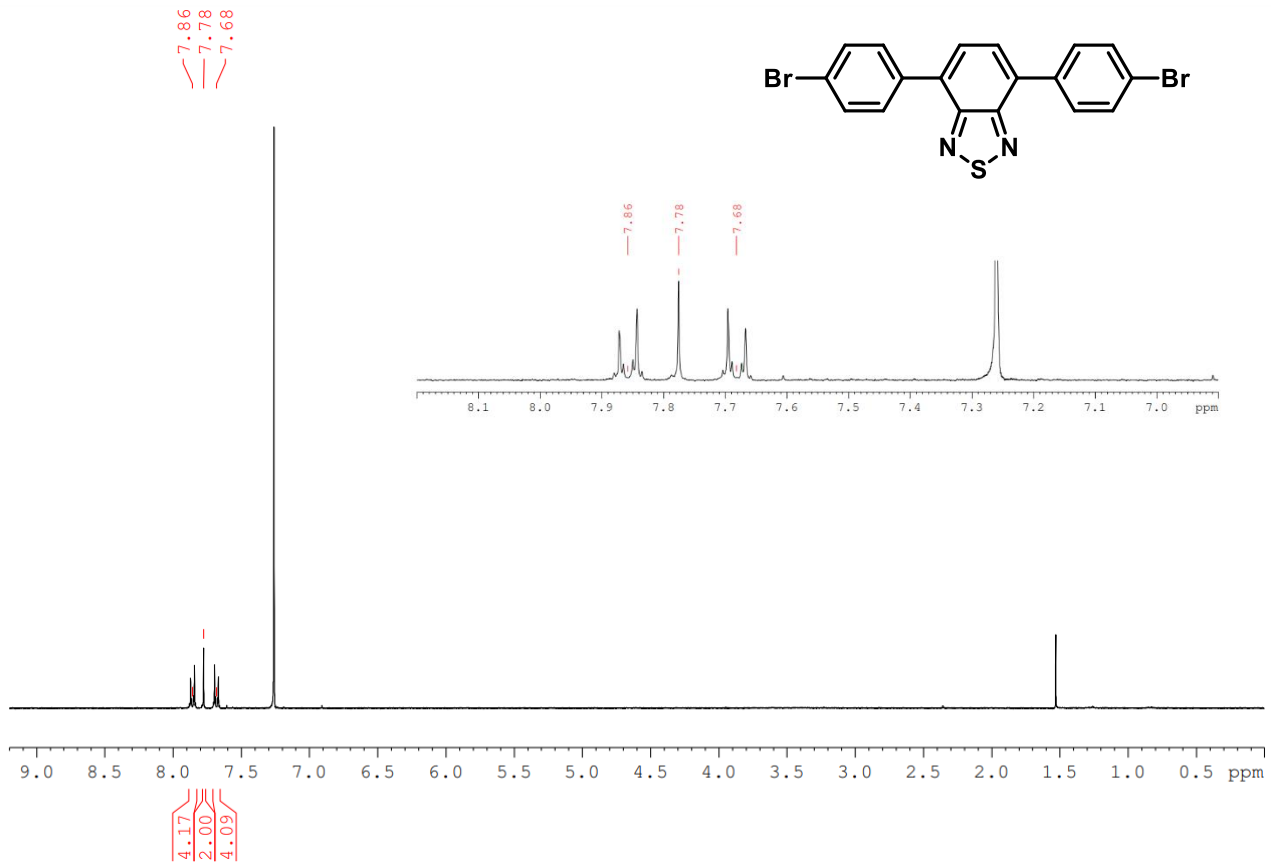

Figure S135 ^{1}H NMR spectra of **pBr-BTZ** in $CDCl_3$.

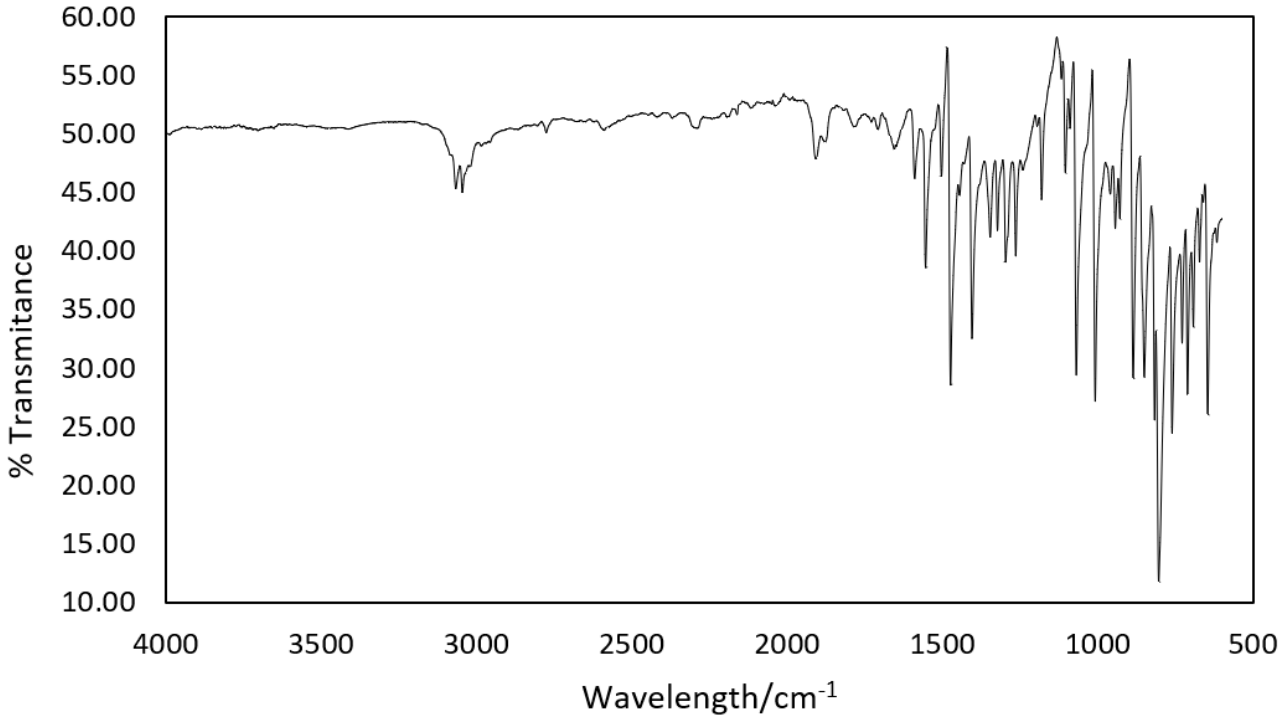

Figure S136 IR spectra of **pBr-BTZ**.

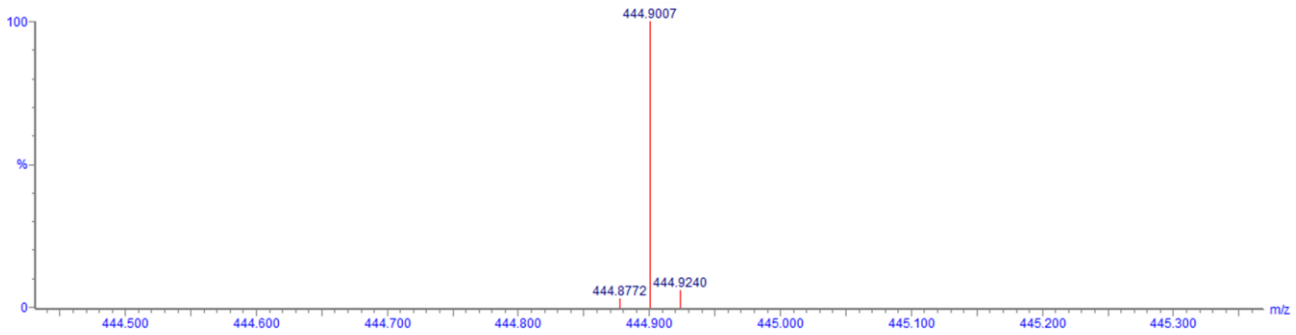

Figure S137 HRMS spectra of **pBr-BTZ**.

4,7-Bis(4-iodophenyl)benzo[*c*][1,2,5]thiadiazole (pI-BTZ)

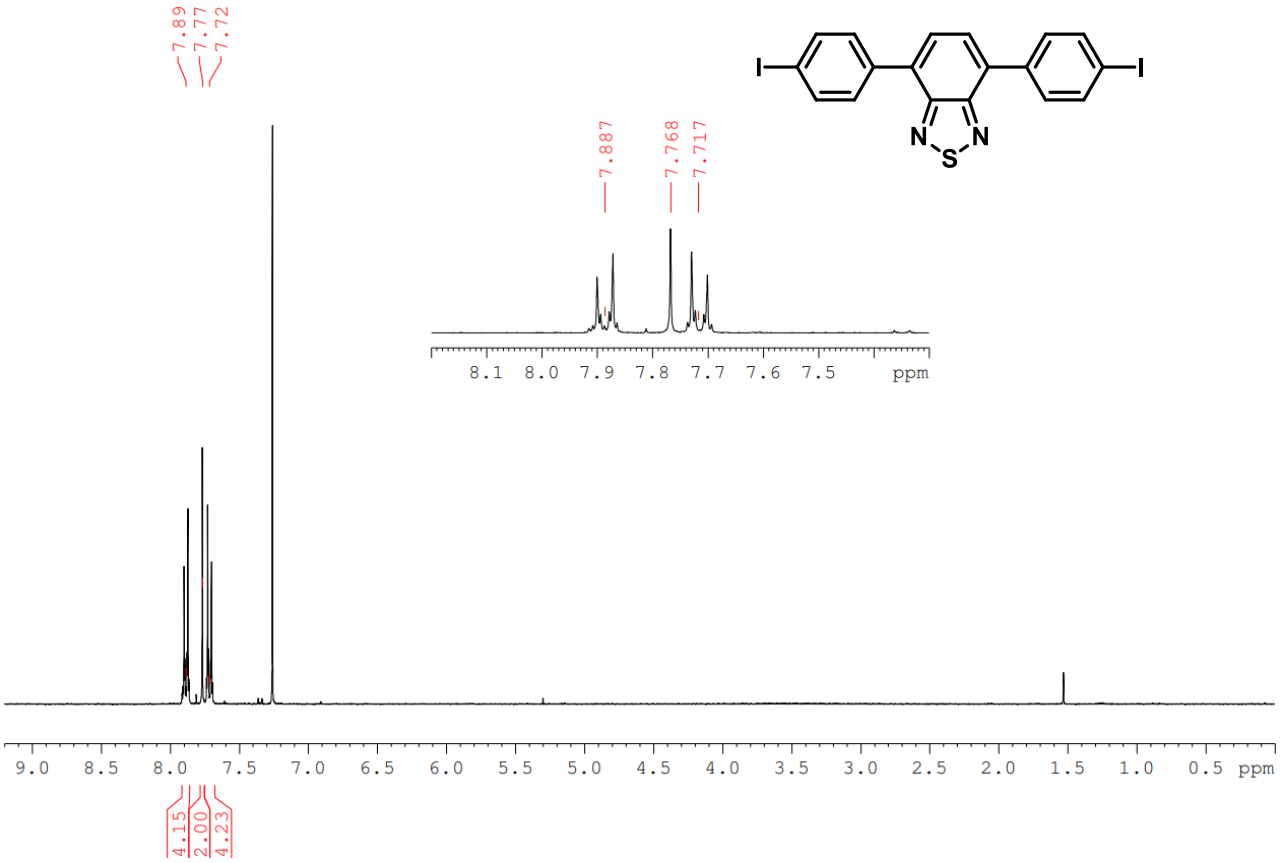

Figure S138 ^{1}H NMR spectra of **pI-BTZ** in $CDCl_3$.

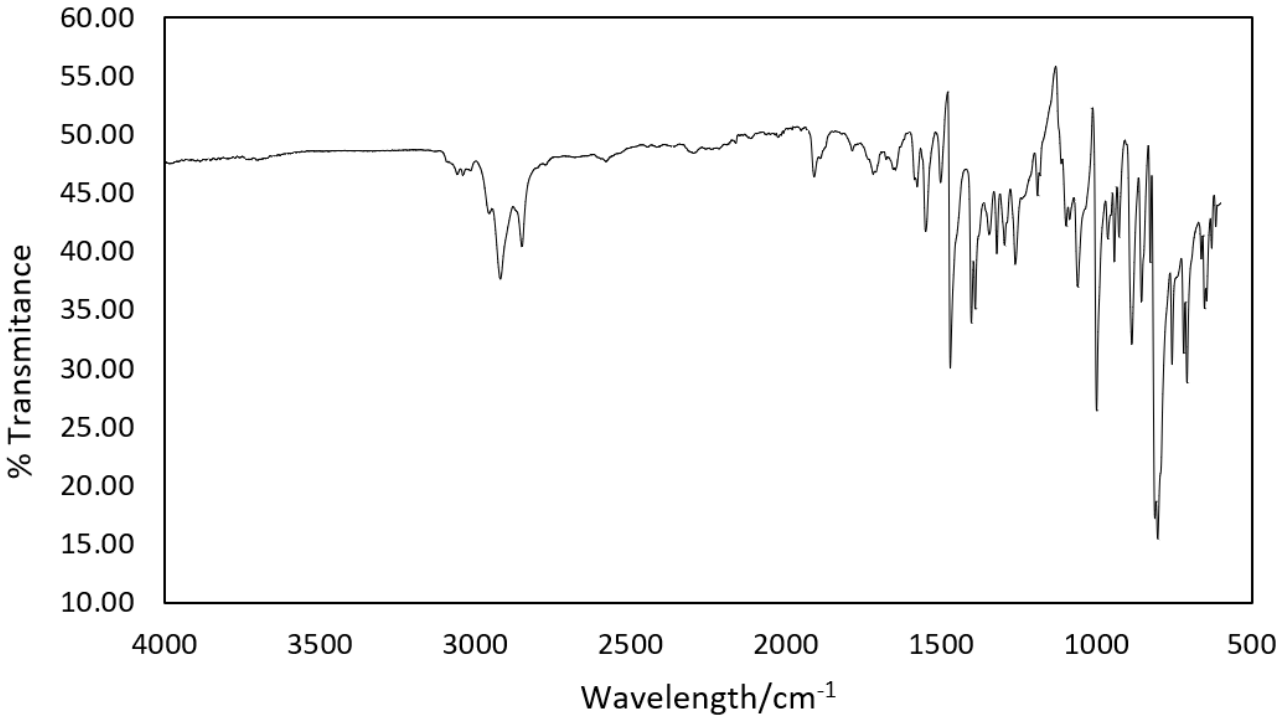

Figure S139 IR spectra of **pI-BTZ**.

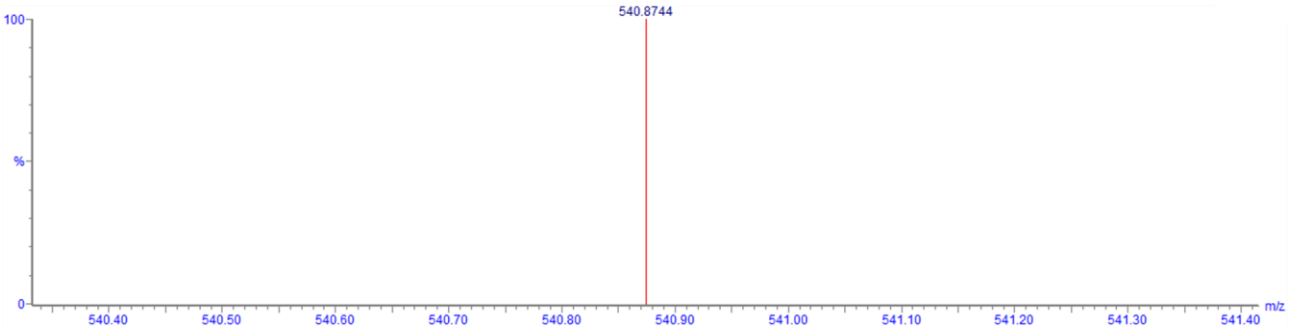

Figure S140 HRMS spectra of **pI-BTZ**.

4,7-Bis(4-(thiophen-2-yl)phenyl)benzo[*c*][1,2,5]thiadiazole (pTh-BTZ)

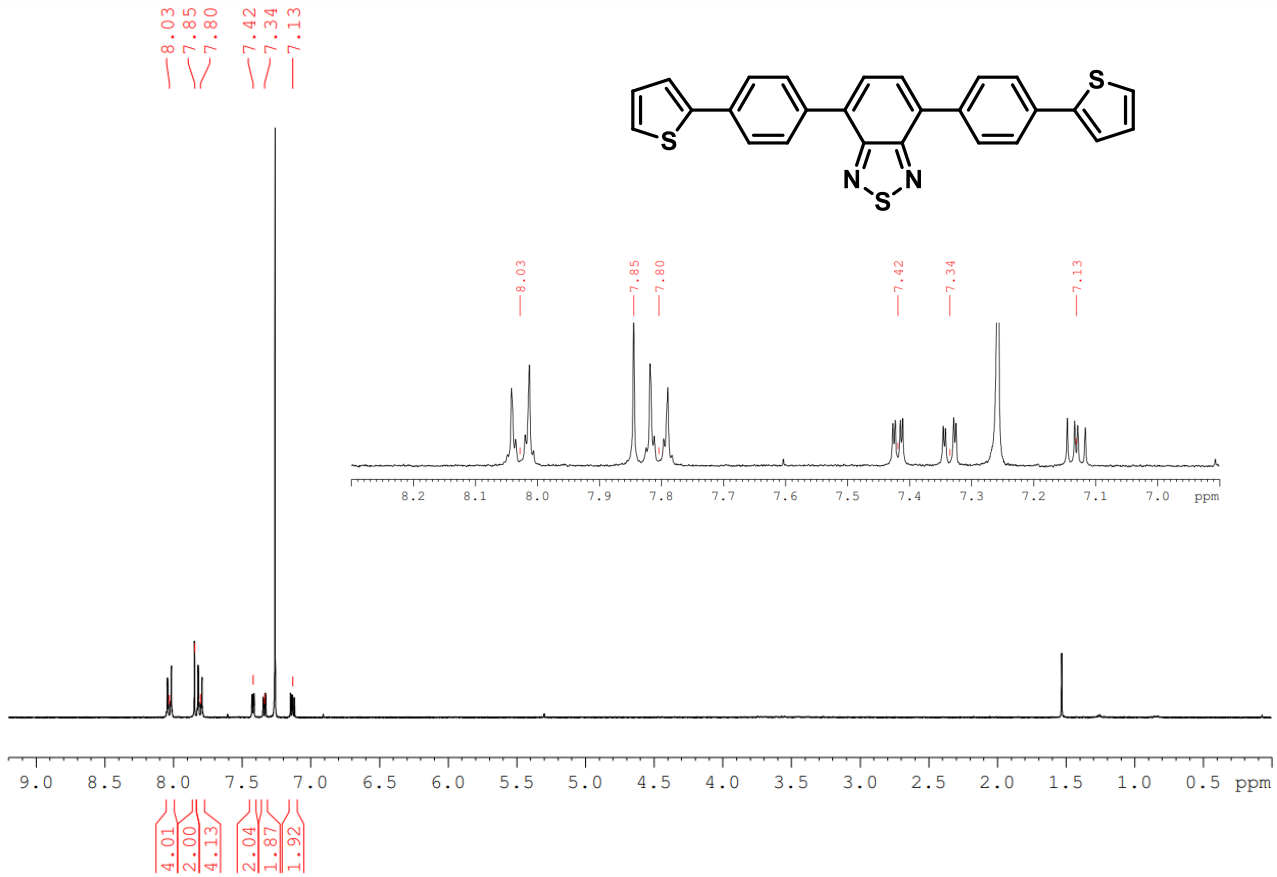

Figure S141 ^{1}H NMR spectra of **pTh-BTZ** in $CDCl_3$.

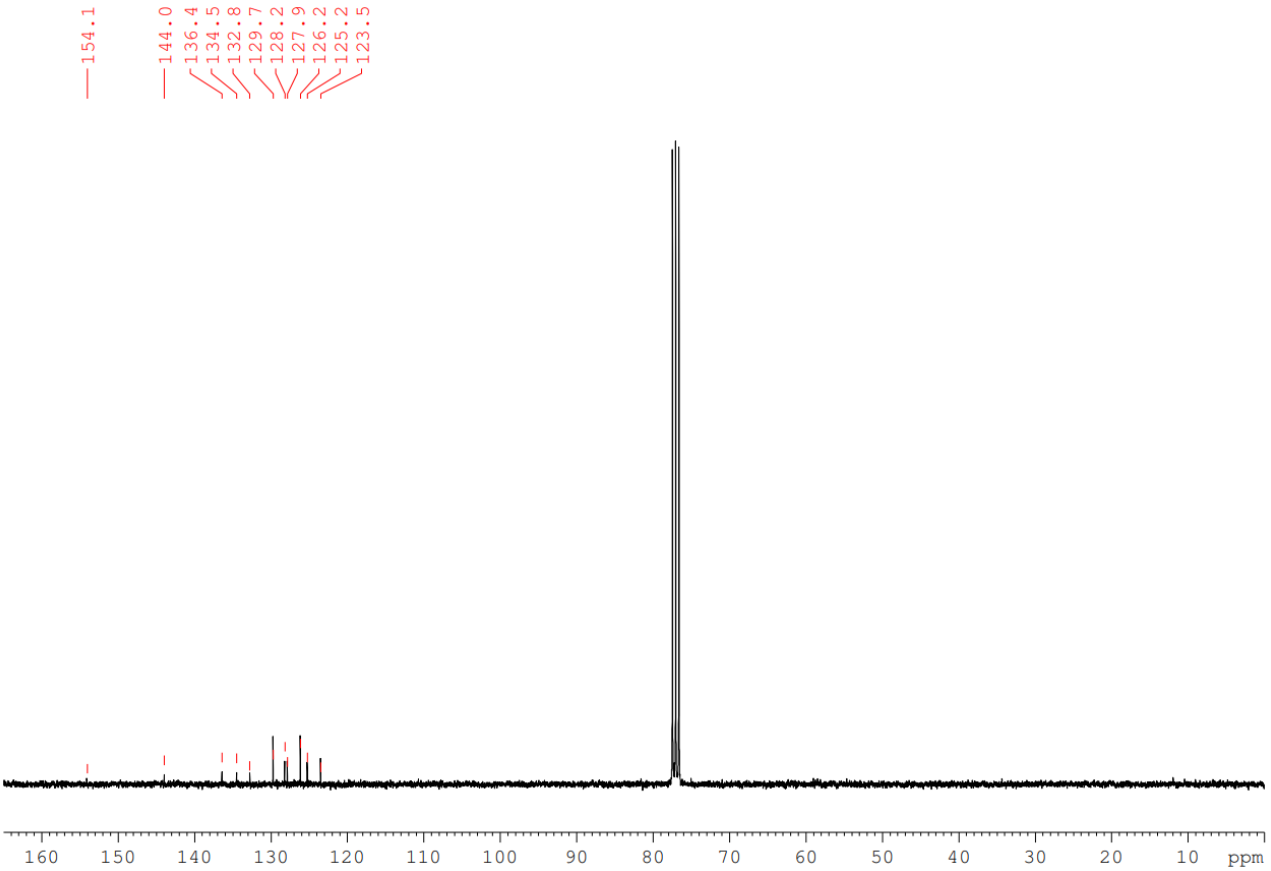

Figure S142 ^{13}C NMR spectra of **pTh-BTZ** in $CDCl_3$.

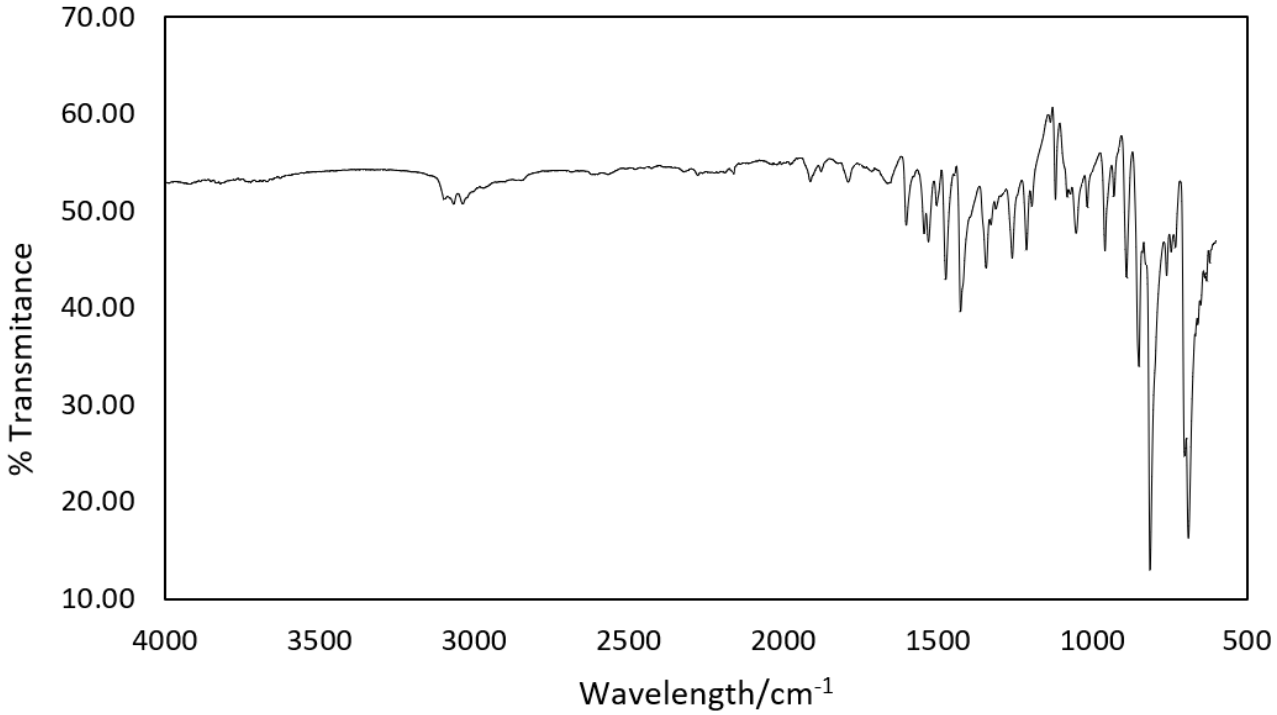

Figure S143 IR spectra of **pTh-BTZ**.

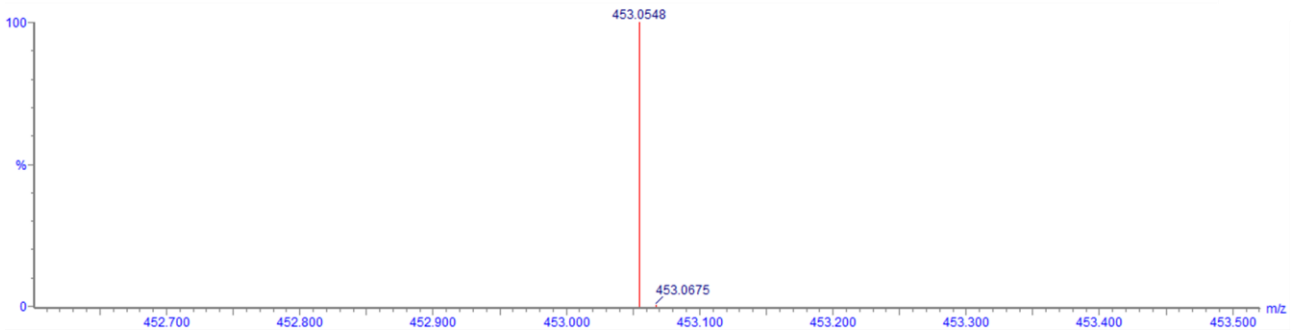

Figure S144 HRMS spectra of **pTh-BTZ**.

4,7-Di(thiophen-2-yl)benzo[*c*][1,2,5]thiadiazole (Th-BTZ)

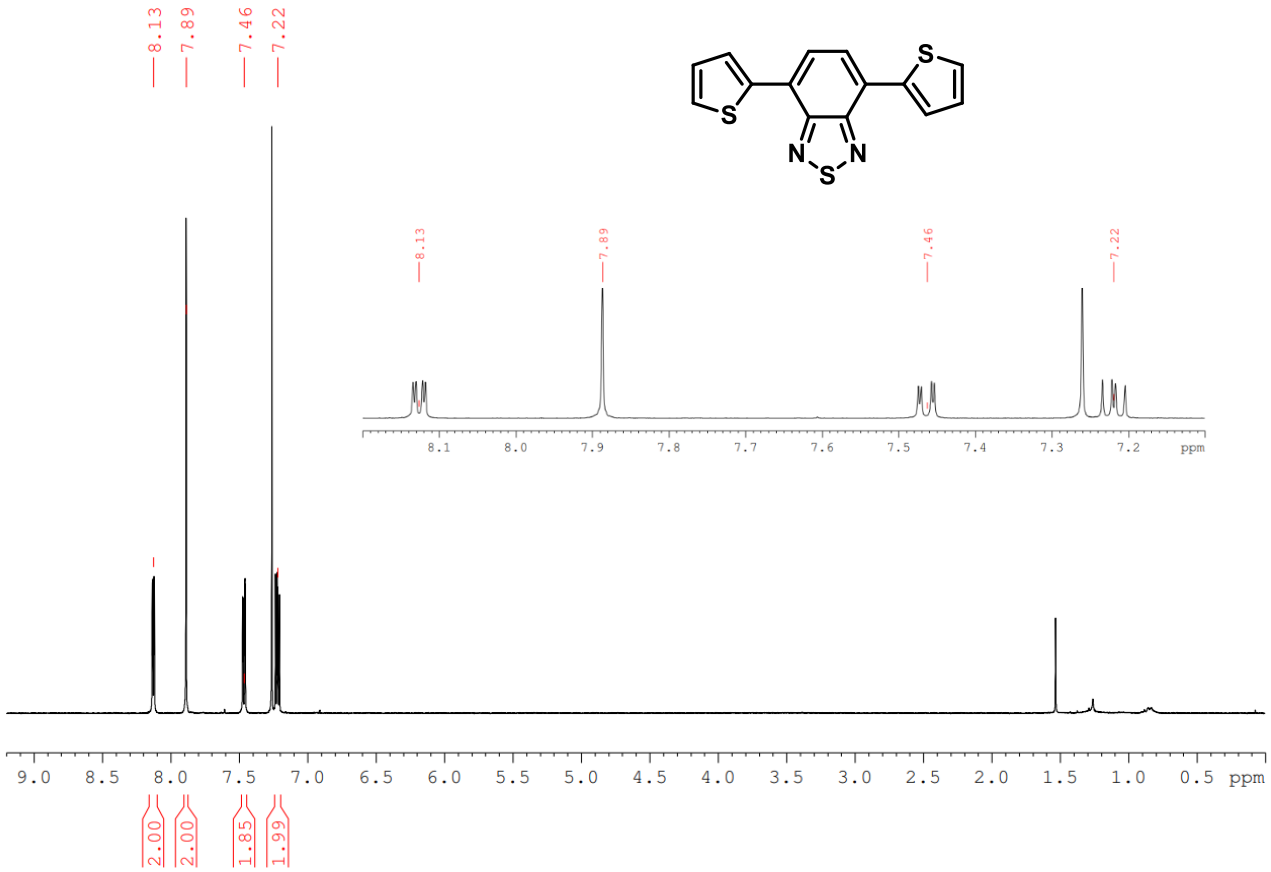

Figure S145 ^{1}H NMR of **Th-BTZ** in $CDCl_3$.

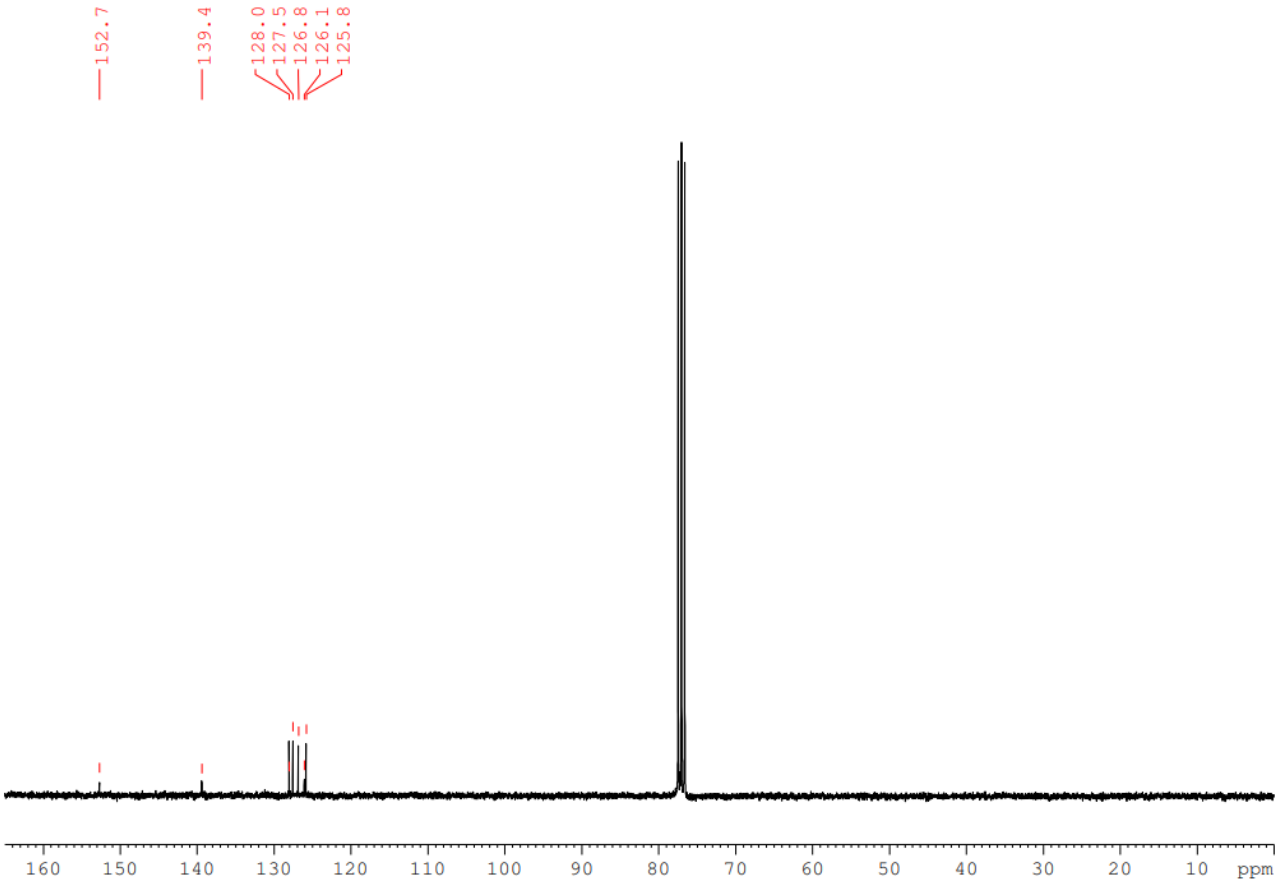

Figure S146 ^{13}C NMR of **Th-BTZ** in $CDCl_3$.

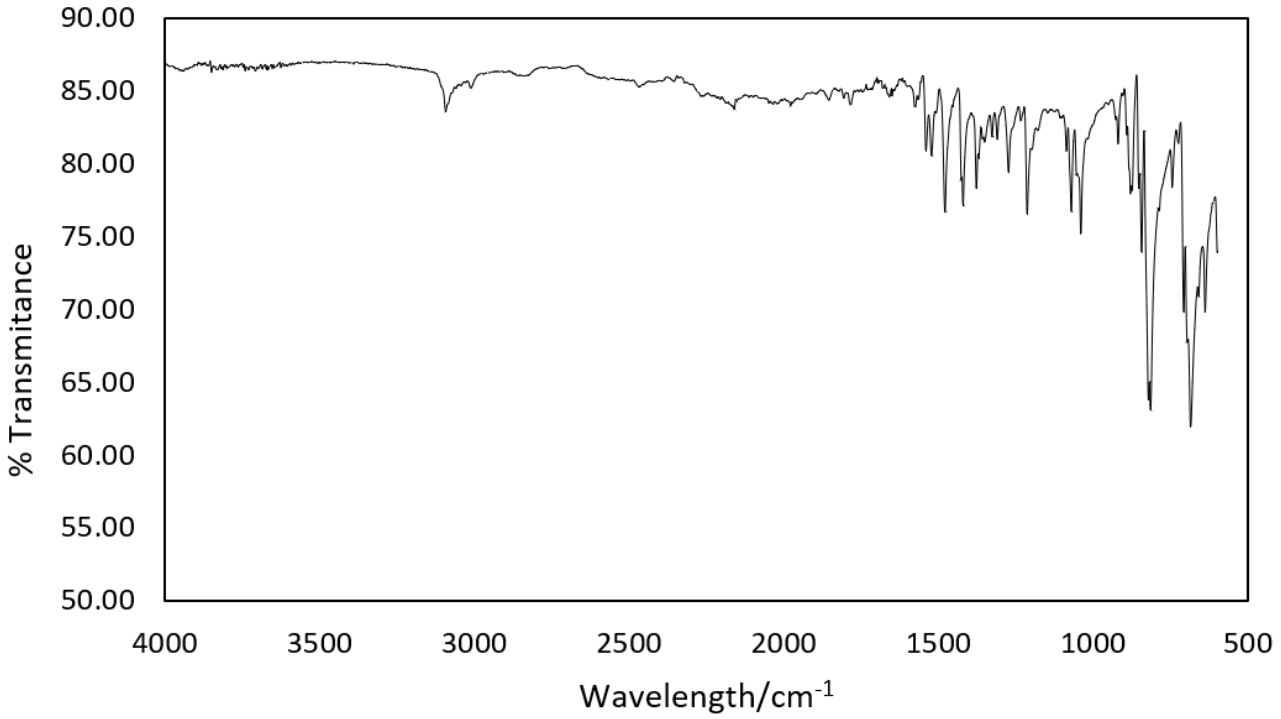

Figure S147 IR spectra of **Th-BTZ**.

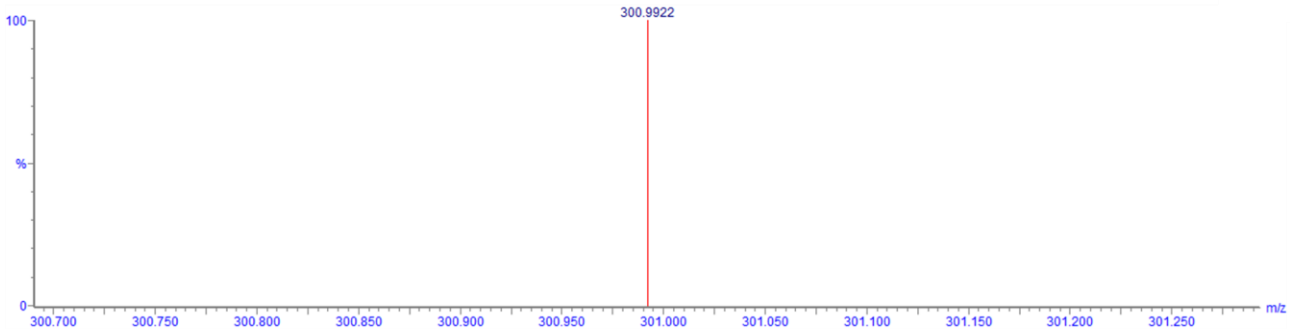

Figure S148 HRMS spectra of **Th-BTZ**.

4,7-Bis(5-bromothiophen-2-yl)benzo[*c*][1,2,5]thiadiazole (ThBr-BTZ)

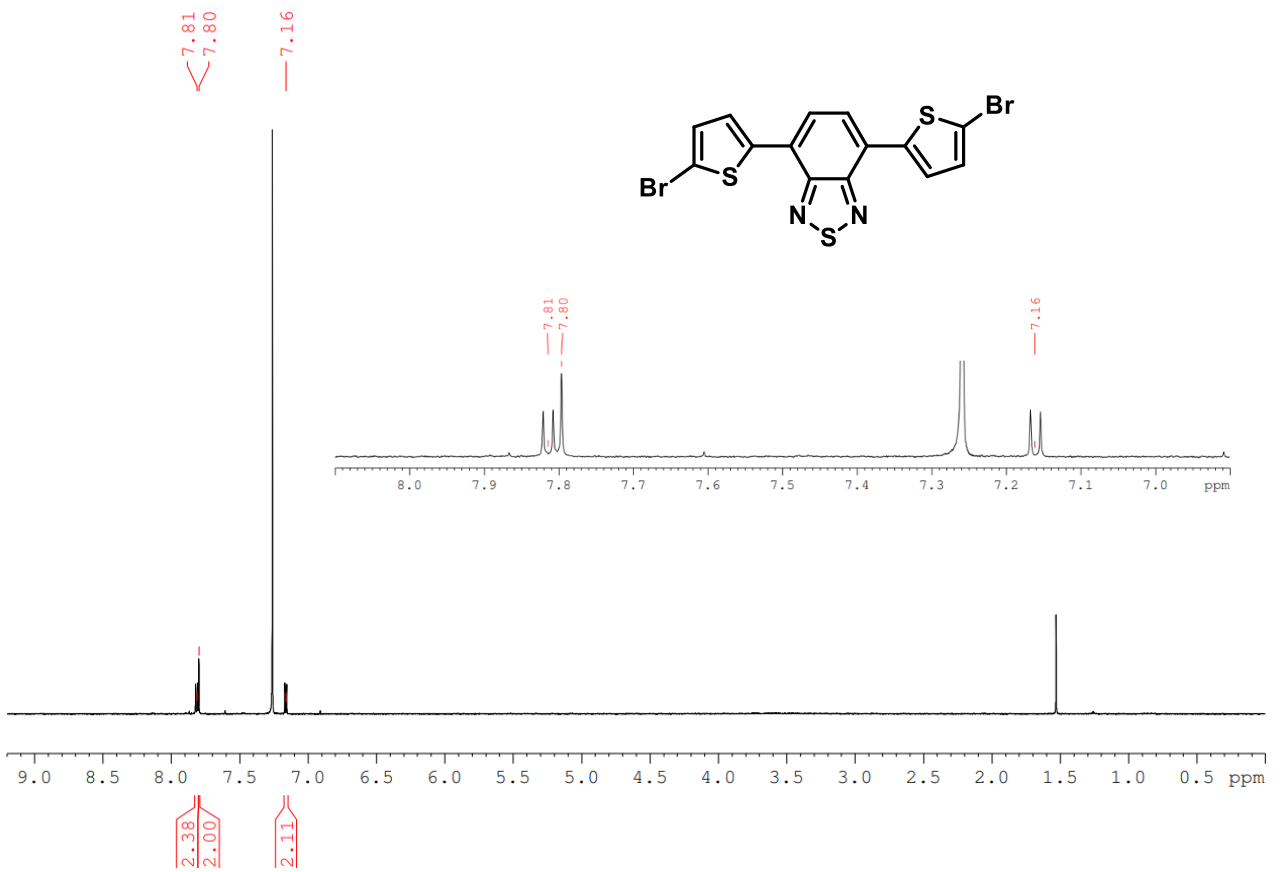

Figure S149 ^{1}H NMR spectra of **ThBr-BTZ** in $CDCl_3$.

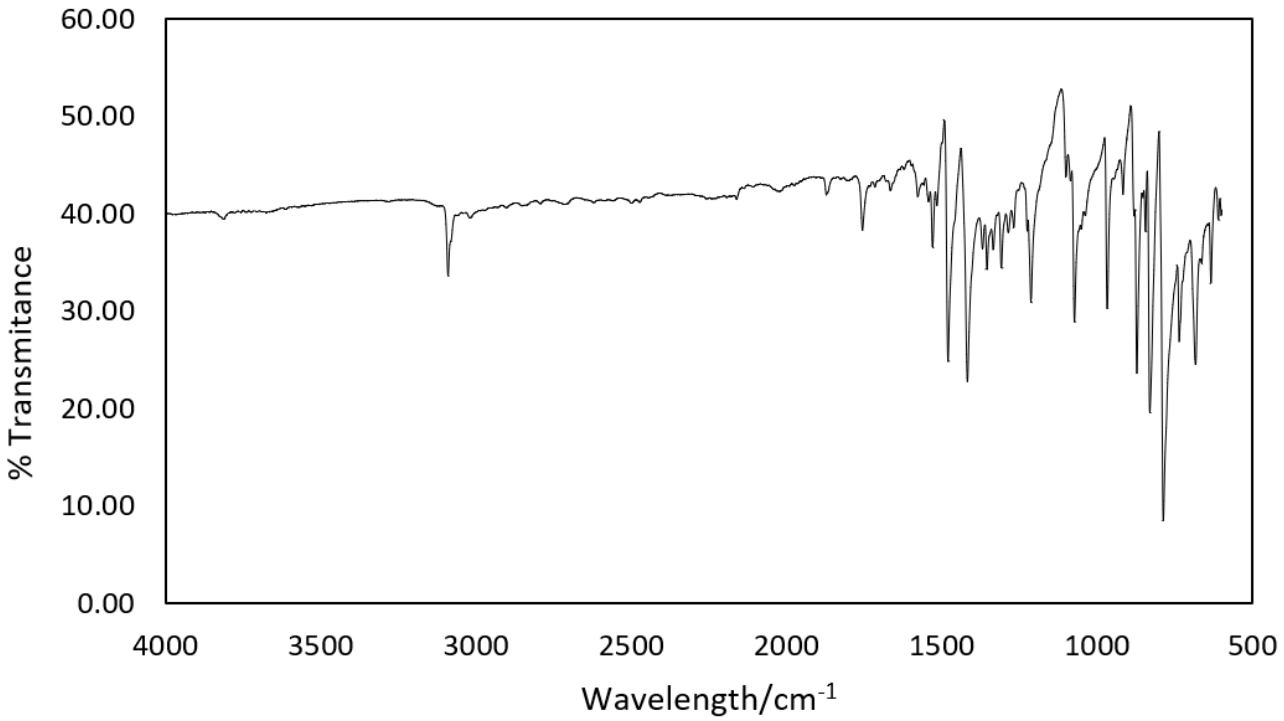

Figure S150 IR spectra of **ThBr-BTZ**.

4,7-Di([2,2'-bithiophen]-5-yl)benzo[*c*][1,2,5]thiadiazole (ThTh-BTZ)

Figure S151 ^{1}H NMR spectra of **ThTh-BTZ** in $CDCl_3$.

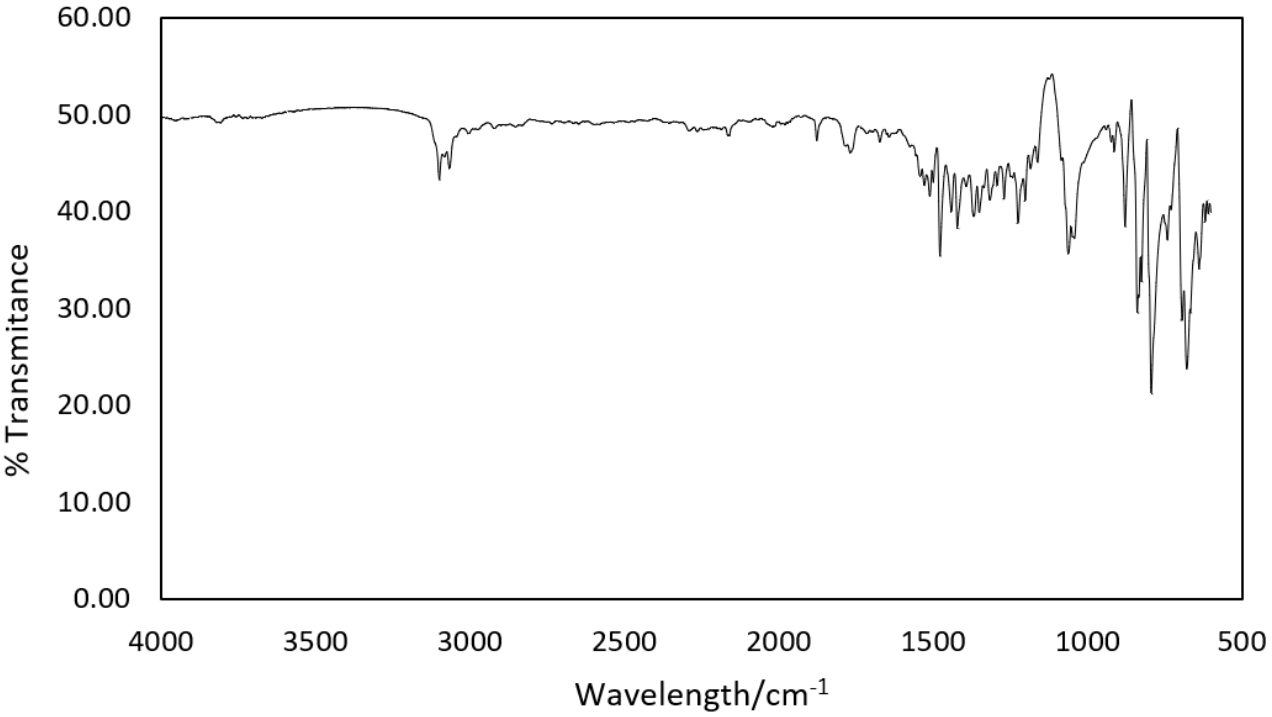

Figure S152 IR spectra of **ThTh-BTZ**.

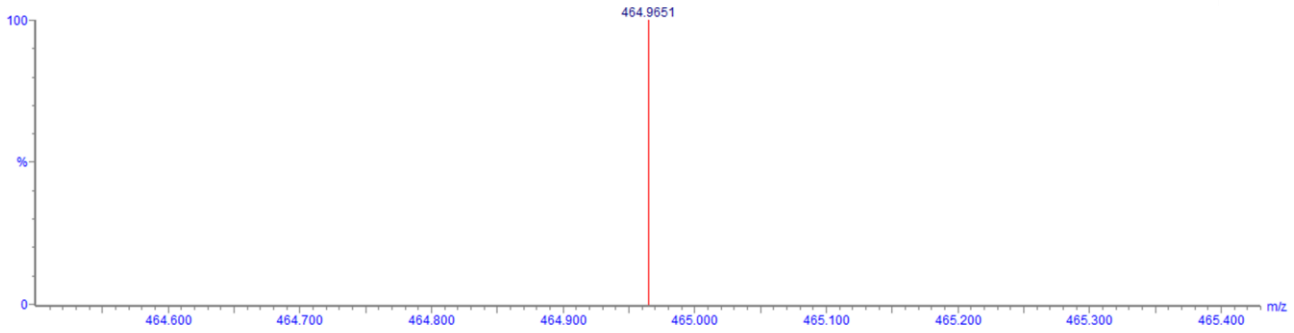

Figure S153 HRMS spectra of **ThTh-BTZ**.

4,7-Bis(benzo[*b*]thiophen-2-yl)benzo[*c*][1,2,5]thiadiazole (BTh-BTZ)

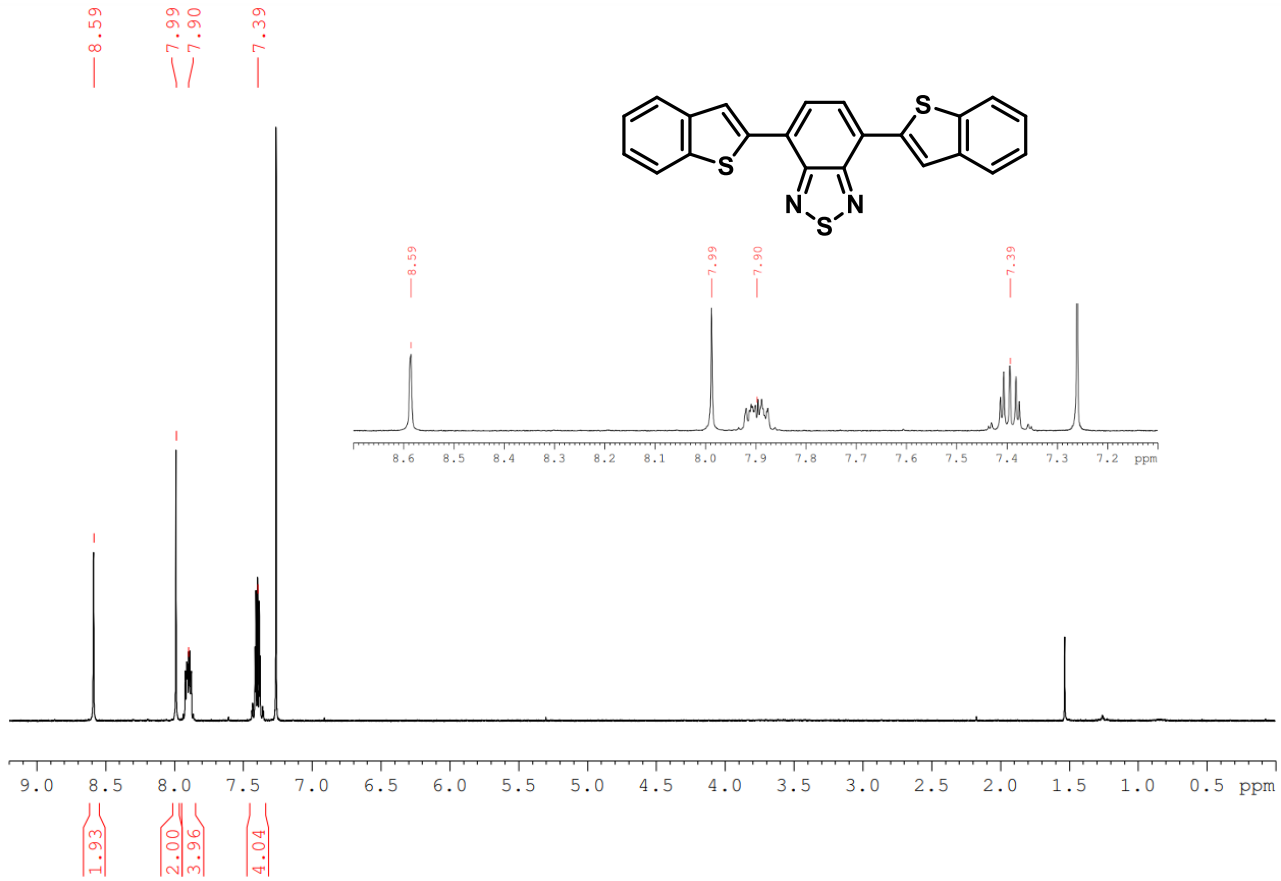

Figure S154 ^{1}H NMR spectra of **BTh-BTZ** in $CDCl_3$.

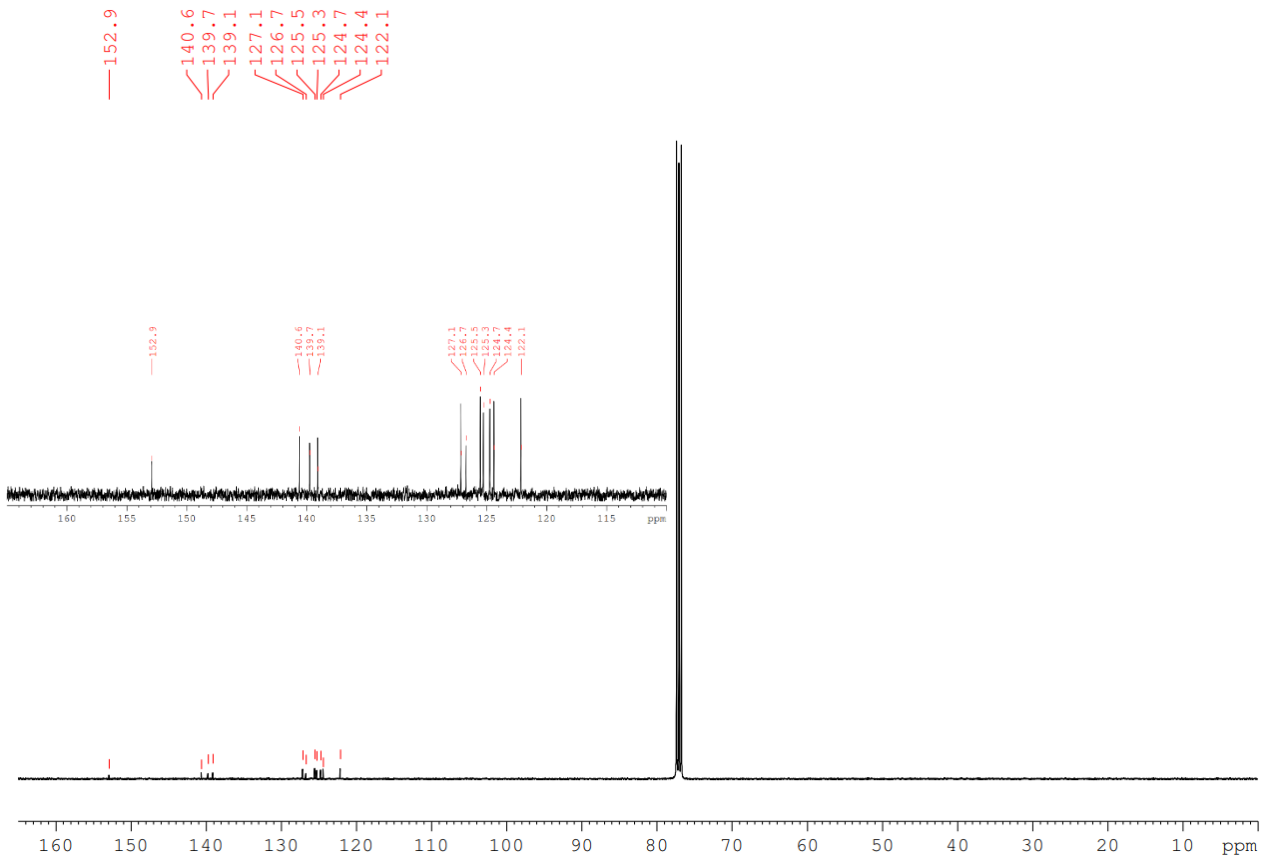

Figure S155 ^{13}C NMR spectra of **BTh-BTZ** in $CDCl_3$. Spectra was obtained using a D_1 of 20 s and increased number of scans.

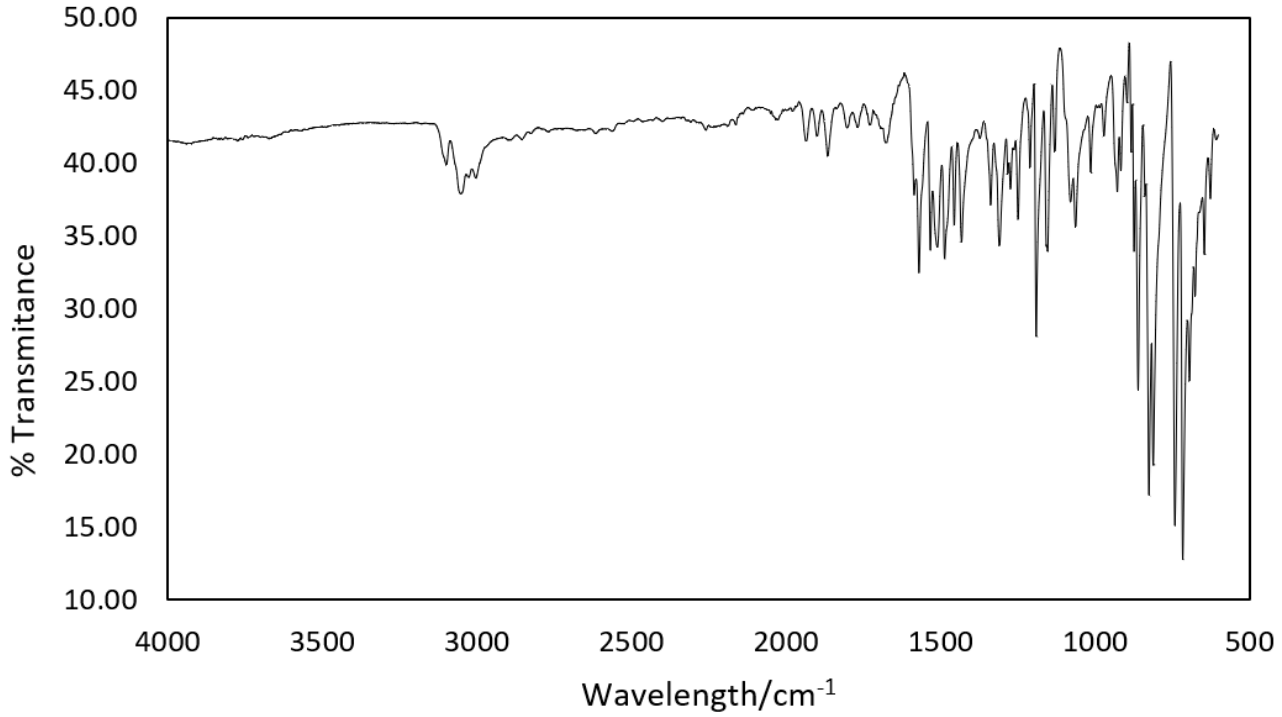

Figure S156 IR spectra of **BTh-BTZ**.

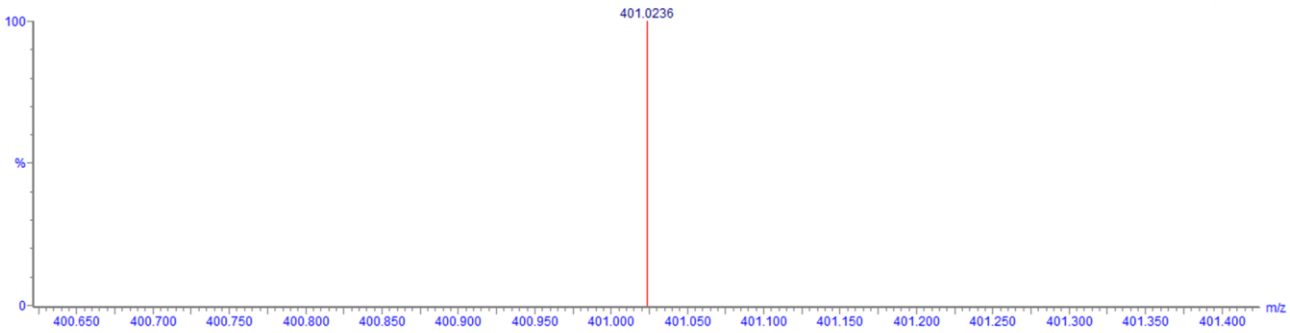

Figure S157 HRMS spectra of **BTh-BTZ**.

4,7-Di(thiazol-2-yl)benzo[*c*][1,2,5]thiadiazole (Tz-BTZ)

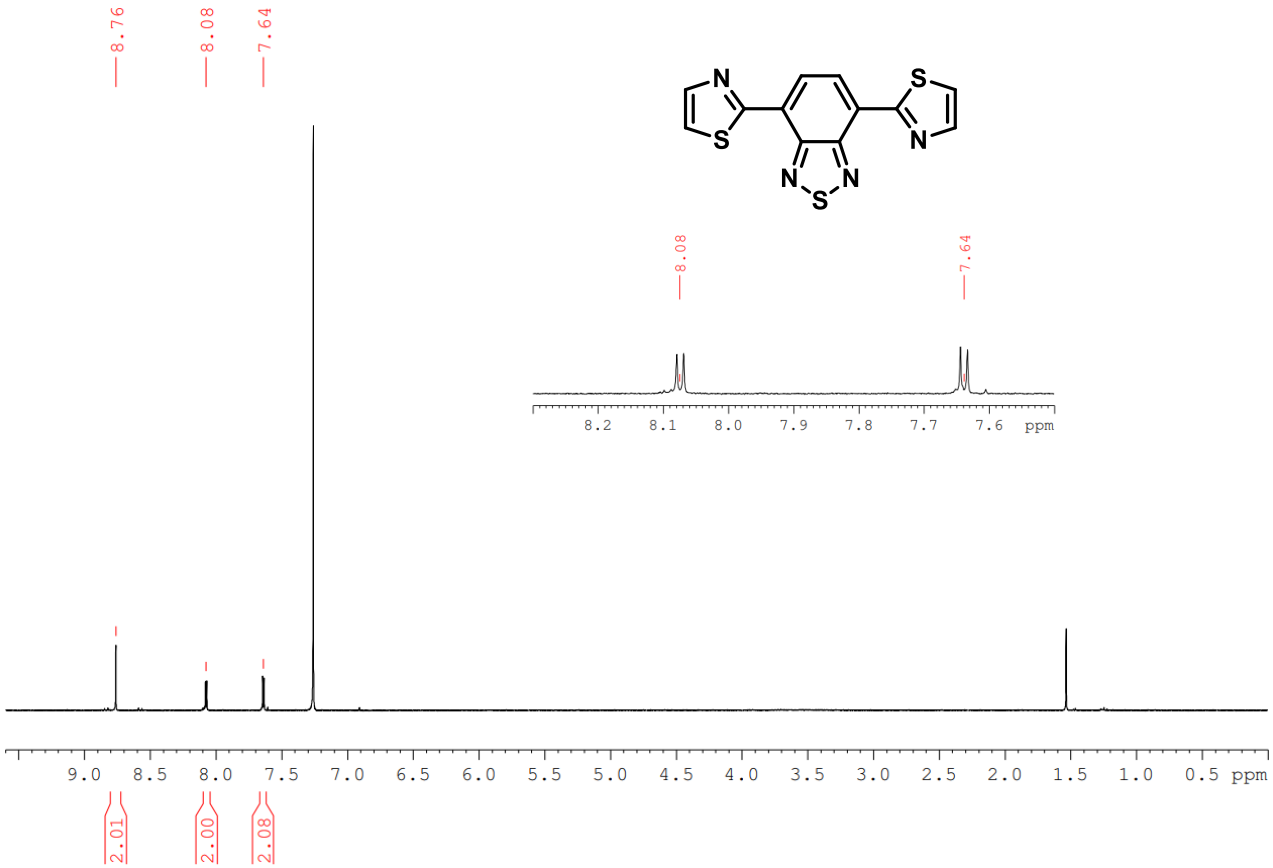

Figure S158 ^{1}H NMR of **Tz-BTZ** in $CDCl_3$.

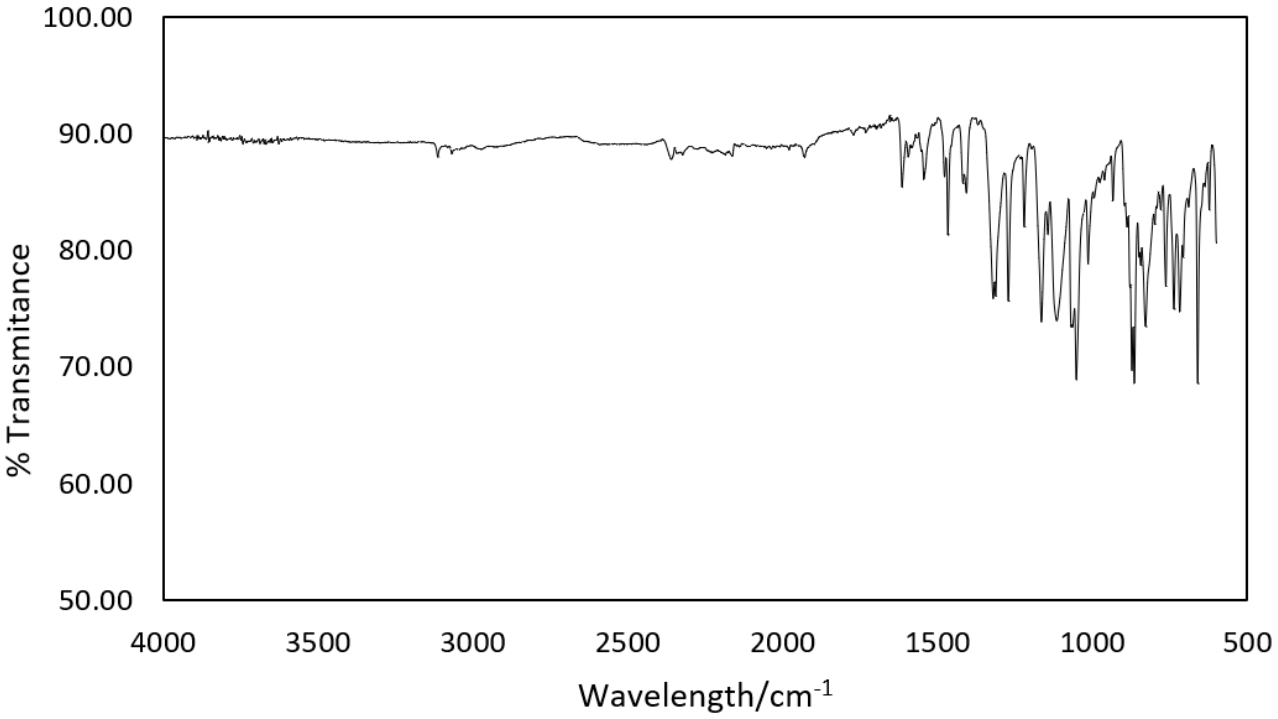

Figure S159 IR spectra of **Tz-BTZ**.

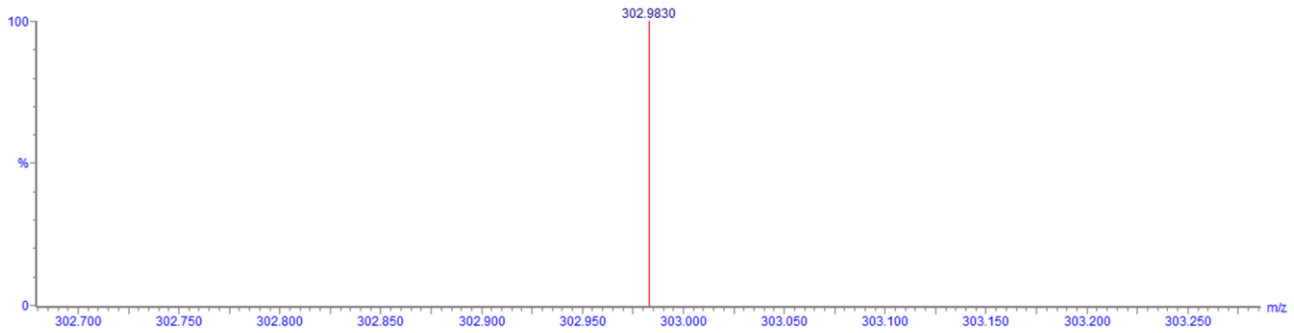

Figure S160 HRMS spectra of **Tz-BTZ**.

Di-*tert*-butyl 2,2'-(benzo[*c*][1,2,5]thiadiazole-4,7-diyl)bis(1*H*-pyrrole-1-carboxylate) (Pyr-BTZ)

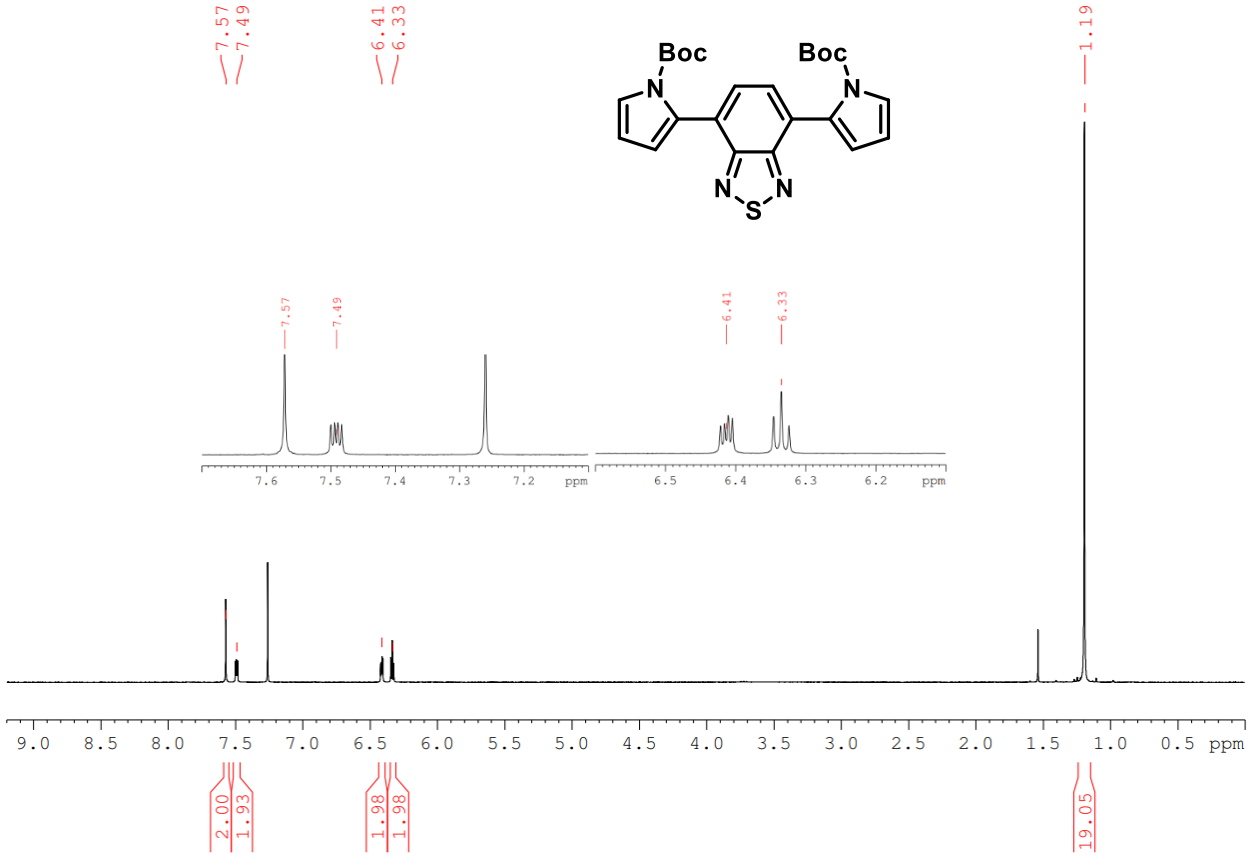

Figure S161 ^{1}H NMR of **Pyr-BTZ** in $CDCl_3$.

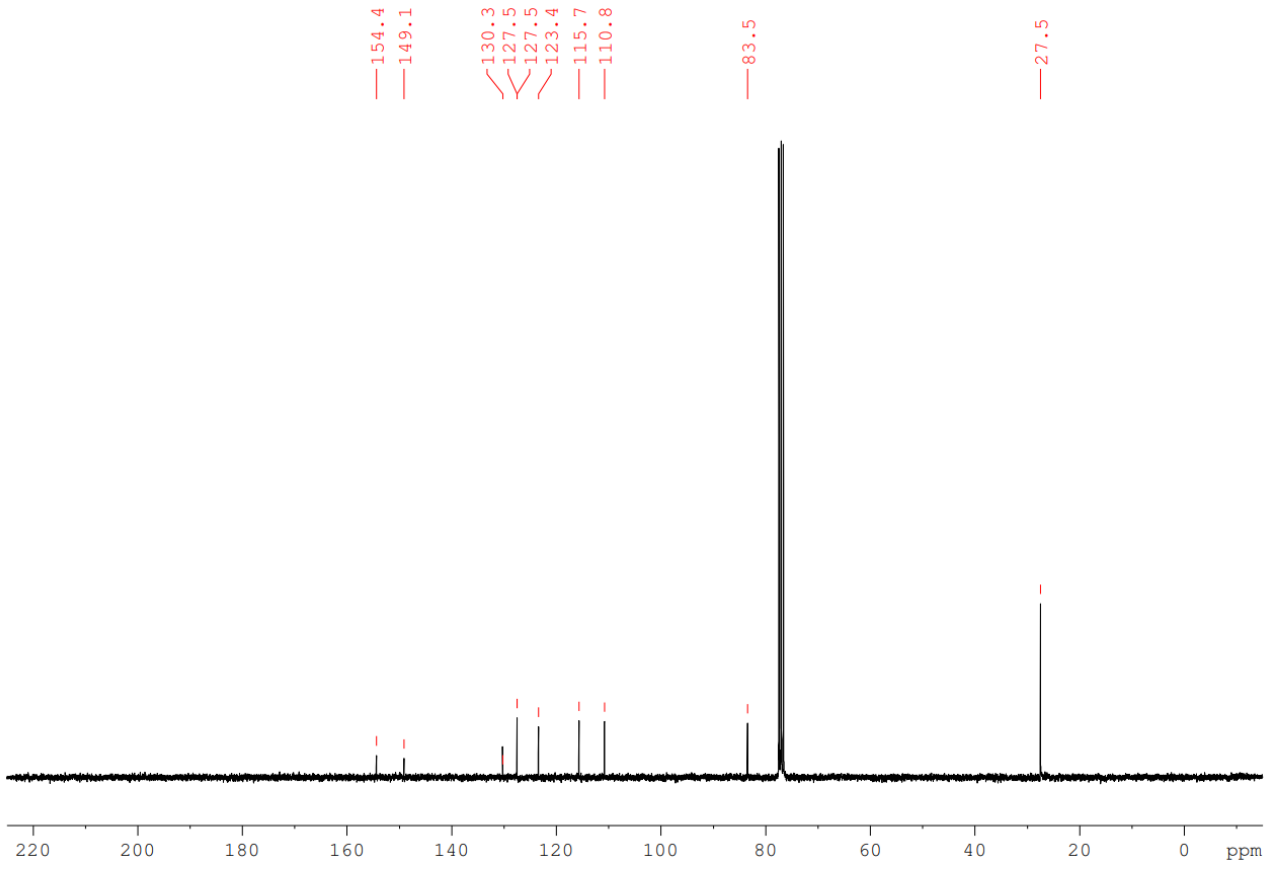

Figure S162 ^{13}C NMR of **Pyr-BTZ** in $CDCl_3$.

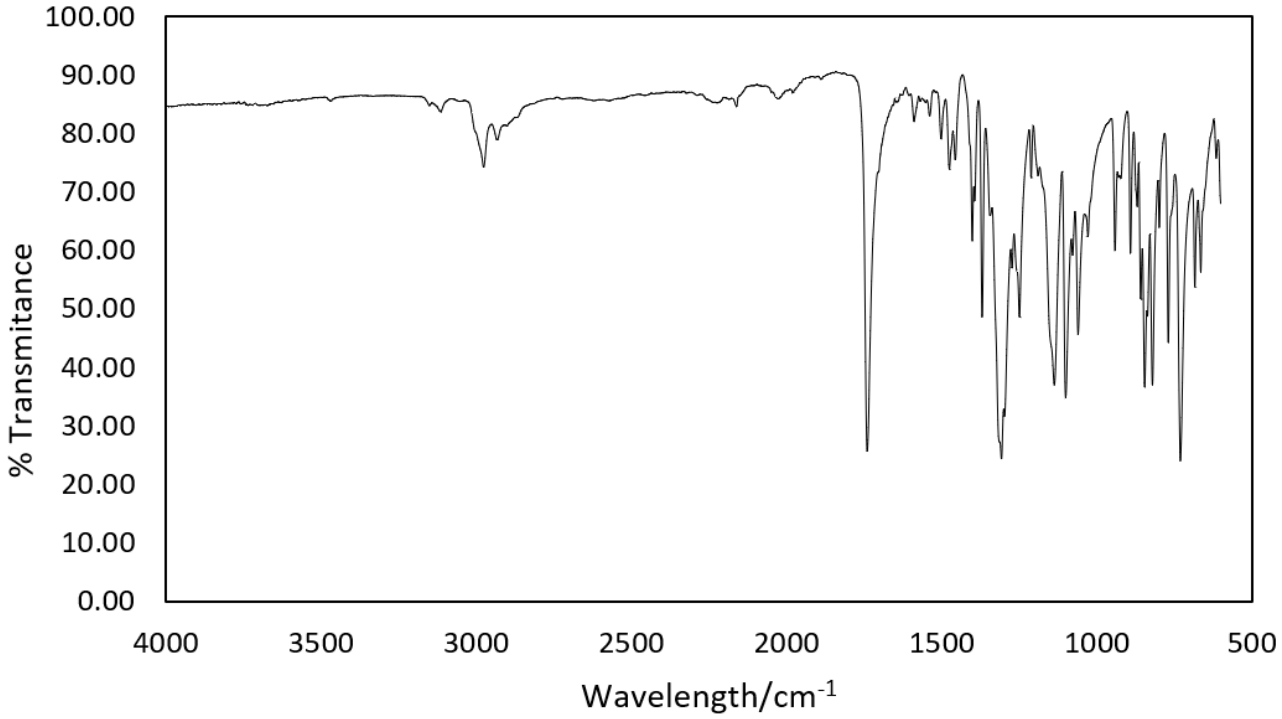

Figure S163 IR spectra of **Pyr-BTZ**.

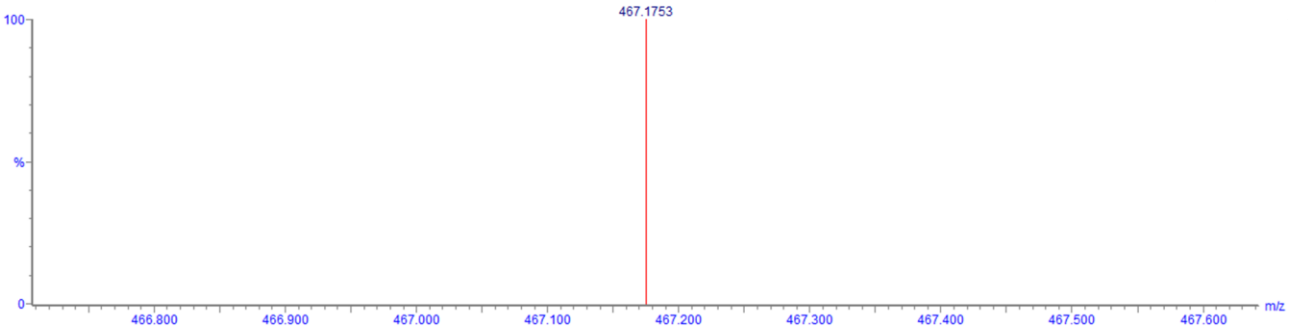

Figure S164 IR spectra of **Pyr-BTZ**.

4,7-Di(pyridin-4-yl)benzo[*c*][1,2,5]thiadiazole (4N-BTZ)

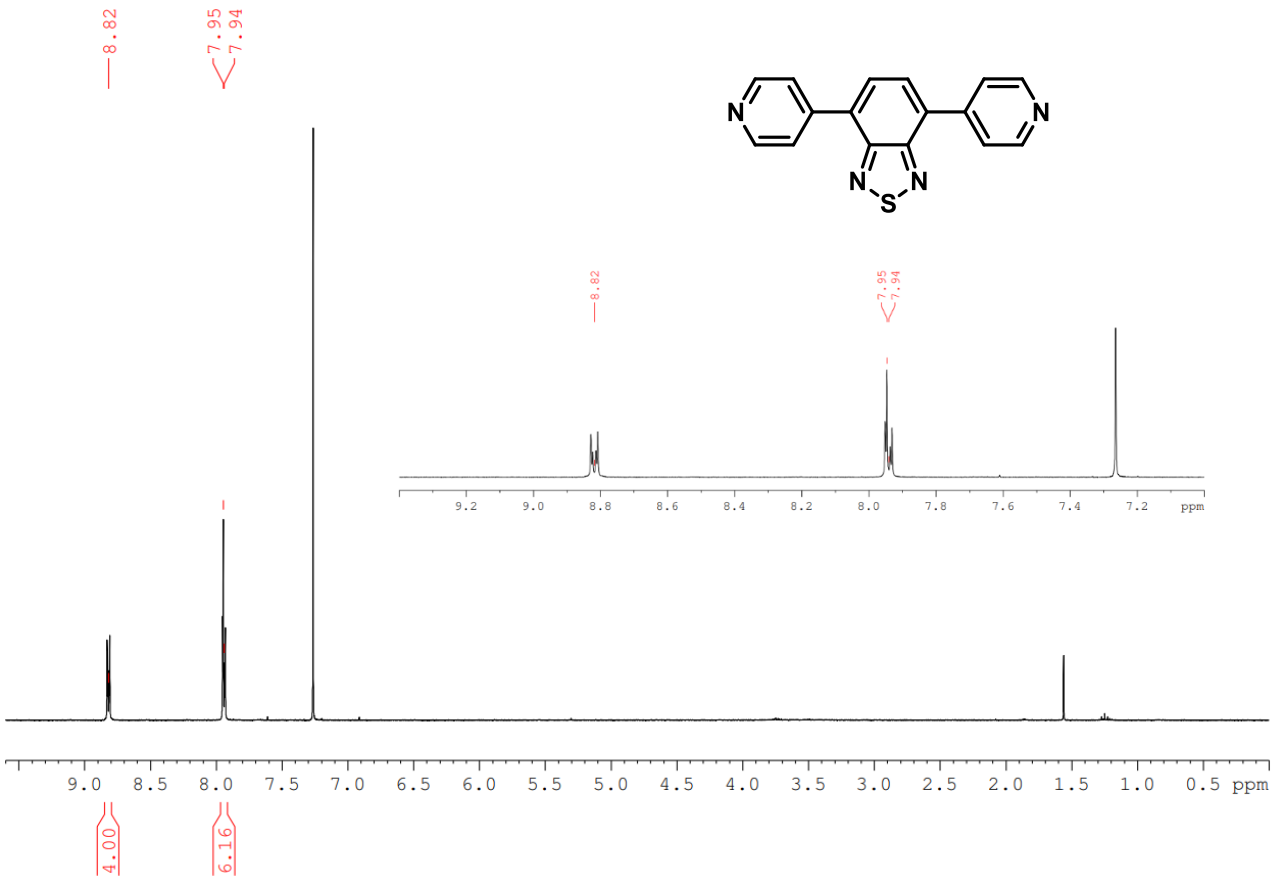

Figure S165 ^{1}H NMR of **4N-BTZ** in $CDCl_3$.

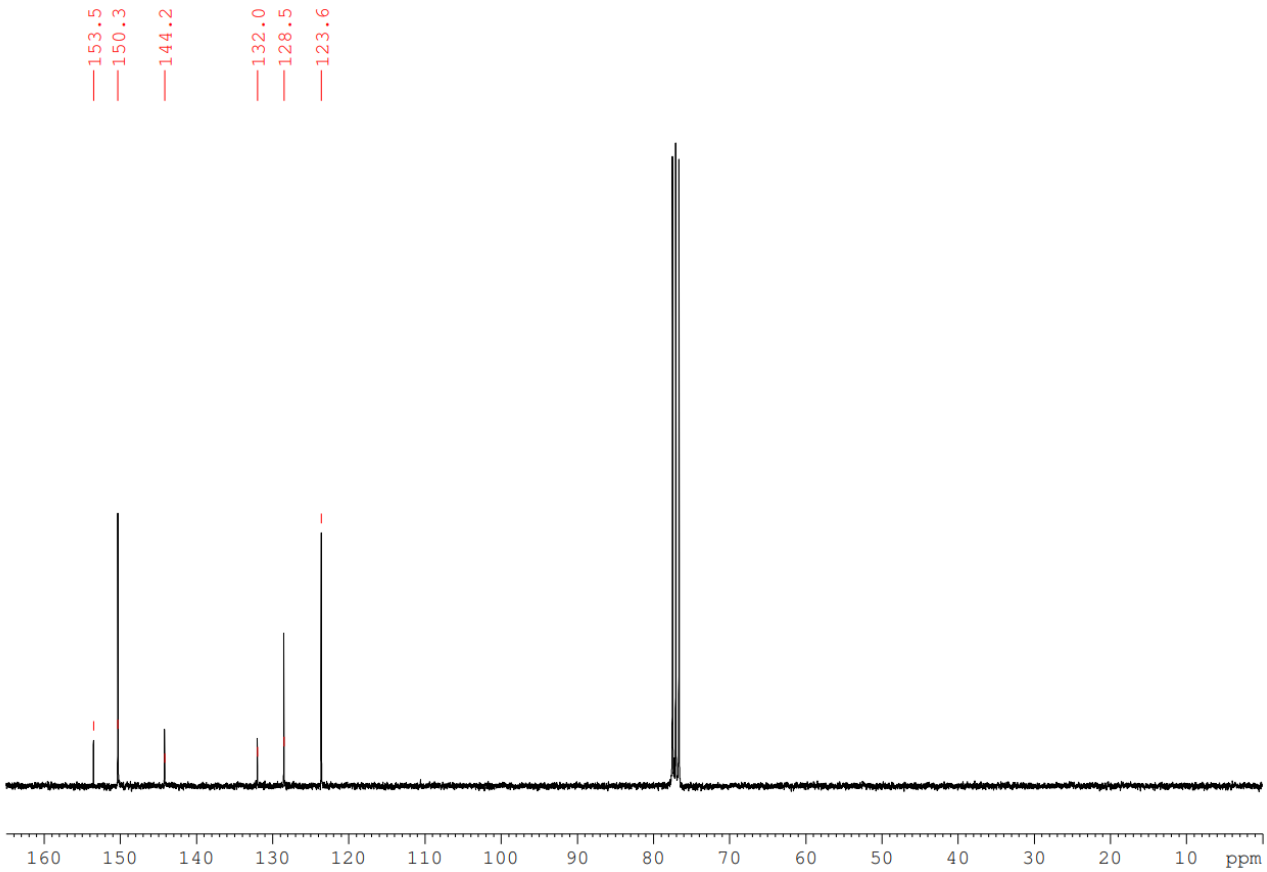

Figure S166 ^{13}C NMR of **4N-BTZ** in $CDCl_3$.

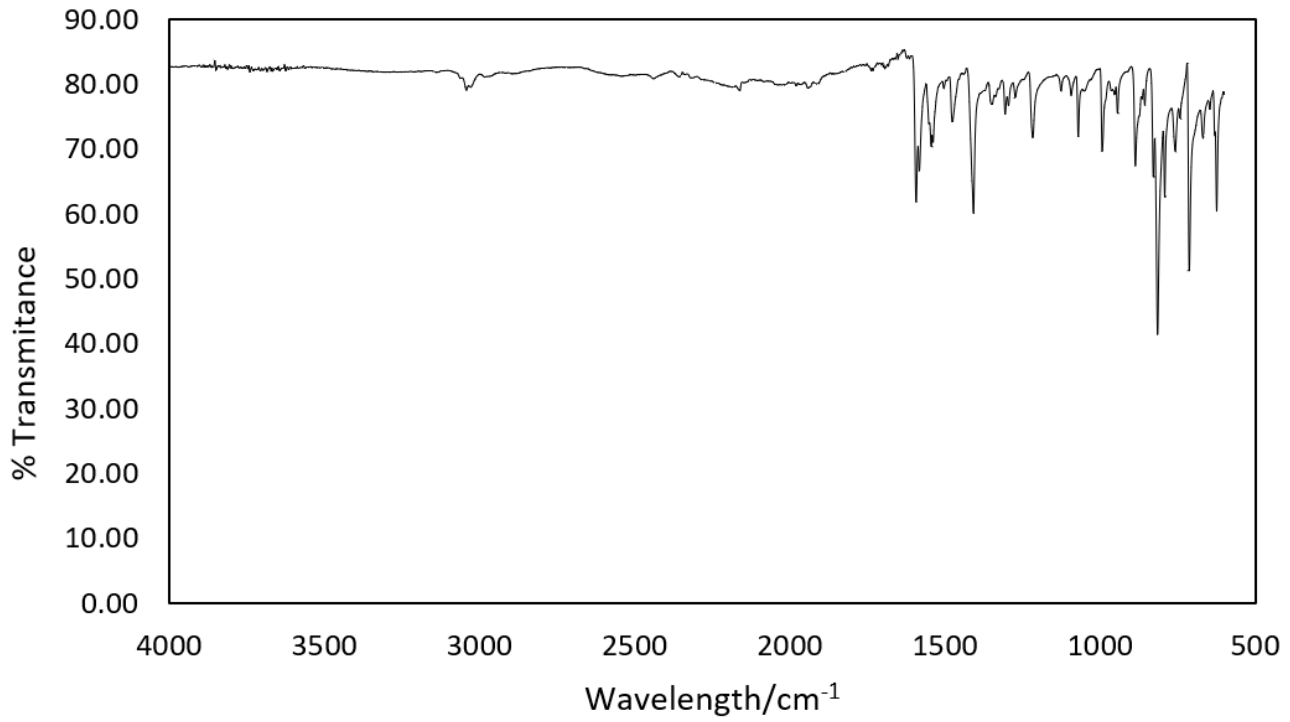

Figure S167 IR spectra of **4N-BTZ**.

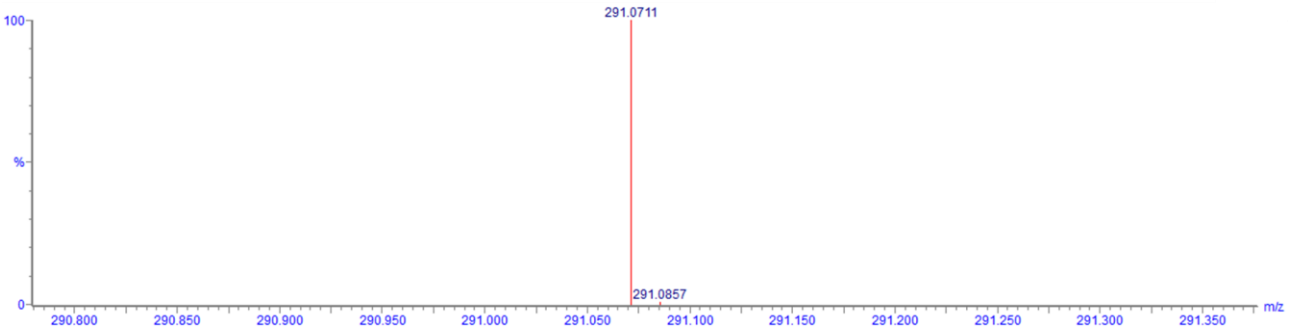

Figure S168 HRMS spectra of **4N-BTZ**.

4,7-Di(biphenyn-2-yl)benzo[*c*][1,2,5]thiadiazole (oPh-BTZ)

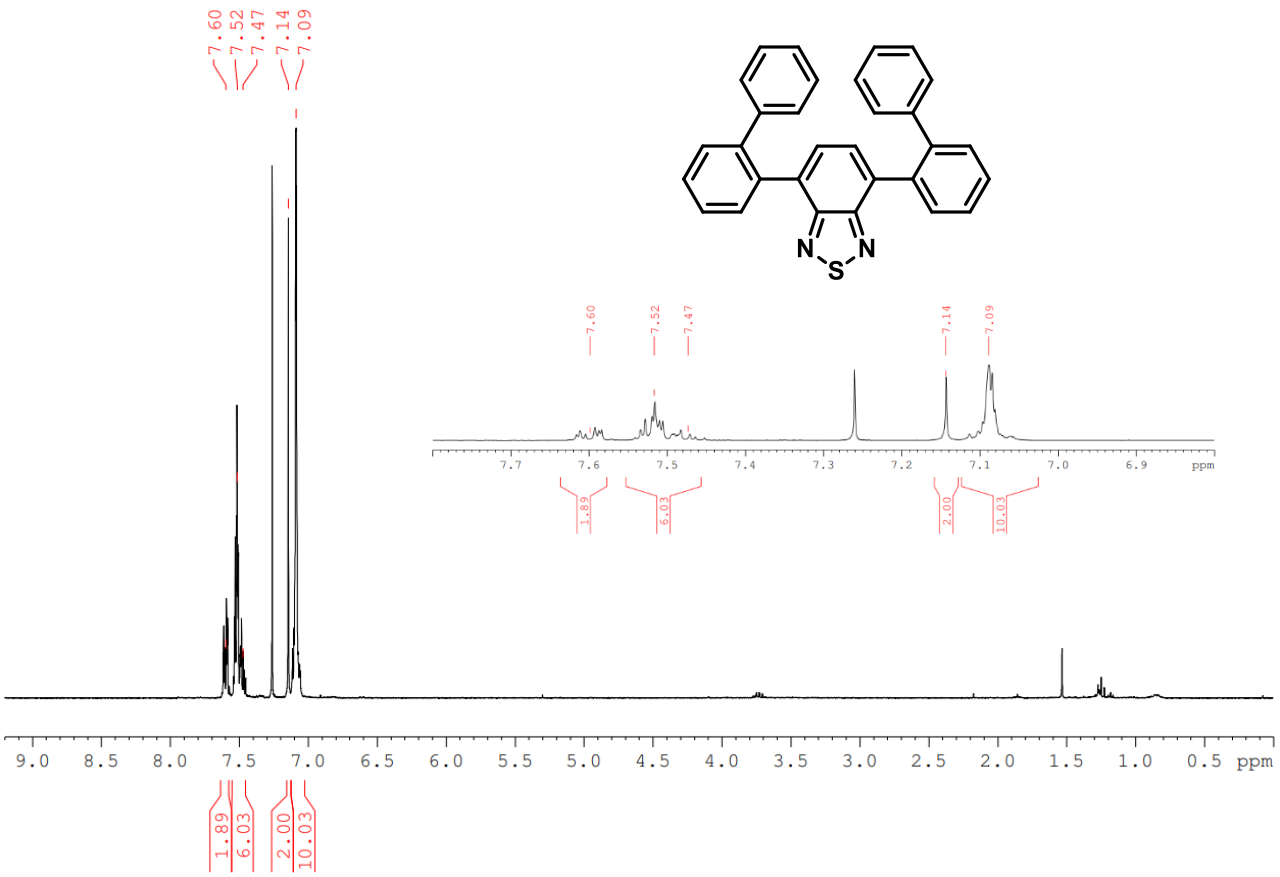

Figure S169 ^{1}H NMR of **oPh-BTZ** in $CDCl_3$.

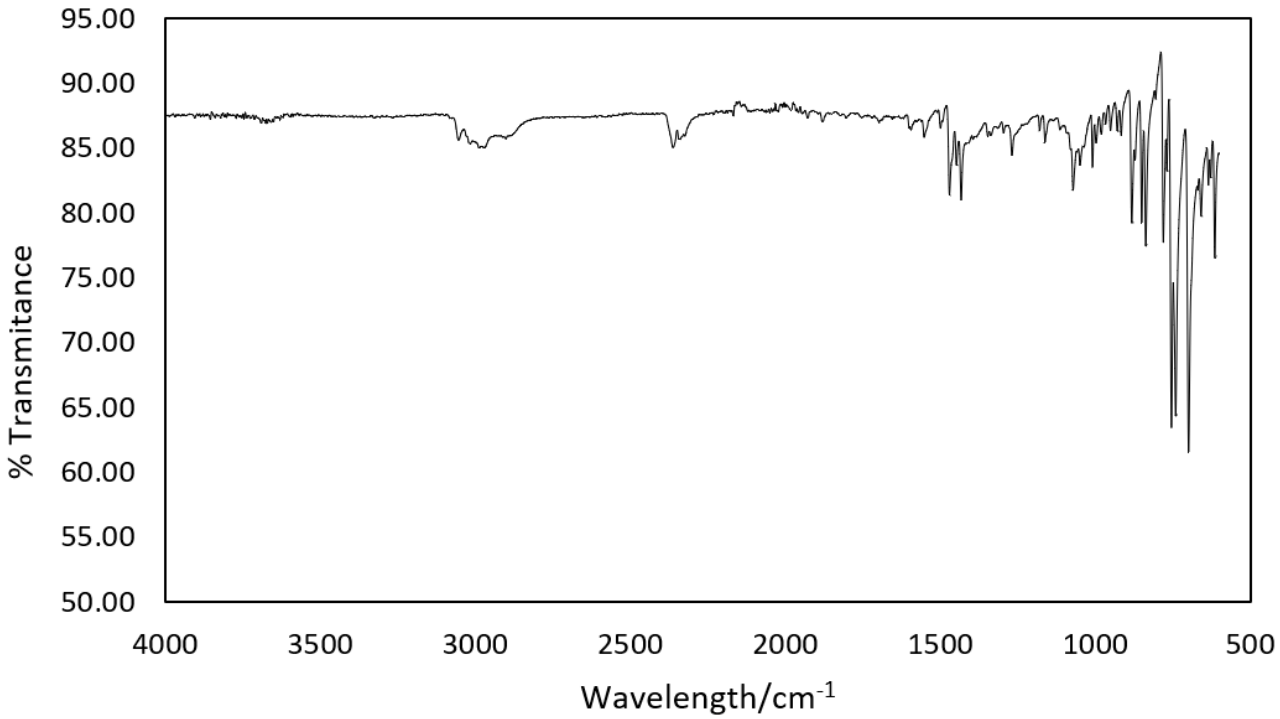

Figure S170 IR spectra of **oPh-BTZ**.

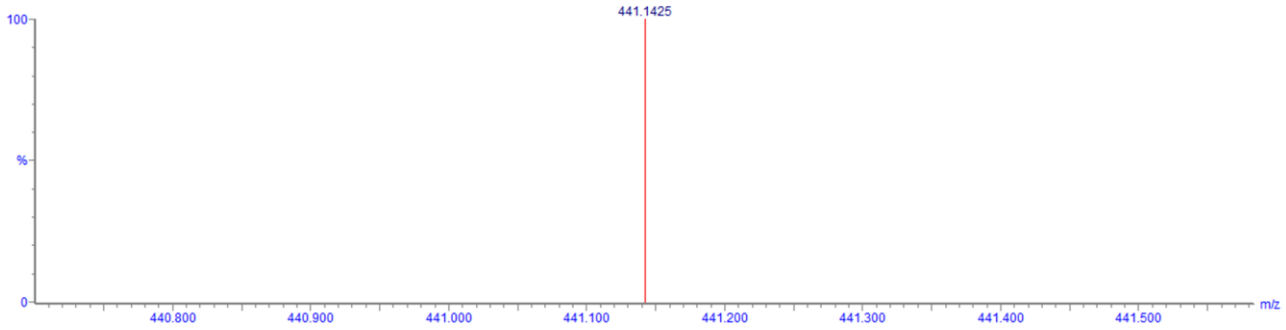

Figure S171 HRMS spectra of **oPh-BTZ**.

4,7-Di(biphenyn-3-yl)benzo[*c*][1,2,5]thiadiazole (mPh-BTZ)

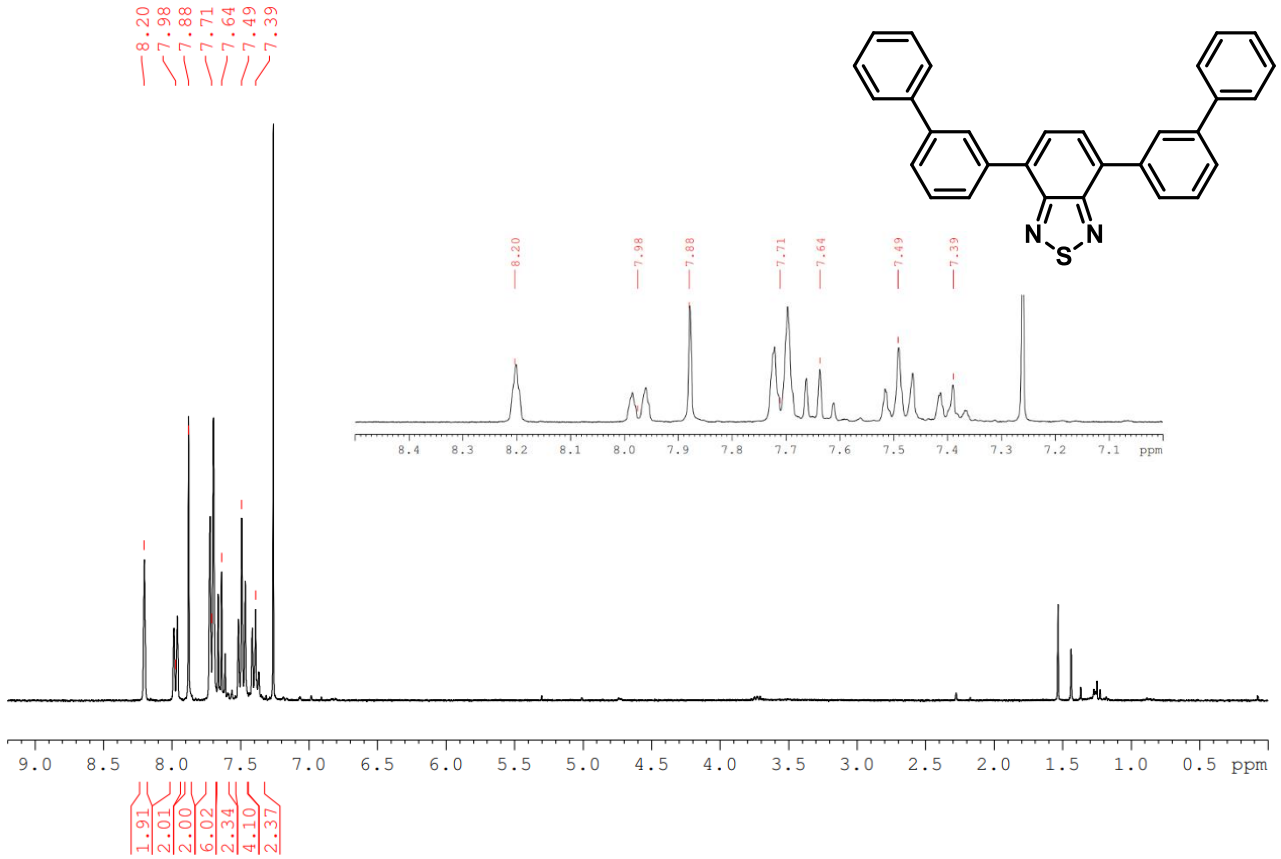

Figure S172 ^{1}H NMR of **mPh-BTZ** in $CDCl_3$.

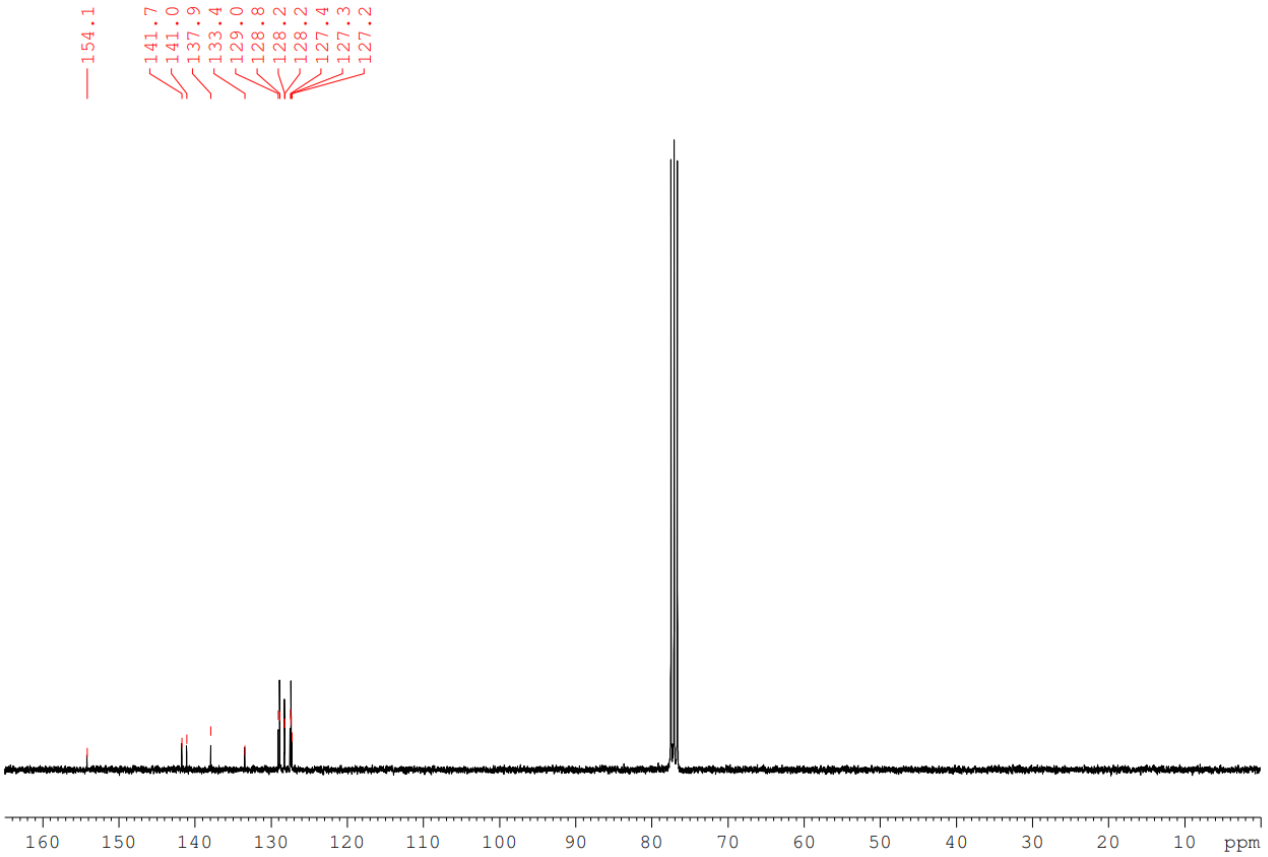

Figure S173 ^{13}C NMR of **mPh-BTZ** in $CDCl_3$.

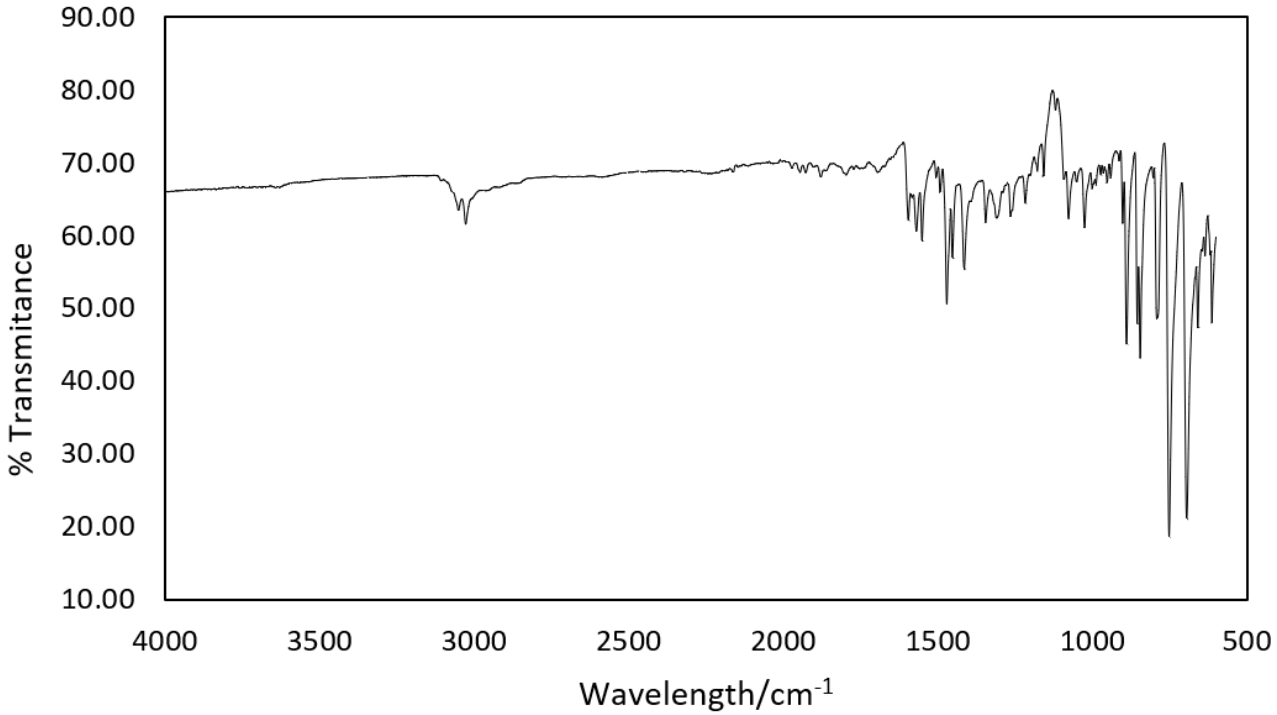

Figure S174 IR spectra of **mPh-BTZ**.

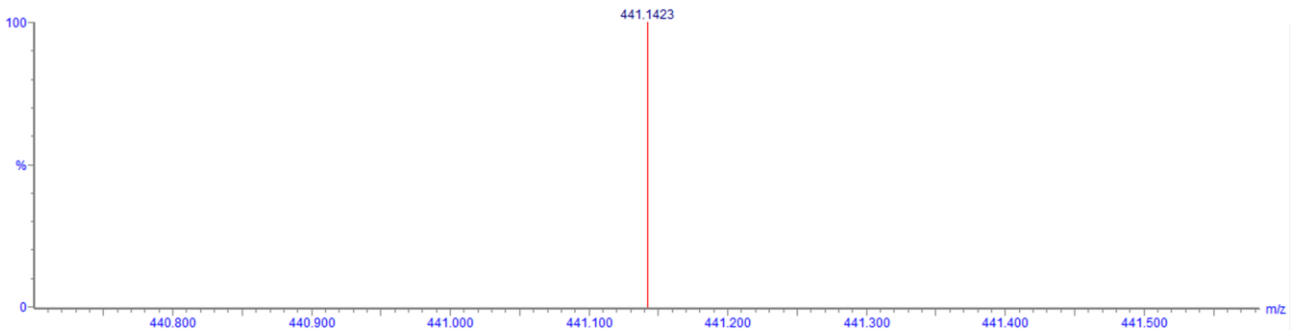

Figure S175 HRMS spectra of **mPh-BTZ**.

4,7-Di(biphenyn-4-yl)benzo[*c*][1,2,5]thiadiazole (pPh-BTZ)

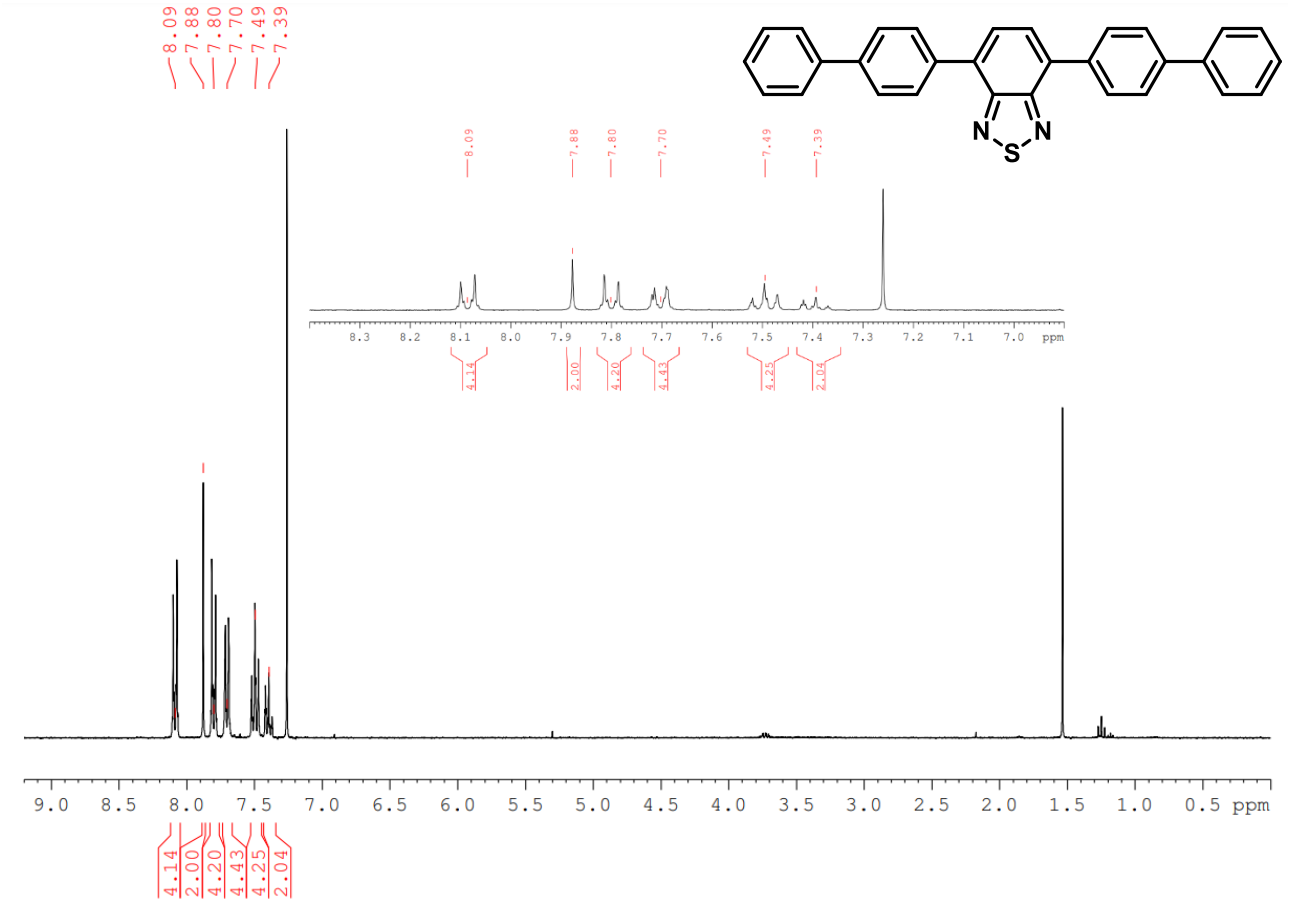

Figure S176 ^{1}H NMR of **pPh-BTZ** in $CDCl_3$.

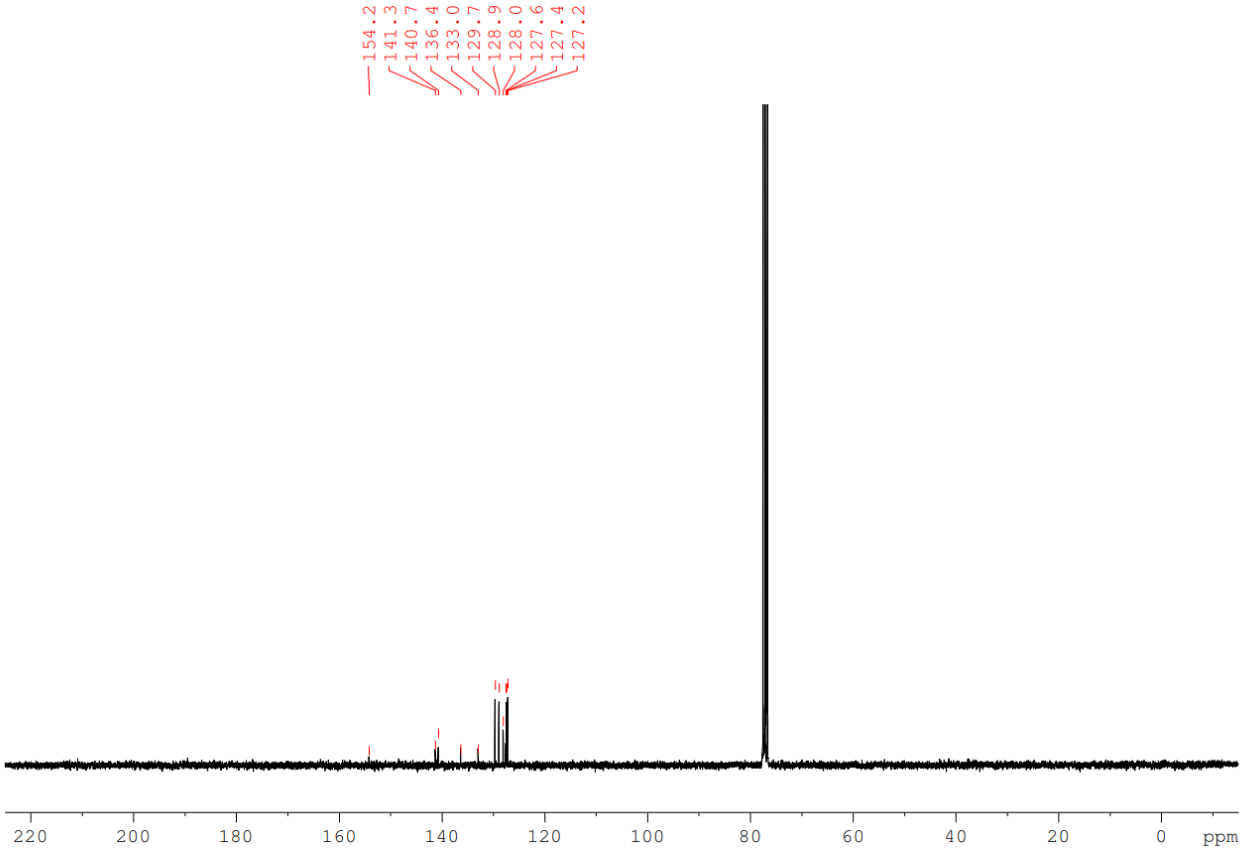

Figure S177 ^{13}C NMR spectra of **pPh-BTZ** in $CDCl_3$.

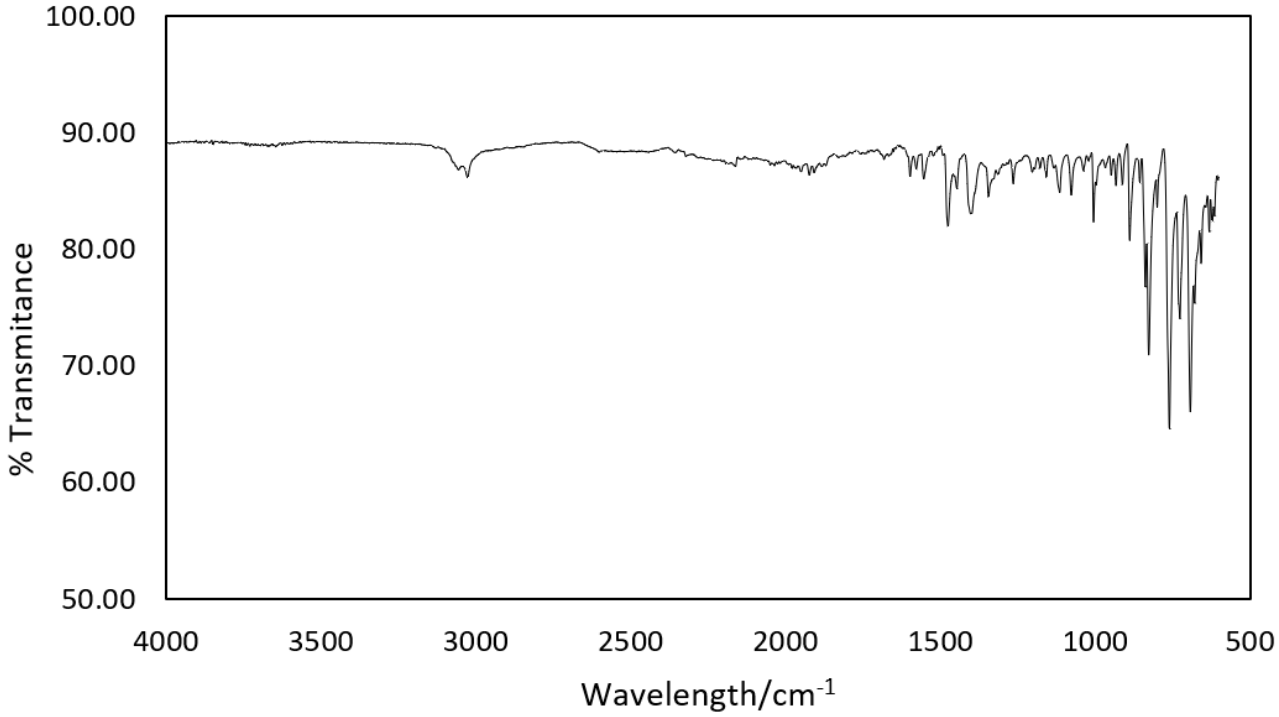

Figure S178 IR spectra of **pPh-BTZ**.

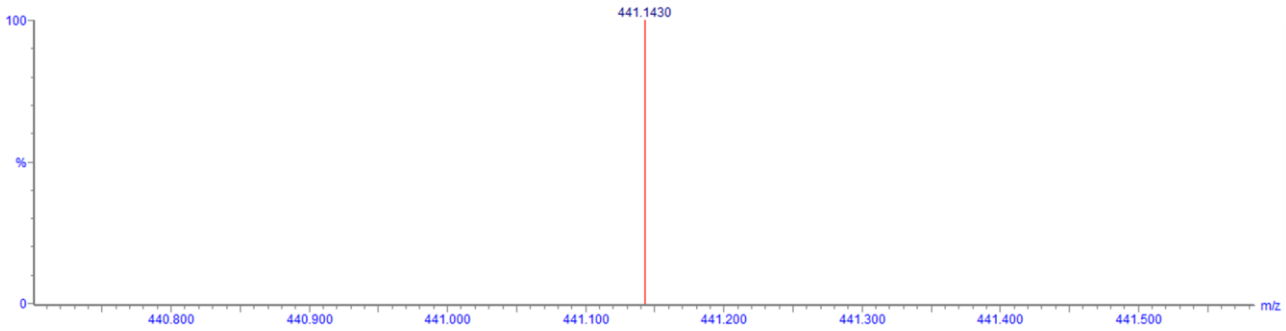

Figure S179 HRMS spectra of **pPh-BTZ**.

4,7-Di(naphthalen-1-yl)benzo[*c*][1,2,5]thiadiazole (1Nap-BTZ)

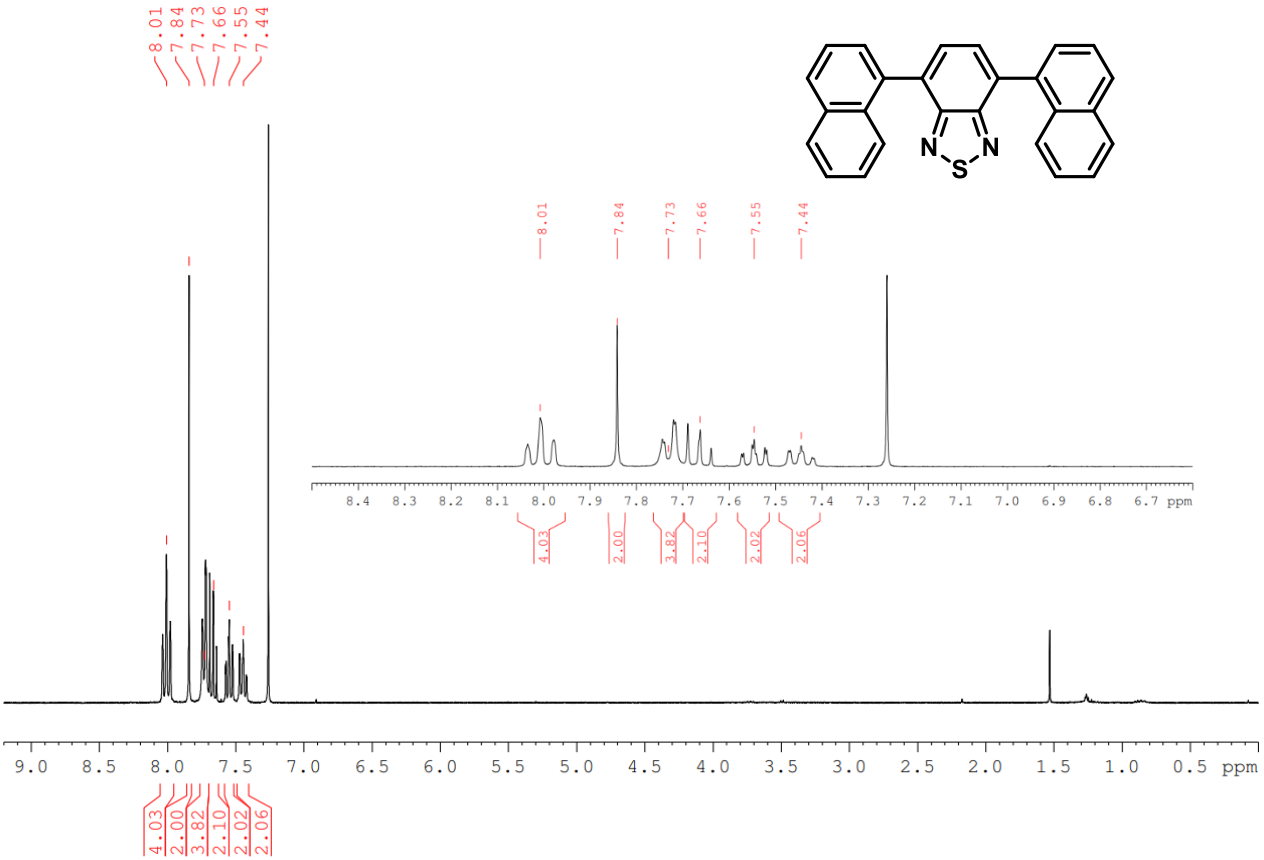

Figure S180 ^{1}H NMR of **1Nap-BTZ** in $CDCl_3$.

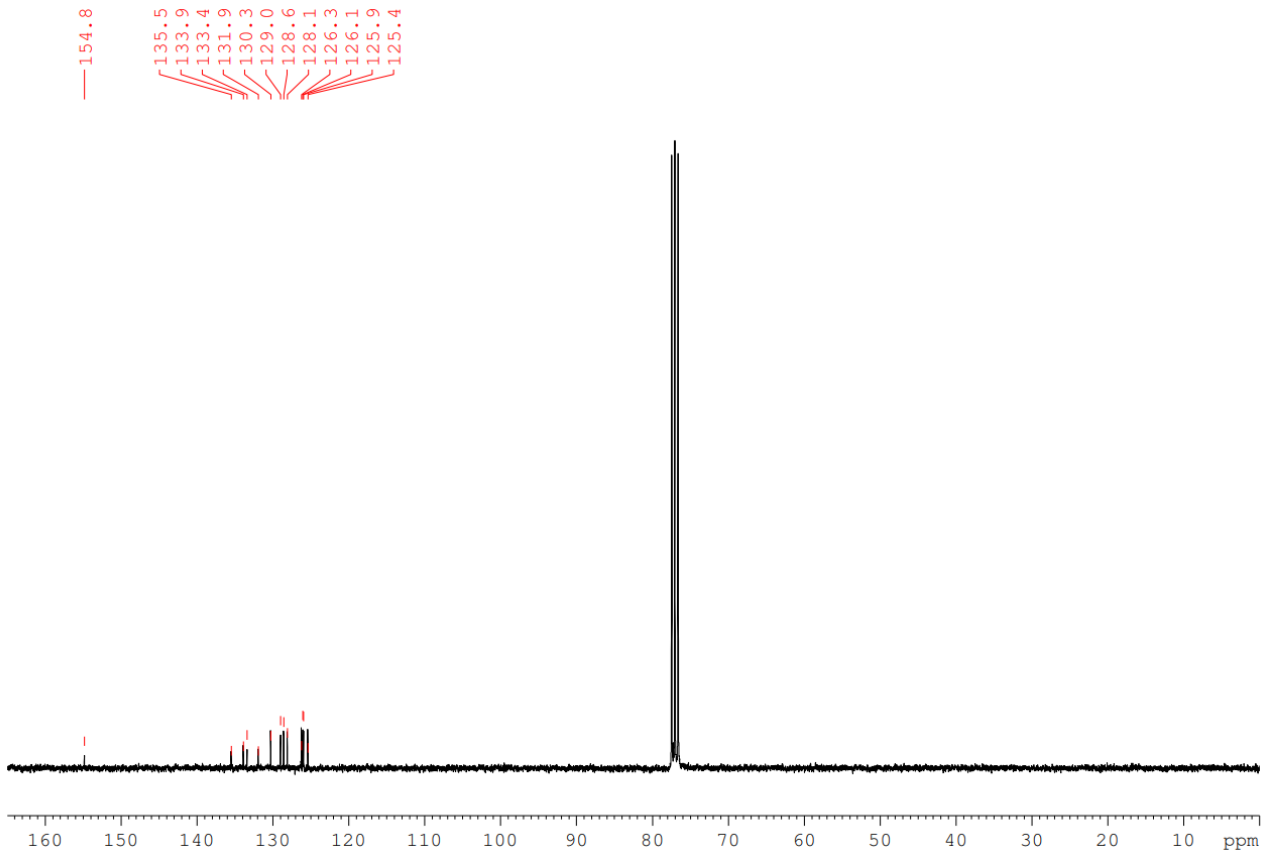

Figure S181 ^{13}C NMR of **1Nap-BTZ** in $CDCl_3$.

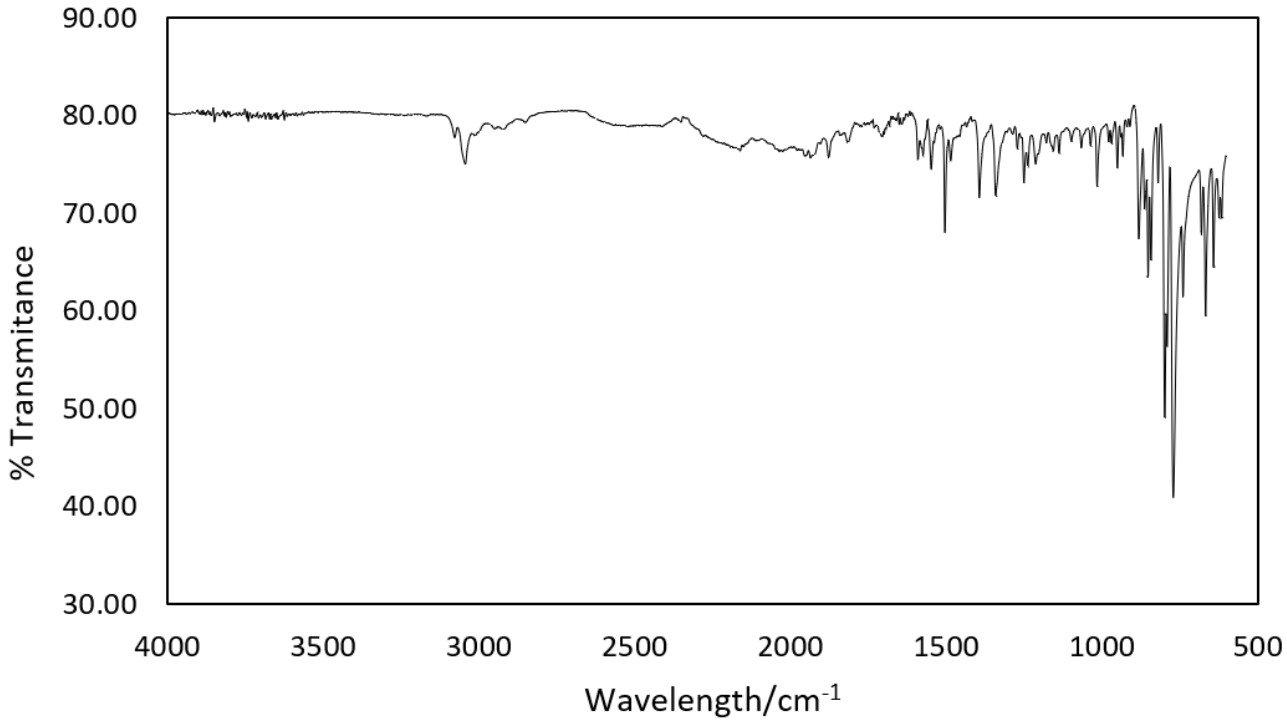

Figure S182 IR spectra of **1Nap-BTZ**.

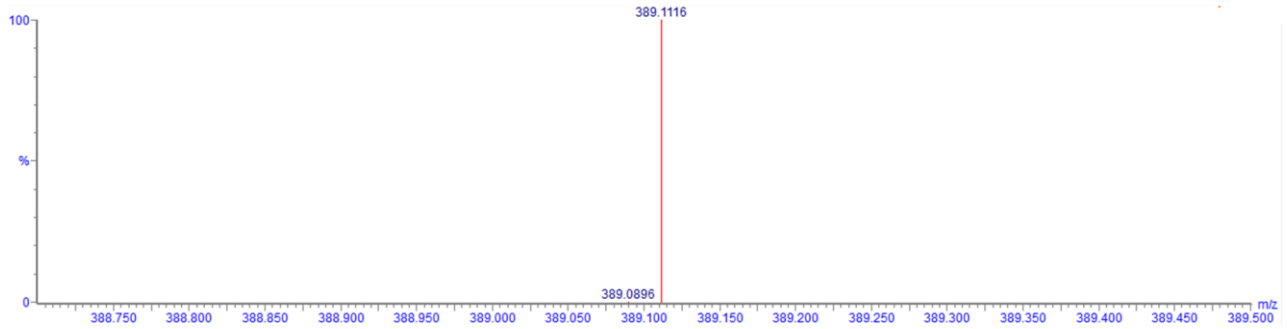

Figure S183 HRMS spectra of **1Nap-BTZ**.

4,7-Di(naphthalen-2-yl)benzo[*c*][1,2,5]thiadiazole (2Nap-BTZ)

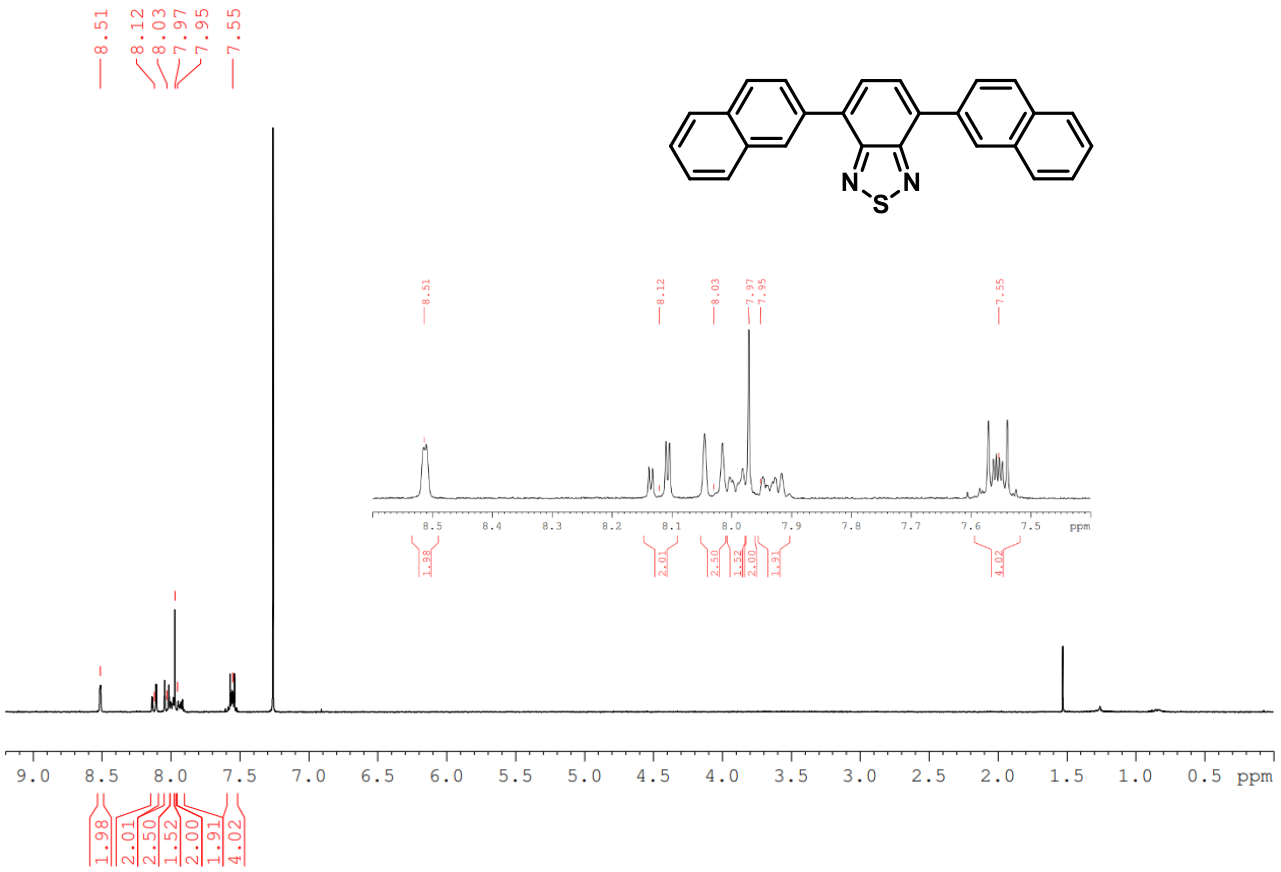

Figure S184 ^{1}H NMR of **2Nap-BTZ** in $CDCl_3$.

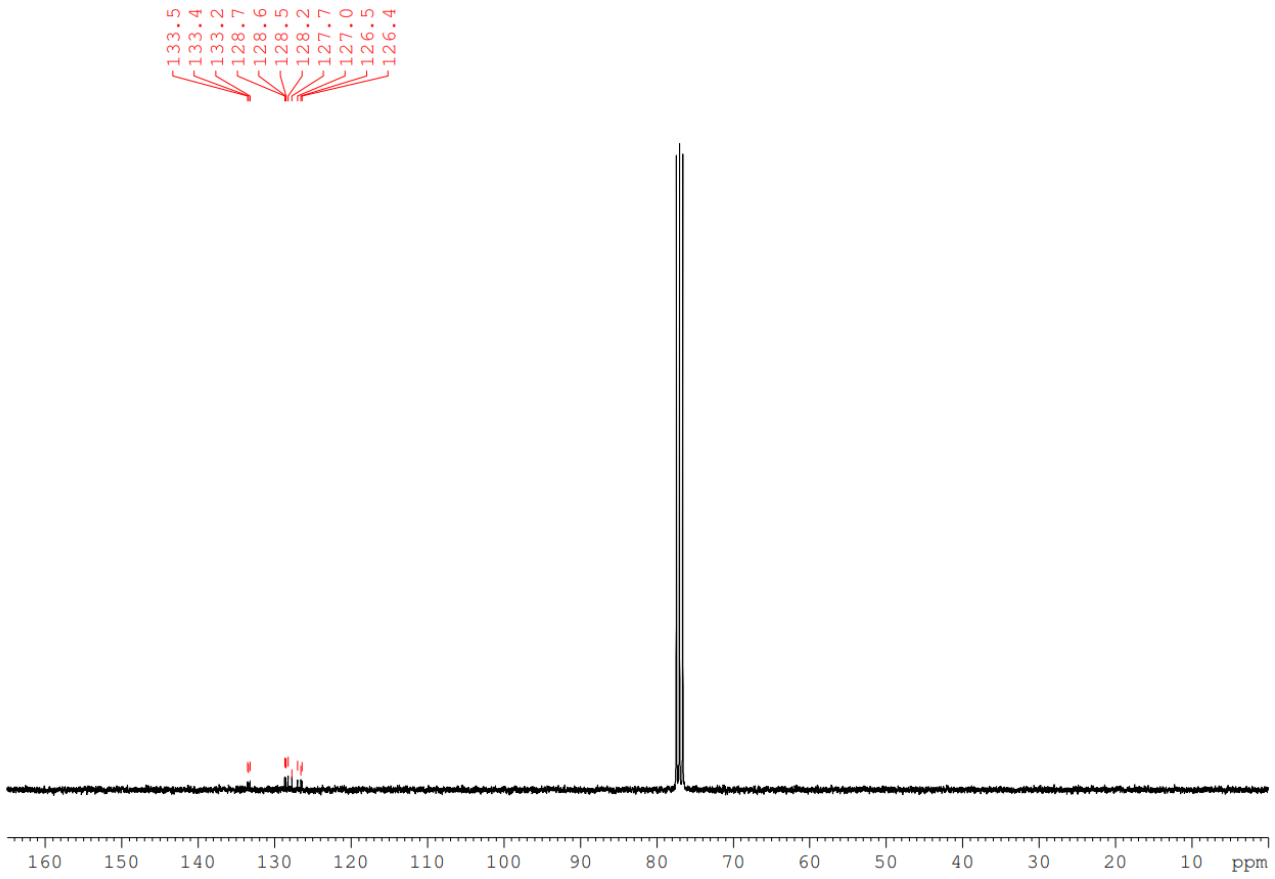

Figure S185 ^{13}C NMR spectra of **2Nap-BTZ** in $CDCl_3$.

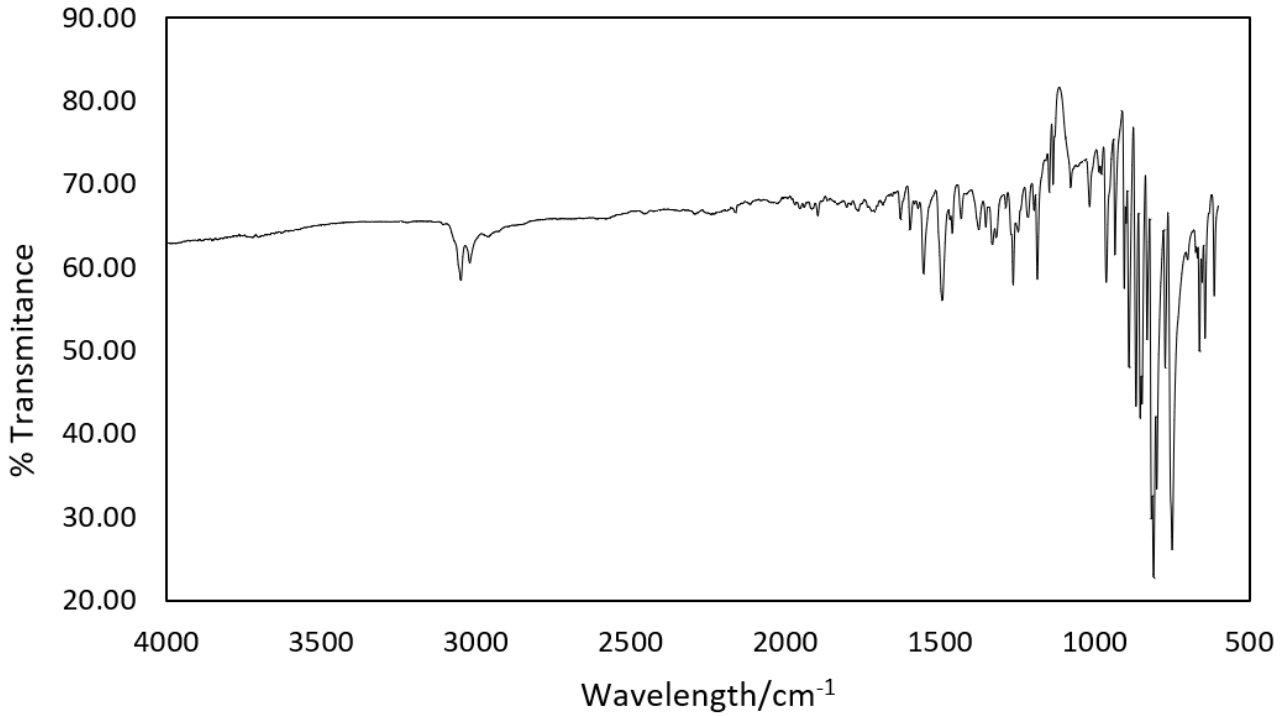

Figure S186 IR spectra of **2Nap-BTZ**.

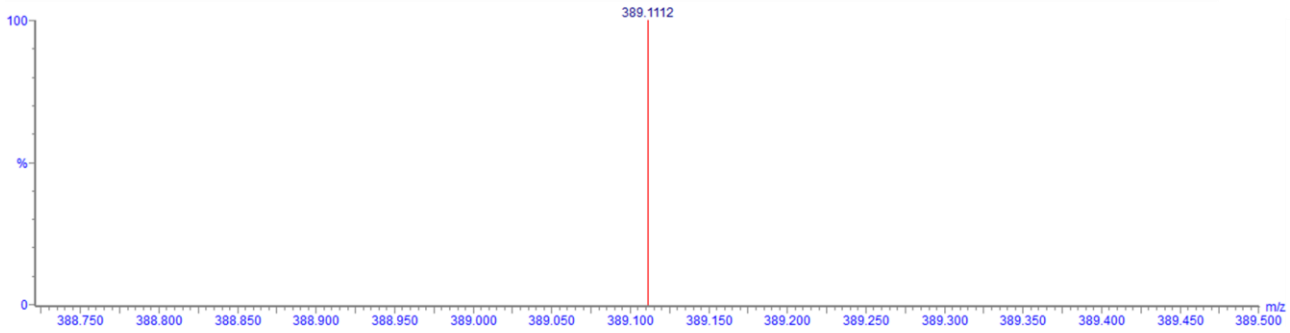

Figure S187 HRMS spectra of **2Nap-BTZ**.

4,7-Bis(9,9-dioctyl-9*H*-fluoren-2-yl)benzo[*c*][1,2,5]thiadiazole (Flu-BTZ)

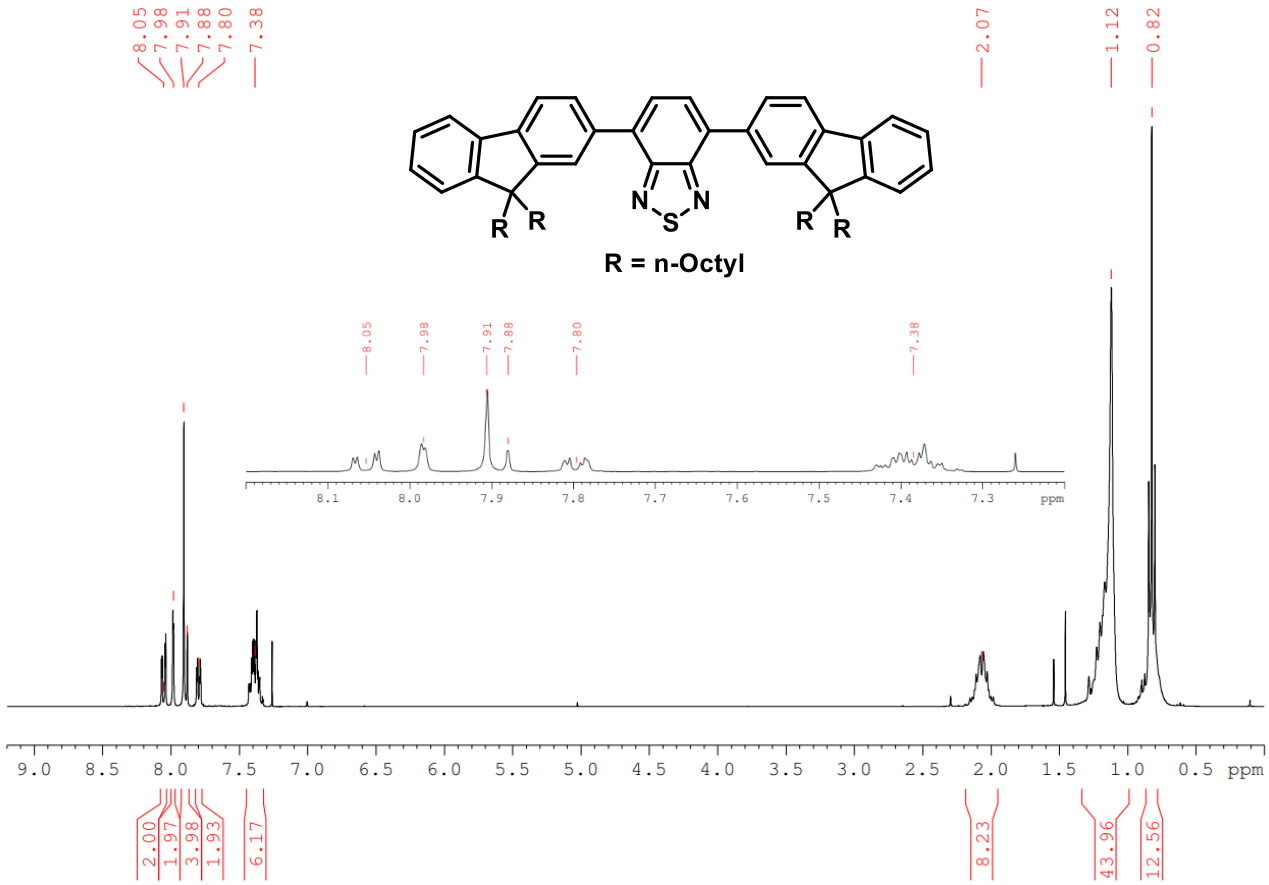

Figure S188 ^{1}H NMR spectra of **Flu-BTZ** in $CDCl_3$.

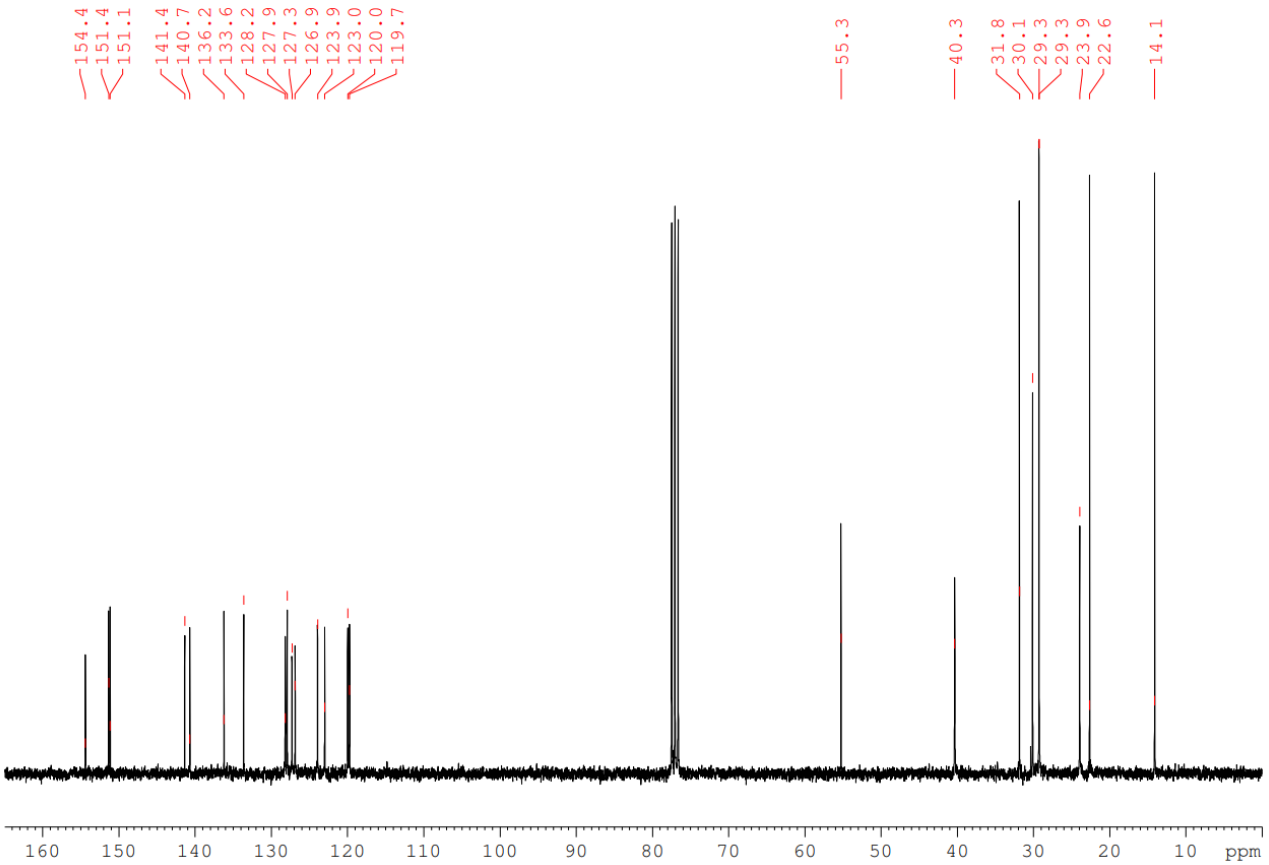

Figure S189 ^{13}C NMR spectra of **Flu-BTZ** in $CDCl_3$.

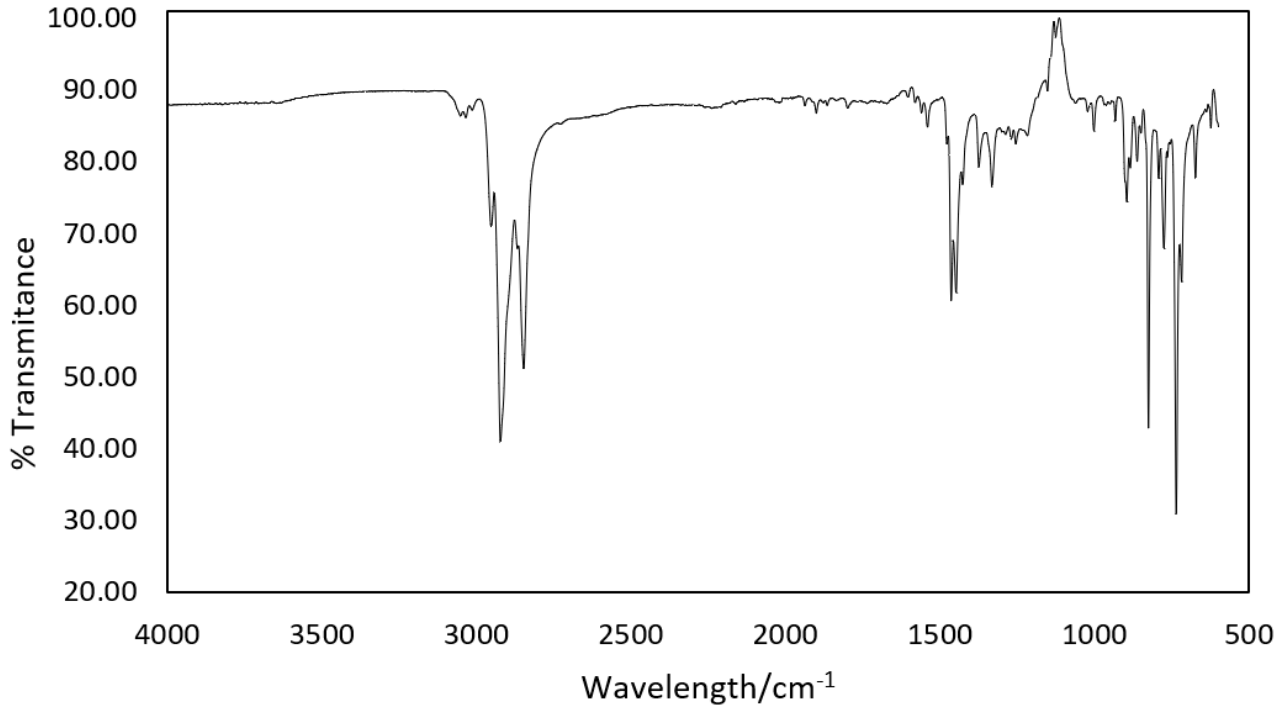

Figure S190 IR spectra of **Flu-BTZ**.

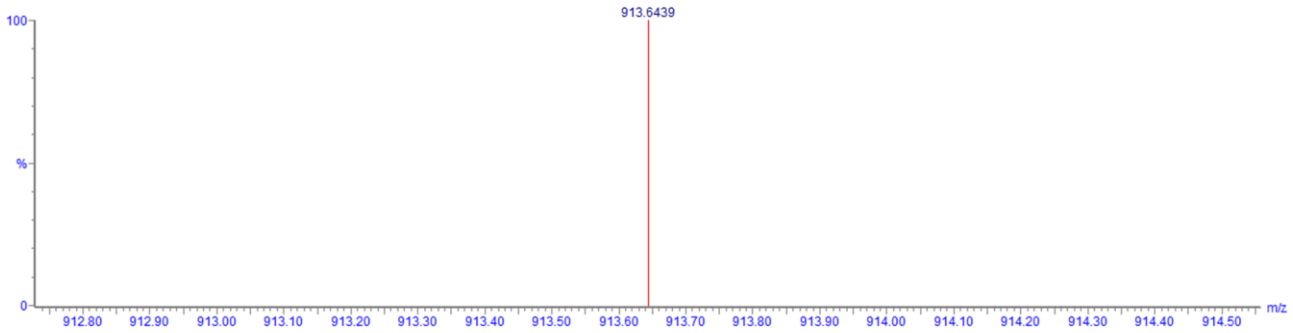

Figure S191 HRMS spectra of **Flu-BTZ**.

4,7-Di-*p*-tolylbenzo[*c*][1,2,5]thiadiazole (pMe-BTZ)

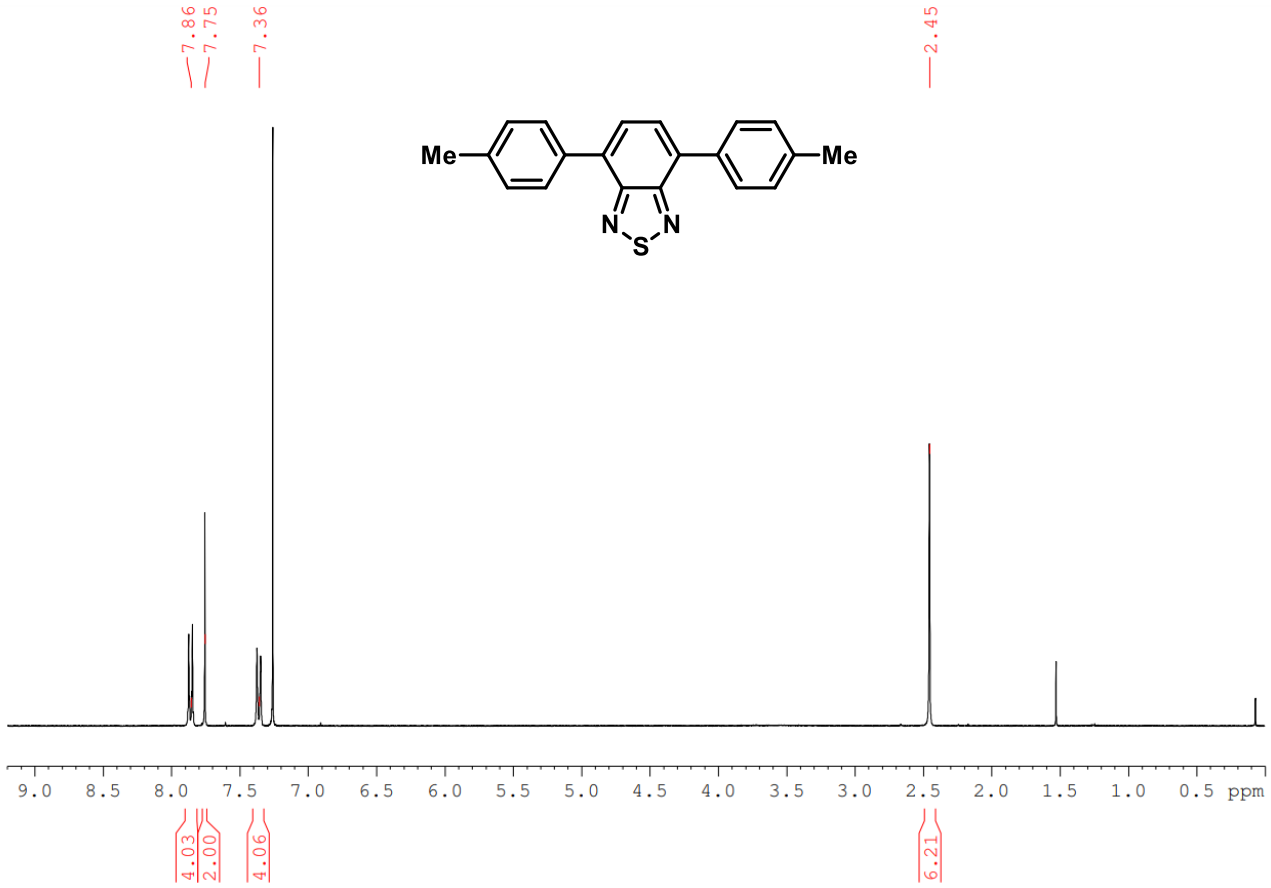

Figure S192 ^{1}H NMR of **pMe-BTZ** in $CDCl_3$.

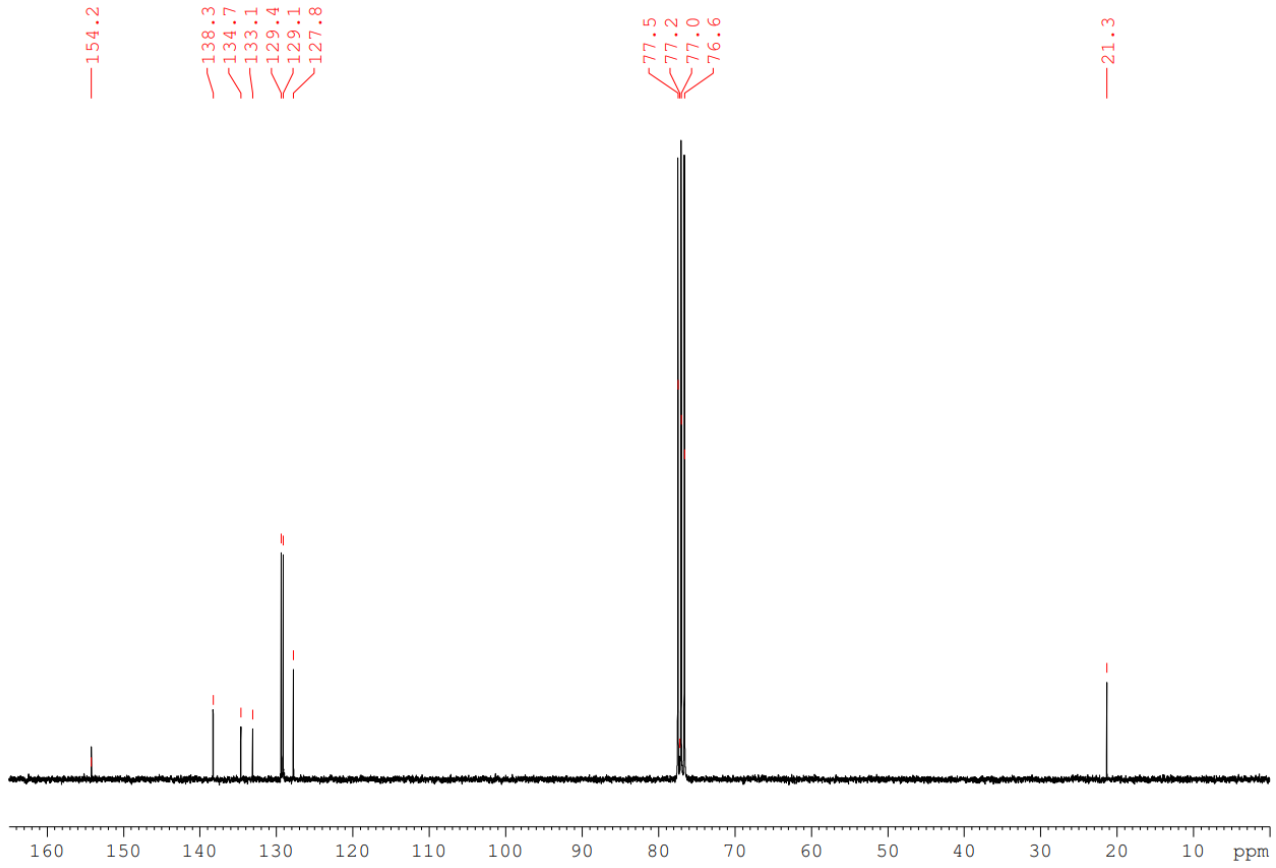

Figure S193 ^{13}C NMR of **pMe-BTZ** in $CDCl_3$.

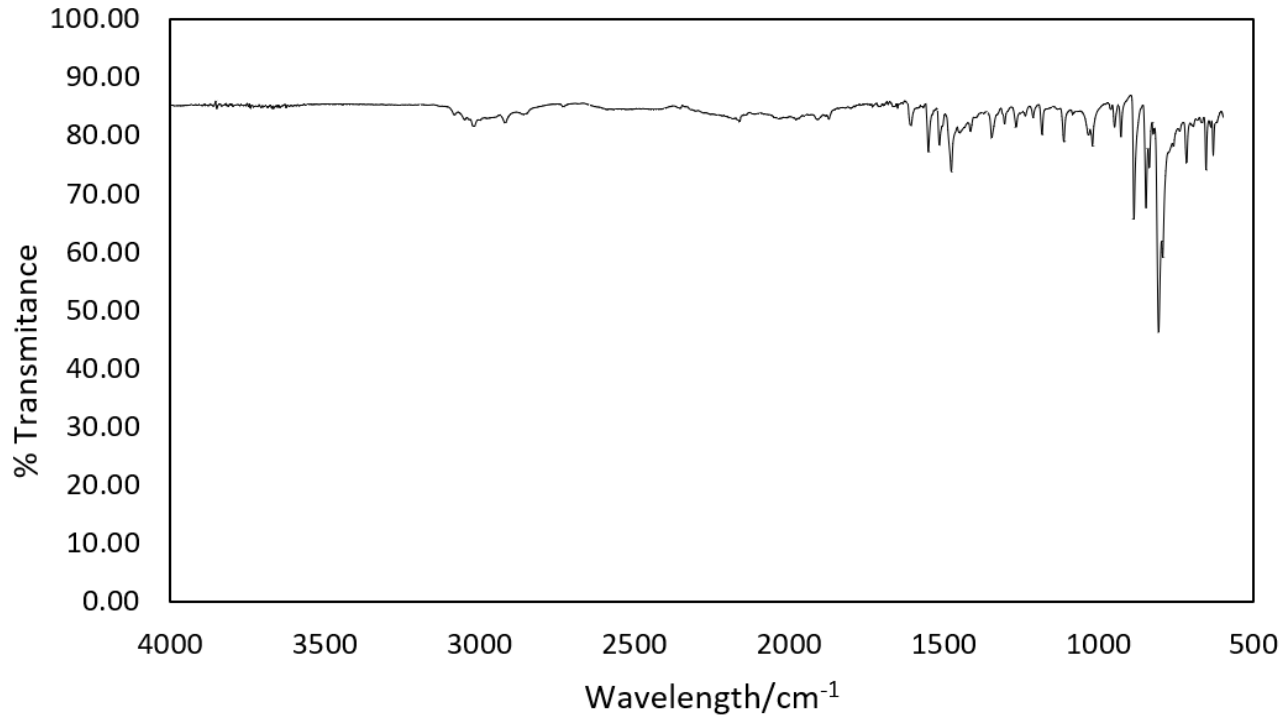

Figure S194 IR spectra of **pMe-BTZ**.

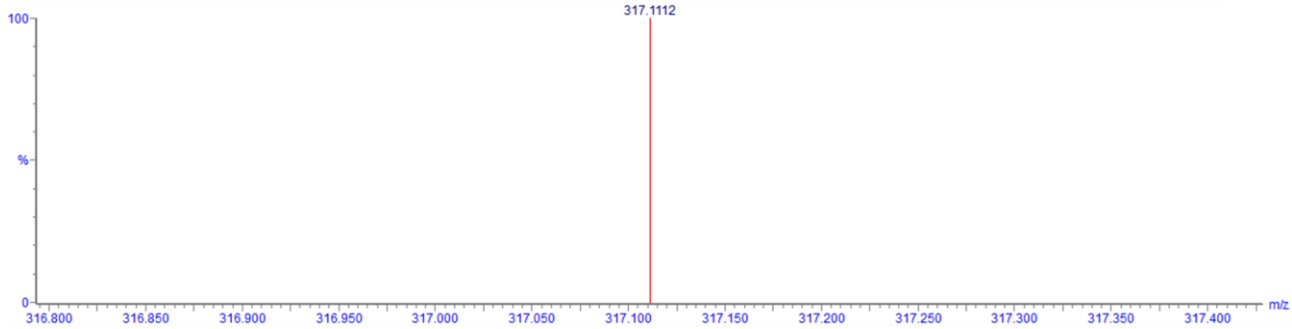

Figure S195 HRMS spectra of **pMe-BTZ**.

4,4'-(Benzo[*c*][1,2,5]thiadiazole-4,7-diyl)diphenol (pOH-BTZ)

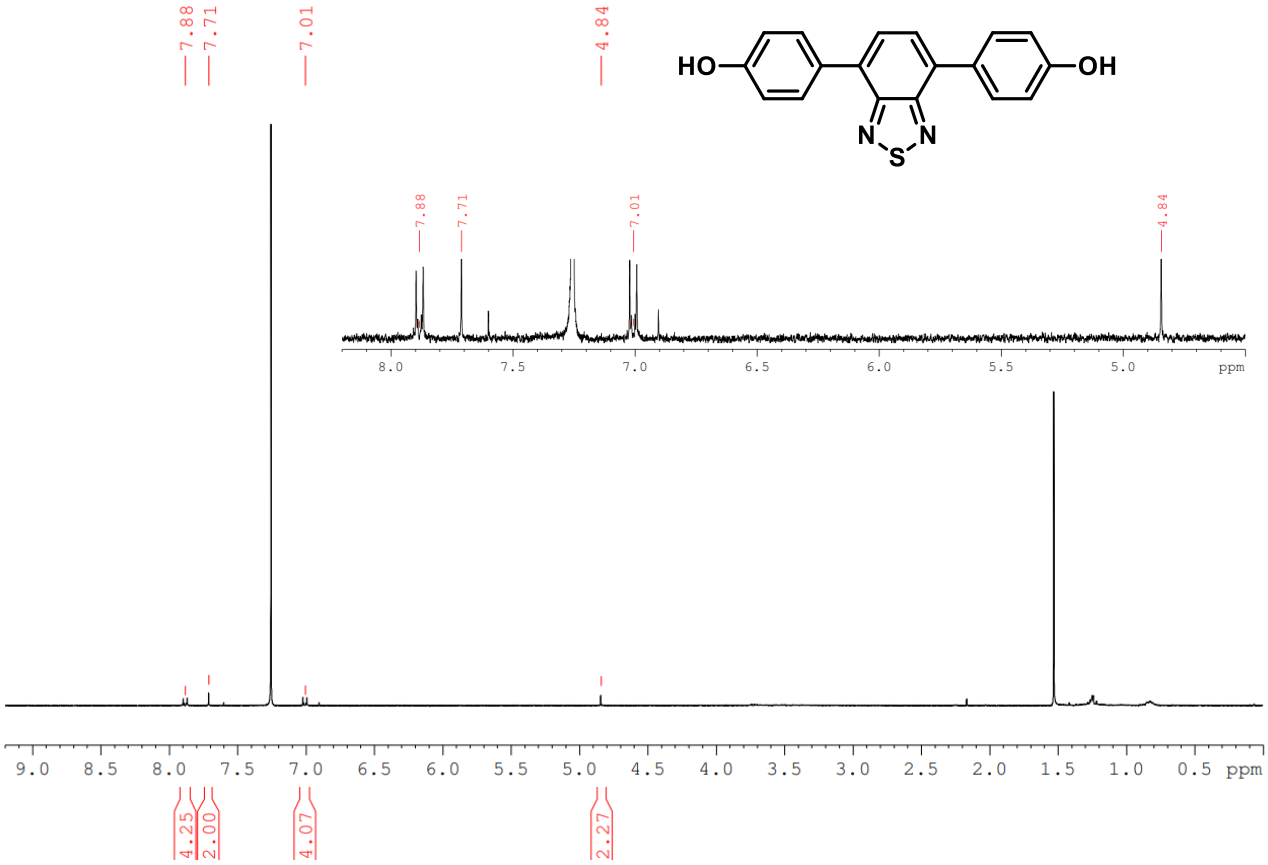

Figure S196 ^{1}H NMR of **pOH-BTZ** in $CDCl_3$.

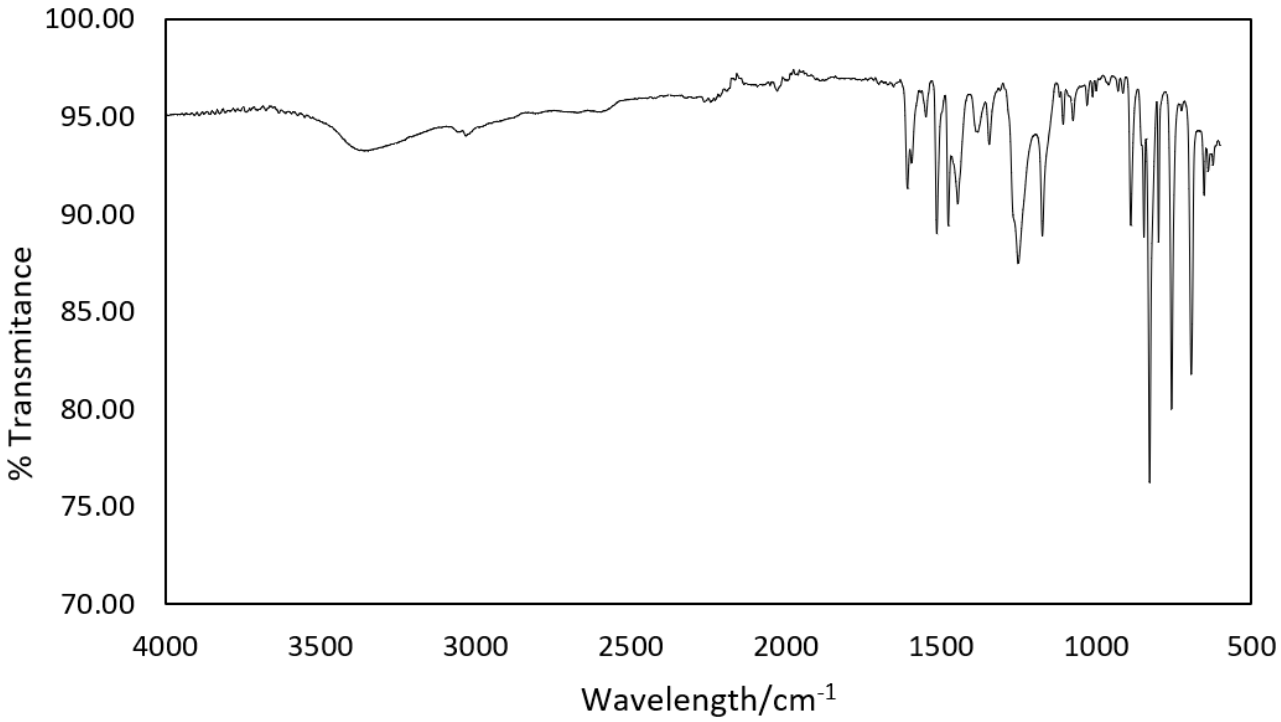

Figure S197 IR spectra of **pOH-BTZ**.

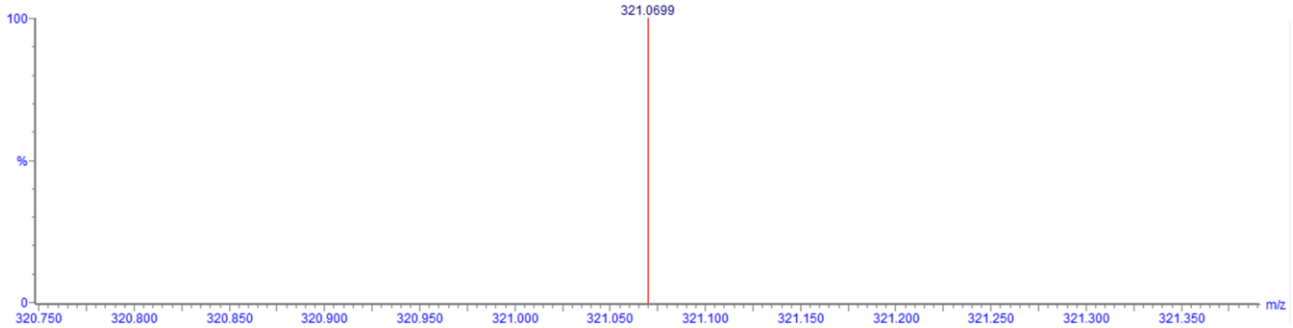

Figure S198 HRMS spectra of **pOH-BTZ**.

4,7-Bis(4-methoxyphenyl)benzo[*c*][1,2,5]thiadiazole (pOMe-BTZ)

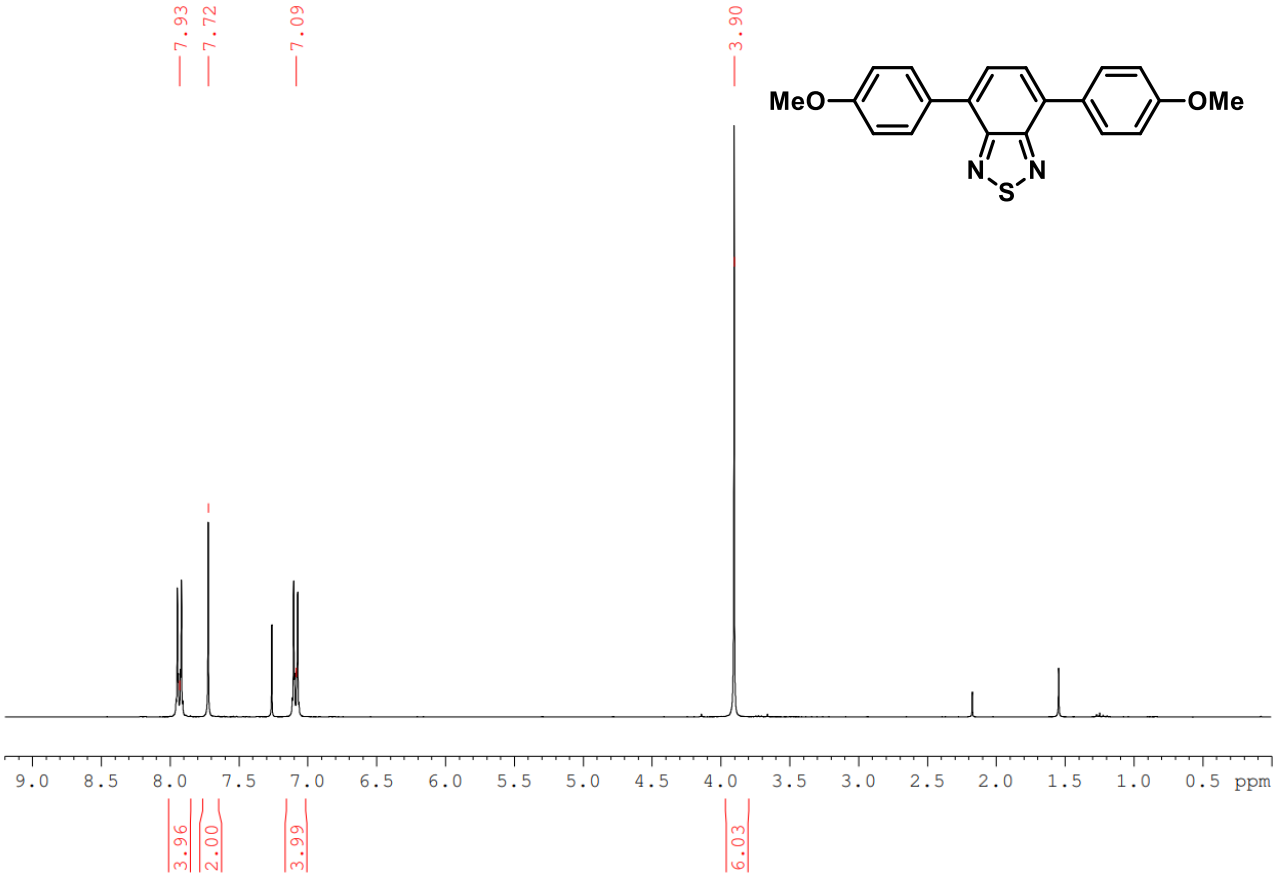

Figure S199 ^{1}H NMR of **pOMe-BTZ** in $CDCl_3$.

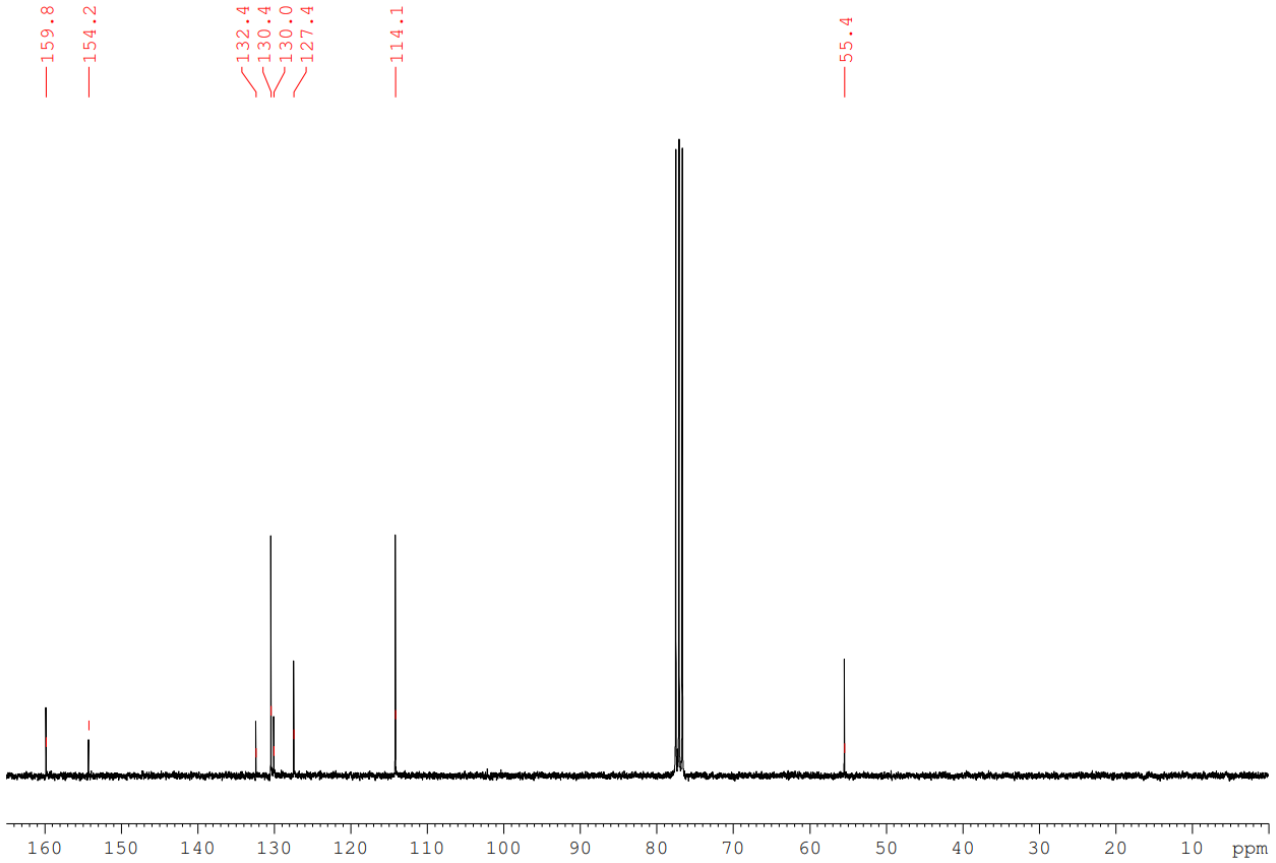

Figure S200 ^{13}C NMR of **pOMe-BTZ** in $CDCl_3$.

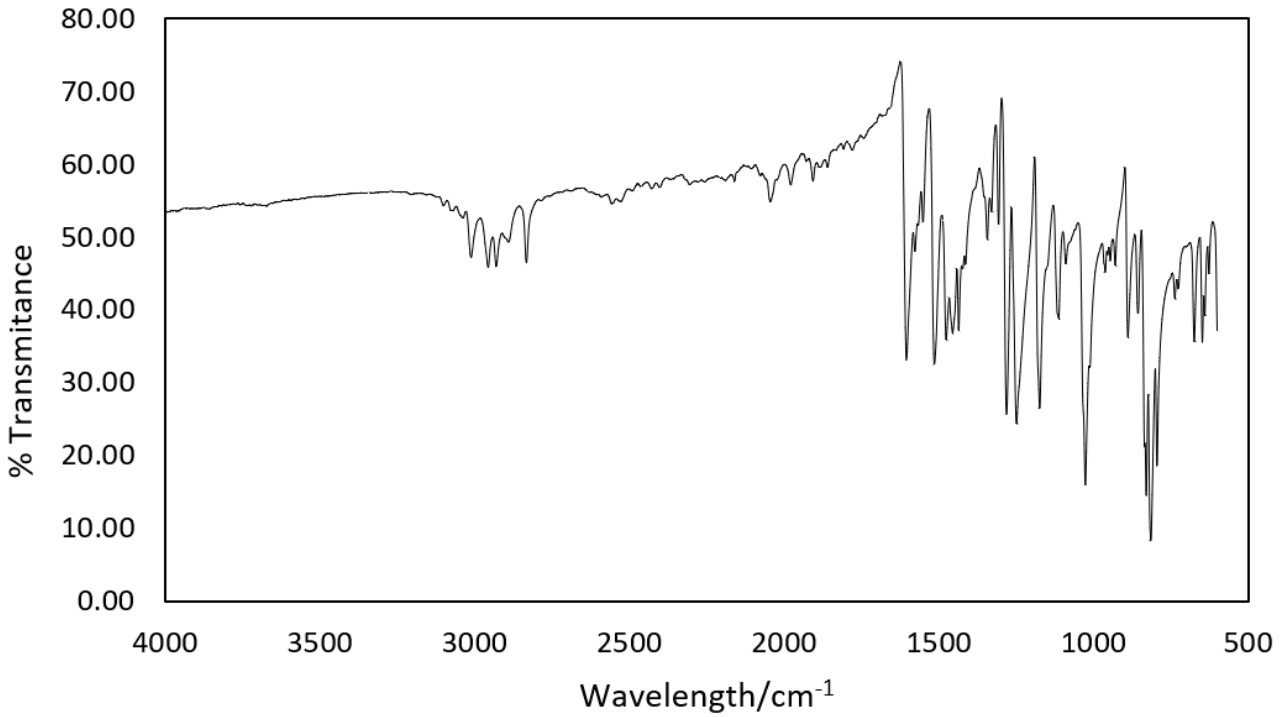

Figure S201 IR spectra of **pOMe-BTZ**.

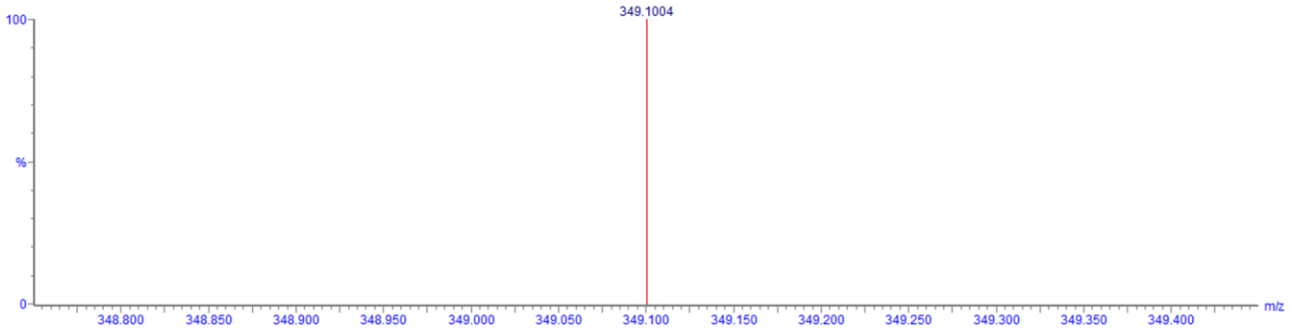

Figure S202 HRMS spectra of **pOMe-BTZ**.

4,4'-(Benzo[*c*][1,2,5]thiadiazole-4,7-diyl)dibenzaldehyde (pCHO-BTZ)

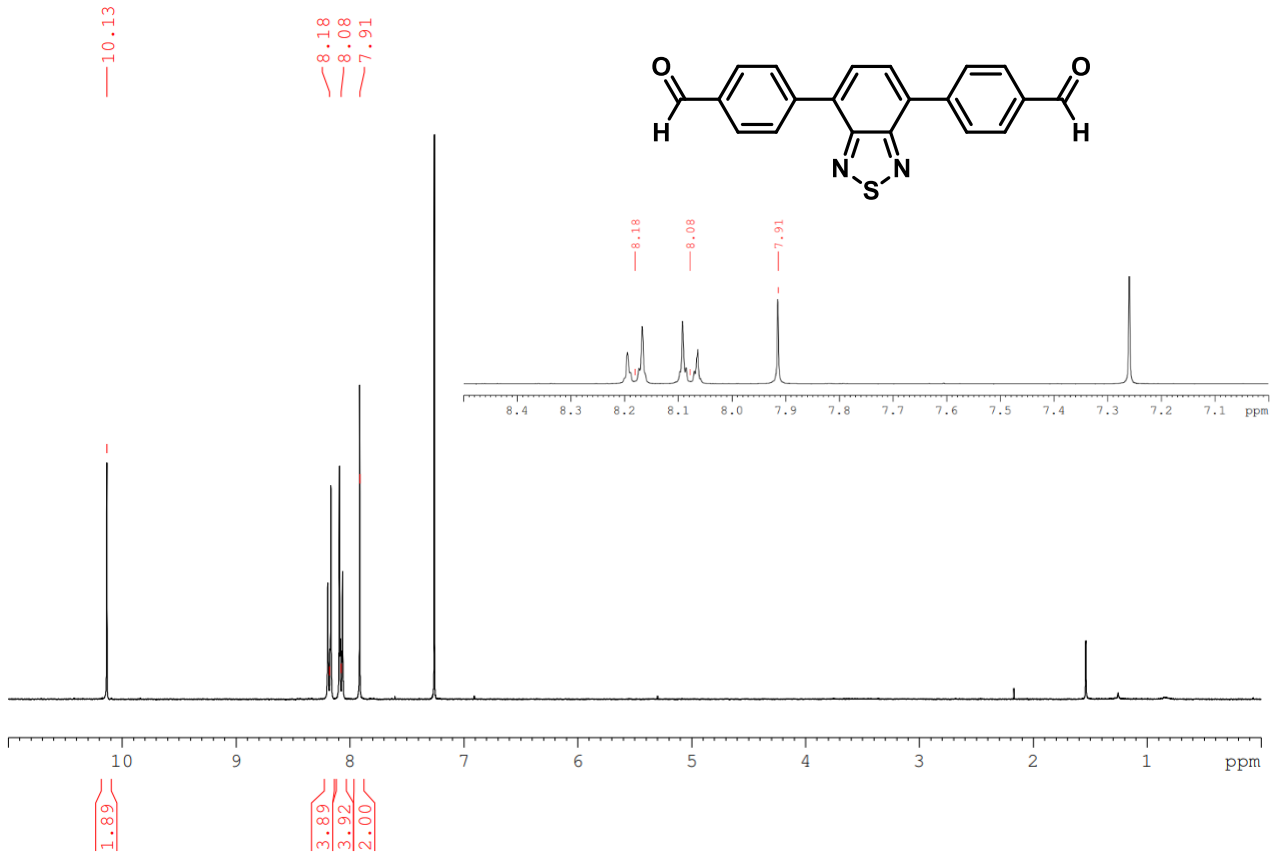

Figure S203 ^{1}H NMR of **pCHO-BTZ** in $CDCl_3$.

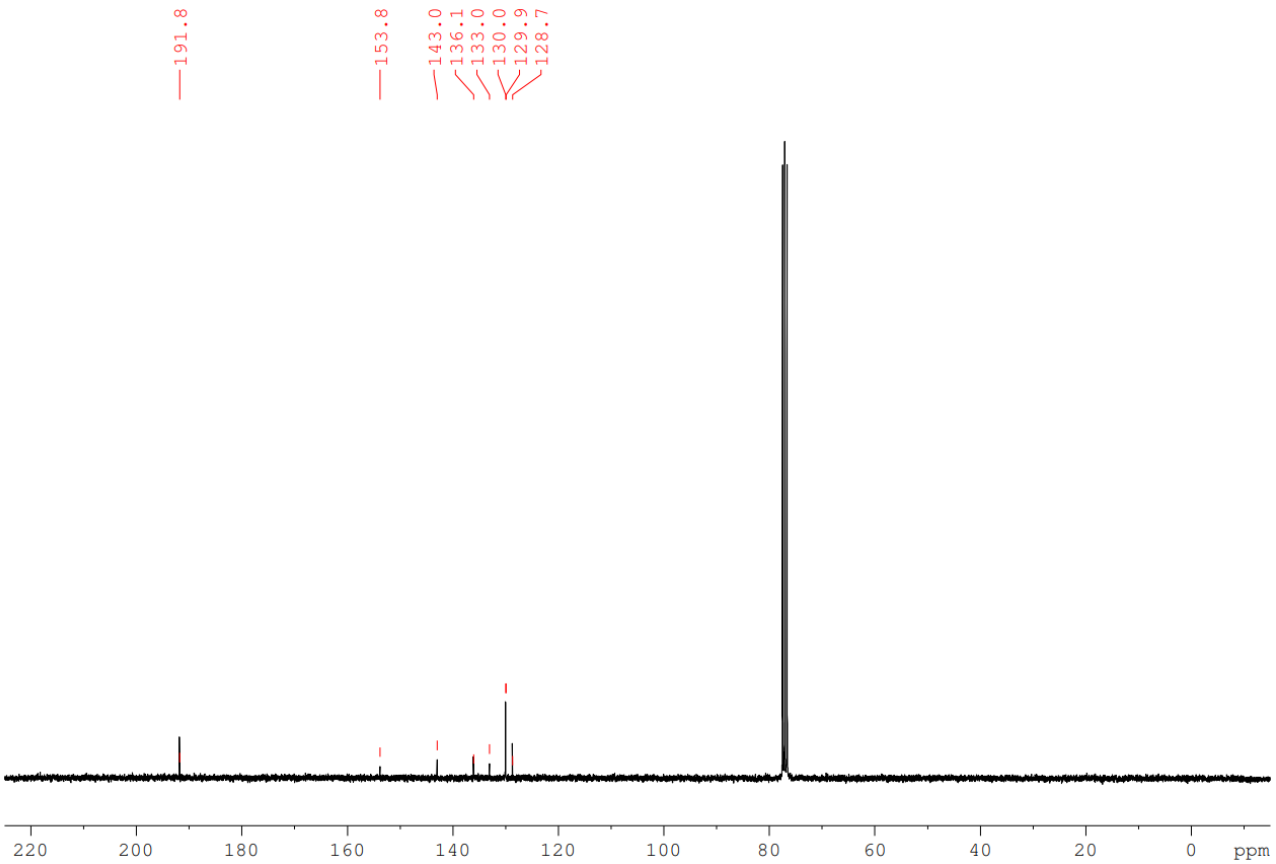

Figure S204 ^{13}C NMR of **pCHO-BTZ** in $CDCl_3$.

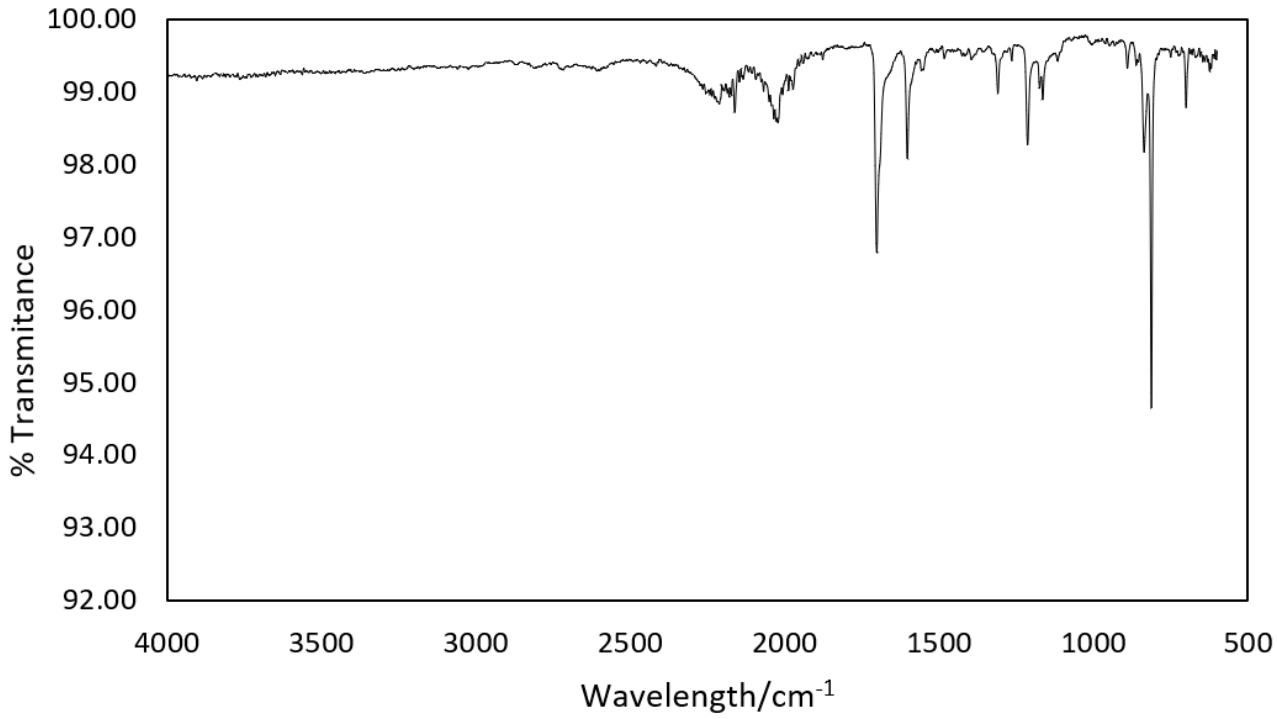

Figure S205 IR spectra of **pCHO-BTZ**.

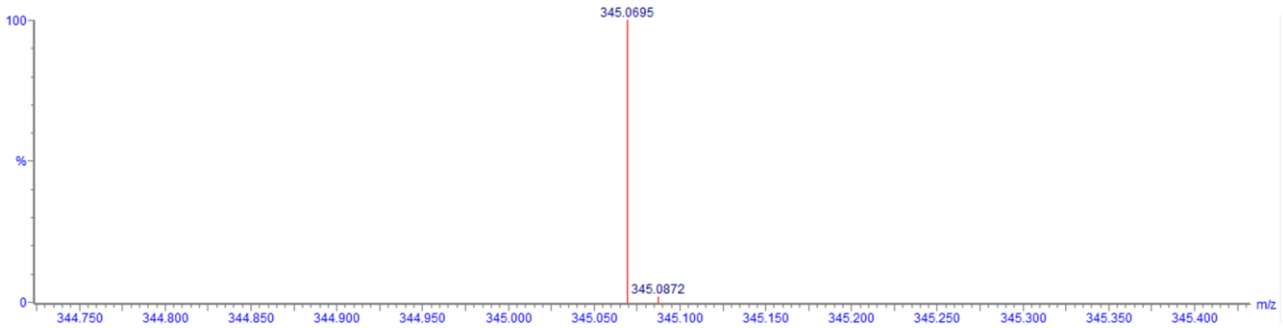

Figure S206 HRMS spectra of **pCHO-BTZ**.

4,4'-(Benzo[*c*][1,2,5]thiadiazole-4,7-diyl)dibenzonitrile (pCN-BTZ)

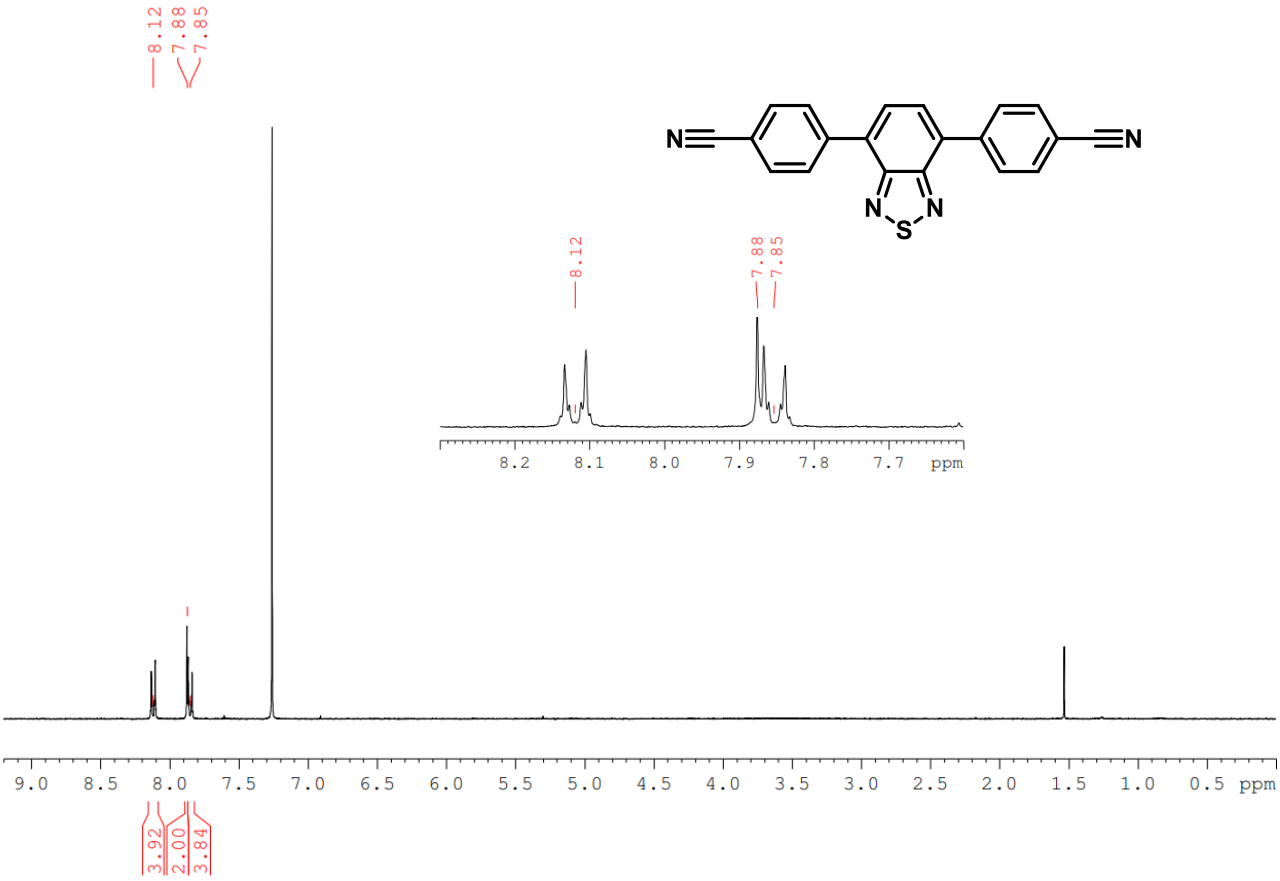

Figure S207 ^{1}H NMR of **pCN-BTZ** in $CDCl_3$.

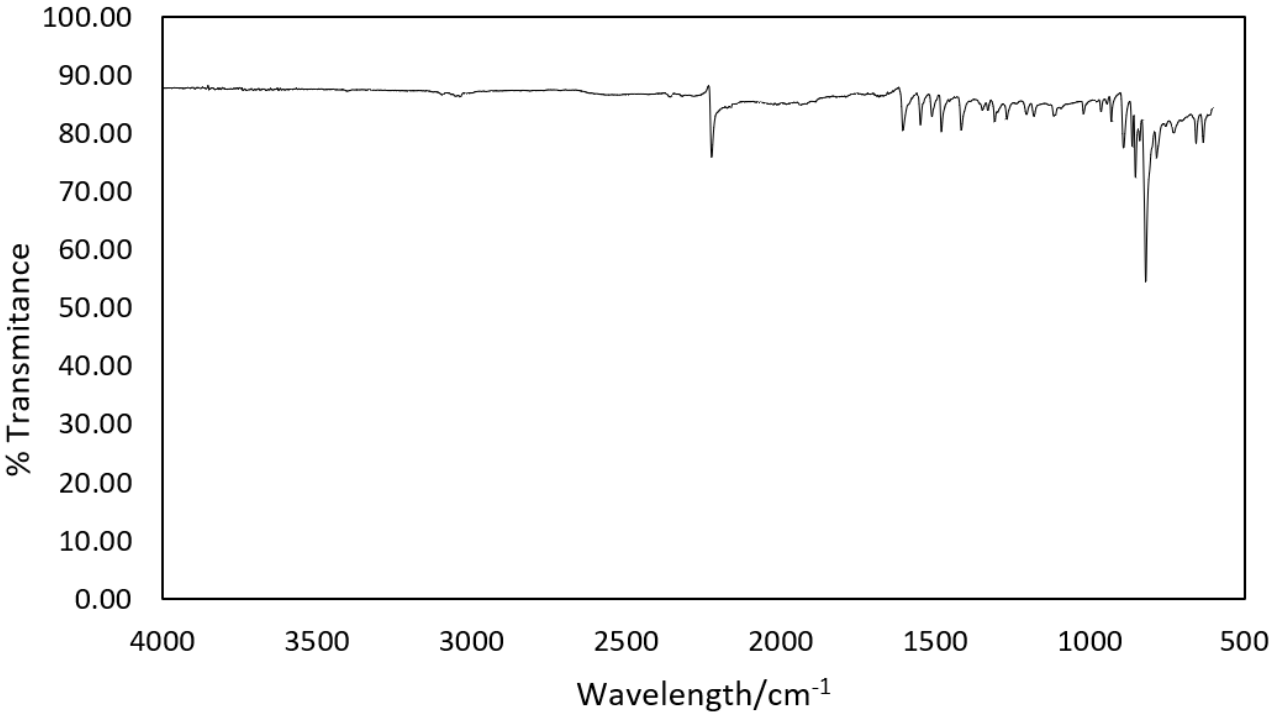

Figure S208 IR spectra of **pCN-BTZ**.

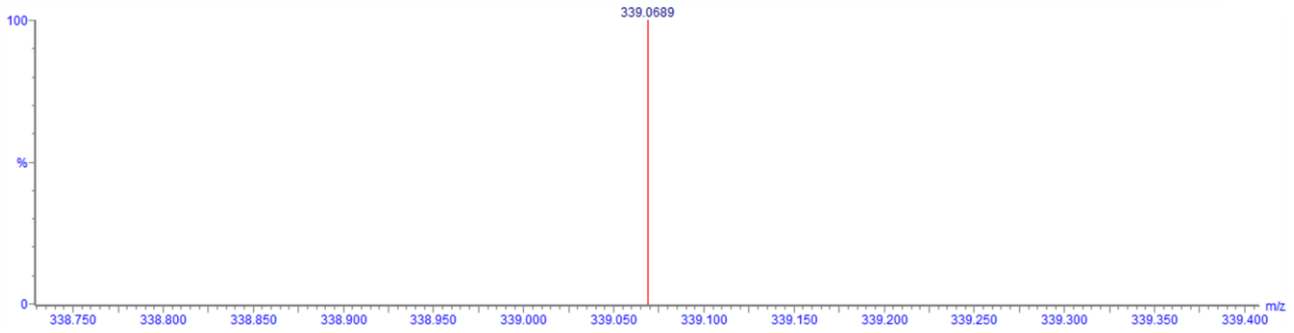

Figure S209 HRMS spectra of **pCN-BTZ**.

4,7-Bis(4-(trifluoromethyl)phenyl)benzo[*c*][1,2,5]thiadiazole (pCF$_3$-BTZ)

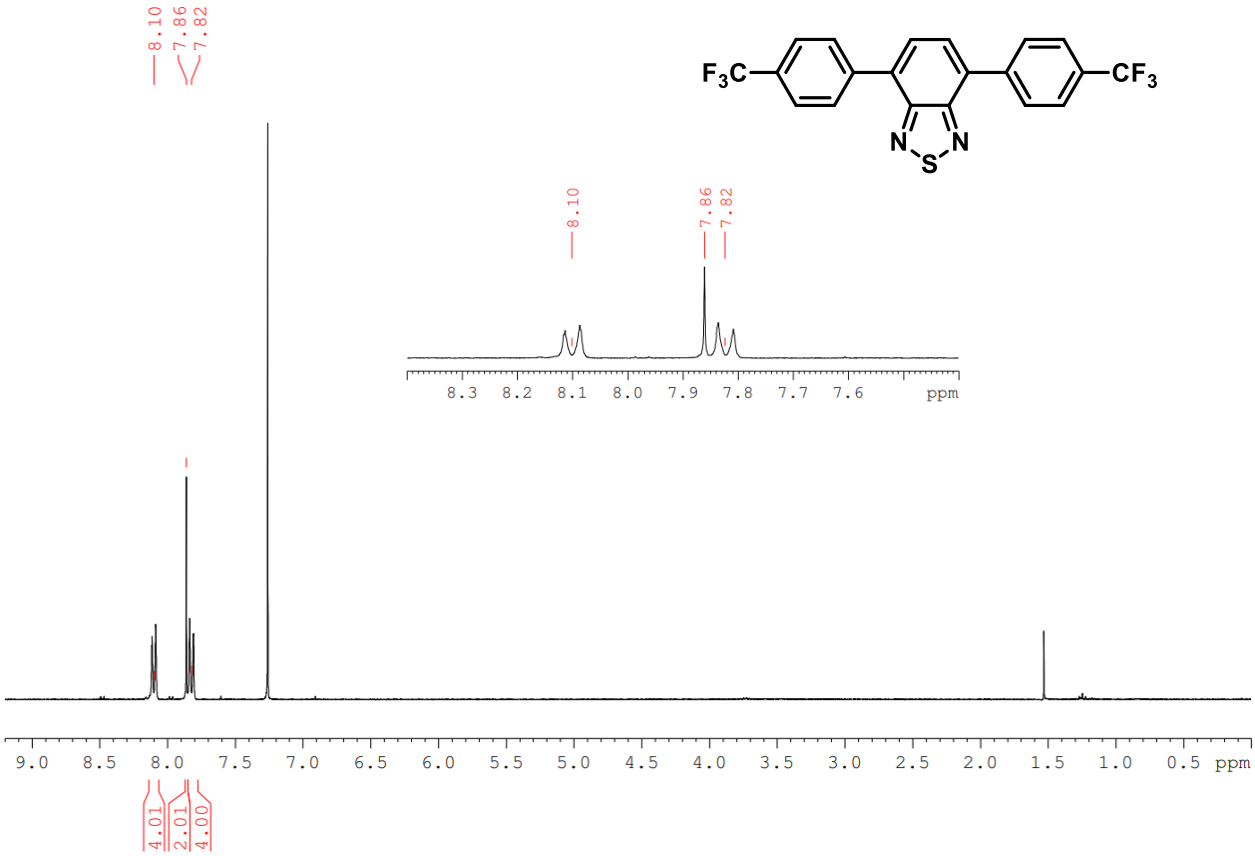

Figure S210 ^{1}H NMR of **pCF$_3$-BTZ** in $CDCl_3$.

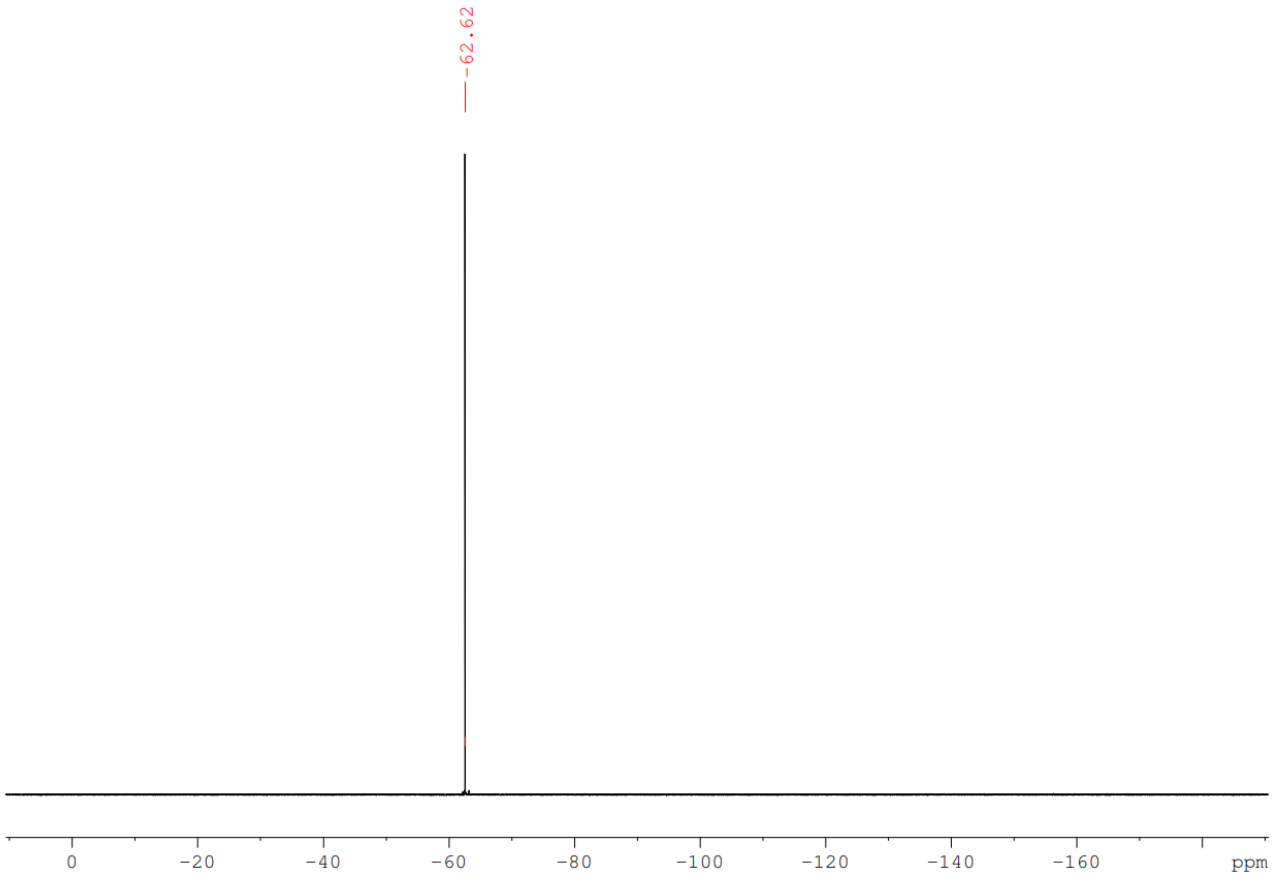

Figure S211 ^{19}F NMR of **pCF$_3$-BTZ** in $CDCl_3$.

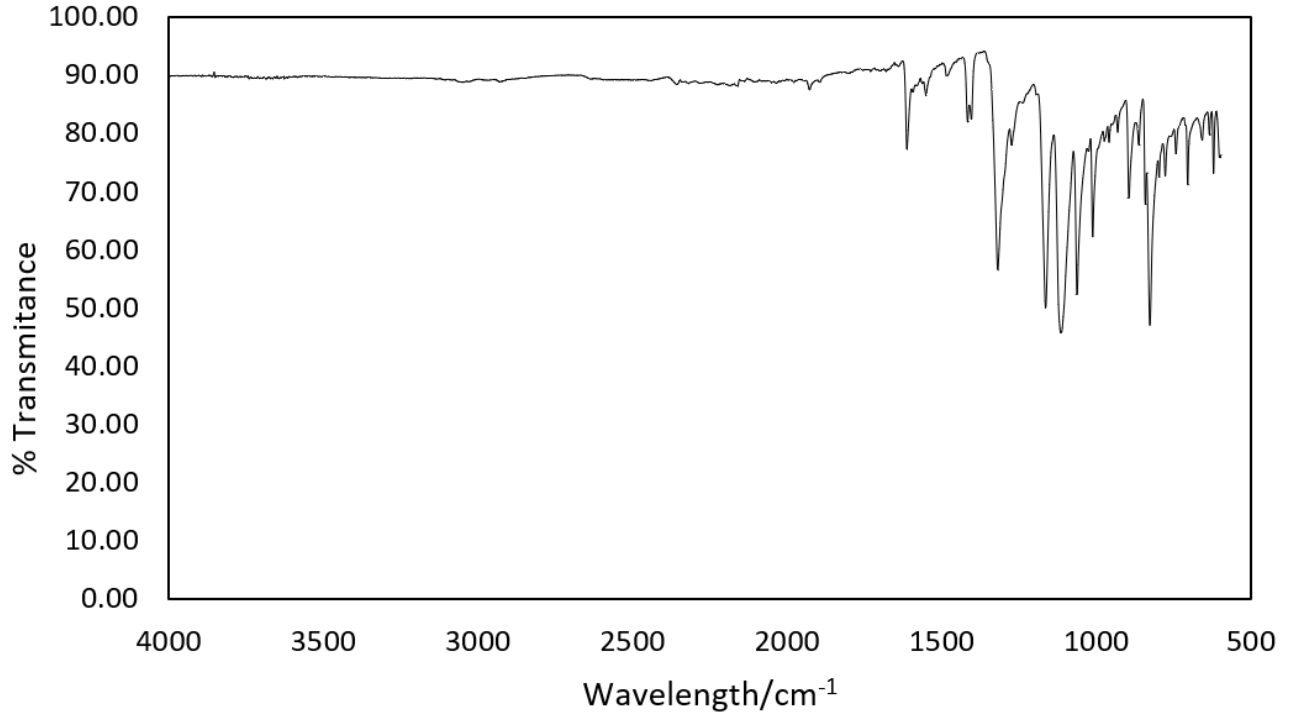

Figure S212 IR spectra of **pCF$_3$-BTZ**.

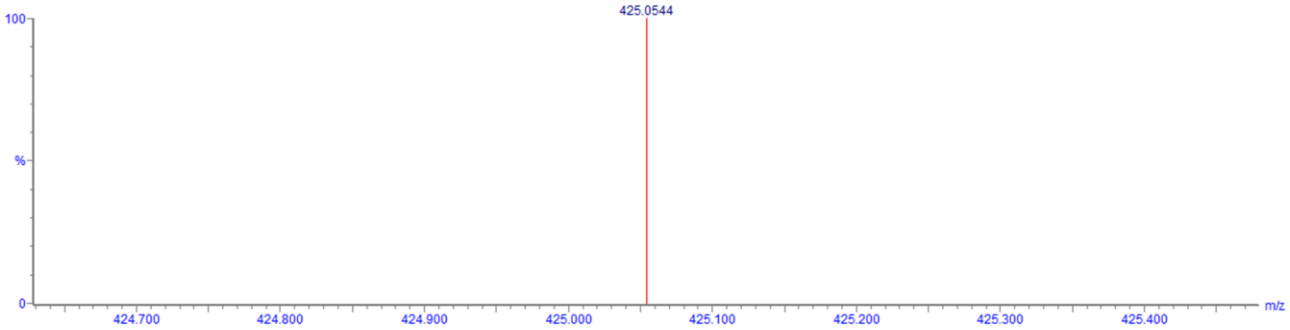

Figure S213 HRMS spectra of **pCF$_3$-BTZ**.

4,7-Bis(4-nitrophenyl)benzo[*c*][1,2,5]thiadiazole (pNO$_2$-BTZ)

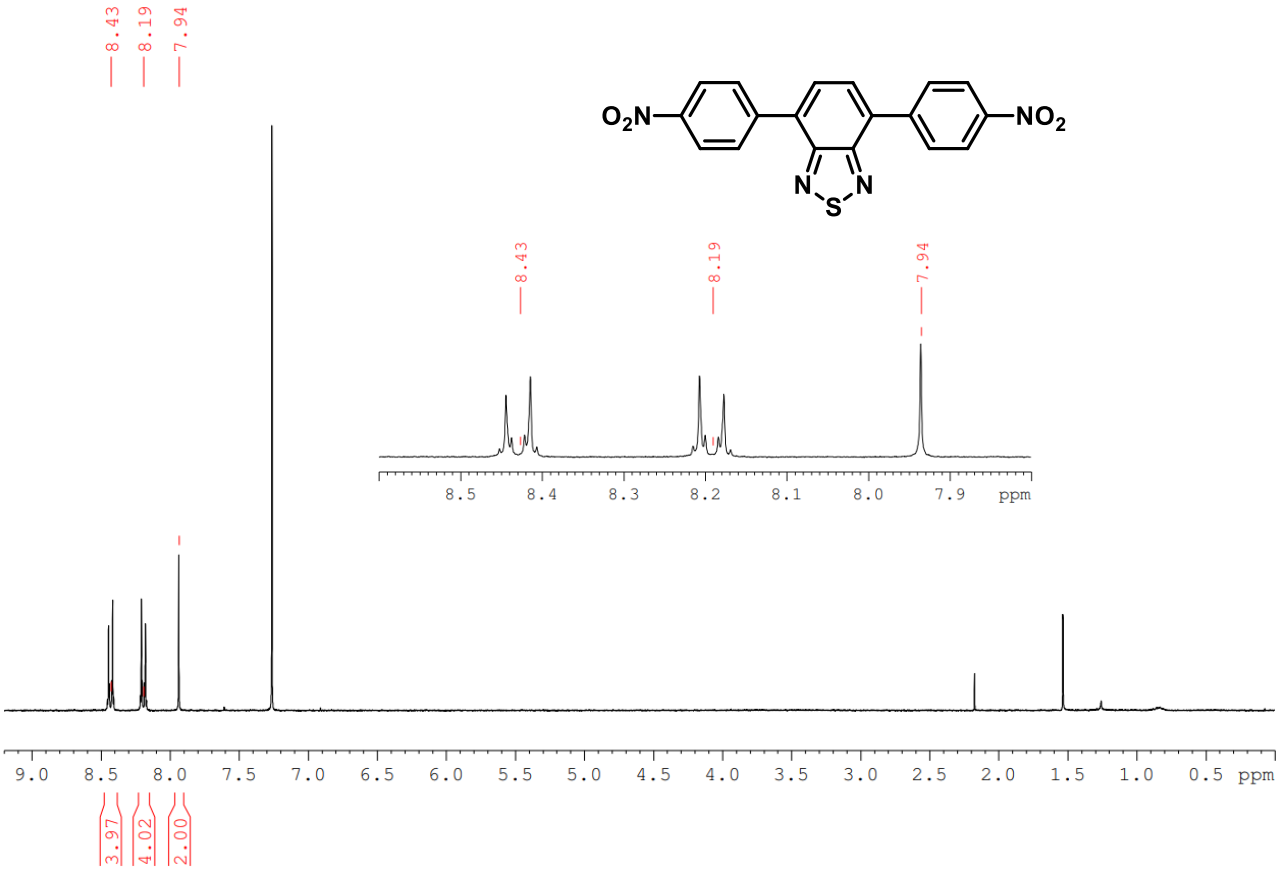

Figure S214 ^{1}H NMR of **pNO$_2$-BTZ**.

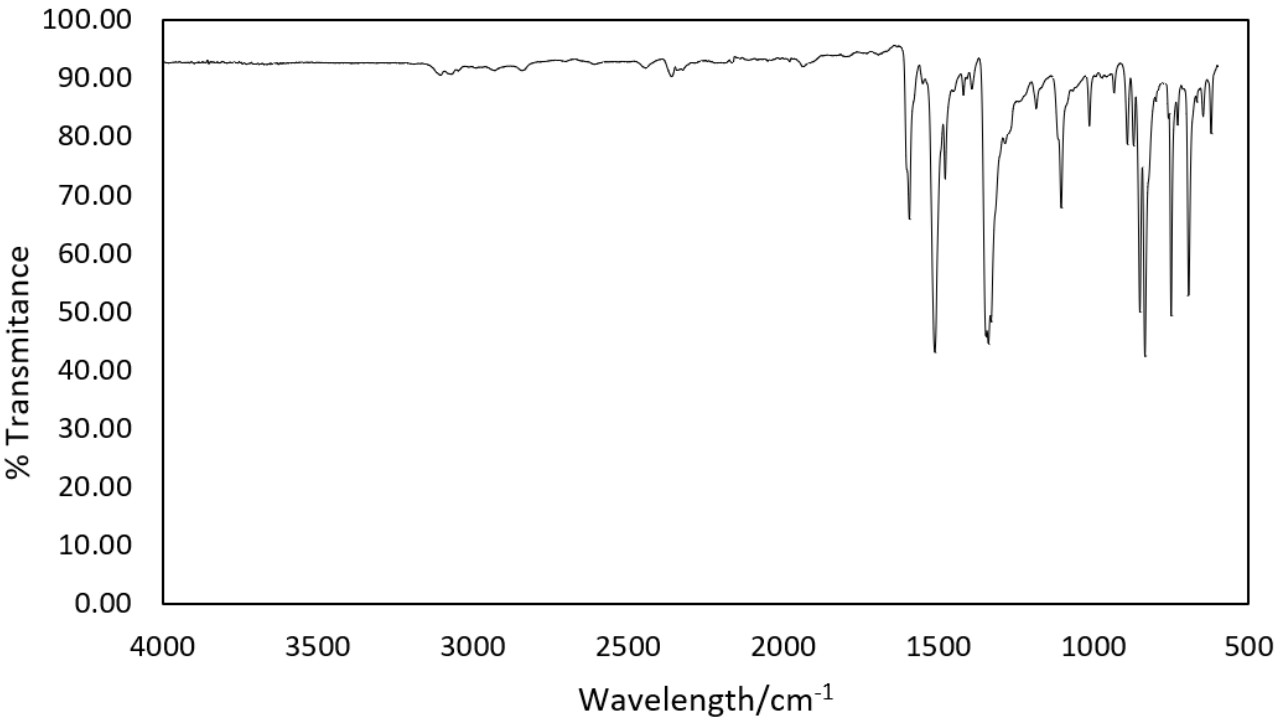

Figure S215 IR spectra of **pNO$_2$-BTZ**.

9. Characterisation of Photocatalytic Reaction Products

2-Cyclohexyl-4-methylquinoline (1)

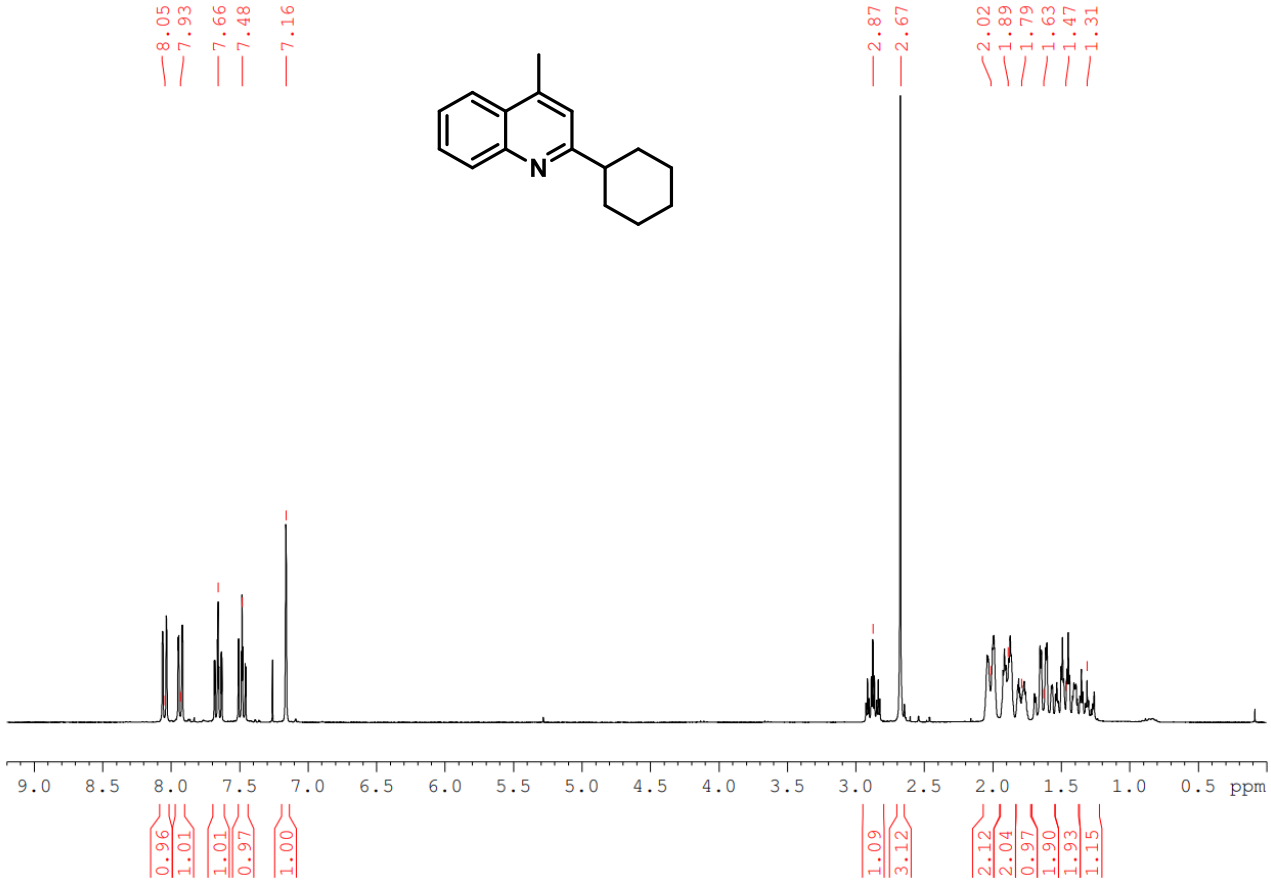

Figure S216 ^{1}H NMR of 2-cyclohexyl-4-methylquinoline in $CDCl_3$.

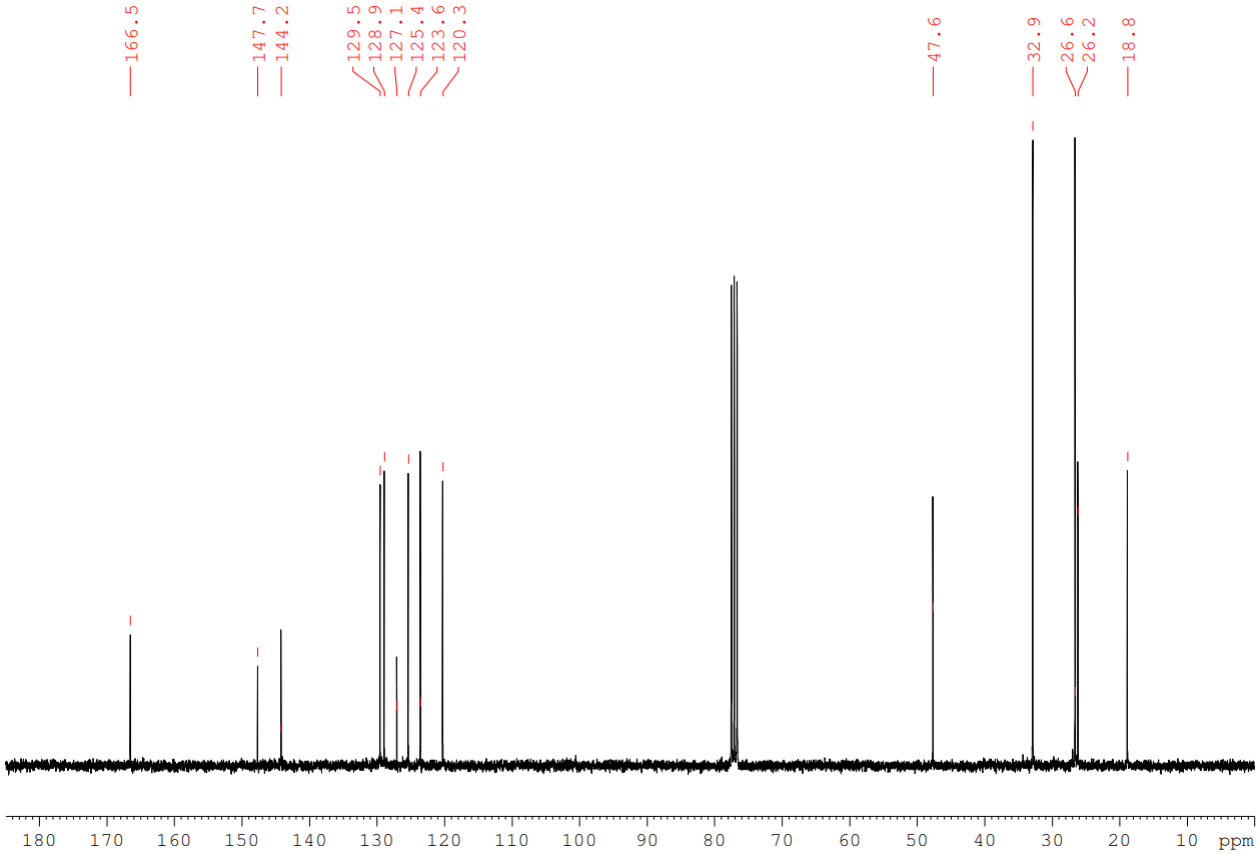

Figure S217 ^{13}C NMR of 2-cyclohexyl-4-methylquinoline in $CDCl_3$.

4-Cyclohexyl-2-methylquinoline (2)

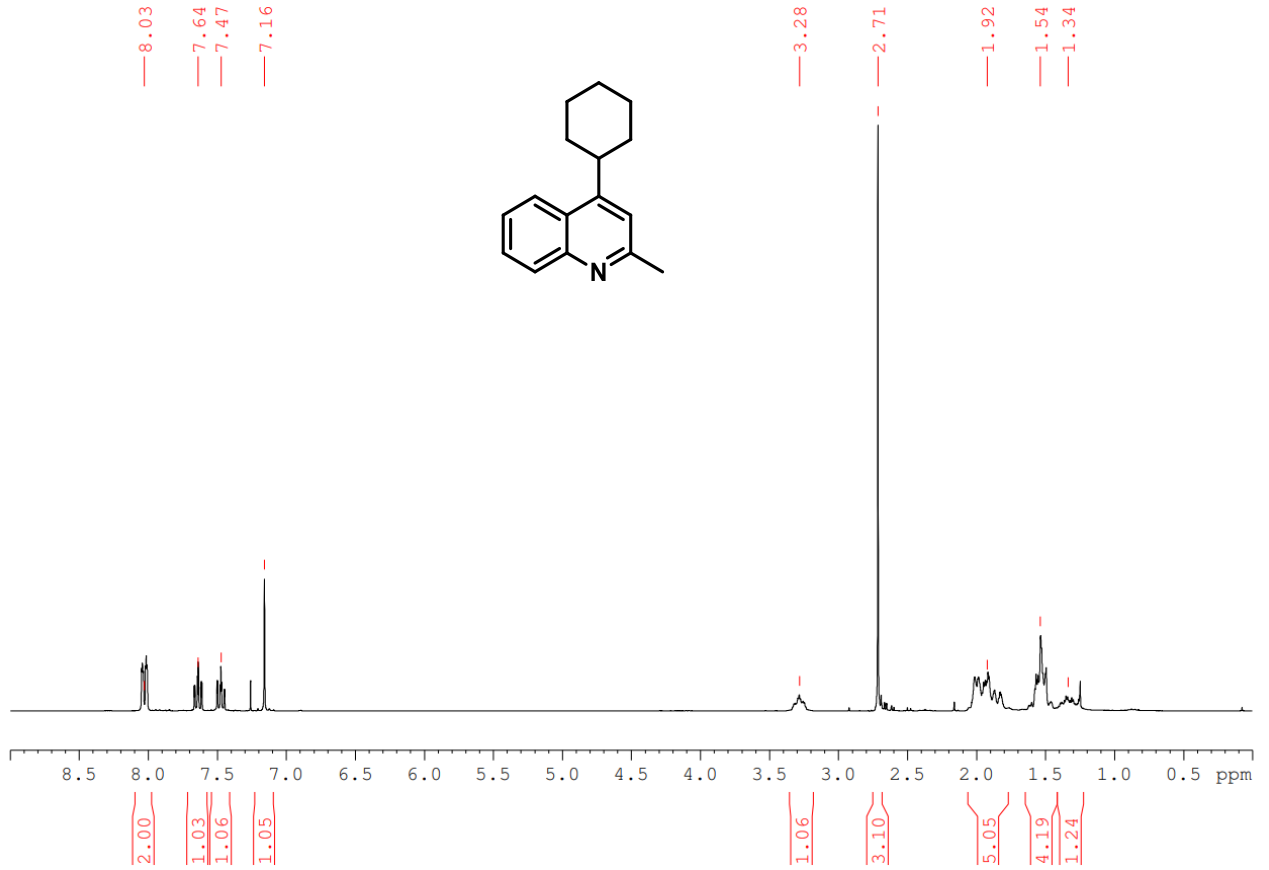

Figure S218 ^{1}H NMR of 4-cyclohexyl-2-methylpyridine in $CDCl_3$.

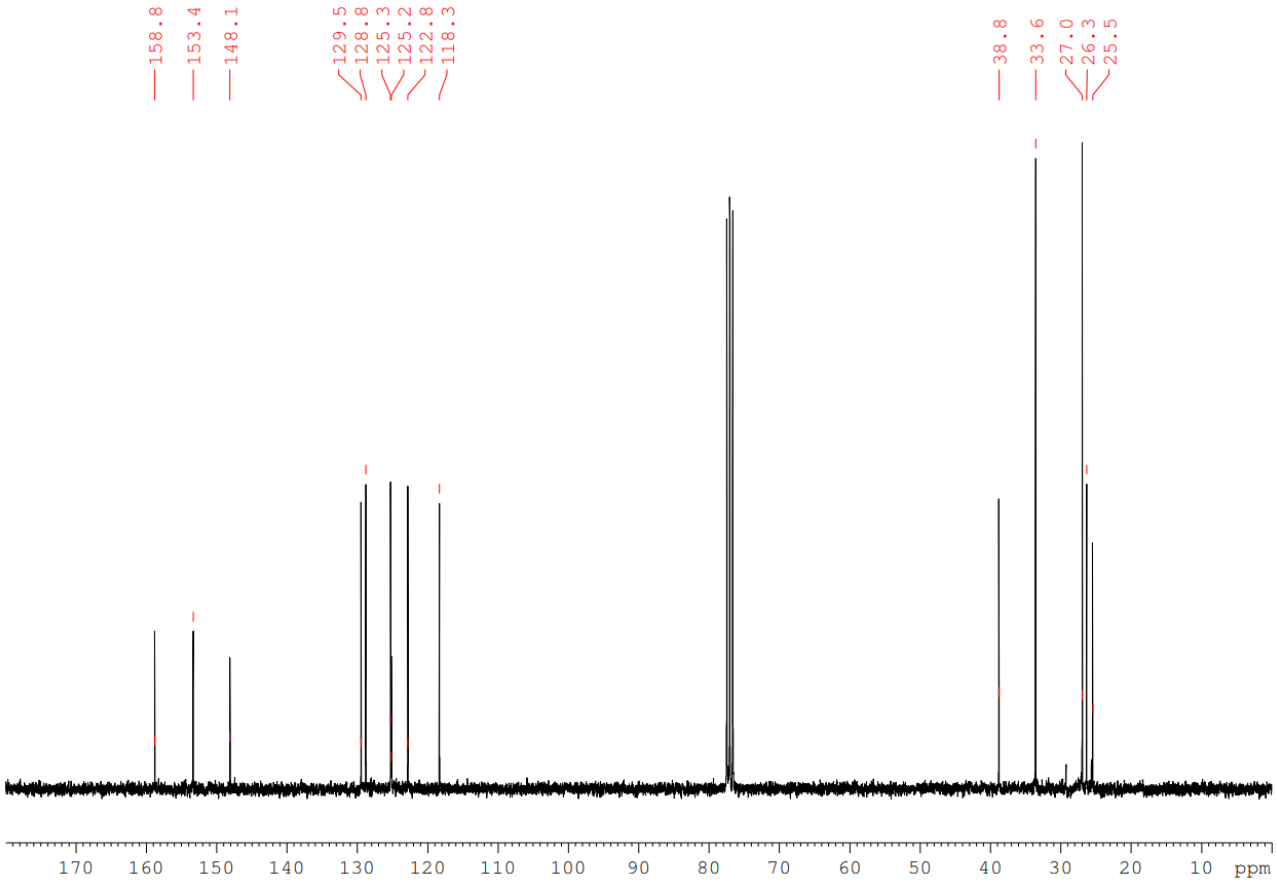

Figure S219 ^{13}C NMR of 4-cyclohexyl-2-methylpyridine in $CDCl_3$.

4-Cyclohexyl-2,6-dimethylpyridine (3)

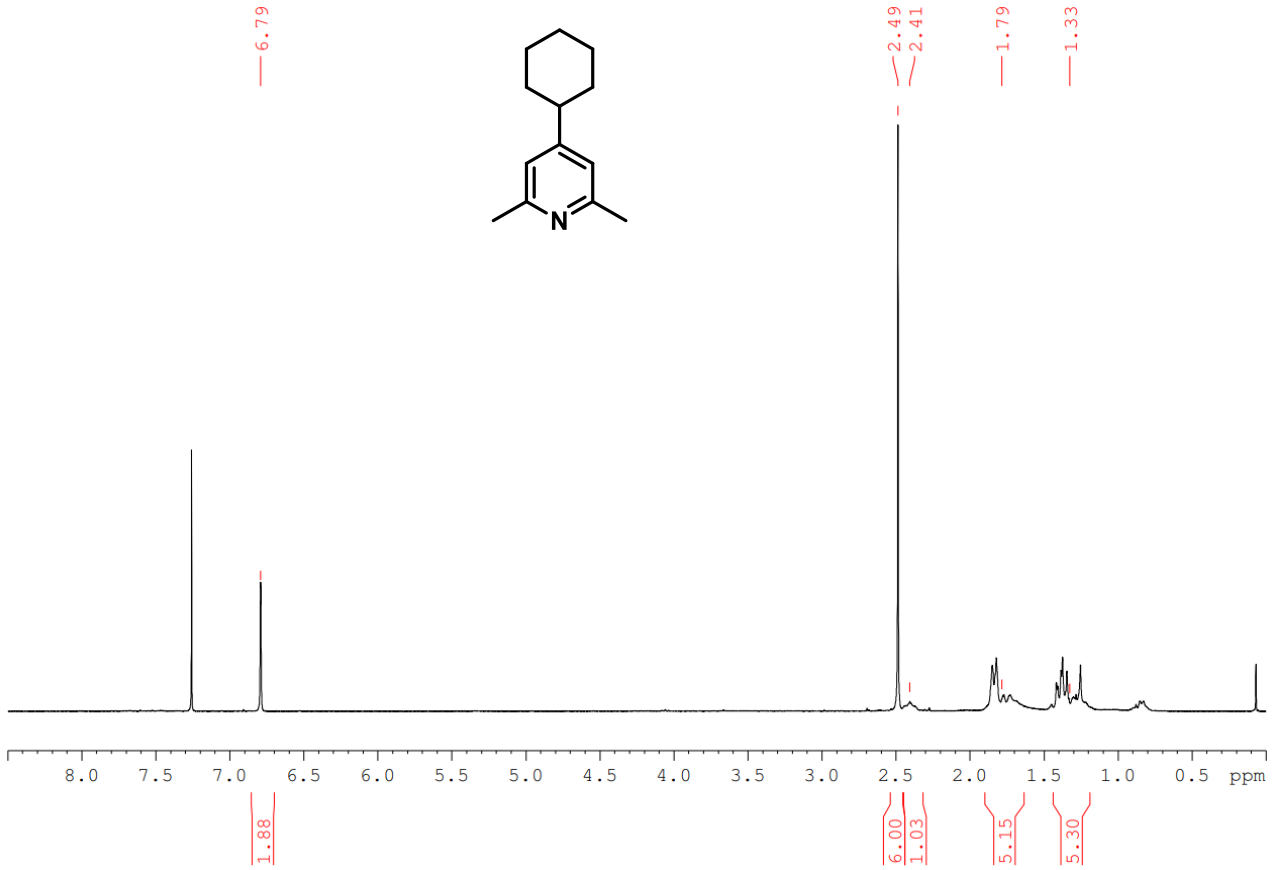

Figure S220 ^{1}H NMR of 4-cyclohexyl-2,6-dimethylpyridine in $CDCl_3$.

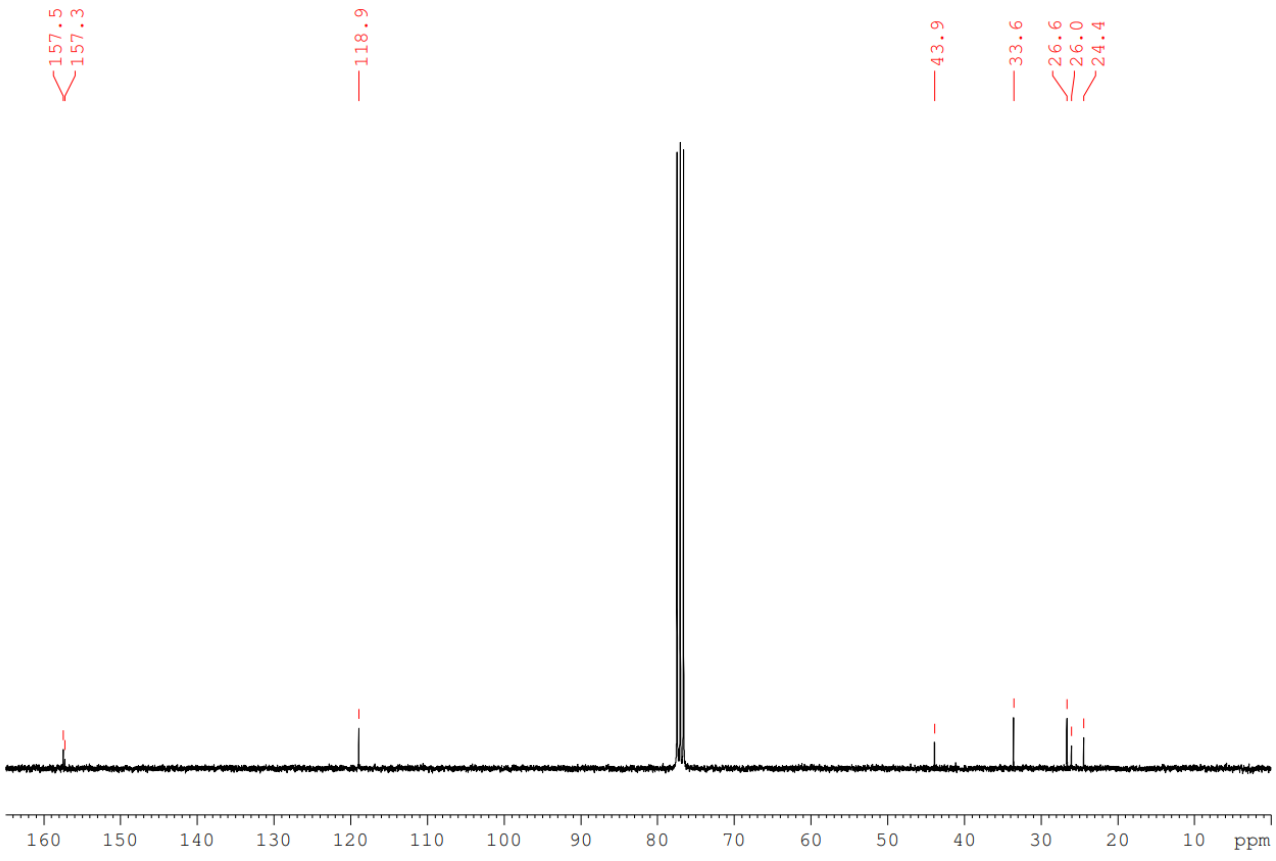

Figure S221 ^{13}C NMR of 4-cyclohexyl-2,6-dimethylpyridine in $CDCl_3$.

4-Cyclohexylquinazoline (4)

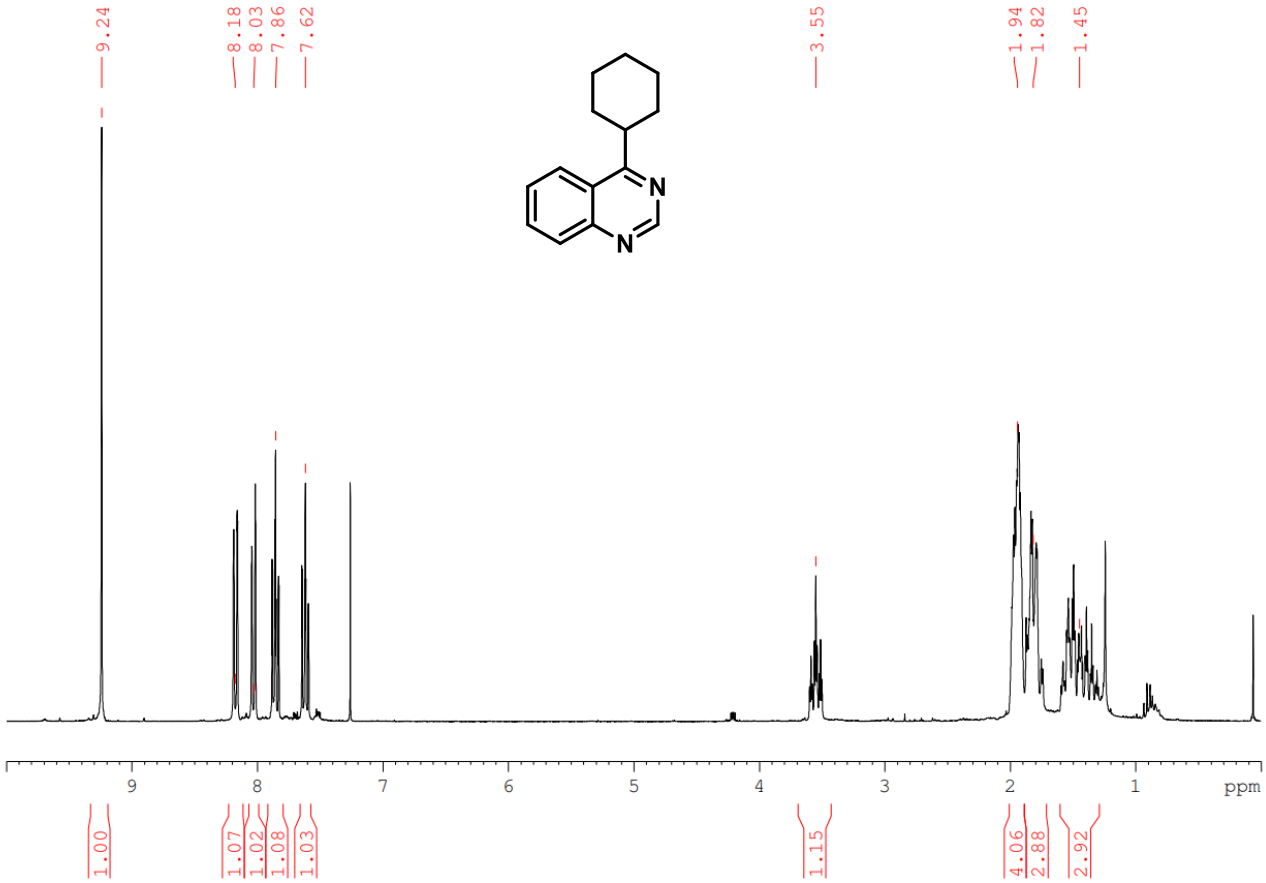

Figure S222 ^{1}H NMR of 4-cyclohexylquinazoline in $CDCl_3$.

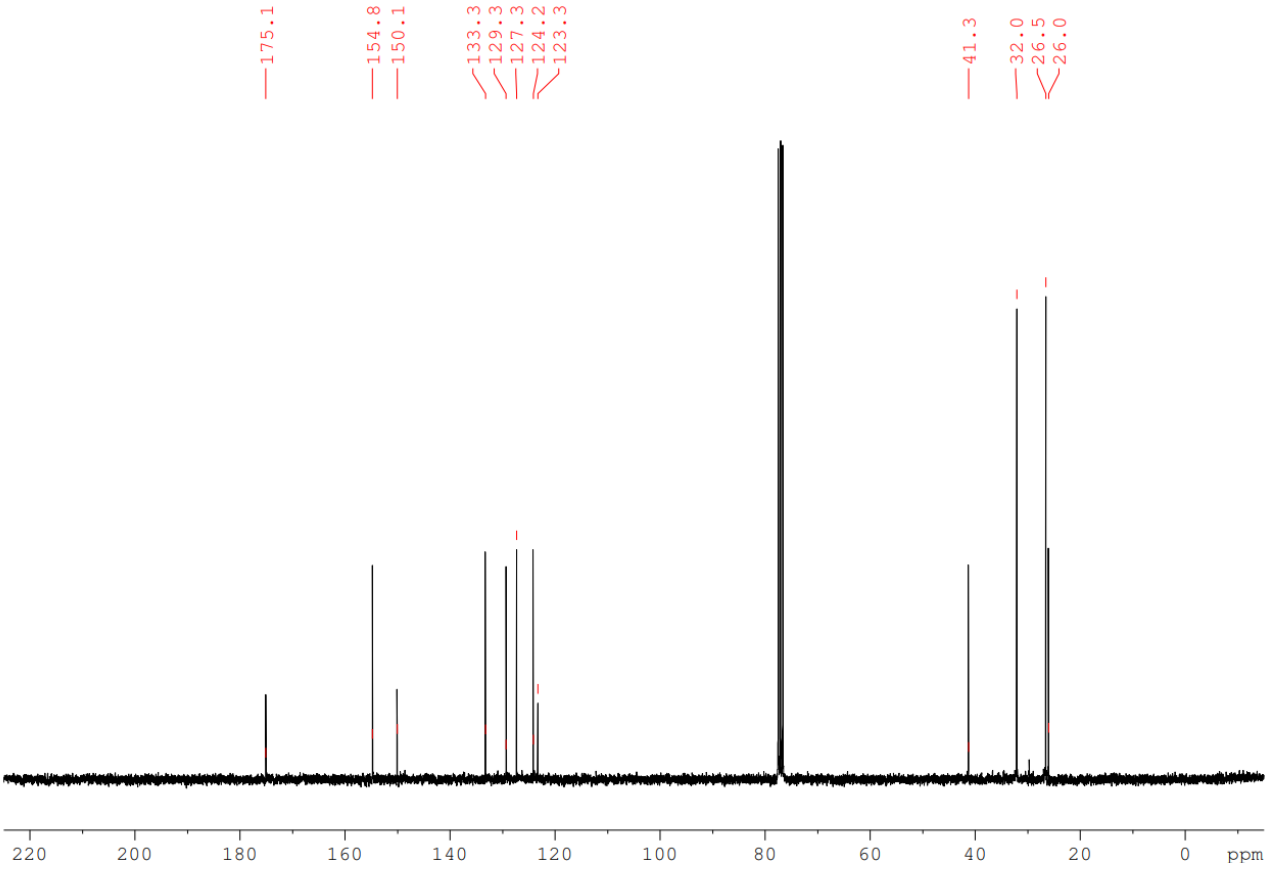

Figure S223 ^{13}C NMR of 4-cyclohexylquinazoline in $CDCl_3$.

1-Cyclohexylisoquinoline (5)

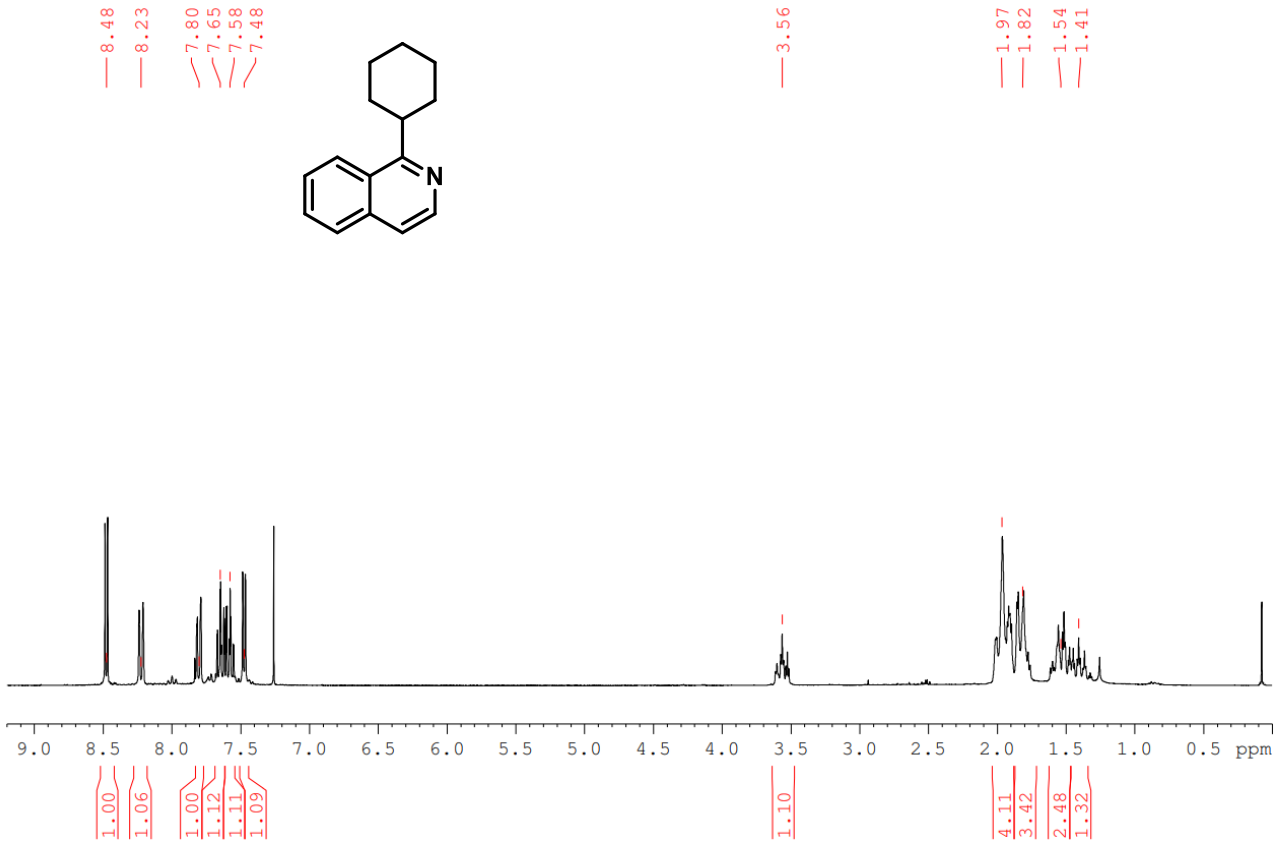

Figure S224 ^{1}H NMR of 1-cyclohexylisoquinoline in $CDCl_3$.

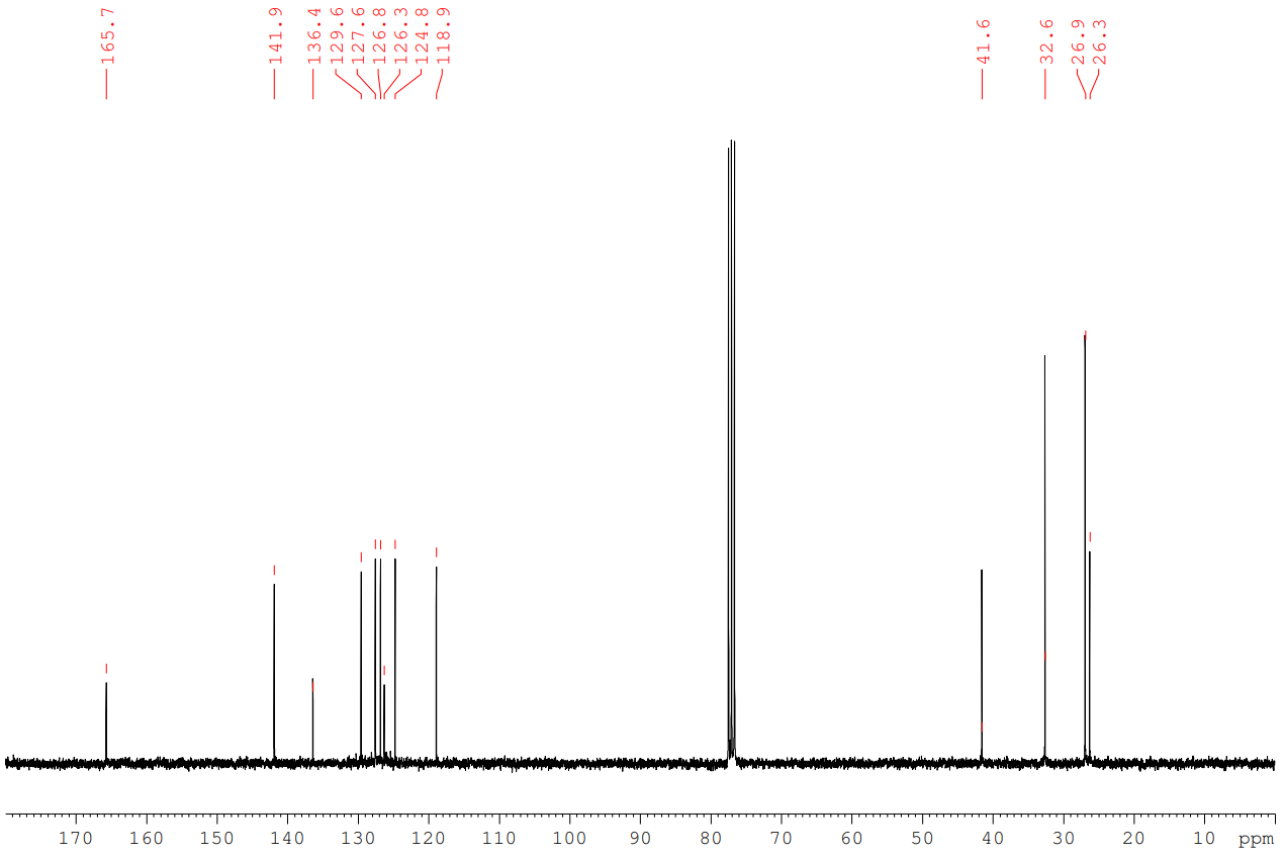

Figure S225 ^{13}C NMR of 1-cyclohexylisoquinoline in $CDCl_3$.

2-Cyclohexyl-1-methyl-1*H*-benzo[*d*]imidazole (6)

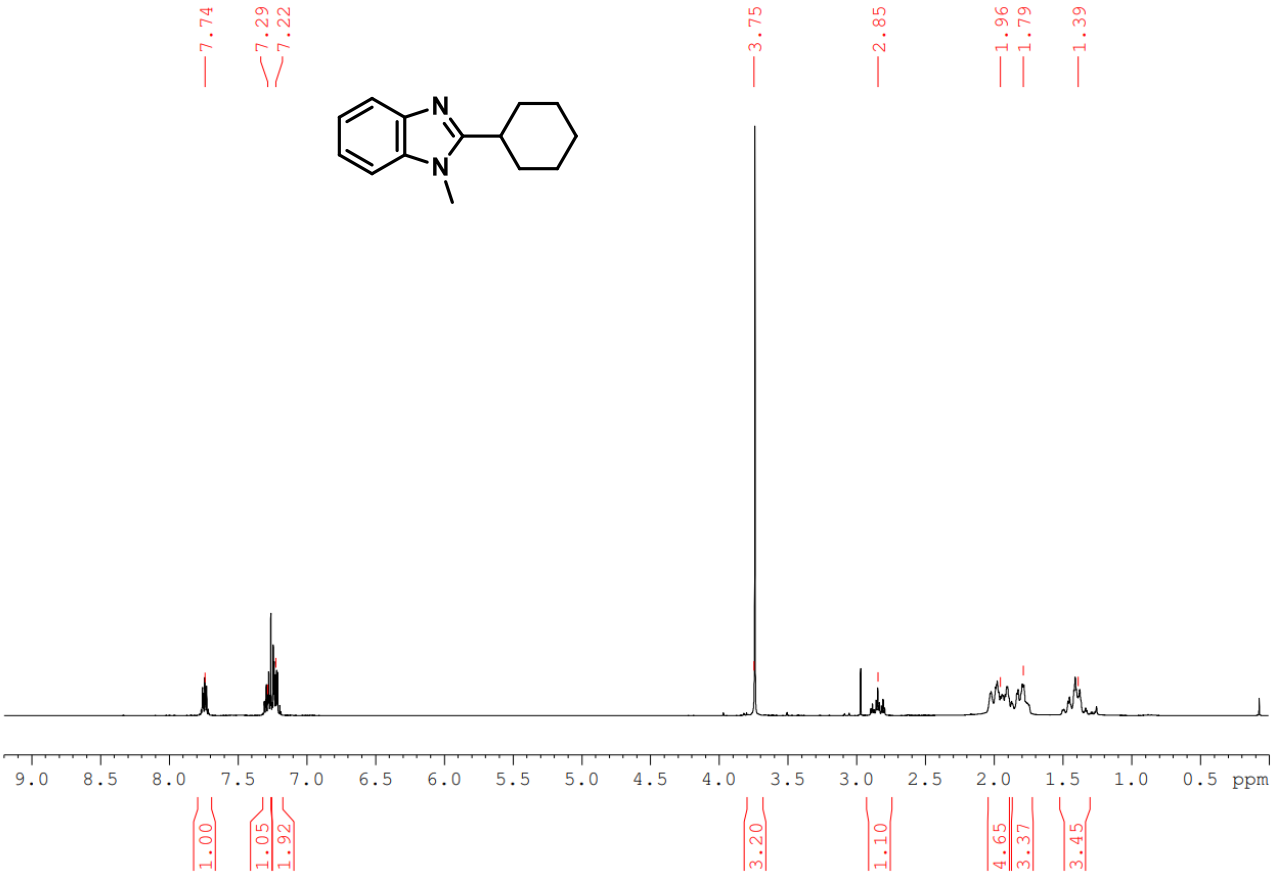

Figure S226 ^{1}H NMR of 4-cyclohexyl-1-methyl-1*H*-benzo[*d*]imidazole in $CDCl_3$.

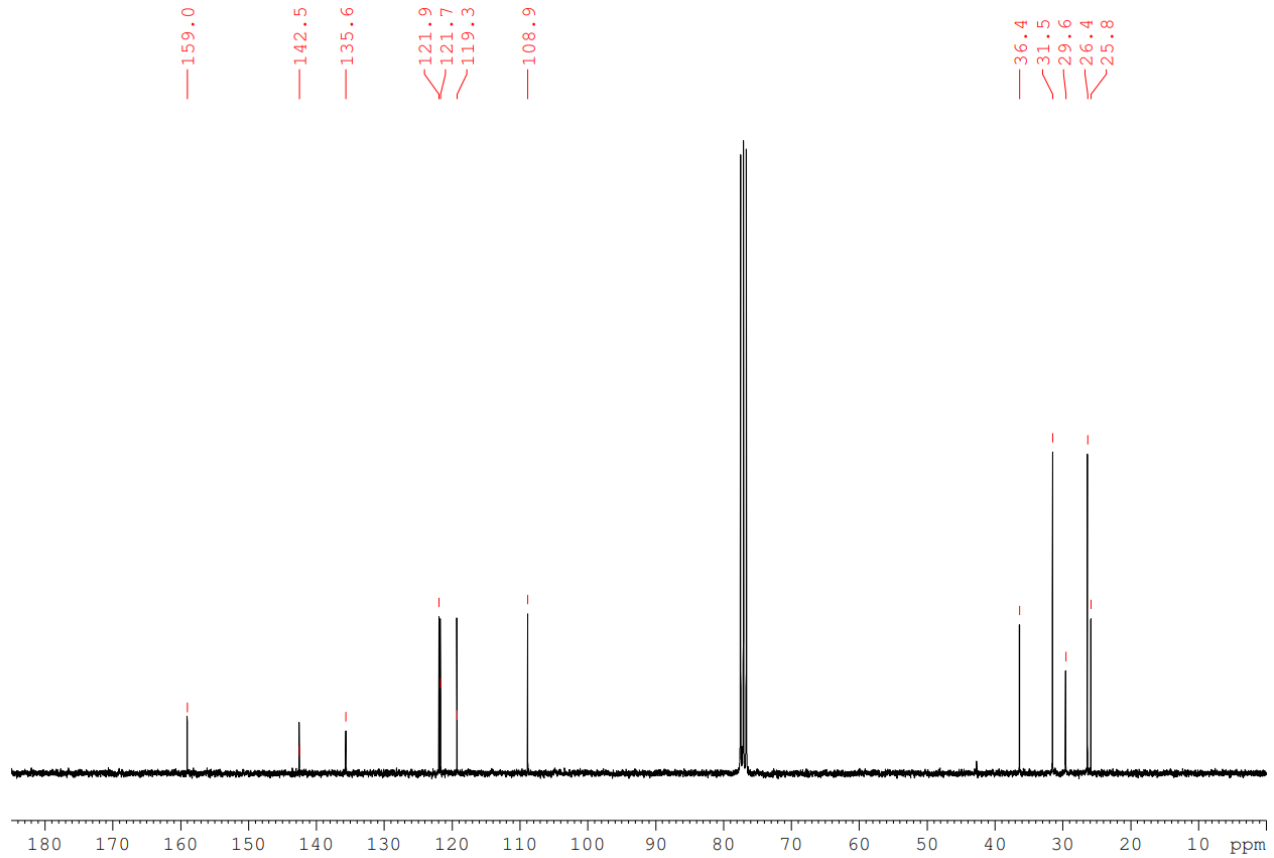

Figure S227 ^{13}C NMR of 4-cyclohexyl-1-methyl-1*H*-benzo[*d*]imidazole in $CDCl_3$.

2-(Adamantan-1-yl)-4-methylquinoline (7)

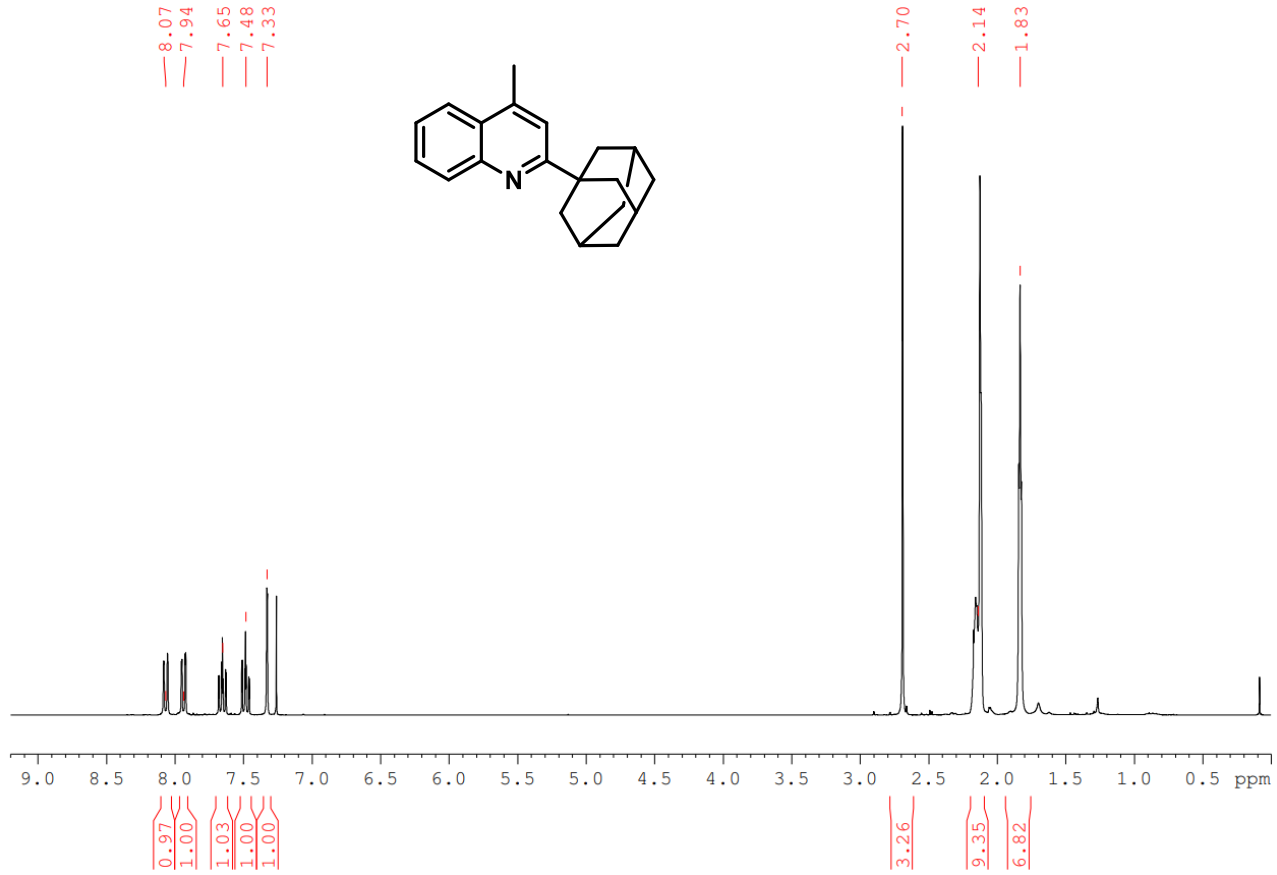

Figure S228 ^{1}H NMR of 2-(adamantan-1-yl)-4-methylquinoline in $CDCl_3$.

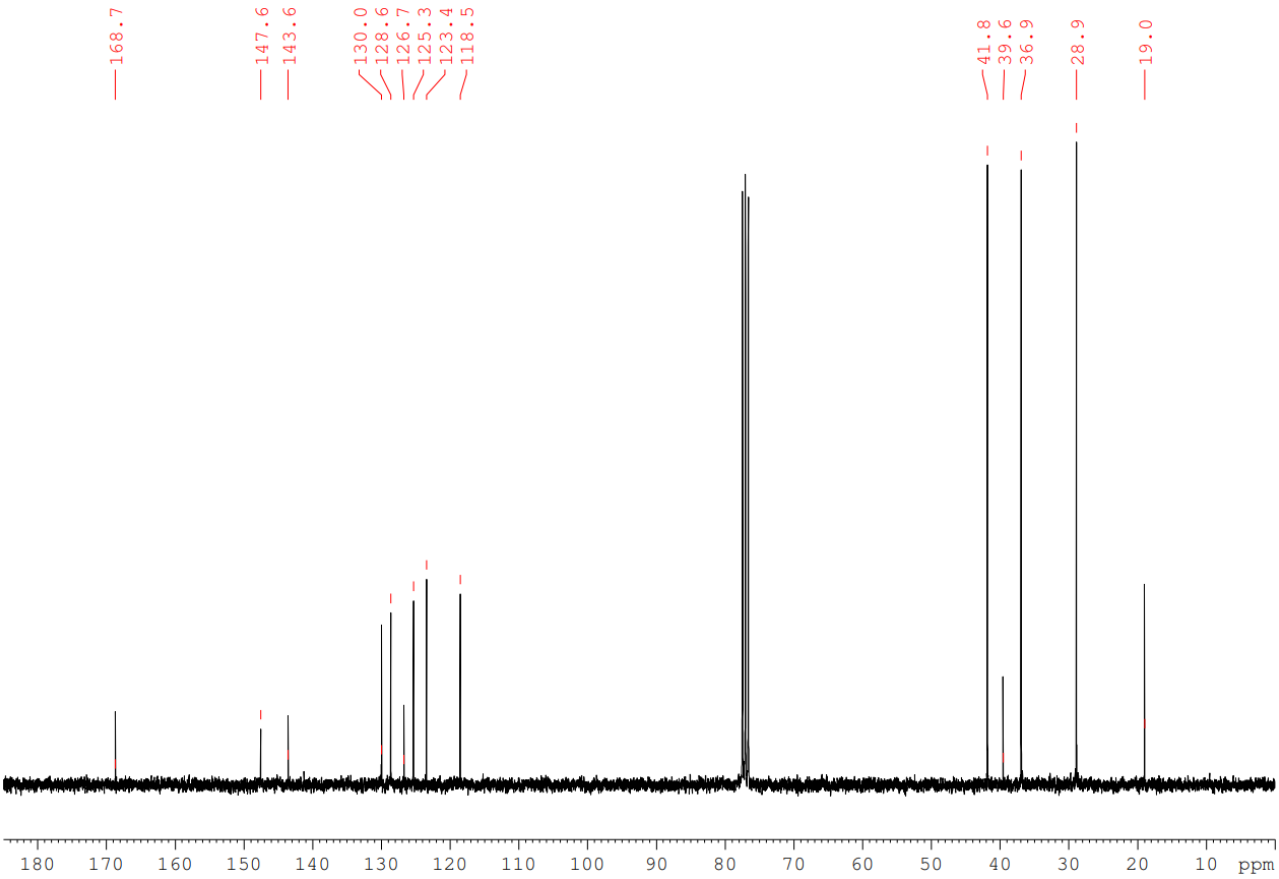

Figure S229 ^{13}C NMR of 2-(adamantan-1-yl)-4-methylquinoline in $CDCl_3$.

2-Isopentyl-4-methylquinoline (8)

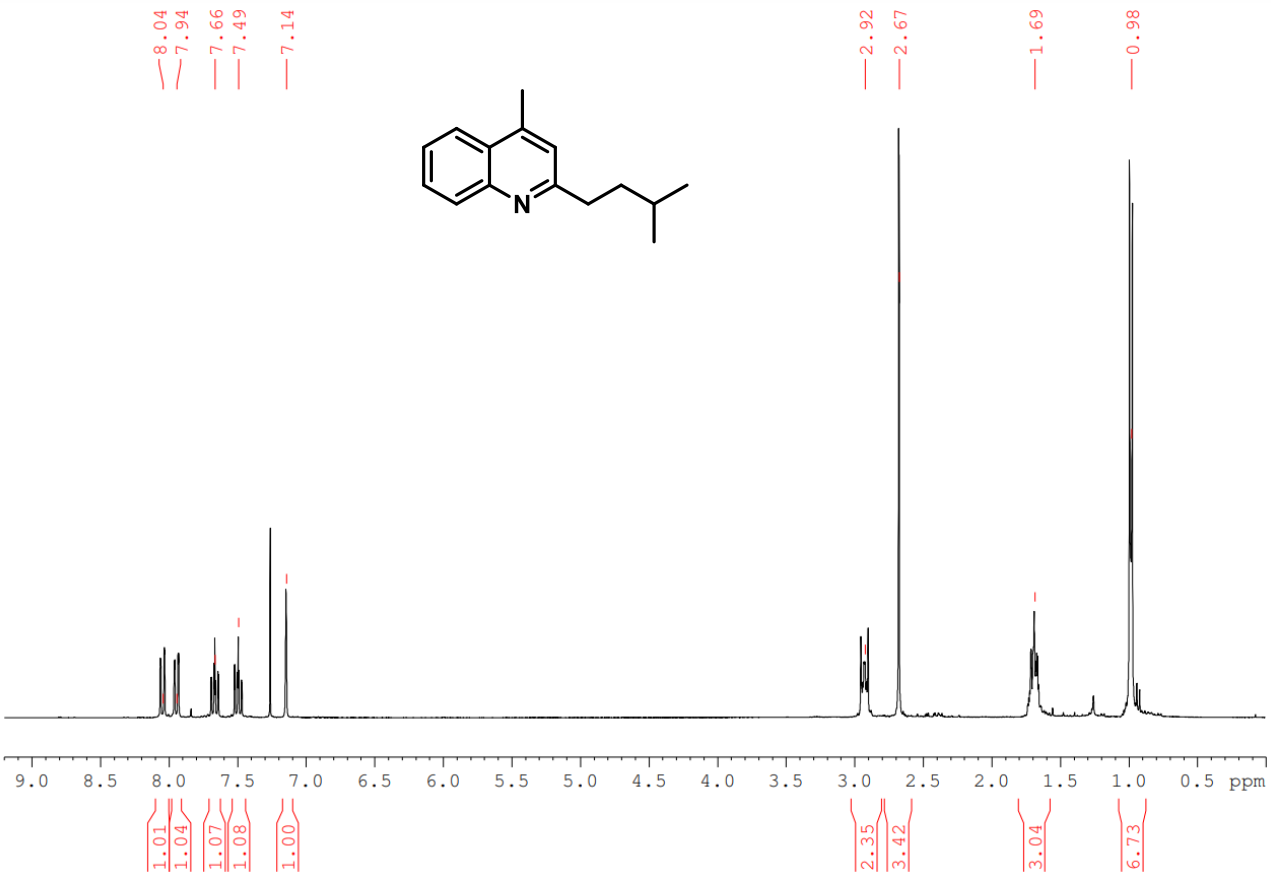

Figure S230 ^{1}H NMR of 2-isopentyl-4-methylquinoline in $CDCl_3$.

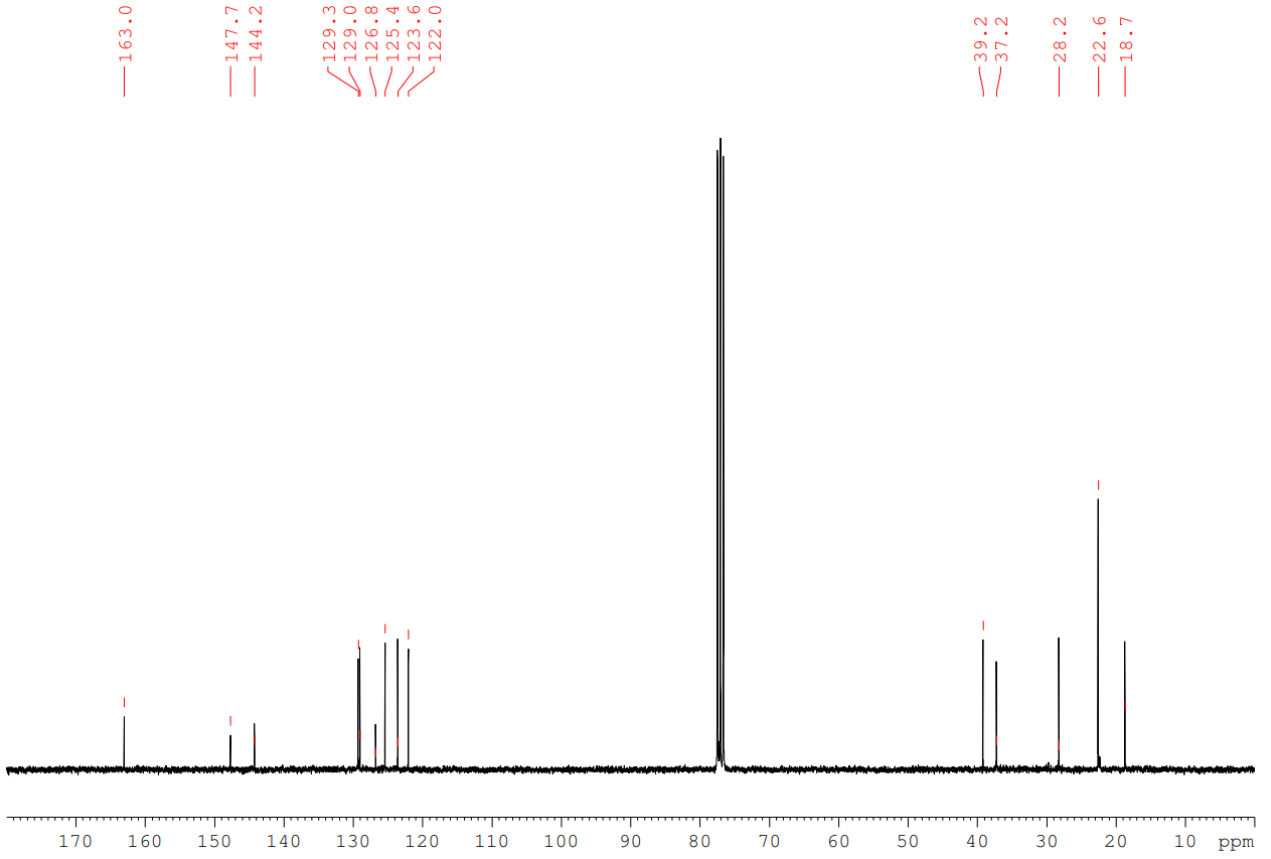

Figure S231 ^{13}C NMR of 2-isopentyl-4-methylquinoline in $CDCl_3$.

N-((4-methylquinolin-2-yl)methyl)acetamide (9)

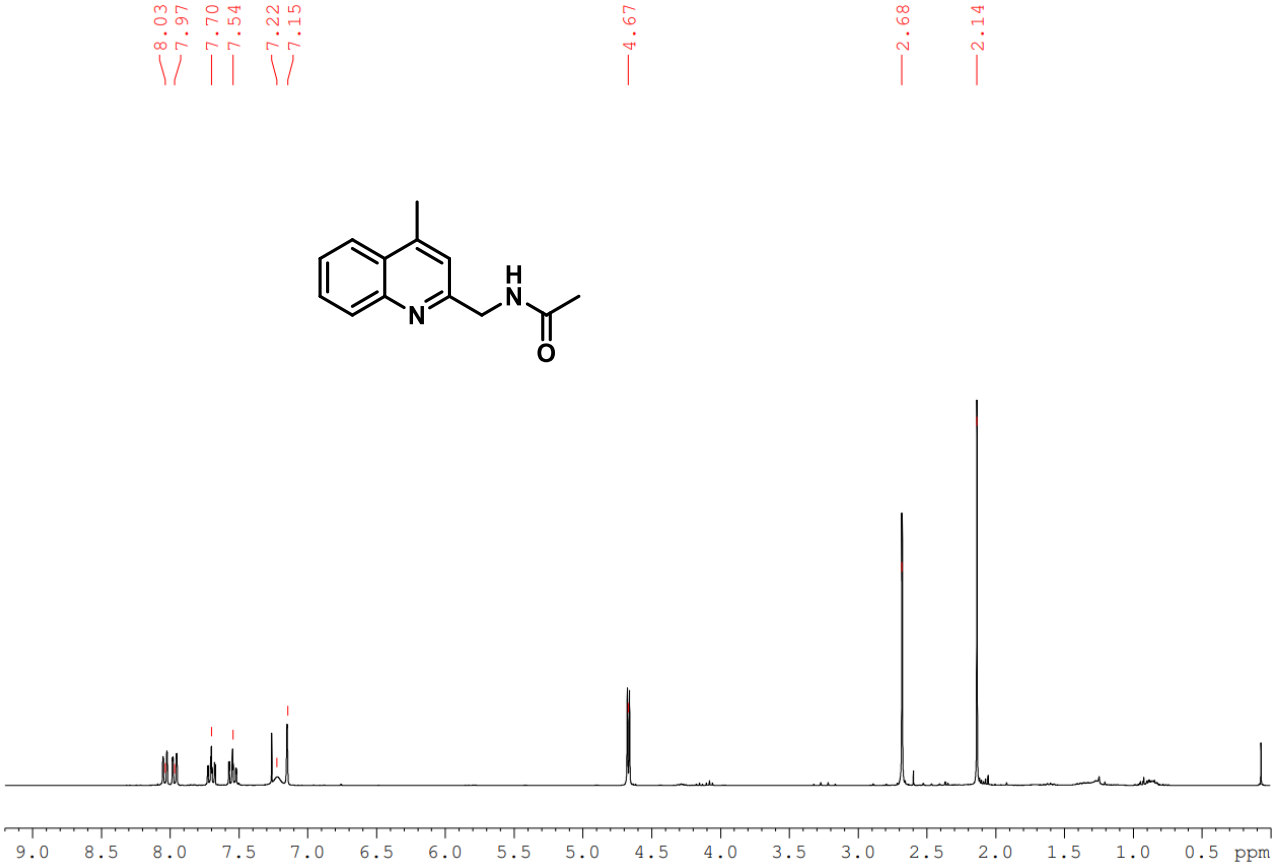

Figure S232 ^{1}H NMR of *N*-((4-methylquinolin-2-yl)methyl)acetamide in $CDCl_3$.

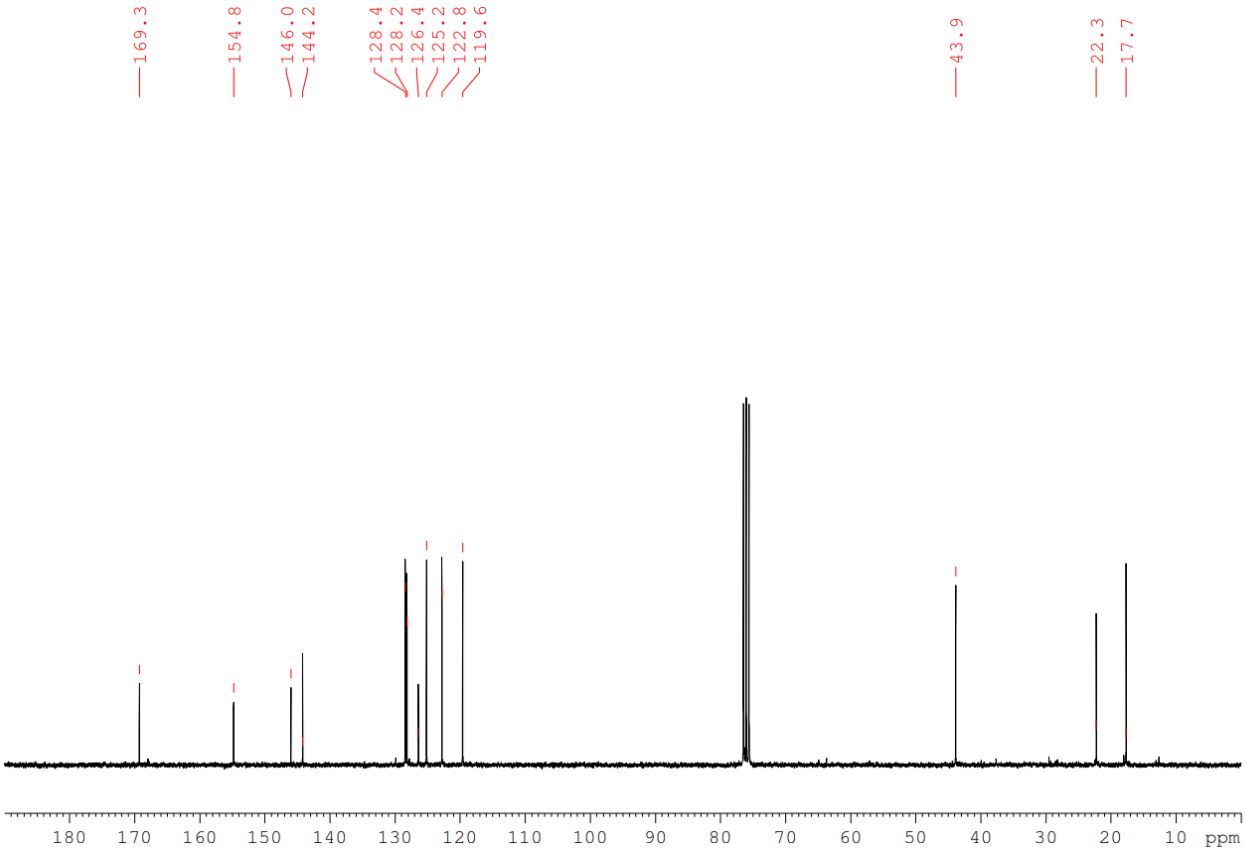

Figure S233 ^{13}C NMR of *N*-((4-methylquinolin-2-yl)methyl)acetamide in $CDCl_3$.

1-(3,4-Dimethoxybenzyl)isoquinoline (10)

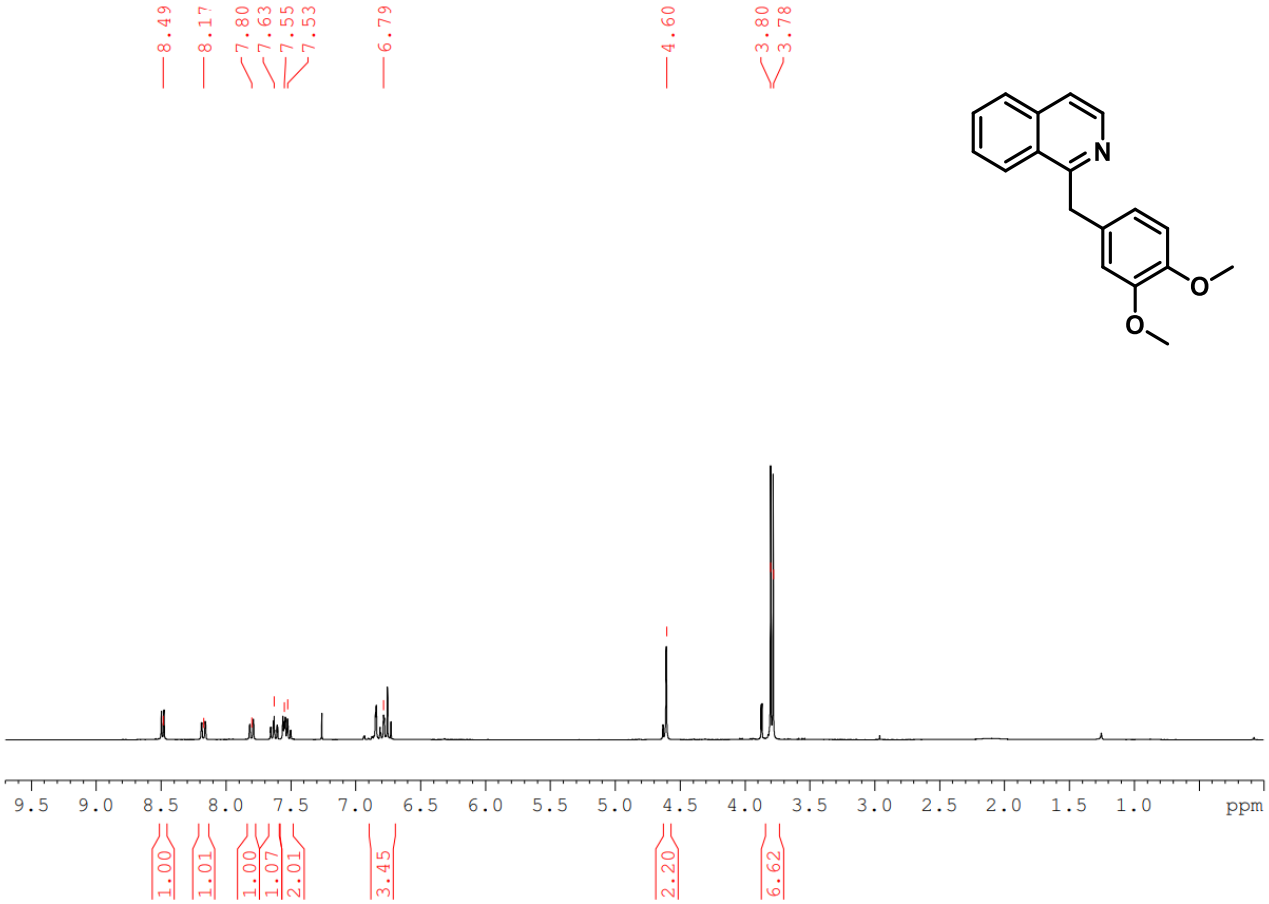

Figure S234 ^{1}H NMR of 1-(3,4-dimethoxybenzyl)isoquinoline in $CDCl_3$.

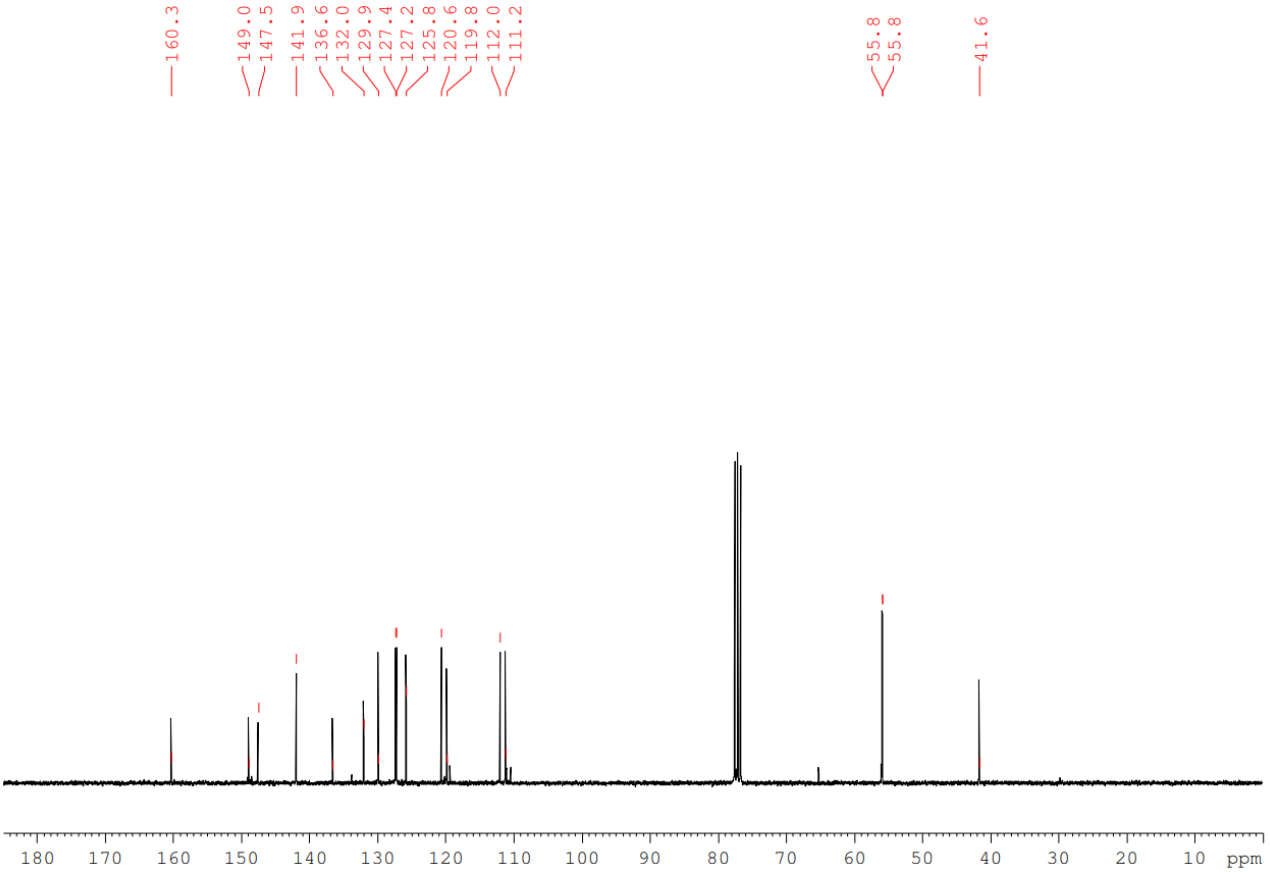

Figure S235 ^{13}C NMR of 1-(3,4-dimethoxybenzyl)isoquinoline in $CDCl_3$.

10. References

1 C. M. S. Jones, A. Gakamsky and J. Marques-Hueso, *Sci. Technol. Adv. Mater.*, 2021, **22**, 810–848.

2 O. V. Dolomanov, L. J. Bourhis, R. J. Gildea, J. A. K. Howard and H. Puschmann, *J. Appl. Crystallogr.*, 2009, **42**, 339–341.

3 G. M. Sheldrick, *Acta Crystallogr. Sect. A Found. Crystallogr.*, 2015, **71**, 3–8.

4 G. M. Sheldrick, *Acta Crystallogr. Sect. C Struct. Chem.*, 2015, **71**, 3–8.

5 M. Ranger, D. Rondeau and M. Leclerc, *Macromolecules*, 1997, **30**, 7686–7691.

6 B. A. DaSilveira Neto, A. S. A. Lopes, G. Ebeling, R. S. Gonçalves, V. E. U. Costa, F. H. Quina and J. Dupont, *Tetrahedron*, 2005, **61**, 10975–10982.

7 J. P. Heiskanen, P. Vivo, N. M. Saari, T. I. Hukka, T. Kastinen, K. Kaunisto, H. J. Lemmetyinen and O. E. O. Hormi, *J. Org. Chem.*, 2016, **81**, 1535–1546.

8 M. Dogru, A. Sonnauer, S. Zimdars, M. Döblinger, P. Knochel and T. Bein, *CrystEngComm*, 2013, **15**, 1500–1502.

9 N. R. Paisley, C. M. Tonge, D. M. Mayder, K. A. Thompson and Z. M. Hudson, *Mater. Chem. Front.*, 2020, **4**, 555–566.

10 D. R. Lide, Ed., *CRC Handbook of Chemistry and Physics*, 87th ed., CRC Press, Boca Raton, 87th edn., 2006.

11 C. Reichardt, *Angew. Chemie Int. Ed.*, 1965, **4**, 555-566.

12 M. J. Frisch, G. W. Trucks, H. B. Schlegel, G. E. Scuseria, M. A. Robb, J. R. Cheeseman, G. Scalmani, V. Barone, G. A. Petersson, H. Nakatsuji, X. Li, M. Caricato, A. V. Marenich, J. Bloino, B. G. Janesko, R. Gomperts, B. Mennucci, H. P. Hratchian, J. V. Ortiz, A. F. Izmaylov, J. L. Sonnenberg, D. Williams-Young, F. Ding, F. Lipparini, F. Egidi, J. Goings, B. Peng, A. Petrone, T. Henderson, D. Ranasinghe, V. G. Zakrzewski, J. Gao, N. Rega, G. Zheng, W. Liang, M. Hada, M. Ehara, K. Toyota, R. Fukuda, J. Hasegawa, M. Ishida, T. Nakajima, Y. Honda, O. Kitao, H. Nakai, T. Vreven, K. Throssell, J. A. Montgomery, Jr., J. E. Peralta, F. Ogliaro, M. J. Bearpark, J. J. Heyd, E. N. Brothers, K. N. Kudin, V. N. Staroverov, T. A. Keith, R. Kobayashi, J. Normand, K. Raghavachari, A. P. Rendell, J. C. Burant, S. S. Iyengar, J. Tomasi, M. Cossi, J. M. Millam, M. Klene, C. Adamo, R. Cammi, J. W. Ochterski, R. L. Martin, K. Morokuma, O. Farkas, J. B. Foresman, and D. J. Fox, Gaussian 16, Revision A.03, Inc., Wallingford CT, 2016.

13 R. Dennington, T. A. Keith and J. M. Millam, GaussView Version 6, Semichem Inc., Shawnee Mission KS, 2016.

14 B. Miehlich, A. Savin, H. Stoll and H. Preuss, *Chem. Phys. Lett.*, 1989, **157**, 200–206.

15 C. Lee, W. Yang and R. G. Parr, *Phys. Rev. B*, 1988, **37**, 785–789.

16 A. D. Becke, *J. Chem. Phys.*, 1993, **98**, 1372–1377.

17 A. D. Becke, *Phys. Rev. A*, 1988, **38**, 3098–3100.

18 R. Krishnan, J. S. Binkley, R. Seeger and J. A. Pople, *J. Chem. Phys.*, 1980, **72**, 650–654.

19 T. H. Dunning, *J. Chem. Phys.*, 1989, **90**, 1007–1023.

20 A. V. Marenich, C. J. Cramer and D. G. Truhlar, *J. Phys. Chem. B*, 2009, **113**, 6378–6396.

21 T. Yanai, D. P. Tew and N. C. Handy, *Chem. Phys. Lett.*, 2004, **393**, 51–57.

22 T. Malcomson and M. J. Paterson, *Photochem. Photobiol. Sci.*, 2020, **19**, 1538–1547.

23 M. J. Paterson, O. Christiansen, F. Pawłowski, P. Jørgensen, C. Hättig, T. Helgaker and P. Sałek, *J. Chem. Phys.*, 2006, **124**, 054322.

24 J. Arnbjerg, M. J. Paterson, C. B. Nielsen, M. Jørgensen, O. Christiansen and P. R. Ogilby, *J. Phys. Chem. A*, 2007, **111**, 5756–5767.

25 M. Johnsen, M. J. Paterson, J. Arnbjerg, O. Christiansen, C. B. Nielsen, M. Jørgensen and P. R. Ogilby, *Phys. Chem. Chem. Phys.*, 2008, **10**, 1177–1191.

26 L. Therese Bergendahl and M. J. Paterson, *Chem. Commun.*, 2012, **48**, 1544–1546.

27 M. Akhtaruzzaman, N. Kamata, J. Nishida, S. Ando, H. Tada, M. Tomura and Y. Yamashita, *Chem. Commun.*, 2005, 3183.

28 C. B. Nielsen, A. J. P. White and I. McCulloch, *J. Org. Chem.,* 2015, **80**, 5045–5048.

29 S. I. Kato, T. Matsumoto, M. Shigeiwa, H. Gorohmaru, S. Maeda, T. Ishi-i and S. Mataka, *Chem. - A Eur. J.*, 2006, **12**, 2303–2317.

30 E. M. Espinoza, J. A. Clark, J. Soliman, J. B. Derr, M. Morales and V. I. Vullev, *J. Electrochem. Soc.*, 2019, **166**, H3175–H3187.

31 H. G. Roth, N. A. Romero and D. A. Nicewicz, *Synlett*, 2016, **27**, 714–723.

32 N. A. Romero and D. A. Nicewicz, *Chem. Rev.*, 2016, **116**, 10075–10166.